DOCTOR OF PHILOSOPHY

Investigation of the physiological function of TTBK2 (tau tubulin kinase 2), a protein kinase mutated in spinocerebellar ataxia type 11 (SCA11)

Esoof, Noor

Award date:
2014

Investigation of the physiological function of TTBK2 (tau tubulin kinase 2), a protein kinase mutated in spinocerebellar ataxia type 11 (SCA11)

Noor Esoof

A thesis submitted for the degree of

Doctor of Philosophy

University of Dundee

January 2014

I. Erratum

The aim of this erratum is to summarise the inconsistencies between data presented in this PhD thesis and the raw data that it is based upon. References to tables and figures in the PhD thesis will be made in the form of "Thesis Table" and "Thesis Figure" to avoid confusion with tables shown in this erratum. File names mentioned reference to files found in Noor Esoof's folder on the MRC group folder network drive ("smb://mrc-smb.lifesci.dundee.ac.uk/mrc-group-folder/Noor Esoof").

Thesis Figure 4.1 and Thesis Table 4.1

It has now been established that the raw data used for Thesis Figure 4.1 and Thesis Table 4.1 are different from what is reported in the PhD thesis. Conclusions drawn from Thesis Figure 4.1 and Thesis Table 4.1 are thus misleading. Thesis Figure 4.1 describes the use of two different anti-TTBK2 antibodies in the same experiment to conduct separate immunoprecipitations that lead to the results summarized in Thesis Table 4.1. The sources identifying the raw data used for this analysis, which also matches with the gel image used as Thesis Figure 4.1, are (a) a word document (file name "NEsoof 110624 MFP b.docx"), used for submission of the samples to the MRC mass spectrometry (MS) facility and (b) the actual MS measurements saved on a central server. The word document states: "Aim of Project is to identify proteins that co-immunoprecipitate with [*sic*] endogenous TTBK2 and TTBK1". The gel image in the submission form (the same image used in the thesis as Thesis Figure 4.1) is labelled with 'TTBK1' and 'TTBK2' above the respective gel lanes. These observations are consistent with the idea that the experiment in Thesis Table 4.1 used antibodies raised against TTBK1 and TTBK2, rather than 2 different antibodies against TTBK2.

As shown in Table 1, the samples from the lane labelled 'TTBK1' contained consistently more TTBK1-related peptides than TTBK2-related peptides. As the well samples from the lane labelled 'TTBK2' contained more TTBK2-related peptides than TTBK1-related peptides, this is also suggests that the experiment used separate antibodies raised against TTBK1 and TTBK2, which means that Thesis Figure 4.1 has been mislabelled.

	TTBK1 lane	TTBK2 lane
TTBK1 peptide count	#35 – 143 (65)	#43 – 2 (1)
[#sample - total (unique)]	#36 – 49 (17)	#44 – 6 (4)
	#37 – 0	#45 – 6 (2)
	#38 – 0	#46 – 0
	#39 – 0	#47 – 0
	#40 – 0	#48 – 0
	#41 – 0	#49 – 0
	#42 – 0	#50 – 0
TTBK2 peptide count	#35 – 16 (9)	#43 – 12 (8)
[#sample - total (unique)]	#36 – 0	#44 – 48 (20)
	#37 – 0	#45 – 24 (10)
	#38 – 0	#46 – 0
	#39 – 0	#47 – 5 (2)
	#40 – 0	#48 – 5 (1)
	#41 – 9 (1)	#49 – 0
	#42 – 0	#50 – 0

Table 1: Raw data from MS submission form "NEsoof 110624 MFP b.docx". The data is formatted as "sample number – total peptides (unique peptides)".

Furthermore, only the data from the column "TTBK2 Ab1" are found in the file "NEsoof 110624 MFP b.docx". The other column of Thesis Table 4.1 labelled "TTBK2 Ab2" corresponds to data found in experiment "NEsoof 110728 MFP b.docx". The timestamp used in the file names shows that these two experiments were conducted over a month apart (24th of June 2011 versus 28th of July 2011). The thesis links all data in Thesis Table 4.1 to Thesis Figure 4.1, therefore use of the data in "NEsoof 110728 MFP b.docx" without addressing the different sources is inappropriate. A correct presentation of data would be to show only the lane labelled "TTBK2 Ab1" of Thesis Figure 4.1 with a gel image representative of experiment "NEsoof 110728 MFP b.docx" next to it, while also addressing the fact that these are independent experiments.

On page 117, the PhD thesis describes how non-specific interacting proteins were filtered out by use of the IgG control samples. Thus, the peptides belonging to key protein interaction partners that were further investigated, such as SV2A and Synaptotagmin-1, should not appear in the IgG samples of these experiments. As

shown in Table 2, the IgG lane samples of experiment “NEsoof 110624 MFP b.docx” contain a substantial number of both SV2A and Synaptotagmin-1 peptides. Thus, without additional experimental evidence and explicit justification, neither one of these proteins should have been selected for further experiments as being strong candidates for specific TTBK2 interaction partners, which has implications for all data presented in the PhD thesis thereafter.

	SV2A (in IgG lane)	**Synaptotagmin-1 (in IgG lane)**
peptide count [#sample - total (unique)]	#27 – 0	#27 – 0
	#28 – 37 (30)	#28 – 0
	#29 – 22 (15)	#29 – 58 (32)
	#30 – 0	#30 – 0
	#31 – 0	#31 – 8 (3)
	#32 – 0	#32 – 0
	#33 – 0	#33 – 0
	#34 – 0	#34 – 0

Table 2: Raw data from MS submission form "NEsoof 110624 MFP b.docx". Data is taken from the IgG lane samples and is formatted as “sample number – total peptides (unique peptides)”.

Similar conclusions can be drawn for the IgG lane samples of experiment “NEsoof 110728 MFP b.docx”, as shown in Table 3. In this case no peptides for Synaptotagmin-1 were detected in the IgG control, but also here multiple SV2A peptides have been measured.

	SV2A (in IgG lane)	**Synaptotagmin-1 (in IgG lane)**
peptide count [#sample - total (unique)]	#33 – 0	#33 – 0
	#34 – 0	#34 – 0
	#35 – 24(17)	#35 – 0
	#36 – 0	#36 – 0
	#37 – 0	#37 – 0
	#38 – 0	#38 – 0
	#39 – 0	#39 – 0

Table 3: Raw data from MS submission form "NEsoof 110728 MFP b.docx". Data is taken from the IgG lane samples and is formatted as “sample number – total peptides (unique peptides)”.

Thesis Table 4.8

The raw data used for Thesis Table 4.8 is derived from two separate experiments. Columns titled "NP1", "pS42", "pS45", "pS47", "pS42+pS45", "pS42+pS47", "pS45+pS47" are derived from data linked in file "NEsoof 120823 MFP_peptide_pulldown.docx". The data in the column titled "pS42+pS45+pS47" are also linked to the same word document, but the link has been altered to point to data from a different experiment. The timestamp in the filename dates the file to the 23rd of August, 2012. The last modification of the file recorded occurred on 9th of April 2014. The altered link points to the data in file "NEsoof 120801 MFP.docx", sample 02, marked as "S45 peptide". As the column of the data this link replaced is titled "pS42+pS45+pS47", this is unlikely to be an independent replicate put into this table, but instead a different experiment performed with differing conditions on a different date (23rd of August 2012 versus 1st of August 2012).

The potential interaction partner listed at the top, "Spectrin beta chain, brain 2" is mixed up with a different Spectrin protein isoform. The raw mass spec data show the entry corresponding to the listed MASCOT scores and peptide counts as follows:
"sp|Q62261|SPTB2_MOUSE (...) Spectrin beta chain, brain 1 OS=Mus musculus GN=Sptbn1 (...)"

This shows that the full name of the correct protein is actually "Spectrin beta chain, brain 1", and the gene identifier is "Sptbn1", not "Sptbn2" as stated in Thesis Table 4.8.

Thesis Page 164

The PhD thesis page 164 states: "SPTBN2 was not present in pull-downs with NP1 or singly-phosphorylated peptides". As shown in Thesis Table 4.8 there are 10 peptides for SPTBN2 detected in sample NP. Therefore the quoted statement is incorrect.

Thesis Table 4.10

The data in Thesis Table 4.10 is based on samples in the submission form “NEsoof 120823 MFP_peptide_pulldown.docx” and the reported MASCOT scores for the listed proteins are correct in the different samples. However, the legend of Thesis Table 4.10 states: "Comparisons are shown only for proteins identified with a MASCOT score of 400 or more." This suggests that only the most abundant proteins in the experiment, above a certain threshold, are reported. This description is incorrect as, for example, the line for SYT1 in the column for sample “pS80+pS81+pT84” shows a MASCOT score of 157 and should therefore not have been included in Thesis Table 4.10 according to the selection criteria stated in the figure legend. This is also the case for protein NEFM with MASCOT scores below 400.

In addition, the raw data corresponding to the samples in submission form “NEsoof 120823 MFP_peptide_pulldown.docx” contain many more protein hits with MASCOT scores greater than 400 that are not listed in Thesis Table 4.10. Therefore, this table not only lists proteins that do not fit the stated selection criteria, but also omits proteins that should have been reported, according to the selection criteria stated in the figure legend.

Thesis Figure 4.16

The Spectrin protein listed in Thesis Table 4.8, SPTBN1, was misidentified as SPTNB2. This also means that the wrong antibody was used for its detection in Thesis Figure 4.16, listed as “SPTBN2, ab58234” on PhD thesis page 65 in the “Materials and Methods” chapter. The detection of STPBN2 protein in whole cell lysate (labelled “input” in Thesis Figure 4.16) has, so far, not been reproduced by other members of the Alessi lab using the materials described in the PhD thesis. The major band detected by the SPTBN2 antibody is detected just below the 100 kDa marker, while the SPTBN2 band shown in Thesis Figure 4.16 and Thesis Figure 4.17 is detected at around 250 kDa. All SPTBN2 blots may therefore be incorrect.

II. Acknowledgements

For the past four years, I have had the marvellous privilege of being able to work autonomously towards this PhD thesis under the expert guidance of Prof. Dario Alessi, to whom I would like to express my heartfelt gratitude. I am immeasurably grateful for the opportunity to work on an exciting project and for allowing me to grow as a research scientist.

A successful science project is always collaborative, and with the way that my PhD project progressed, collaborations became a necessity. I would like to gratefully acknowledge Dr. Paul Davies for his biophysical expertise that was invaluable to the project and for being a friend throughout my PhD. I would also like to acknowledge Dr. Sarah Gordon and Prof. Michael Cousin (University of Edinburgh) for their substantial contribution to the project with their complementary expertise on how to expand the project in terms of functional experiments. My thanks also go out to the three postdocs who joined the TTBK2 endeavour: Ning, Max and Thomas.

This project would not have been possible without the exceptional work of the MRC PPU technical support staff and the DSTT teams for providing all the cDNA constructs, antibodies, purified proteins and other reagents. I would like to thank David Campbell, Bob Gourlay and Joby Varghese for the mass spectrometry analysis. Special thanks to the DSTT cloning team: Maria Deak, Mark Peggie, Thomas McCartney, Simone Weidlich for their expertise in making all the cDNA constructs used in this thesis. I would also like to thank Fiona Brown from the antibody production team, everybody in the protein production team, James Hastie and Hilary McLauchlan. Many thanks also to the administrative team: Alison Hart, Allison Bridges, Gail Fraser, Elaine Forsyth, and Judith Hare.

I take this opportunity to express my gratitude to the people who have been instrumental in the successful evolution of this project. I would like to show my greatest appreciation to Prof. John Rouse and Dr. Anton Gartner, my thesis committee members. A special thank you to Dr. Miratul Muqit, for being a supportive colleague and for always finding time for helpful scientific discussions.

Apart from the efforts of myself, the success of any project depends largely on the encouragement and guidelines of many others. I would like to thank all past and present members of the lab and all the MRC PPU PhD students, postdocs and PIs. I cannot thank everybody by name, but I would like to record my great debts of gratitude to the following: Youcef, Fran, Ayaz, Sourav, Chandana, Eeva, Agne, Jinwei, Kristina, Laia, Piotr, Ana, Jenny, Vanessa, Paola, Ciaran, Akihito, Francesca, Esther, Helen, Charlie and Jevgenia.

Last but not least, I would like to thank my parents, to whom this thesis is dedicated.

III. Declarations

I hereby declare that the following thesis is based on the results of investigations conducted by myself, and that this thesis is of my own composition. Work other than my own is clearly indicated in the text by reference to the researchers or their publications. This dissertation has not in whole, or in part, been previously presented for a higher degree.

Noor Esoof

I certify that Noor Esoof has spent the equivalent of a least nine terms in research work in the College of Life Sciences, University of Dundee, and that she has fulfilled the conditions of the Ordinance General No. 14 of the University of Dundee and is qualified to submit the accompanying thesis in application for the degree of Doctor of Philosophy.

Dario R. Alessi

IV. List of Abbreviations

Ach	Acetylcholine
ADCA	Autosomal dominant cerebellar ataxia
AFG3L2	ATPase family gene 3-like 2
AGC	Kinase group containing PKA, PKC and PKG.
AMP	Adenosine Monophosphate
AP2	adaptor-related protein complex 2
APS	Ammonium persulfate
ATP	Adenosine Triphosphate
ATN1	Atrophin 1
ATXN	Ataxin
BSA	Bovine Serum Albumin
CACNA1A	Calcium channel, voltage-dependent, P/Q type, alpha 1A subunit
CamK2a	$Ca^{2+/}$calmodulin-dependent protein kinase II
cAMP	cyclic adenosine-3', 5'-monophosphate
CBB	Coomassie brilliant blue
CD	Circular dichroism
CDK	Cyclin-dependent kinase
CH	Calponin homology
CK1	Casein kinase 1
CLK	CDC2-Like kinase
cpm	Counts per minute
C. elegans	Caenorhabditis elegans
cpm	Counts per minute
CSP	Cysteine string protein
Da	Dalton
DMEM	Dulbecco's Modified Eagle's Medium
DMP	Dimethyl pimelimidate
DNA	Deoxyribonucleic acid
DRPLA	Dentatorubral-pallidoluysian atrophy
DSTT	Division of signal transduction therapy
DTT	Dithiothreitol
E. coli	Escherichia coli

ECL	Enhanced chemiluminescence
EDTA	Ethylenediamine tetra acetic acid
EF	Calcium-binding motifs composed of two helixes (E and F) joined by a loop.
EGTA	Ethyleneglycol bis (2-aminoethylether)-N, N-tetra acetic acid
ER	Endoplasmic reticulum
Erk	Extracellular signal-regulated kinase
FBS	Foetal bovine serum
FGF	Fibroblast growth factor
FP	Fluorescence polarisation
GABA	γ-aminobutyric acid
GFP	Green fluorescent protein
GSK	Glycogen synthase kinase
GST	Glutathione S-transferase
HDL-4	Huntington's disease-like 4
HEPES	4-(2-hydroxyethyl)-1-piperazineethanesulfonic acid
HEK293	Human embryonic kidney 293
HPLC	High performance liquid chromatography
HSP70	70 kDa Heat shock protein
HSR	Heat shock response
IgG	Immunoglobulin G
IHPS	Inositol high-polyphosphate series
IP6	Inositol hexaphosphate
ITC	Isothermal titration calorimetry
ITPR1	Inositol 1,4,5-trisphosphate receptor, type 1
KCNC3	Voltage-gated potassium channel subunit $K_v3.3$
KD	Kinase-dead
KLH	Keyhole limpet hemocyanin
LB	Luria broth
MALDI	Matrix-assisted laser desorption ionisation
MAP	Microtubule-associated protein
MAPK	Mitogen-activated protein kinase
MEF	Mouse embryonic fibroblast
MEM	Minimum essential medium
mGluR1	Metabotropic glutamate receptor type 1

mRNA	Messenger ribonucleic acid
MS/MS	Tandem mass spectrometry
NMD	Nonsense-mediated decay
NMR	Nuclear magnetic resonance
NOE	Nuclear Overhauser effect
NSF	N-ethylmaleimide sensitive factor
N-terminal	Amino-terminal
PBS	Phosphate buffered saline
PCR	Polymerase chain reaction
PDK1	3-phosphoinositide-dependent kinase 1
PH	Pleckstrin homology
PI3K	Phosphoinositide 3-kinase
PKA	Protein kinase A (cAMP-dependent protein kinase)
PKB	Protein kinase B (also known as Akt)
PKC	Protein kinase C
PLEKHG4	Pleckstrin homology domain-containing, family G member4
PMSF	Phenylmethanesulphonylfluoride
PP2	Protein phosphatase 2
PP2R2B	Protein phosphatase 2, regulatory subunit B, beta
PRKCG	Protein kinase C gamma type
PSPL	Positional scanning peptide library
ROS	Reactive oxygen species
rpm	Revolutions per minute
SCA	Spinocerebellar ataxia
SCAMP	Secretory carrier-associated membrane protein
SNARE	Soluble NSF attachment receptor
SPR	Surface plasmon resonance
SPTBN2	β2-spectrin
SH3	Src homology 3
SUMO	Small ubiquitin-like modifier
SV2	Synaptic vesicle glycoprotein 2
SVOP	SV2 related protein homolog
TEMED	Tetramethylethylenediamine
TFA	Trifluoroacetic acid

TK	Thymidine kinase
TBP	TATA-binding protein
TTBK1	Tau tubulin kinase 1
TTBK2	Tau tubulin kinase 2
UPR	Unfolded protein response
UPS	Ubiquitin-dependent proteasome system
VAMP	Vesicle associated membrane proteins
WT	Wild-type

V. Amino acid code

Amino acid or residue	Three letter symbol	One letter symbol
Alanine	Ala	A
Arginine	Arg	R
Asparagine	Asn	N
Aspartate	Asp	D
Cysteine	Cys	C
Glutamate	Glu	E
Glutamine	Gln	Q
Glycine	Gly	G
Histidine	His	H
Isoleucine	Ile	I
Leucine	Leu	L
Lysine	Lys	K
Methionine	Met	M
Phenylalanine	Phe	F
Proline	Pro	P
Serine	Ser	S
Threonine	Thr	T
Tryptophan	Trp	W
Tyrosine	Tyr	Y
Valine	Val	V
Any amino acid	Xaa	X

VI. Summary

TTBK2 was first identified based on its physical association with microtubules and its ability to phosphorylate microtubule-associated proteins (tau, tubulin, MAP2) *in vitro* (Takahashi et al., 1995, Tomizawa et al., 2001). Since this discovery by Japanese scientists in 1995, considerable work has been invested in examining TTBK2's relationship with aberrant tau phosphorylation and neurodegeneration in Alzheimer's disease. However, these studies have never been substantiated *in vivo*.

The identification of TTBK2 truncating mutations as the cause of spinocerebellar ataxia type 11 (SCA11), in 2007, emphasised that TTBK2 has a prominent physiological role in the nervous system. When I started my PhD, there was little known about TTBK2 and many fundamental questions about TTBK2 remained unanswered.

In Chapter 3, I describe an initial analysis of TTBK2 substrate specificity by using an unbiased positional scanning peptide library and show that it has a conspicuous preference for a phosphotyrosine residue at the +2 position relative to the phosphorylation site. This information was then exploited to develop an optimised peptide substrate, named TTBKtide, to assess TTBK2 catalytic activity. TTBKtide was used to demonstrate that SCA11 truncating mutations lead to marked inhibition of TTBK2 kinase activity.

The identification of TTBK2's interacting proteins was of paramount importance to advance our understanding of both biological and disease processes. Identifying and characterising the key targets (substrates) of TTBK2 in the nervous system would provide vital new insights into the physiological role of TTBK2, which in turn, may uncover the molecular pathogenic mechanism underpinning the development of spinocerebellar ataxia type 11 (SCA11). To this end, I identified a number of TTBK2 interactors by co-immunoprecipitation of endogenous TTBK2 from mouse brain homogenates (Chapter 4). This screen provided tantalising evidence that TTBK2 operates in a distinct step of the synaptic vesicle cycle. An analysis of potential

protein substrates identified synaptic vesicle glycoprotein 2A (SV2A) as a substrate of TTBK2. Phosphopeptide mapping revealed that SV2A is phosphorylated at two clusters of three highly-conserved residues by TTBK2. These two phosphorylation clusters were then shown to mediate the phospho-dependent interactions of SV2A with AP2 clathrin adaptors, β2-spectrin and synaptotagmin 1.

SV2A and synaptotagmin 1 are both synaptic vesicle membrane proteins. Their interaction is both physical and functional. In chapter 5, I describe the characterisation of the SV2A/synaptotagmin 1 interaction using biophysical and functional methods. I have used two different biophysical methods: Isothermal titration calorimetry (ITC) and fluorescence polarisation, for quantitative analyses of the SV2A/synaptotagmin 1 phosphospecific interaction. Also, in collaboration with Prof. Michael Cousin's laboratory (University of Edinburgh), the role of SV2A phosphorylation and the effect of disrupting the SV2A/synaptotagmin 1 interaction were examined via mutagenesis and optical imaging of pHluorin-tagged proteins in cultured neurons from wild-type mice.

VII. TABLE OF CONTENTS

1 General Introduction

1.1 Signal transduction in the brain

The human brain is an organ of staggering complexity. This jelly-like mass of tissue, weighing in at around 1.4 kilograms, contains approximately 86 billion nerve cells, or neurons (Herculano-Houzel, 2009) and an equal or slightly greater number of neuroglia (or glial cells) which serve to support and protect the neurons. Each neuron consists of a cell body, dendrites, and an axon (Figure 1.1). The cell body contains the nucleus and cytoplasm. The axon extends from the cell body and often gives rise to many smaller branches before ending at nerve terminals. Dendrites extend from the neuron cell body and receive messages from other neurons.

All brain functions involve changes in the efficiency of communication between nerve cells via synapses, which are specialised intercellular junctions between neurons or between neurons and other excitable cells where signals are propagated from one cell to another with high spatial precision and speed. The dendrites are covered with synapses formed by the ends of axons from other neurons.

Each of the billions of neurons in the human brain can have up to 10,000 synaptic connections. By establishing an ever-changing network of synapses, the brain is able to attain the level of functional complexity that underlies human behaviour. The formation and withdrawal of synaptic connections between neurons is a dynamic process that can be modified by experience. In addition, experience can change the efficacy of existing synapses. This constant change in the synaptic communication between neurons is called synaptic plasticity and is critical for higher brain functions such as learning and memory.

Synaptic transmission is the currency of information exchange in the brain. Each of the 86 billion neurons can form thousands of synapses. Each synapse is independently regulated and this results in a vastly complex and intricate network. Nevertheless, from this apparent chaos emerges this pristine order of information processing by the

brain. Understanding the mechanisms that underlie brain activity and function remains one of the major challenges of modern science.

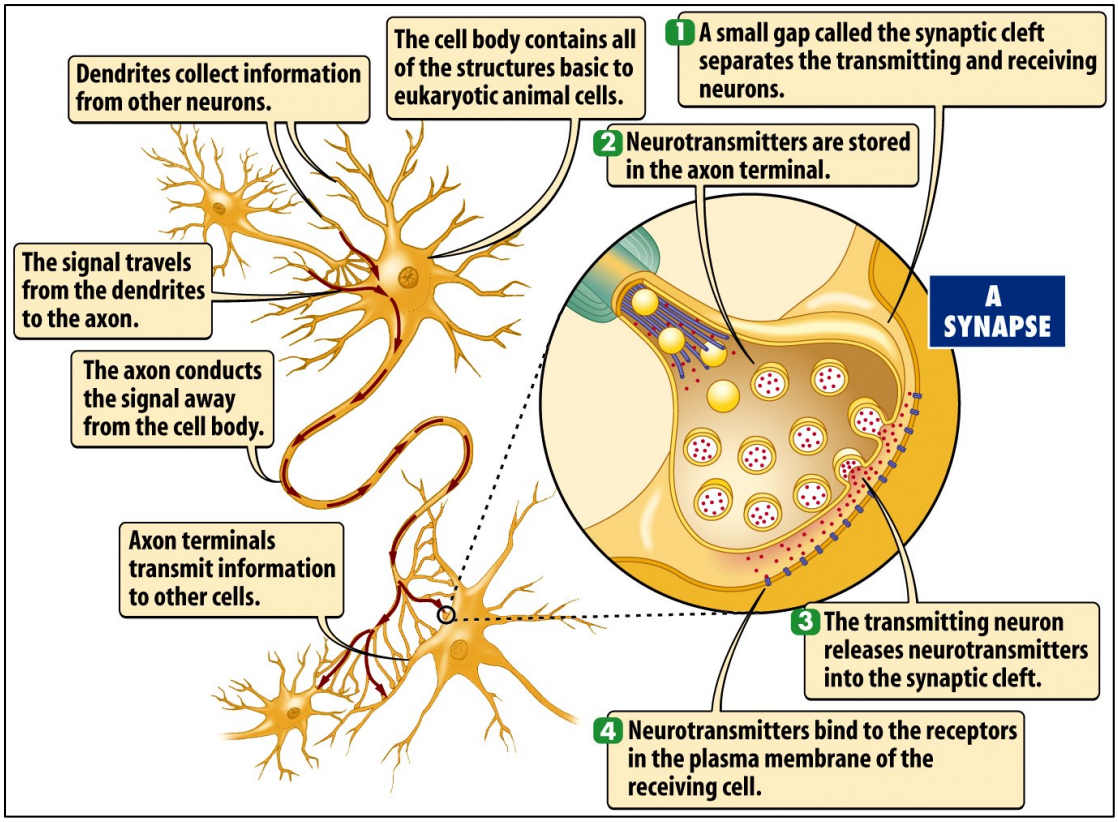

Figure 1.1. Neurons are cells within the nervous system that transmit information to other nerve cells, muscle, or gland cells. Synapses are the contact points where one neuron communicates with another. This communication involves the release of neurotransmitters, which diffuse across the synapse, and bind to receptors on the surface of the target cell. [adapted from (Byrne, 2013)].

All the processes of how we react to stimuli, learn and retain information, and how we coordinate our movements rely on the complicated networks of neurons that communicate with each other and their targets. Knowledge of the molecular mechanisms underlying this fast and accurate intercellular signalling across synapses has expanded tremendously over the last century but much still remains to be discovered.

1.2 Electrical versus chemical transmission

By the early 1930s, it was well accepted that neurons are physically separated from one another by a narrow space. Discovering how neurons communicate across this

cleft was the major challenge facing neuroscience and would set the stage for the next great conceptual leap in the understanding of the nervous system.

A vigorous debate went on from the 1930s through the 1960s as to whether communication across the synapses, was electrical or chemical in nature. The electrical school of thought, championed by electrophysiologists, held that the nerve impulse or action potential was propagated along the axon to the nerve ending, changed the electrical field across the plasma membrane of the postsynaptic cell, and thereby produced a physiological response. The chemical school of thought, advocated by pharmacologists, believed that when the action potential came down the axon to the nerve terminal, it caused the fusion of neurotransmitter-containing vesicles with the presynaptic plasma membrane, releasing the neurotransmitter, which then diffused across the synaptic cleft and, through activation of a (hypothetical) receptor, produced a physiological response.

The chemical school won this debate: over 99% of all synapses in the brain use chemical transmission (Figure 1.1). This hotly debated argument between physiologists and pharmacologists encompasses one of the key periods in the history of neuroscience and is now facetiously referred to as “the war of the soups and the sparks” (Valenstein, 2006).

1.3 Communication between neurons occurs across the synapse

Neuronal information processing requires exquisitely specific and rapid signalling mechanisms that must be flexible and easily modified. Neurons communicate primarily via the process of chemical synaptic transmission at a specialised site, the synapse. Synapses are specialised intercellular junctions between neurons and other excitable cells where signals are propagated from one cell to another with high spatial precision and speed.

Synaptic signalling is mediated by a variety of chemical neurotransmitters that carry a signal from the presynaptic to the postsynaptic neuron. Independent of the neurotransmitter type, the same fundamental mechanisms are used at all synapses: Neurotransmitters are stored in synaptic vesicles in presynaptic nerve terminals and

are released when excitation of a presynaptic terminal triggers vesicle exocytosis. Released neurotransmitters then stimulate postsynaptic receptors to complete synaptic transmission (Figure 1.1).

The basic feature of a synapse is a close apposition of specialised regions of the plasma membranes of two participating cells to form the synaptic interface. On the presynaptic side a cluster of neurotransmitter-filled synaptic vesicles is associated with the presynaptic plasma membrane (Figure 1.2). On the postsynaptic membrane, a thickening of the membrane marks an accumulation of neurotransmitter receptors.

Figure 1.2. Visualisation of a synapse. Illustration of a synapse, showing the synaptic vesicles (green) packaged with neurotransmitters collected at the active zone ready to fuse and release neurotransmitter into the synaptic cleft in response to stimulation by an action potential [Adapted from the Science illustration visualisation challenge, (Johnson, 2005)].

Bernard Katz and co-workers developed the first cellular picture of the mechanism of transmitter release in the 1950s, Electrophysiological recordings of the frog neuromuscular junctions demonstrated that neurotransmitters are released in discrete quanta (Fatt and Katz, 1952). With the advent of electron microscopy, abundant membrane-bound organelles were observed in the presynaptic nerve terminal, leading to the discovery of synaptic vesicles. These observations resulted in the vesicle

hypothesis, which states that a vesicle contains a single quantum of transmitter (Katz, 1969). This hypothesis was validated when synaptic vesicles were purified and shown to contain neurotransmitters (Whittaker, 1968). More sophisticated morphological techniques, including the examination of rapidly stimulated nerve terminals, resulted in a clearer picture of the flow of membranes in the presynaptic nerve terminal (Heuser and Reese, 1973).

1.4 Synaptic vesicles

Synaptic vesicles are uniformly small (20-nm radius), abundant organelles whose only known function is to take up and release neurotransmitters. They are relatively simple because only a limited number of proteins fit into a sphere of 40-nm diameter. Purified vesicles have a protein:phospholipid ratio of 1:3 with an unremarkable lipid composition (40% phosphatidylcholine, 32% phosphatidylethanolamine, 12% phosphatidylserine, 5% phosphatidylinositol, 10% cholesterol) (Benfenati et al., 1989). Calculations suggest that each synaptic vesicle is composed of approximately 10, 000 molecules of phospholipids and of proteins with a combined approximate molecular weight of 5-10 x 10^3 kDa (Jahn and Sudhof, 1993). Since an average protein has a molecular weight of around 50 kDa, synaptic vesicles contain approximately 200 protein molecules. Each of the 200 synaptic vesicle proteins must have a specific role and all parts must be carefully orchestrated and co-regulated to produce a productive outcome.

1.5 Neurotransmitters

1.5.1 What is a neurotransmitter?

Neurotransmitters are chemical signals released from presynaptic nerve terminals into the synaptic cleft. The subsequent binding of neurotransmitters to specific receptors on postsynaptic neurons (or other classes of target cells) transiently changes the electrical properties of the target cells, leading to an enormous variety of postsynaptic effects.

Over the years, a number of formal criteria have emerged that definitively identify a substance as a neurotransmitter. Nonetheless, identifying the neurotransmitters active at any particular synapse remains a difficult undertaking, and for many synapses (particularly in the brain), the nature of the neurotransmitter is not well established (Snyder and Innis, 1979). Substances that have not met all the criteria outlined in below are referred to as "putative" neurotransmitters.

1.5.2 Criteria that define a neurotransmitter

In an influential review published in 1958, William Paton set out five criteria that must be satisfied before a substance can be considered a neurotransmitter (Paton, 1958): (1) the enzymes involved in the synthesis of the substance must be present within the presynaptic neurons; (2) the substance must be released from the axon terminals when the presynaptic fibers are stimulated; (3) the action of the substance when applied to the postsynaptic cells must accurately mimic that seen during normal synaptic transmission; (4) a mechanism must be present at the site of synapses to terminate the action of the putative transmitter; and (5) the effect of drugs (whether agonists and antagonists) on the postsynaptic cells must be the same when the putative transmitter substance is applied to the synapse. Since then, a sixth criterion has been added to this list by neuroscientists, namely, that the postsynaptic cells must bear the appropriate receptors for the transmitter.

The distinctive characteristics of neurotransmitters, compared to other signalling molecules, are made clearer by comparison with the actions of the hormones secreted by the endocrine system. Hormones typically influence target cells far removed from the hormone-secreting cell. This "action at a distance" is achieved by the release of hormones into the bloodstream. In contrast, the distance over which neurotransmitters act is miniscule. At many synapses, transmitters bind only to receptors on the postsynaptic cell that directly underlies the presynaptic terminal (Figure 1.3A); in such cases, the transmitter acts over distances less than a micrometre. Even when neurotransmitters diffuse locally to alter the electrical properties of multiple postsynaptic (and sometimes presynaptic) cells in the vicinity (Figure 1.3B), they act only over distances of tens to hundreds of micrometres. While the elongated axonal

processes of neurons allow neurotransmitters to be released as much as a metre away from the neuronal cell body, these transmitters still act only near the presynaptic site of release (Figure 1.3C).

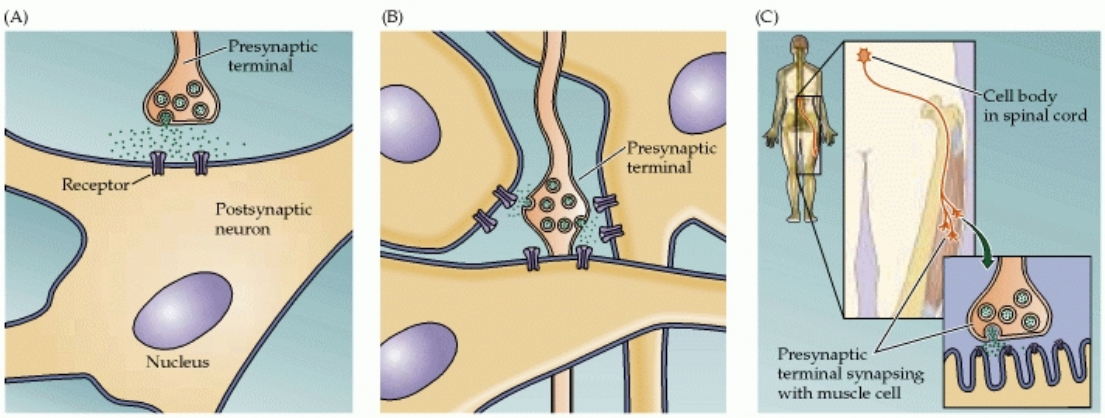

Figure 1.3. Localisation of neurotransmitter action. Neurotransmitters in general act either locally (A), by altering the electrical excitability of a small region of a single postsynaptic cell, or more diffusely (B), by altering the electrical excitability of a few postsynaptic cells. (C) Neurons can exert their actions over greater distances by having long axons that locally release neurotransmitters onto distant targets. [Adapted from (Purves, 2001)]

1.5.3 Two major categories of neurotransmitters

Acetylcholine (ACh), the first neurotransmitter discovered, was originally described as "vagus stuff" in 1921 by Otto Loewi because of its ability to mimic the electrical stimulation of the vagus nerve (Sakmann, 1992). It is now known to be a neurotransmitter at all autonomic ganglia, at many autonomically innervated organs, at the neuromuscular junction, and at many synapses in the central nervous system (CNS). By the 1950s, the list of neurotransmitters (defined by the criteria described previously) had expanded to include four amines — adrenaline, noradrenaline, dopamine, and serotonin — in addition to acetylcholine (ACh). Over the following decade, three amino acids — glutamate, γ-aminobutyric acid (GABA), and glycine — were also shown to be neurotransmitters. Subsequently, other small molecules were added to the list, and considerable evidence now suggests that histamine, aspartate, and ATP should be included. The most recent class of molecules discovered to be transmitters are a large number of polypeptides (neuropeptides). Since the 1970s, more than 100 such molecules have been shown to meet at least some of the criteria outlined.

It is useful to separate this variety of agents into two broad categories based simply on their size. Neuropeptides, which include somatostatin and cholecystokinin, are relatively large transmitter molecules composed of 3 to 36 amino acids. Individual amino acids, such as glutamate and γ-aminobutyric acid (GABA), as well as the transmitters acetylcholine, serotonin, and histamine, are much smaller than neuropeptides and have therefore come to be called small-molecule neurotransmitters. Within the category of small-molecule neurotransmitters, the biogenic amines (dopamine, noradrenaline, adrenaline, serotonin, and histamine) are often discussed separately because of their similar chemical properties and postsynaptic actions.

By far the most prevalent transmitter is glutamate, which is excitatory at well over 90% of the synapses in the human brain (Izquierdo et al., 1993). The next most prevalent is GABA, which is inhibitory at more than 90% of the synapses that do not use glutamate. Even though other transmitters are used in far fewer synapses, they may be very important functionally - the great majority of psychoactive drugs exert their effects by altering the actions of some neurotransmitter systems, often acting through transmitters other than glutamate or GABA.

1.5.4 Excitatory and inhibitory neurotransmitters

Some neurotransmitters are commonly described as "excitatory" or "inhibitory". The only direct effect of a neurotransmitter is to activate one or more types of receptors. The effect on the postsynaptic cell depends, therefore, entirely on the properties of those receptors. It happens that for some neurotransmitters (for example, glutamate), the most important receptors all have excitatory effects: that is, they increase the probability that the target cell will fire an action potential. For other neurotransmitters, such as GABA, the most important receptors all have inhibitory effects (although there is evidence that GABA is excitatory during early brain development). There are, however, other neurotransmitters, such as acetylcholine, for which both excitatory and inhibitory receptors exist; and there are some types of receptors that activate complex metabolic pathways in the postsynaptic cell to produce effects that cannot

appropriately be called either excitatory or inhibitory. Thus, it is an oversimplification to call a neurotransmitter excitatory or inhibitory - nevertheless it is convenient to call glutamate excitatory and GABA inhibitory so this usage is seen frequently.

1.6 Molecular mechanisms of neuronal signal transduction

On the basis of those initial studies, elucidating the biochemical mechanisms by which neurotransmitters, through activation of their receptors, produce their physiological effects within their postsynaptic, target nerve cells, would be an essential step toward understanding nervous system function. Indeed, the molecular mechanisms underlying signal transduction in the nervous system have been the subject of intense scrutiny over the past five decades.

Paul Greengard pioneered research in neuronal signal transduction in the 1960s. He was inspired by earlier studies carried out by Earl Sutherland and Edwin Krebs**,** who were interested in understanding how the hormones glucagon and adrenaline break down glycogen to glucose in liver and muscle cells. Sutherland and his colleagues found that these hormones stimulated the formation of cyclic adenosine monophosphate (cAMP) from adenosine triphosphate (ATP) by virtue of activating a class of enzymes termed hormone-sensitive adenylyl cyclases. Sutherland then showed that cAMP could mimic the hormones, causing the breakdown of glycogen to glucose (Sutherland, 1972). Krebs and his colleagues subsequently showed that cAMP caused the breakdown of glycogen to glucose by activating an enzyme that they called cAMP-dependent protein kinase (PKA). Krebs further showed that one substrate for PKA, when phosphorylated, was itself an enzyme that caused the breakdown of glycogen to glucose. The action of protein kinases is reversed by means of enzymes called protein phosphatases.

Greengard's initial hypothesis was that the same signalling machinery used by the endocrine system to break down glycogen to glucose might be used for communication between nerve cells. His team searched the brain for signalling enzymes analogous to those in liver and muscle and they found a family of adenylyl cyclases, analogous to the hormone-sensitive adenylyl cyclases described by

Sutherland, which converted ATP to cAMP in the presence of neurotransmitters. The first of these was a dopamine-sensitive adenylyl cyclase: in the presence of dopamine, this membrane-bound enzyme stimulated formation of cAMP. Moreover, the data indicated that this enzyme might play a role in neuronal signal transduction (Kebabian and Greengard, 1971).

At about the same time, Eishichi Miyamoto and J. F. Kuo (also from Paul Greengard's laboratory) demonstrated PKA activity in the brain (Miyamoto et al., 1969). The concentration of this enzyme was enormously higher in brain than in liver. Even more intriguing was the fact that the enzyme was concentrated in the synaptic region of nerve cells. These data were consistent with a possible role for PKA in synaptic transmission. Soon thereafter, a second distinct class of regulated protein kinase was discovered. It was named cyclic guanosine monophosphate (cGMP)–dependent protein kinase (PKG) and which was activated selectively by cGMP rather than cAMP (Kuo and Greengard, 1970). PKG was present both in brain and in non-neural tissues. Subsequently, Howard Schulman, in collaboration with Paul Greengard, discovered a third group of regulated protein kinases, which were stimulated by calcium in the presence of an unidentified endogenous heat-stable protein, later shown to be the calcium effector protein calmodulin (Schulman and Greengard, 1978).

The discovery in the nervous system of several neurotransmitter-sensitive enzymes that made cAMP and of several second messenger–dependent protein kinases reinforced the notion that second messengers and protein kinases are involved in signalling in the brain. This idea was supported by the discovery of a large number of brain-specific substrate proteins for these protein kinases. More than 100 substrate proteins for protein kinases that were highly enriched in or exclusively localised to the brain, some of which were present in very high concentrations were identified (Greengard et al., 1999). Moreover, injections of various second messengers, protein kinases, and protein phosphatases, as well as activators, inhibitors and substrates of these enzymes, were able to either mimic or antagonise the ability of neurotransmitters to produce physiological responses in nerve cells, such as changes in ligand-gated ion channels, voltage-gated ion channels, ion pumps, and transcription

factors. Combined, these data have provided overwhelming evidence of a role for those signal transduction pathways in synaptic transmission (Greengard et al., 1999).

In addition, studies in which purified protein kinases or kinase inhibitors have been microinjected into defined cells while a specific response is monitored have demonstrated that protein phosphorylation is both necessary and sufficient to mediate responses of excitable cells to extracellular signals (Llinas et al., 1985, Llinas et al., 1991, Greengard et al., 1993, Castellucci et al., 1980, Castellucci et al., 1982). Those independent studies conclusively demonstrated that the efficacy of neurotransmitter release from the presynaptic terminal, in response to the nerve impulse, is regulated by protein phosphorylation and dephosphorylation.

Paul Greengard was awarded (jointly with Arvid Carlsson and Eric R. Kandel) the Nobel Prize for Physiology or Medicine for his discoveries concerning signal transduction in the nervous system in 2000.

1.7 Protein phosphorylation

The rapid and reversible phosphorylation of proteins catalysed by protein kinases and protein phosphatases is a well-recognised mechanism of regulation in cells. This bidirectional process is a highly flexible method of influencing cellular activity in response to a variety of incoming stimuli. The first physiological role for protein phosphorylation was identified about 50 years ago while investigating the regulation of glycogen metabolism (Krebs and Fischer, 1955, Sutherland, 1972). In fact, many aspects of gene regulation; cell cycle control, transport, and secretion; actin remodelling; and cell adhesion are controlled by this mechanism (Krebs, 1985, Hunter, 1995, Pawson and Scott, 1997, Cohen, 2000, Goodman and Smolik, 2000, Pawson and Nash, 2000). The utility of protein phosphorylation as the predominant form of covalent modification of proteins *in vivo* is exemplified by the finding that ~30% of intracellular proteins are phosphoproteins (Hunter, 1987). Not surprisingly, the breakdown in signal transduction may be the cause or consequence of many diseases, including cancer, diabetes, arthritis, and Alzheimer's (Cohen, 1999).

1.8 Protein phosphorylation systems

All protein phosphorylation systems consist minimally of three components. These include the phosphoproteins (substrates) themselves, which change their biological properties during phosphorylation/dephosphorylation. In addition, two classes of enzymes are needed for phosphorylation/dephosphorylation reactions. One set of these enzymes includes the protein kinases, phosphotransferases that catalyse transfer of phosphate from ATP to proteins on specific serine, threonine or tyrosine residues. The other set of enzymes includes the phosphoprotein phosphatases, which dephosphorylate the phosphoproteins and thereby return the particular protein phosphorylation system to its basal state (Figure 1.4).

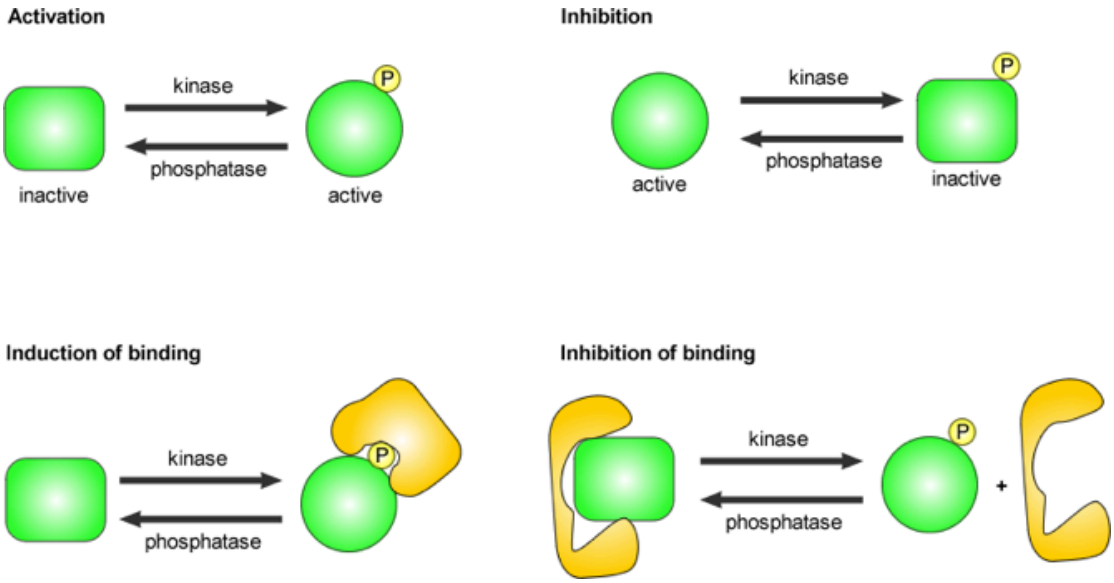

Figure 1.4. Effects of protein phosphorylation. Fundamental outcomes of phosphorylation of proteins by kinases and dephosphorylation by phosphatases are the regulation of the activity and the modulation of protein-protein interactions.

Most signalling pathways are composed of common elements. The initial signal is transduced through a receptor at the plasma membrane (such as a G-protein coupled receptor, or a receptor tyrosine kinase or phosphatase), which results in activation of the receptor or the mobilisation of receptor-associated proteins to generate some form of intracellular message (Figure 1.5). This signal is then directed throughout the cell either by the diffusion of a small soluble second messenger or the translocation of an activated enzyme.

At a molecular level, phosphorylation mediates the regulation of enzymatic activities by causing allosteric conformational changes, or by directly enhancing or blocking access to enzyme catalytic sites (Johnson and Barford, 1990, Barford, 1991, Johnson and O'Reilly, 1996). More recently it has been realised that an essential feature of signalling by protein phosphorylation is the modulation of protein–protein interactions. These are mediated by a growing number of protein interaction modules domains that may associate with their binding partners in a phosphorylation-dependent manner. Examples of these domains include the Src homology 2 (SH2) domain, which is a sequence-specific phosphotyrosine-binding module present in many signalling molecules and the forkhead-associated (FHA) domain, which is a small protein that recognises phosphothreonine epitopes on proteins (Cantley et al., 1991, Pawson and Gish, 1992, Pawson, 1995). These protein–protein interactions generate molecular networks that drive intracellular signalling events. Phosphorylation is a crucial part of the underlying biochemical mechanisms through which specificity is generated during signal transduction, and it provides the means by which signalling molecules may act in combination to generate complex biological responses (Pawson and Nash, 2000).

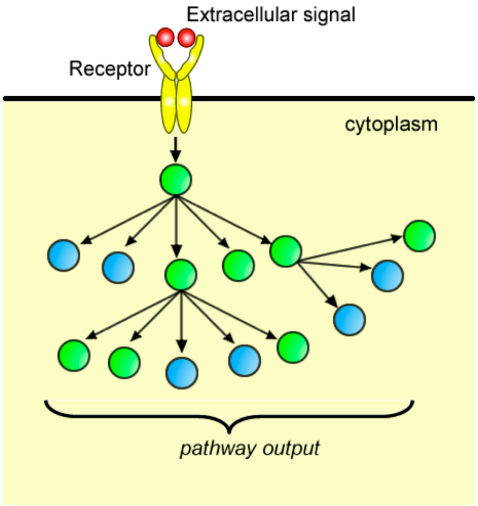

Figure 1.5. An outline of a signal transduction cascade. In a typical signal transduction cascade, extracellular signal molecules (red) bind to receptors (yellow) and initiate intracellular cascades that relay and amplify the signal at each step of the cascade via activation of enzymes (green), which regulate other enzymes and non-enzymatic substrates (blue). The net output of such signal transduction "pathways" induces cellular changes such as changes in gene expression, cell division, cell death or differentiation, or the modulation of protein-protein interactions.

1.6 Protein kinases

Ever since the discovery nearly 50 years ago that reversible phosphorylation regulates the activity of glycogen phosphorylase, there has been intense interest in the role of protein phosphorylation in regulating protein function. With the advent of DNA cloning and sequencing in the mid-1970s, it rapidly became clear that a large family of eukaryotic protein kinases exists, and the identification of novel protein kinases led to the speculation that a vertebrate genome might encode as many as 1001 protein kinases (Hunter, 1987).

However, the near-completion of working draft of the human genome sequence in 2001 paved the way for the systematic identification of almost all human protein kinases. This venture, dubbed as the 'kinome project' (Manning et al., 2002), involved the use of automated computational predictions to screen genomic, complementary DNA (cDNA) and EST (expressed sequence tag) sequences from genomic sequence databases for the characteristic motifs of protein kinases. Using this approach, the authors catalogued the protein kinase complement of the human genome and a total of 518 kinases were identified. The total number of kinases was about half that predicted earlier, but it is still a strikingly large number, constituting about 1.7% of all human genes.

To compare related kinases in human and model organisms and to gain insights into kinase function and evolution, all the kinases were classified into a hierarchy of groups, families, and subfamilies. Kinases were classified primarily by sequence comparison of their catalytic domains, aided by knowledge of sequence similarity and domain structure outside of the catalytic domains.

With the exception of a few atypical kinases, the kinase domains of most members of this superfamily share very similar catalytic motifs that are responsible for the phosphoryl transfer. Thus, the kinome can be classified into eight families, based on their sequence similarity: AGC (PKA, PKG and PKC family), CAMK (Ca^{2+}/calmodulin- dependent family), CK1 (Casein kinase 1 family), CMGC (CDK, MAPK, GSK3 and CLK family), STE (homologues of the yeast *Sterile* kinases

family), TK (Tyrosine kinases family), TKL (Tyrosine kinase-like kinases family) and atypical kinases family (Figure 1.6 on the next page).

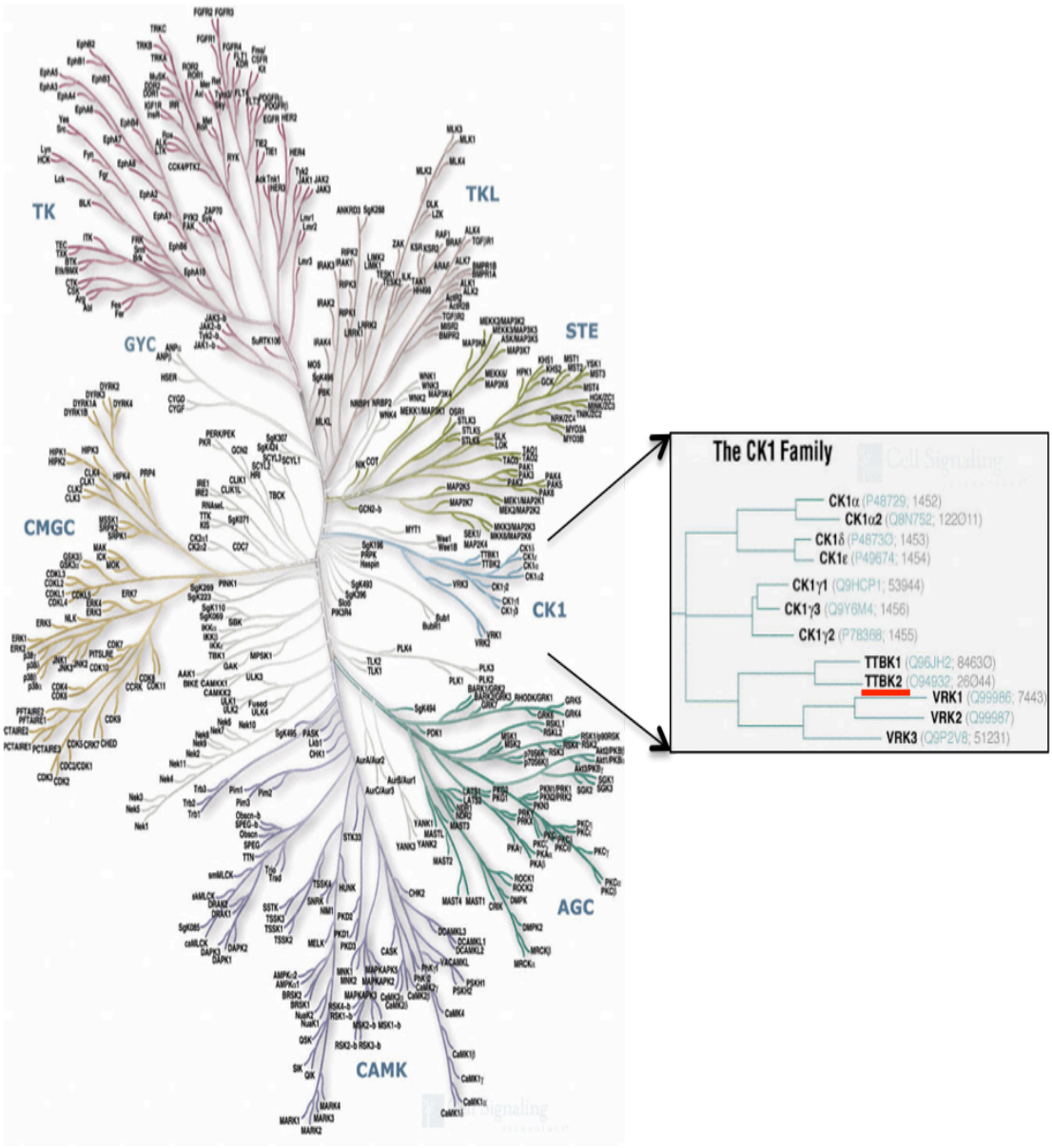

Figure 1.6. The human kinome. 518 kinases are currently found in the human genome, which constitute the human kinome. Kinases were classified into eight families based on the similarity of the kinase domains. TTBK1 and TTBK2 (underlined in red) are part of the CK1 family of kinases. Adapted from (Manning et al., 2002)**.**

1.9 First description of TTBK2

In the course of the purification of proteins associated with microtubules from bovine brain, Takahashi *et al.* (1995) identified a novel protein kinase. Further biochemical characterisation of this newly-discovered kinase showed that it was a serine/threonine kinase with molecular mass of 32 kDa and that it phosphorylated proteins tau, MAP2 (microtubule-associated protein 2), tubulin and α-casein *in vitro*. Hence, it was initially named '**Tau Tubulin Kinase'** (TTK) (Takahashi et al., 1995).

The discoverers of TTK had an enduring interest in the role of tau hyperphosphorylation and its complex role in Alzheimer's disease (AD) and invested considerable work in identifying the specific phosphorylation sites and their relationship to proteinaceous tau aggregates characteristic of AD brains. However, they obtained only *in vitro* evidence that TTK phosphorylates tau at Ser208 and Ser210 (Tomizawa et al., 2001), which are priming sites for the phosphorylation of tau by GSK-3β (Glycogen synthase kinase 3 beta), which is known to influence tau pathology (Noble et al., 2005).

As a consequence of the 'kinome project' in 2002 (Manning et al., 2002), TTK was renamed as TTBK2 (tau tubulin kinase 2), while another protein kinase, whose kinase domain shares significant sequence homology with TTBK2's kinase domain was identified and named TTBK1 (tau tubulin kinase 1). TTBK1 and TTBK2 share 84% sequence homology within the catalytic kinase domain, but display modest homology in the non-catalytic region (Figure 1.7).

Both TTBK isoforms (TTBK1 and TTBK2) belong to the CK1 (casein kinase 1) group of eukaryotic protein kinases composed of CK1 isoforms (CK1α, CK1α2, CK1δ, CK1ϵ, CK1γ1, CK1γ2 and CK1γ3), VRK (vaccinia-related kinase) isoforms (VRK1, VRK2 and VRK3) (Manning et al., 2002). CK1 differs from most other protein kinases by the presence of the S-I-N motif instead of A-P-E in kinase domain region VIII (Hanks and Hunter, 1995). TTBK1 and TTBK2 possess a P-P-E motif at this site. TTBK2 possesses 38% identity with CK1δ within the kinase domain, but

there is no obvious homology beyond the catalytic moiety of TTBK to CK1 or VRK isoforms.

1.9.1 Expression of TTBK isoforms in different tissues

The TTBK1 gene is located on human chromosome 6p21.1 and is composed of 14 exons and 15 introns with a cDNA length of 6932 bp (Ensembl transcript ENST00000259750). The TTBK1 protein is 1321 amino acids in length, has a serine-threonine kinase domain (residues 34-297), and a unique polyglutamate domain in the middle region of the sequence (Figure 1.7). Human TTBK1 homologs were found in mice, *Caenorhabditis elegans* and *Drosophila melanogaster* (Sato et al., 2006).

The gene encoding TTBK2 is located on human chromosome 15q15.2 and is composed of 14 exons and 15 introns with a cDNA length of 10905 bp (Ensembl transcript ENST00000267890). The longest open reading frame is 3,732 nucleotides long, encoding a protein of 1244 amino acids. The gene is alternatively spliced yielding six shorter transcripts, with ubiquitous expression in human adult and foetal tissues (Houlden et al., 2007). The N-terminus of TTBK2 encodes a serine-threonine kinase domain (residues 21-284). However, the C-terminal region possesses no obvious functional domains or motifs and therefore its function has not been delineated. Notably, TTBK1's polyglutamate region is not conserved in TTBK2 (Figure 1.7).

TTBK1 is specifically expressed in the brain. Northern blotting of a human tissue panel showed TTBK1 mRNA in adult brain cortex and cerebellum, as well as in foetal brain. Weak expression of TTBK1 was detected in the spinal cord and testis. No apparent TTBK1 expression was seen in a range of other tissues, including heart, liver, kidney and lung. *In situ* hybridisation (ISH) of mouse brain has shown TTBK1 gene expression in perinuclear and cytoplasmic regions of large cortical pyramidal cells in the temporal cortex cortical layers, layers of the hippocampus and granular layer of cerebellum. Neuronal expression of TTBK1 in both mouse and human brain has been confirmed by immunohistochemistry (IHC) (Sato et al., 2006).

In contrast to TTBK1, TTBK2 expression can be detected in other tissues, including heart, muscle, liver, thymus, spleen, lung, kidney, testis and ovary (Takahashi et al., 1995, Tomizawa et al., 2001). In the mouse and rat brain, TTBK2 mRNA expression was found at high levels in the cerebellum and hippocampus as shown by *in situ* hybridisation (Sato et al., 2006). Another study revealed that TTBK2 mRNA was also detected in all brain regions in human, rat and mouse (Houlden et al., 2007) by *in situ* hybridisation. The highest level of expression of TTBK2 mRNA was observed in the cerebellum Purkinje cells, granular cell layer, hippocampus, midbrain and substantia nigra (Houlden et al., 2007). Lower expression was seen in the cortex of human, rat and mouse brains.

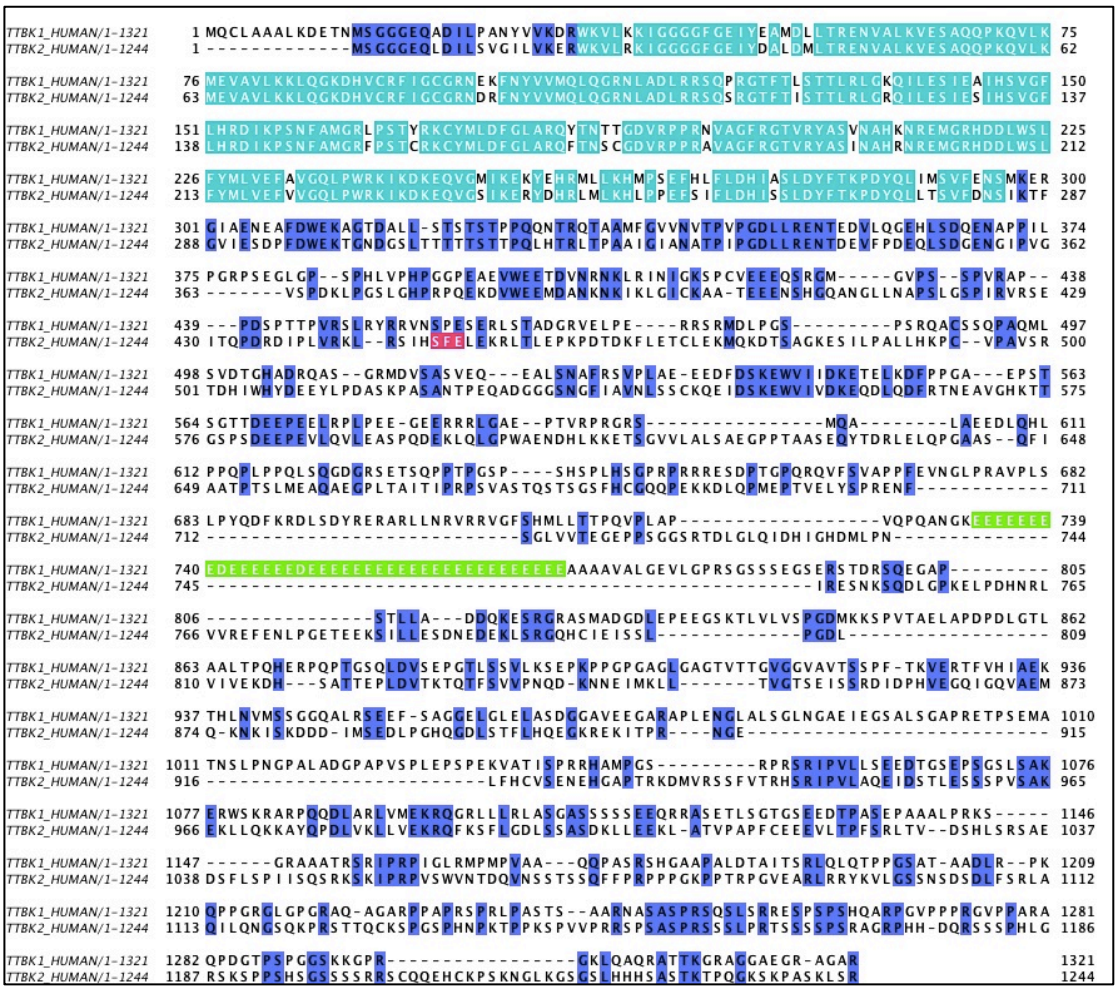

Figure 1.7. Pairwise sequence alignment of human TTBK1 and TTBK2. TTBK1 and TTBK2 share 84% sequence homology (shaded in turquoise blue) in their kinase domain sequences. SCA11-causing mutations truncate the TTBK2 protein at amino acids 448, 449 and 450 (highlighted in red). The polyglutamic acid stretch (highlighted in green) of TTBK1 is not shared by TTBK2 and both kinases share modest homology outside their kinase domains.

1.10 Putative function of TTBKs in tau regulation

The putative function of TTBK1, with respect to AD pathogenic mechanisms, has been studied by Sato et al. (2008). TTBK1 has been shown, by partial phosphopeptide mapping, to phosphorylate tau *in vitro* (Sato et al., 2006). Similarly, TTBK2 has also been shown to phosphorylate tau *in* vitro at Ser208 and Ser210 (Tomizawa et al., 2001).

The examination of a transgenic TTBK1 mouse model, in which the protein is highly expressed in the subiculum and cortical pyramidal layers, has been reported (Sato et al., 2006). Those mice show increased phosphorylation of both tau at Ser262/356 residues and of the neurofilament protein. The mice also showed significant age-dependent memory impairment as determined by a spatial learning radial arm water maze test. The fact that TTBK1 has not been shown to directly phosphorylate tau at Ser262/356 *in vitro* indicated that TTBK1 might enhance phosphorylation at this site either by activation of other kinases or through priming of tau by direct phosphorylation at other sites (Sato et al., 2008).

Subsequently, Xu et al. (2010) used the same TTBK1 mice to generate bigenic mice that overexpress full-length TTBK1 and the disease-causing P301L tau mutant (Xu et al., 2010). These mice show accumulation of tau aggregates in cortical and hippocampal neurons at 12-13 months of age as well as enhanced tau phosphorylation. The bigenic mice also showed significant locomotor dysfunction as well as enhanced loss of motor neurons.

The potential importance of TTBK1 in AD is supported by human genetic data from two independent genome-wide association studies. Vázquez-Higuera et al. (2011) analysed nine TTBK1 gene single nucleotide polymorphisms (SNPs) in a group of Spanish AD patients and controls (Vazquez-Higuera et al., 2011). Based on the data generated, it was speculated that reduced TTBK1 expression in minor allele homozygotes (rs2651206 in intron 1, rs10807287 in intron 5 and rs7764257 in intron 9) could lead to lower tau phosphorylation and neurofibrillary tangle formation. Subsequently, Yu et al. (2011) confirmed that minor alleles of the rs2651206

polymorphism were significantly associated with a reduced risk of late onset AD in a Han Chinese population (Yu et al., 2011).

Interestingly, both TTBK1 and TTBK2 can phosphorylate tau *in vitro* at sites that are found in paired helical filaments (PHFs) that constitute the characteristic Alzheimer's disease (Sato et al., 2006, Tomizawa et al., 2001). One would therefore expect that an upregulation or overactivation of each one of these kinases would lead to increased tau phosphorylation and predispose to neurodegeneration. Indeed, genetic variations in TTBK1, which are thought to result in decreased TTBK1 activity, can decrease the risk of AD (Vazquez-Higuera et al., 2011, Yu et al., 2011).

1.11 Identification of TTBK2 as the causative gene for SCA11

Apart from the tentative *in vitro* evidence of tau phosphorylation by TTBK2, its physiological role has not been explored since its discovery. However, in 2007, the discovery of a pathogenic mutation in the TTBK2 gene, causing a neurological condition, underscored the fundamental physiological importance of TTBK2.

Worth *et al.* (1999) identified a British family with a relatively pure form of autosomal dominant cerebellar ataxia, a genetic syndrome with progressive degeneration of the cerebellum (Figure 1.8), causing uncoordinated movements in gait, eye movement, speech, and other motor coordination skills. The affected family from Devon, on the southwest coast of England, stretched over 8 generations and affected individuals had progressive cerebellar ataxia, abnormal eye signs and pyramidal features, as well as cerebellar atrophy visible upon magnetic resonance imaging (Figure 1.8).

1.11.1 The cerebellum and cerebellar atrophy

The cerebellum ("little brain" in Latin) is a structure that is located at the back of the brain, underlying the occipital and temporal lobes of the cerebral cortex (Figure 1.8). Although the cerebellum accounts for approximately 10% of the brain's volume, it contains more than 50% of the total number of neurons in the brain. On average the

human cerebellum weighs 154g and packs 69 billion neurons, while the human cerebral cortex weighs, on average 1233 grams and contains 16 billion neurons (Herculano-Houzel, 2009).

Historically, the cerebellum has been considered a motor structure, because cerebellar damage leads to impairments in motor control and posture and because the majority of the cerebellum's outputs are to parts of the motor system. Motor commands are not initiated in the cerebellum; rather, the cerebellum modifies the motor commands of the descending pathways to make movements more adaptive and accurate (Passot et al., 2012). Two types of neurons play dominant roles in the cerebellar circuit: Purkinje cells and granule cells. Purkinje cells are among the most distinctive neurons in the brain, and also among the earliest types to be recognised — they were first described by the Czech anatomist Jan Evangelista Purkyně in 1837 (Zarsky, 2012). Purkinje cells use GABA as their neurotransmitter (Sastry et al., 1997), and therefore exert inhibitory effects on their targets. Cerebellar granule cells, in contrast to Purkinje cells, are among the smallest neurons in the brain. They are also the most numerous neurons in the brain: In humans, estimates of their total number average around 50 billion (D'Angelo, 2013), which means that about 3/4 of the brain's neurons are cerebellar granule cells.

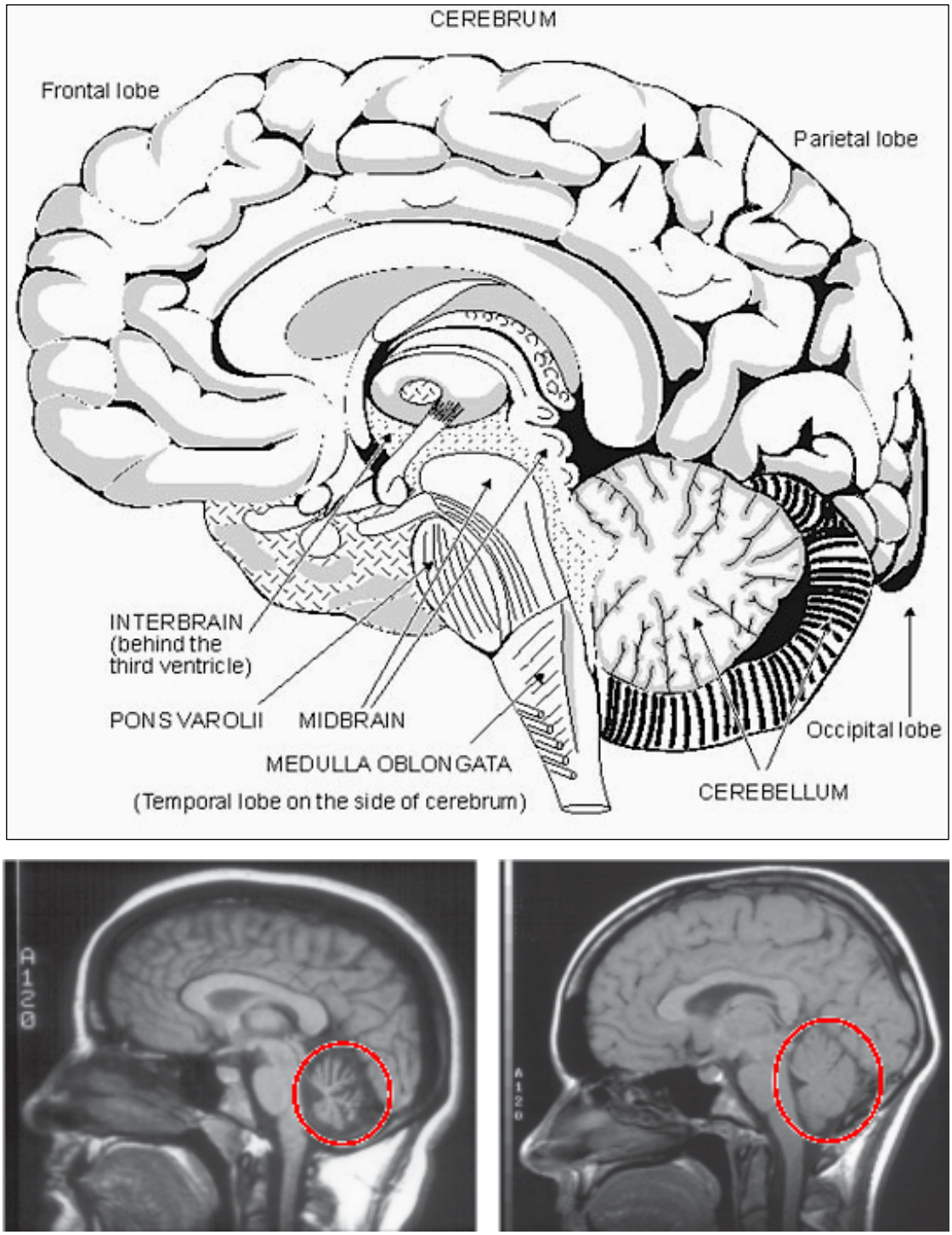

Figure 1.8. Upper panel: Drawing of the human brain. The cerebellum is a structure that is located at the back of the brain, underlying the occipital and temporal lobes of the cerebral cortex. **Lower panel: Magnetic resonance imaging (MRI) scans of two brains.** The brain on the left shows atrophy of the cerebellum, a pathological hallmark of ataxia patients, compared to the brain on the right shows a normal cerebellum. [adapted from http://pedclerk.bsd.uchicago.edu/page/ataxia]

1.11.2 Genome-wide linkage and identification of causative mutation

Using a genome-wide linkage strategy to screen the members of the affected family, Worth *et al.* (1999) found linkage to marker D15S1039. Construction of haplotypes defined a 7.6 centimorgan (cM) interval between the flanking markers D15S146 and D15S1016, thereby assigning the disease locus, designated **SCA11 (**spinocerebellar ataxia type 11), to chromosome 15q14-q21.3.

Houlden et al. (2007) narrowed the SCA11 locus further to a 5.6 cM region containing 134 protein-coding genes. After screening 54 genes in the linked region identified on chromosome 15q15-q21, none of which had a pathogenic mutation, the gene encoding tau tubulin kinase 2 (TTBK2) was sequenced and a 1-base insertion of an adenosine in exon 13 at nucleotide 1329, codon 444 was exposed (Figure 1.9). This insertion created a premature stop codon (TGA) in the mRNA at codon 450, truncating the normal protein from 1244 to 450 amino acids.

The authors proceeded to screen another cohort of 40 families with autosomal dominant pure SCA, for which no genetic mutations were identified, for TTBK2 mutations. A frameshift deletion of 2 bases (GA) in exon 13 of TTBK2 at nucleotides 1284-1285, codons 428 and 429 (Figure 1.9) was found in one of the families screened. This created a premature stop site (TGA) in the mRNA at codon 449. The family was of Pakistani ancestry, with five affected individuals present over three generations (family 2). Both mutations segregated in the affected family members, and neither was detected in over 400 elderly European-descended British or in 50 elderly Pakistani controls individuals.

The discovery of TTBK2 mutations prompted other research groups assess the prevalence and phenotypic spectrum of SCA11. Bauer et al. (2010) screened a cohort of 148 index patients of predominantly German and French descent with autosomal dominant spinocerebellar ataxia, who were negative for repeat expansions and mutations in known SCA genes, for mutations in TTBK2. All 148 patients were negative for all the conventional known SCA mutations. In two of 148 patients - one German and one French - the authors identified two SCA11-causing mutations.

Remarkably, both carried an identical two-base pair deletion (c.1306_1307delGA) in exon 12 leading to a premature stop codon, truncating the normal protein from 1244 to 448 amino acids.

Two other cohorts of SCA patients were screened for TTBK2 mutations. To investigate the frequency of SCA11 in Chinese SCA patients, Xu et al. (2010) examined the TTBK2 gene in 68 unrelated probands diagnosed with dominantly inherited ataxia using the denaturing high-performance liquid chromatography (dHPLC) method. All analysed samples displayed the normal elution profile, which signified that no disease-related mutation was identified, thus providing evidence that SCA11 is a rare form of ataxia in China.

Edener and colleagues (2009) screened 49 unrelated familial cases with ataxia for TTBK2 mutations. Sequencing all coding exons revealed, amongst others, two novel missense exchanges at evolutionarily conserved amino acid positions. A disease causing effect was excluded with high probability for both variations as they were also detected in control samples (Edener et al., 2009).

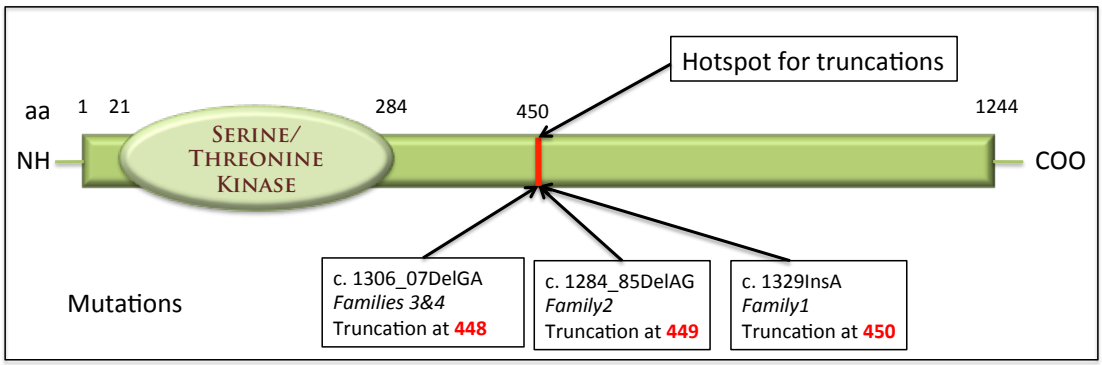

Figure 1.9. Domain architecture of the TTBK2 protein. The longest transcript produces a 1244-residue protein with a kinase domain (amino acids 21-284) at its N-terminus. The rest of the protein possesses no defined functional domains or motifs. The SCA11-causing truncating mutations identified leave the kinase domain intact but eliminate most of the non-catalytic portion of the protein.

In summary, four SCA11-causing TTBK2 mutations have been identified so far. Strikingly, all four are frameshift mutations that truncate the wild-type TTBK2 protein from 1244 to 450, 449 and 448 (two mutations) amino acids respectively (Figure 1.9). The mutations mapped to the conserved serine-rich region of the protein,

and all four mutations do not affect the kinase domain but, however, eliminate most of the non-catalytic portion of the protein.

1.12 Spinocerebellar ataxia

Ataxia, a term derived from a Greek word meaning ‘loss of order’, is used clinically to describe lack of voluntary coordination of muscle movements, with poor coordination between limbs. It is a neurological dysfunction of motor coordination that can affect gaze, speech, gait and balance. Individuals suffering from ataxia are at first clumsy and unable to walk steadily, and have slurred speech. Patients can eventually lose the ability to swallow and breathe in a coordinated fashion, which can eventually be fatal (Orr, 2012).

Ataxia is the consequence of a neurodegenerative process that affects a specific population of nerve cells, whose vulnerability determines the clinical manifestations of the disease. The origin of many forms of ataxia can be traced back to dysfunction of the parts of the nervous system that coordinate movement, especially the cerebellum, which plays a very important role in motor coordination and the fine adjustments of movement. Ataxia can result from the variable degeneration of neurons in the cerebellum, brain stem, spinocerebellar tracts, and their afferent/efferent connections. Cerebellar ataxia is the most common form of ataxia and is caused by dysfunction either within the cerebellum or in its afferent and efferent pathways. Spinocerebellar ataxia (SCA) is caused by anomalous function of the spinocerebellum, the part of the cerebellar cortex that receives somatosensory input from the spinal cord.

Although there are sporadic forms of SCAs, the term is most often used to refer to the hereditary forms, and in particular the autosomal dominant forms. The autosomal dominant SCAs are typically late-onset, progressive, and often fatal neurodegenerative disorders. They are characterised by cerebellar ataxia and frequently other symptoms related to dysfunction of additional neural pathways.

1.12.1 Clinical Features of the Spinocerebellar Ataxias

Autosomal dominant spinocerebellar ataxias (SCAs) comprise a highly heterogeneous group of dominantly-inherited ataxias, where the age of onset of the clinical symptoms is typically between 30 and 50 years of age, although early onset in childhood and onset in later decades after 60 years have been reported for specific SCA subtypes (Duenas et al., 2006). During the past 20 years, more than 30 SCA subtypes have been described (Table 1.1.). They are designated as SCA1 to SCA30, where the numbers indicate the chronological order of discovery of the genomic locus by genome-wide linkage of affected families.

The prognosis is variable depending on the underlying cause of the spinocerebellar ataxia subtype. Epidemiological data indicate that SCAs might be more common than previously estimated with prevalences over 5–7 in 100,000 in some geographical areas reaching 18.5/100,000 in Japan when including dominant, recessive and sporadic SCAs and familial spastic paraplegia (Tsuji et al., 2008). This is similar to the prevalences reported for other uncommon motor neurodegenerative diseases, such as Huntington's disease or motor neuron diseases.

Although ataxia is the prominent symptom in SCAs, few mutations cause an almost pure cerebellar syndrome and isolated neurodegeneration in the cerebellar cortex. Most SCAs are multisystemic disorders presenting clinical variability and even those SCA subtypes regarded as 'pure' cerebellar forms reveal neurodegeneration not only in the cerebellum and spinocerebellar tracts, but also in many other areas of the central and peripheral systems. SCAs are characterised by progressive ataxia that is variably associated with other neurological symptoms. The clinical hallmarks result from a progressive degenerative process that mostly affects the cerebellum, brainstem and spinal cord (Figure 1.10).

SCAs are associated with several genomic loci. The disease gene has been identified for several genetic variants of familial ataxias (SCA1–3, 6–8, 10, 11, 12, 14, 17, FGF14 (fibroblast growth factor 14)–SCA and dentatorubral-pallidoluysian atrophy (DRPLA)) (Table 1.1.). SCA1–3, 6, 7, 17 and DRPLA are associated with an

expanded CAG-repeat in the open reading frames of the corresponding genes, which are translated into long polyglutamine tracts. Longer expansions are associated with earlier onset and more severe disease in subsequent generations. The most common presentation of SCA is dominantly transmitted ataxia 'plus', which is characterised by variable associations between cerebellar dysfunction, supranuclear ophthalmoplegia, slow saccades, optic atrophy, pyramidal and extrapyramidal features, mild-to-moderate dementia, amyotrophy and peripheral neuropathy. SCA's diagnostic pathological feature is usually olivopontocerebellar atrophy, which is the degeneration of neurons in specific areas of the brain – the cerebellum, pons, and inferior olives (Zoghbi and Orr, 2000) (Figure 1.10).

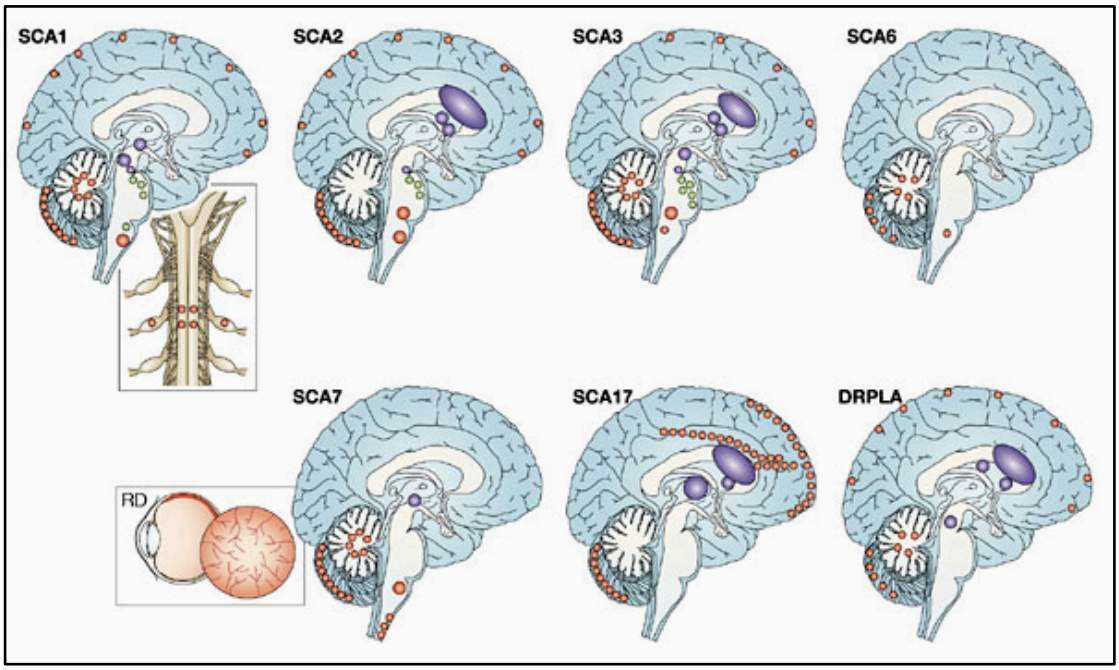

Figure 1.10. The principal sites of neuronal loss and organ dysfunction in spinocerebellar ataxia type 1 (SCA1), SCA2, SCA3, SCA6, SCA7, SCA17 and dentatorubral-pallidoluysian atrophy (DRPLA) (see also Table 1.1.). Large dots indicate severe neuronal loss. Blue dots indicate involvement of extrapyramidal nuclei. Green dots indicate cranial nerve involvement. Retinal degeneration is associated with SCA7. [Adapted from (Taroni and DiDonato, 2004)].

1.12.2 Genetic mutations causing neurodegeneration in the spinocerebellar ataxias

To date, more than 30 SCA genes or loci have been identified (Matilla-Duenas, 2008) (Table 1.1). Recognised mechanisms leading to spinocerebellar neurodegeneration

include polyglutamine expansions (SCAs 1, 2, 3, 6, 7, 17 and DRPLA); non-coding expansions (SCA10 and SCA12); as well as conventional mutations in genes encoding a cytoskeletal protein (βIII spectrin (SPTBN2), SCA5), an ion channel (voltage gated potassium channel $K_v3.3$, SCA13), a protein kinase (protein kinase C gamma (PRKCG), SCA14), an intracellular calcium channel (inositol 1,4,5-triphosphate receptor 1, SCA15), a fibroblast growth factor (FGF14, SCA27) and an ATPase family gene 3-like 2 (AFG3L2, SCA28).

SCAs 1, 2, 3, 6, 7, 17 and DRPLA are all caused by the expansion of a translated CAG repeat sequence leading to an abnormally long polyglutamine (polyQ) tract in the encoded proteins named ataxins 1, 2 and 3, alpha 1A-voltage-dependent calcium channel, ataxin 7, TATA-box-binding protein and atrophin 1, respectively, hence included in the group regarded as polyglutaminopathies. They all show common features, the progressive neurodegeneration of neuronal subsets in distinct brain areas and the formation of polyQ-containing protein aggregates forming characteristic nuclear or cytoplasmic inclusions (Duenas et al., 2006). The age at onset and severity of disease symptoms inversely correlate with the length of the glutamine repeat.

SCAs 8, 10 and 12, are caused by repeat expansions located outside of the coding region of the disease genes (Holmes et al., 1999, Wakamiya et al., 2006, Daughters et al., 2009). While SCAs 8 and 10 appear to be caused by toxic RNA gain-of-function mechanisms (although SCA8 might be also caused by polyglutamine expansions), SCA12 is caused by dysregulation of the activity of the crucial enzyme protein phosphatase 2 (PP2, formerly named PP2A) in cerebellar Purkinje cells. Different mechanisms are responsible for cerebellar ataxia and neurodegeneration in SCAs 5, 13, 14, 15, 27 and 28 where alterations in amino acid composition in beta-III spectrin (SPTBN2) (Ikeda et al., 2006), potassium channel KCNC3 (Waters et al., 2006), protein kinase C gamma (PRKCG) (Chen et al., 2003, Yabe et al., 2003), the Inositol 1,4,5-triphosphate receptor (ITPR1) (van de Leemput et al., 2007), fibroblast growth factor 14 (FGF14) (van Swieten et al., 2003), and the ATPase family gene 3-like 2 protein (AFG3L2) (Maltecca et al., 2009), respectively, elicit disease symptoms in these SCA subtypes.

Table 1.1. Genetic heterogeneity and molecular pathogenesis in the spinocerebellar ataxias (adapted from (Matilla-Duenas et al., 2010)).

SCA subtype	Genomic location	Gene	Protein	Function	DNA mutation
SCA1	6p22.3	ATXN1	Ataxin 1	Transcription regulation	(CAG)n
SCA2	12q24.12	ATXN2	Ataxin 2	RNA metabolism	(CAG)n
SCA3/MJD	14q32.12	ATXN3	Ataxin 3	De-ubiquitination, Transcription regulation	(CAG)n
SCA4	16q24-ter	SCA4	U	U	U
SCA5	11q13.2	SPTBN2	ß2-spectrin	Neuronal membrane skeleton	ID, MM
SCA6	19p13.2	CACNA1A	CACNA1A	Ca^{2+} signalling/homeostasis	(CAG)n
SCA7	3p14.1	ATXN7	Ataxin 7	Transcription regulation	(CAG)n
SCA8	13q21	ATXN8OS/ ATXN8	Ataxin 8	U	(CUG/CAG)n
SCA9	U	U	U	U	U
SCA10	22q13.31	ATXN10	Ataxin 10	Neuritogenesis	Intronic (ATTCT)n
SCA11	15q15.2	TTBK2	Tau tubulin kinase 2	U	FM
SCA12	5q32	PPP2R2B	PPP2R2B	Regulation of PP2 activity transcription regulation	5′-UTR (CAG)n
SCA13	19q13.33	KCNC3	KCNC3	K^{+} signalling	MM
SCA14	19q13.42	PRKCG	PRKCG	Phosphorylation	ID, MM
SCA15[b]	3p26.1	ITPR1	Inositol 1,4,5-triphosphate receptor 1	Inositol 1,4,5-triphosphate calcium signalling	D,MM
SCA16	8q23–q24.1	U	U	U	U
SCA17/HDL4	6q27	TBP	TBP	General transcription (TFIID complex)	(CAG)n
SCA18	7q22–q32[a]	U	U	U	U

SCA19	1p21–q21[a]	U	U	U	U
SCA20	11q12.2–11q12.3[a]	U	U	U	Chromosomal duplication
SCA21	7p21.3–p15.1[a]	U	U	U	U
SCA22	1p21–q23[a]	U	U	U	U
SCA23	20p13–p12.2[a]	U	U	U	U
SCA24	U	U	U	U	U
SCA25	2p21–p15[a]	U	U	U	U
SCA26	19p13.3[a]	U	U	U	U
SCA27	13q33.1	FGF14	FGF14	Signal transduction, Regulation NaV channels, Excitability of Purkinje cells	FM, MM, translocation
SCA28	18p11.21	AFG3L2	ATPase family gene 3-like 2	ATPase	MM
SCA29[b]	3p26	U	U	U	U
SCA30	4q34.3–q35.1[a]	U	U	U	U
DRPLA	12p13.31	ATN1	Atrophin 1	Transcription repression (nuclear receptor corepressor)	(CAG)n
16q-ADCA	16q22.1	PLEKHG4	Puratrophin 1	Intracellular signalling, cytoskeleton dynamics	5′-UTR SNP
Unknown	U	U	U	U	U

Table 1.1. (continued). Genetic heterogeneity and molecular pathogenesis in the spinocerebellar ataxias (adapted from (Matilla-Duenas et al., 2010)).

Genes noted in genomic location according to Ensembl

D: deletion, FM: frameshift mutation, ID: in-frame deletion, MM: missense mutation, SNP: single nucleotide polymorphism, UTR: untranslated region, U: unknown

[a]Genes not noted according to HUGO Gene Nomenclature Committee

[b]SCA29 maps to the same genomic location than SCA15

HDL4: Huntington's disease-like 4; MJD: Machado-Joseph disease

In the rest of SCAs, the mutations and, therefore, the genes remain to be identified and characterised. Understanding the pathogenic mechanisms underlying neurodegeneration in spinocerebellar ataxias is leading to the identification of potential therapeutic targets that will ultimately facilitate drug discovery.

1.12.3 Cellular and molecular pathways implicated in neurodegeneration in the spinocerebellar ataxias.

More than 30 genes have been identified triggering the well-described clinical and pathological phenotype of SCAs. The underlying cellular and molecular events are, however, still poorly understood. Studies of the functions of the proteins implicated in SCAs and the corresponding altered cellular pathways point to major aetiological roles for defects in transcriptional regulation, protein aggregation and clearance, alterations of calcium homeostasis, and activation of pro-apoptotic routes among others, all leading to synaptic neurotransmission deficits (Figure 1.11), spinocerebellar dysfunction, and, ultimately, neuronal demise (Matilla-Duenas et al., 2010).

Table 1.2 summarises the known cellular and molecular pathways that are known to be perturbed in some SCA subtypes. More mechanistic and detailed insights are emerging on these molecular routes. The growing understanding of how dysregulation of these pathways trigger the onset of symptoms and mediate disease progression is leading to the identification of conserved molecular targets influencing the critical pathways in pathogenesis that will serve as effective therapeutic strategies *in vivo*, which may also prove beneficial in the treatment of SCAs.

1.12.4 Common occurring pathways mediating polyglutamine neurotoxicity: protein aggregation, misfolding, stability and clearance

Seven spinocerebellar ataxia subtypes including SCAs 1, 2, 3/Machado–Joseph disease, 6, 7, 17 and DRPLA, are all caused by the expansion of a CAG repeat sequence in specific genes leading to abnormally long polyglutamine (polyQ) tracts in

SCA subtype	Identified cellular and molecular pathways	Numbers on Fig. 1.11
SCA1	Aggregation, apoptosis/caspases, autophagy, calcium and dopaminergic signalling, dysruption of vesicular transport, ER, gene transcription, HSR, mitochondrial dysfunction, PI3K/Akt, PP2, PRKC, SUMOylation, synaptic neurotransmission deficits (glutamate, GABA), UPR, UPS	(1–12, 14, 16)
SCA2	Aggregation, apoptosis/caspases, autophagy, calcium and dopaminergic signalling, ER, gene transcription, HSR, mitochondrial dysfunction, synaptic neurotransmission deficits (glutamate, GABA), UPR, UPS	(1–4, 7–12, 17)
SCA3	Aggregation, apoptosis/caspases, autophagy, dopaminergic signalling, ER, gene transcription, HSR, mitochondrial dysfunction, SUMOylation, synaptic neurotransmission deficits (glutamate, GABA), UPR, UPS	(1–3, 7–12)
SCA5	Neuronal membrane skeleton, synaptic neurotransmission deficits (glutamate, GABA)	(6, 11, 15)
SCA6	Aggregation, apoptosis/caspases, autophagy, dopaminergic signalling, ER, gene transcription, HSR, mitochondrial dysfunction, synaptic neurotransmission deficits (glutamate, GABA), UPR, UPS	(1–4, 7–12)
SCA7	Aggregation, apoptosis/caspases, autophagy, ER, gene transcription, mitochondrial dysfunction, SUMOylation, synaptic neurotransmission deficits (glutamate, GABA), UPR, UPS	(1–3, 6–12)
SCA8	Aggregation, apoptosis/caspases, gene transcription, mitochondrial dysfunction, synaptic neurotransmission deficits (glutamate, GABA), UPR, UPS	(1, 2, 6–9, 11, 12, 15)
SCA10	Neuritogenesis.	(16)
SCA12	Apoptosis/caspases, dysruption of vesicular transport, gene transcription, PP2, tau phosphorylation	(2, 5, 7, 14)
SCA13	Potassium channel signalling	(13)
SCA14	Calcium, neuritogenesis, synaptic neurotransmission deficits (glutamate, GABA)	(4, 11, 16)
SCA15	Calcium homeostasis	(2, 4, 16)
SCA17/HDL4	Aggregation, apoptosis/caspases, autophagy, dopaminergic signalling, ER, gene transcription, HSR, mitochondrial dysfunction, synaptic neurotransmission deficits (glutamate, GABA), UPR, UPS	(1–3, 7–12)
SCA27	Dopaminergic signalling, signal transduction, sodium voltage channel	(11, 17)
SCA28	Mitochondrial dysfunction	(2, 9)
DRPLA	Aggregation, apoptosis/caspases, autophagy, ER, gene transcription, HSR, mitochondrial dysfunction, synaptic neurotransmission deficits (glutamate, GABA), UPR, UPS	(1–3, 7–12)
19q-ADCA	Actin dynamics, intracellular signalling, synaptic neurotransmission deficits	(7, 11)

Table 1.2. Cellular and molecular pathways implicated in the spinocerebellar ataxia. [adapted from (Matilla-Duenas et al., 2010)]

ER: endoplasmic reticulum; GABA: γ-aminobutyric acid; HDL4: Huntington's disease-like 4; HSR: heat shock response; UPR: unfolded protein response; UPS: Ubiquitin-dependent proteasome system.

the encoded proteins (Zoghbi and Orr, 2000). A similar pathogenic pathway is likely to underlie these SCAs, since each of the expanded CAG repeats encodes

polyglutamine and the pathogenic minimum number of repeats that cause disease is roughly the same, at around 40 copies of the repeat in most of the different subtypes. Toxic gain-of-function mechanisms are likely to be responsible for the polyglutamine-containing protein is aggregation and deposition of misfolded proteins leading to neuronal dysfunction and eventually cell death.

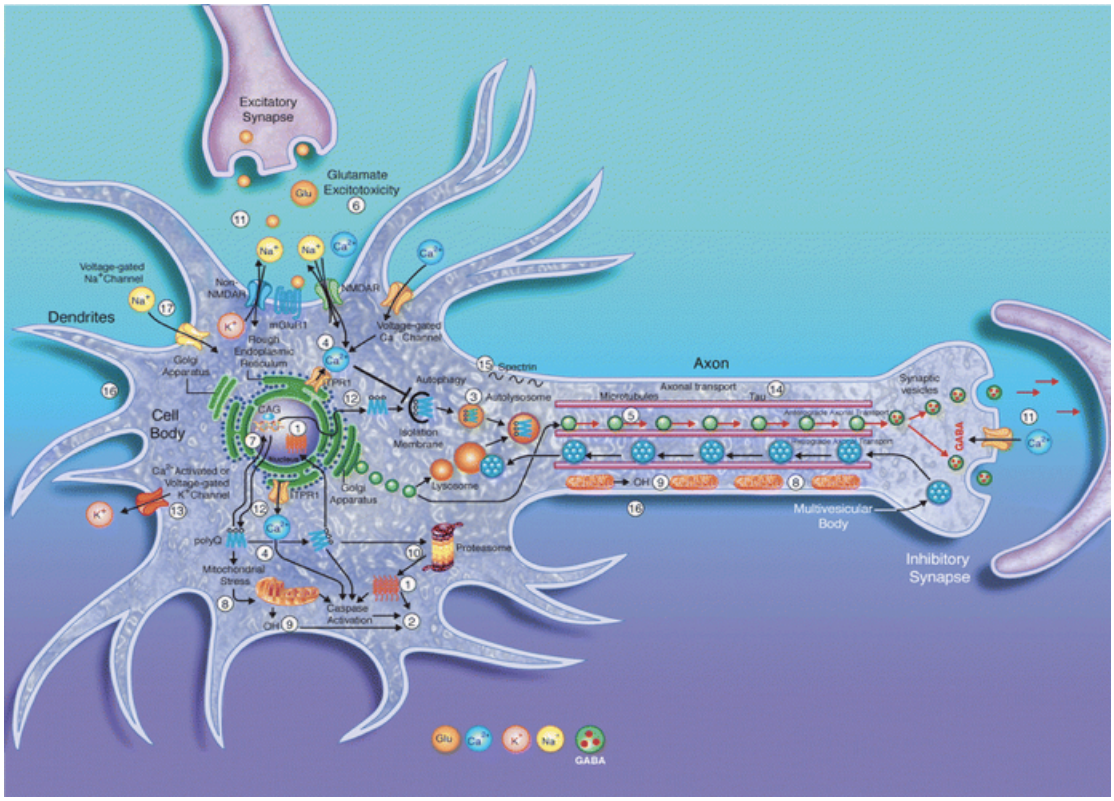

Figure 1.11. Molecular mechanism of neurodegeneration in the spinocerebellar ataxias. [adapted from (Matilla-Duenas et al., 2010)]

1 aggregation, *2* apoptosis, *3* autophagy, *4* Ca^{2+} homeostasis/signalling alterations, *5* disruption of axonal transport and vesicle trafficking, *6* excitotoxicity, *7* interference with gene transcription, *8* mitochondrial impairment, *9* oxidative stress, *10* alterations of proteasome degradation, *11* synaptic neurotransmission deficits, *12* unfolded protein response (UPR), *13* potassium channel dysfunction, *14* tau phosphorylation, *15* neuronal membrane skeleton, *16* neuritogenesis, *17* voltage-gated Na^{+} channels. Ca^{2+} calcium ions, ER endoplasmic reticulum, GABA γ-aminobutyric acid, Glu glutamate, ITPR1 inositol 1,4,5-triphosphate receptor type 1, K^{+} potassium ions, mGluR1 metabotropic glutamate receptor type 1, Na^{+} sodium ions, Q glutamine. [Adapted from (Matilla-Duenas et al., 2010)]

Proteins with expanded stretches of polyglutamine adopt an abnormal configuration resulting in the formation and deposition of polyglutamine aggregates in disease neurons forming characteristic nuclear or cytoplasmic inclusions, which are neuropathological hallmarks in these diseases (Ross and Poirier, 2004). These inclusions contain cellular components such as ubiquitin, the proteasome, HSP70 (70

kDa heat shock protein), and transcription factors among others (Cummings et al., 1998, McCampbell et al., 2000, Schmidt et al., 2002). Whether the toxicity is a direct result of the aggregates or results from intermediary structures formed during the process of aggregation has been the object of controversy, but blocking aggregation is still one approach attempted to minimise toxicity.

A possible mechanism for aggregate formation by the mutant protein would be by loss of native state stability by the expanded polyglutamine and, thus, leading to the formation and accumulation of a partially unfolded, aggregation-prone species, resulting in fibrillisation. This phenomenon probably accounts for the earlier age of onset and higher severity of disease symptoms observed when mutant ataxins contain longer numbers of glutamines.

1.12.5 Dysregulation of transcription and gene expression

Several lines of evidence implicate those ataxins containing long stretches of polyglutamines in the regulation of gene transcription. Nuclear expression of polyglutamine-expanded proteins is an essential step in polyglutamine pathogenesis, and the resulting transcriptional dysregulation caused by ataxins containing expanded polyglutamines results in neuronal dysfunction and death in a few SCAs (Helmlinger et al., 2006). Interference with gene expression occurs by the effects of the mutation exerted on the interaction of ataxins with transcriptional regulatory proteins and DNA or on chromatin remodelling.

For instance, in SCA1, ataxin 1 interacts with several transcription factors regulating transcription including the transcriptional co-repressors/activators (Matilla et al., 1997). The mutant forms of ataxin-1 exert alterations in the expression levels of genes regulated by those transcriptional regulators leading to alterations of Wnt-receptor signalling, retinoid acid/thyroid hormone signalling, and nucleic acid binding (Matilla-Duenas et al., 2008). Similarly, ataxins 2, 3 and 7, and the SCA17 and DRPLA gene products, the basal transcription factor TATA-binding protein (TBP) and atrophin 1, respectively, are directly involved in transcription as components of transcriptional regulatory complexes (Shimohata et al., 2000, Li et al., 2002, Zhang et

al., 2002, Helmlinger et al., 2004), and the genes and pathways regulated by these factors are just being identified. Interference with transcriptional regulations of specific subset of genes by polyglutamine expansions lead to neuronal dysfunction such as axonal and neurite integrity (Friedman et al., 2007) and accounts for the cell-type specificity degeneration observed in spinocerebellar ataxias, through the sequestration of factors by the long glutamine stretches within the mutant proteins, whose expression are confined to cells that degenerate in these conditions (Matilla et al., 1997).

1.12.6 Alterations in calcium homeostasis

Several lines of evidence point to derangements of neuronal calcium signalling in neurodegeneration of spinocerebellar ataxias. Cerebellar Purkinje cells seem to be particularly sensitive to fluxes in intracellular calcium levels, which could result from different sources, such as the reduction of chaperone activity and endoplasmic reticulum (ER) stress. Several neuronal genes, abundantly expressed in Purkinje cells that are involved in calcium signalling or homeostasis, are down-regulated in the cerebellum of SCA1 mutant mice before the occurrence of detectable motor impairment or pathology (Worth et al., 2000, Serra et al., 2004). This suggests a major role of disruption of calcium homeostasis in cerebellar Purkinje cells that could be importantly involved in the pathogenic process and/or the survival of these cells in SCA1.

In SCA2, mutant ataxin 2, but not wild-type, specifically associates with the cytosolic C-terminal region of type 1 ITPR1 (Inositol 1,4,5-triphosphate receptor type 1), an intracellular calcium release channel (Liu et al., 2009). Association of Atxn2[58 glutamines] with the receptor increases the sensitivity of ITPR1 to activation by inositol-tri-phosphate in planar lipid bilayer reconstitution experiments. This evidence indicates that disturbed neuronal Ca^{2+}-signalling may play an important role in SCA2 neuropathology.

Furthermore, SCA6 is caused by polyglutamine expansion in the CACNA1A gene, which encodes an alpha (2.1) subunit, formerly named [alpha]1A, the major pore-

forming subunit of the $Ca_V2.1$ voltage-dependent P/Q-type calcium channel (Zhuchenko et al., 1997, Pietrobon, 2013).

Also, SCA14 is caused by mutations in protein kinase C gamma (PKC gamma). Interestingly, 18 of 22 mutations are concentrated in the C1 domain, which binds diacylglycerol and is necessary for translocation and regulation of PKC gamma kinase activity. Wild-type PKC gamma, but not C1 domain mutants, inhibits Ca^{2+} influx in response to muscarinic receptor stimulation (Adachi et al., 2008). The resulting sustained Ca^{2+} entry imbalances Ca^{2+} homeostasis and Ca^{2+}-mediated signalling in Purkinje cells and contributes to the neurodegeneration characteristic of SCA14.

SCA15 is caused by deletions and missense mutations in the ITPR1. The ITPR1 couples to intracellular Ca^{2+} channels to facilitate Ca^{2+} release from the endoplasmic reticulum after activation by the intracellular second messenger inositol 1,4,5-triphospate. SCA15 results then from impaired inositol 1,4,5-triphospate-mediated intracellular second-messenger signalling and disturbed calcium release altering intracellular calcium homeostasis.

1.12.7 Mitochondrial stress and apoptosis

There is mounting evidence to suggest that neuronal death in spinocerebellar ataxias results from the direct activation of apoptotic pathways (Lipinski and Yuan, 2004). In addition to the role of mitochondria in intracellular calcium homeostasis as discussed earlier, polyglutamine-expanded cellular death of cerebellar neurons by polyglutamine-expanded containing proteins, is preceded by recruitment of caspases into polyQ aggregates (Sanchez et al., 1999).

Further indication of mitochondrial dysfunction resulting or contributing to ataxia is exemplified by AFG3L2 (ATPase family gene 3-like 2), a ubiquitous nuclear-encoded mitochondrial protease that forms hetero-oligomeric paraplegin-AFG3L2 and homo-oligomeric AFG3L2 complexes in the inner mitochondrial membrane. These complexes ensure protein quality control in the inner membrane, jointly with a chaperone-like activity on the respiratory chain complexes. Mutations in AFG3L2

have been identified in SCA28 (Taroni and DiDonato, 2004). In this SCA subtype, respiratory chain dysfunction and increased reactive oxygen species production caused by AFG3L2 haploinsufficiency seem to lead to degeneration of Purkinje cells and cerebellar dysfunction (Maltecca et al., 2009). This data implicates impaired mitochondrial proteolysis as a novel pathway in cerebellar neurodegeneration.

1.12.8 Alterations in synaptic neurotransmission

Alterations in glutamate synaptic neurotransmission represent another mechanism mediating neurodegeneration in SCAs. In SCA1 transgenic mice, motor dysfunction precedes neuronal death, demonstrating that mutant ataxin-1 produces disruption of motor functions in SCA1 not by killing cells, but by affecting some Purkinje cellular functions including alterations in synaptic plasticity (Clark et al., 1997). Elevated intracellular calcium levels mediated by calcium-permeable glutamate receptors have been proposed as a possible mechanism (Serra et al., 2004). The importance of maintaining proper glutamate transmission in the Purkinje cell/parallel fibre synapse for proper motor function is supported from studies with ataxia mouse mutants. For instance, mice lacking mGluR1 (metabotropic glutamate receptor type 1) display significant motor deficits and, importantly, introduction of mGlur1 expression into Purkinje cells of mGluR1$^{-/-}$ mice restores normal motor function (Ichise et al., 2000).

RNA-mediated neurotoxicity has been implicated in SCA8 pathogenesis (Daughters et al., 2009). Recent studies have revealed that the SCA8 expansion is expressed in both directions (CUG and CAG) and that a novel gene expressed in the CAG direction encodes a pure polyglutamine expansion protein (ataxin 8; ATXN8) (Ikeda et al., 2008). Moreover, the expression of non-coding (CUG)(n) expansion transcripts (ataxin 8 opposite strand, ATXN8OS) and the discovery of intranuclear polyglutamine inclusions suggests that SCA8 pathogenesis may involve toxic gain-of-function mechanisms at both the protein and RNA levels. The SCA8 mice have revealed a loss of cerebellar GABAergic inhibition and, similar to human patients, intranuclear inclusions containing expanded polyQ in Purkinje cells and other

neurons. This data could provide a convincing explanation for the lack of penetrance observed in SCA8 patients (Worth et al., 2000, Corral et al., 2005).

Two SCA mutations impinge on glutamate signalling just upstream of calcium release. SCA5 is caused by mutations in β-III spectrin (SPTBN2), which stabilises the EAAT4 (excitatory amino acid transporter 4) glutamate transporter at the cell surface (Ikeda et al., 2006). Deleterious mutation in SPTBN2 would then lead to a decrease in reuptake of glutamate from the synapse and a strengthening of glutamatergic signalling. SCA20 is caused by a chromosomal duplication of 260 kb on chromosome 11q12 (Knight et al., 2008). A prominent candidate gene in this genomic region is DAGLA (diacylglycerol lipase alpha), which is highly expressed in Purkinje cell dendritic spines and serves to weaken glutamatergic signalling (Knight et al., 2008). Further experiments are necessary to determine whether duplication of DAGLA itself is primarily responsible for symptoms or if other genes in the critical region are more important.

1.12.9 Additional pathways to ataxia

While many of the genes mutated in the SCAs play a clear role in gene expression, calcium homeostasis, mitochondrial stress and apoptosis and synaptic neurotransmission; the existence of additional pathways to ataxia underline the complexity of this phenotype. Some of the emerging pathways that play an important role in SCA cerebellar dysfunction were highlighted in Table 1.2 and Figure 1.11. Whether these pathways function independently of each other or are all interconnected remains to be determined, though the fact that 18 of 23 proteins that cause hereditary ataxia in humans connect to each other either directly or indirectly via protein-protein interactions suggests a high degree of convergence (Lim et al., 2006).

Notably, three SCA genes are involved in phosphorylation-dependent intracellular signalling. Firstly, a CAG repeat expansion in the 5′UTR of PPP2R2B (Protein Phosphatase 2, Regulatory Subunit B) causes SCA12. PP2R2B encodes BB1 and BB2, regulatory subunits of protein phosphatase A (PP2A) involved in determining

subcellular localisation and substrate specificity of the enzyme. The pathogenic consequences of the SCA12 mutation remain unknown, though PP2R2B may play a role in recruiting PP2A to the outer mitochondrial membrane, where it helps to regulate mitochondrial morphology and promote apoptosis (Dagda et al., 2008).

Secondly, multiple mutations in the brain-specific serine/threonine kinase PKCγ can cause SCA14 (Dalski et al., 2006). Both cell culture experiments and an SCA14 transgenic mouse model demonstrate that these mutations in PKCγ alter the downstream signalling ability of PKCγ (Verbeek et al., 2008).

Thirdly, SCA11 is caused by truncating mutations in TTBK2 (tau tubulin kinase 2) (Houlden, 1993). TTBK2 is also a serine/threonine kinase, the investigation of which is the focus of this thesis.

1.13 Pathogenesis of SCA11

How do TTBK2 truncating mutations lead to neuronal dysfunction and ultimately neuronal demise of Purkinje cells of the cerebellum?

Semiquantitative PCR with reverse transcription (RT-PCR) on RNA extracted from lymphoblasts of affected individuals in families 1 and 2, showed that each mutation was associated with an approximate 50% reduction in total TTBK2 mRNA relative to lymphoblast mRNA from unaffected individuals (Houlden et al., 2007). Treating lymphoblasts from affected individuals of both families with cycloheximide, a potent inhibitor of protein synthesis that also blocks the nonsense-mediated decay (NMD) pathway, resulted in increased total TTBK2 mRNA and a selective increase in the abundance of the mutant mRNA, which became roughly equal to that of the normal transcript. Some mutant transcript was detected on fragment analysis, which suggests that a proportion of the mutant mRNA escapes NMD. Thus, all four TTBK2 mutations, which insert premature stop codons in the mRNA, lead to the production of a truncated protein and/or nonsense-mediated decay (NMD) of the mutant transcript.

Nonsense-mediated mRNA decay (NMD) is one of the major cellular surveillance mechanisms for mRNA quality control (Isken and Maquat, 2007). The NMD pathway detects and degrades mRNA bearing a premature termination codon, thus preventing the accumulation of potentially toxic protein or eliminating the detrimental effects of truncated protein expressed from the mRNA containing the premature stop codon (Frischmeyer and Dietz, 1999). In mammalian cells, RNA with a premature stop codon located more than 50 nucleotides upstream of the exon-exon junction is usually recognised (Nagy and Maquat, 1998) and degraded by the NMD pathway during the initial round of translation (Ishigaki et al., 2001). The NMD pathway has been shown to be involved in the pathological development of a number of inherited disorders (Frischmeyer and Dietz, 1999).

Rather than generating a truncated TTBK2 protein, analyses of fibroblasts from the affected members of SCA11-family 1 revealed substantial loss of the mutant mRNA through the NMD pathway (Houlden et al., 2007). As a consequence, most of the expression of TTBK2 protein was from the normal allele as an approximate 50% reduction in total TTBK2 mRNA relative to lymphoblast mRNA from unaffected individuals was observed. This may result in haploinsufficiency of TTBK2, which can produce a concomitant reduction in the phosphorylation of its targets, which leads to the pathogenesis of SCA11.

However, low levels of the truncated TTBK2 mRNA encoded by the mutant allele could be detected in the fibroblasts of affected individuals, indicating that a small proportion of the mutant mRNA escapes NMD. The truncating mutations could result in a mutant TTBK2 that lacks the non-catalytic C-terminal portion and act in a dominant-negative manner to inhibit the function of the wild-type TTBK2 expressed from the normal allele.

Therefore, two plausible pathogenetic mechanisms of SCA11 should be contemplated: haploinsufficiency (loss of half of the kinase activity) or dominant negative effects of mutant TTBK2 protein. Identifying and characterising the key targets (substrates) of TTBK2 in neurons would provide vital new insights into the physiological role of TTBK2, which may, in turn, uncover the molecular pathogenic mechanism underpinning the development of spinocerebellar ataxia type 11 (SCA11).

1.14 Recently-discovered role of TTBK2 in ciliogenesis

Recently, a specific role of TTBK2 was defined in mouse development: it acts at the mature basal body to promote the initiation of ciliogenesis (Goetz et al., 2012). In the course of a genetic screen for mutations that affect neural patterning in the mouse embryo, TTBK2 was identified as an essential gene for Sonic Hedgehog (Shh) signalling because it was required for formation of primary cilia.

The primary cilium has critical roles in human development and disease, but the mechanisms that regulate ciliogenesis are not understood. Crucially, SCA11 disease-associated mutants of TTBK2 can inhibit ciliogenesis in wild-type (WT) cells, suggesting that the mutations cause disease by interfering with the product of the WT allele. The authors hypothesised that ciliogenesis may be perturbed in individuals with SCA11 (Goetz et al., 2012). However, it cannot be distinguished whether the pathology of SCA11 is due to interference with ciliogenesis or to other targets of TTBK2 in the nervous system. Nevertheless, These findings raise the possibility that cilia may play a role in preventing neural degeneration.

1.15 Aims and scope of the thesis

TTBK2 was first identified based on its physical association with microtubules and its ability to phosphorylate microtubule-associated proteins (tau, tubulin, MAP2) *in vitro* (Takahashi et al., 1995, Tomizawa et al., 2001). This discovery was made by Japanese scientists in 1995, and since then considerable work has been invested in examining TTBK2's relationship with aberrant tau phosphorylation and neurodegeneration in Alzheimer's disease. However, these studies have never been substantiated *in vivo*.

The identification of TTBK2 truncating mutations as the cause of spinocerebellar ataxia type 11 (SCA11), in 2007, highlighted the physiological importance of TTBK2 in the nervous system. When I began my PhD, there was little known about TTBK2 and many fundamental questions about TTBK2 remained unanswered: how do the disease mutations impact on TTBK2 activity, what was its physiological substrate, what signal transduction network it participates in and what is its physiological function?

To fully appreciate the role of any given protein kinase plays in cellular signalling, one needs to identify interacting partners as well as downstream substrate(s). To achieve this objective, the basic biochemistry of the protein kinase needs to be investigated first.

TTBK2's substrate specificity and selectivity had not been investigated and the question of how SCA11-causing truncating mutations affect protein expression and kinase activity was not addressed. Therefore, I sought to characterise the substrate specificity of TTBK2 (Chapter 3) by using an unbiased positional scanning peptide library. This screen revealed that it has a conspicuous preference for a phosphotyrosine residue at the +2 position relative to the phosphorylation site. This information was then exploited to develop an optimised peptide substrate, named TTBKtide, to assess TTBK2 catalytic activity. TTBKtide was used to demonstrate that SCA11 truncating mutations lead to marked inhibition of TTBK2 kinase activity.

Regarding the physiological function of TTBK2, the identification and characterisation of the interacting partners and key targets (substrates) of TTBK2 in the nervous system would provide vital new insights into the physiological role of TTBK2. This, in turn, may uncover the molecular pathogenic mechanism underpinning the development of spinocerebellar ataxia type 11 (SCA11). To this end, I aimed to identify TTBK2 interactors and substrate(s) by co-immunoprecipitation of endogenous TTBK2 from mouse brain homogenates (Chapter 4). This screen provided tantalising evidence that TTBK2 operates in a distinct step of the synaptic vesicle cycle. An analysis of potential protein substrates identified synaptic vesicle glycoprotein 2A (SV2A) as a potential substrate of TTBK2. Further work involved the mapping of the TTBK2 phosphorylation sites on SV2A and the exploration of the functional significance of the phosphorylation sites.

This corpus of work provides the first fundamental clues to the physiological function of the TTBK2 protein kinase in neurons. The tantalising evidence points towards a role for TTBK2 in synaptic vesicle trafficking. It also uncovers a hitherto unknown signalling pathway. This opens up several avenues of investigation into the molecular mechanisms that underlie synaptic vesicle trafficking deficits caused by TTBK2

mutations. Further work will thus allow us to arrive at a more complete picture of the impact of TTBK2 truncating mutations on synaptic vesicle trafficking and hence its contribution to the pathogenesis of SCA11.

2 MATERIALS AND METHODS

2.1 MATERIALS

2.1.1 Commercial reagents

Common reagents and buffers were from BDH (Lutterworth, UK) or Sigma-Aldrich (Poole, UK) unless otherwise stated. Cellophane films and All Blue Precision Plus pre-stained protein markers were from BioRad (Herts, UK). Dialysed foetal calf serum (FCS) was from Biowest (Nuaillé, France). CHAPS detergent was from Calbiochem (Merck Biosciences Ltd, Nottingham, UK). Cell culture dishes, cryovials and Spin-X columns were from Corning Incorporated (New York, USA). Cell scrapers were from Costar (Cambridge, USA). 40% (w/v) 29:1 Acrylamide: Bis-Acrylamide solution was from Flowgen Bioscience. Protein G-sepharose, Glutathione-sepharose, Enhanced chemiluminescence (ECL) kit, Hyperfilm MP and [γ^{32}P]-labelled ATP were purchased from GE Healthcare (Piscataway, USA). Dulbecco's modified eagle medium (DMEM), L-15 Leibovitz medium, Opti-MEM reduced serum media, Foetal bovine serum (FBS), tissue culture grade Dulbecco's phosphate buffered serum (PBS), Trypsin/EDTA solution, L-glutamine, non-essential amino acids, vitamins, sodium pyruvate and antibiotic/antimycotic were from GIBCO (Paisley, UK). Pre-cast NuPAGE Novex SDS polyacrylamide 4-12% Bis-Tris gels, NuPAGE MES and MOPS running buffer (20X), 10X NuPAGE sample reducing agent, 4X NuPAGE LDS sample buffer, Colloidal blue staining kit, ProLong Gold, SYBR DNA gel stain were from Invitrogen (Paisley, UK). Instant Blue staining solution was purchased from Expedion (Cambridgeshire). Photographic developer (LX24) and liquid fixer (FX40) were from Kodak (Liverpool, UK). X-ray films were from Konica Corporation (Japan). Agarose was from Melford Laboratories (Chelsworth, UK). Restriction enzymes, DNA ligase and DNA ladder were from New England Biolabs (Hertfordshire, UK). Coomassie protein assay reagent (Bradford reagent) was from Pierce (Chester, UK). Polyethylenimine (PEI) was from Polysciences (Warrington, PA). Skimmed milk (Marvel) was from Premier Beverages (Stafford, UK). Taq DNA polymerase in storage buffer A, sequencing grade trypsin and nucleotide mix (dNTP) were from Promega (UK). Site-directed mutagenesis was carried out using the QuikChange® site-directed mutagenesis method. Plasmid Maxiprep kits were from Qiagen Ltd (Crawley, UK). Acetonitrile (HPLC grade) and

trifluoroacetic acid (TFA) were from Rathburn Chemicals (Walkerburn, UK). Protease inhibitor cocktail tablets and proteinase K were purchased from Roche (Lewes, UK). Protran BA nitrocellulose membrane was purchased from Schleicher and Schuell (Anderman and Co. Ltd., Surrey, UK). Adenosine 5'-triphosphate sodium salt (ATP), anti-HA-agarose, anti-FLAG-agarose, ammonium persulphate (APS), ampicillin, benzamidine, benzonase, bovine serum albumin (BSA), bromophenol blue (BPB), brilliant blue, doxorubicin, dimethyl pimelimidate (DMP), dimethyl sulphoxide (DMSO), ethidium bromide, etoposide glutathione, hydrogen peroxide, iodoacetamide, nocodazole, phenylmethanesulphonylfluoride (PMSF), Ponceau S, sodium dodecyl sulphate (SDS), sodium tetraborate, thymidine, N, N, N', N'-Tetramethylethylenediamine (TEMED), triethylammonium bicarbonate, Triton-X-100 and Tween-20 were from Sigma-Aldrich (Poole, UK). HRP-conjugated secondary antibodies and SuperSignal West Dura extended duration substrate were from Thermo-scientific (Essex, UK). P81 paper and 3mm chromatography paper were from Whatman International Ltd (Maidstone, UK). Spin-X columns were from Corning Incorporated (NY, USA).

2.1.2 In-house reagents

Primers were synthesised by the University of Dundee oligonucleotide synthesis service. Bacterial culture medium Luria Bertani (LB) broth and LB agar plates were provided by the University of Dundee media kitchen facility. Substrate peptides for kinase activity assays were obtained from GS Biochem (Shanghai, China) or the Division of Signal Transduction Therapy (DSTT, University of Dundee).

In addition, purified kinases, phosphatases and other proteins (Table 2.1) and also substrate peptides for kinase activity assays were obtained from the Division of Signal Transduction Therapy (DSTT, University of Dundee).

2.1.3 Antibodies

In-house total and phospho-specific antibodies (Table 2.1) were produced by the DSTT (University of Dundee). Antisera were raised in sheep by Diagnostics Scotland

(Carluke, Lanarkshire, UK). In addition, pre-immune IgG was purified from non-immunised sheep serum using a protein G-sepharose column. All antibodies were affinity purified on CH-sepharose that had been covalently coupled to the appropriate antigen.

Phospho-specific antibodies were generated as follows: first, the peptide immunogen was conjugated to BSA and separately to keyhole limpet haemocyanin (KLH). The BSA and KLH immunogen carrier protein conjugates were then injected into sheep along with Freunds' Adjuvant. Sheep were injected with a booster 3 weeks later and the first bleed was collected after 1 week. This was repeated twice in order to obtain 3 separate bleeds. Each bleed was allowed to clot overnight at 4 ºC, centrifuged at 1500 x g for 60 min at 4 ºC and decanted through glass wool prior to storage at -20 °C. For purification, the serum was heated for 20 min at 56 ºC followed by filtration through a 0.45 µM filter. The anti-serum was diluted 1:1 in 50mM Tris/HCl pH 7.5 with 2% Triton X- 100 and purified on a column of the peptide immunogen coupled to sepharose. Elution was carried out using 50mM glycine pH 2.5 and dialysed overnight into PBS. Total protein antibodies were used at 1 µg/ml in 5% skimmed milk in TBS- T. Phosphospecific antibodies were also used at a concentration of 1µg/ml in the presence of the non-phospho peptide antigen (10 µg/ml) to increase specificity.

The antibodies listed in Table 2.2 were purchased from the indicated sources. Antibodies were prepared in either 5% skimmed milk or 5% BSA in TBS-T and used at the concentration recommended by the manufacturer as shown.

Antibody	Immunogen	Sheep no.	Bleed No.
GST	GST purified from E. coli	S902A	2nd
TTBK2	Human TTBK2 [residues 314-385]	S572C	3rd
TTBK2	Human TTBK2 [residues 300-630]	S533C	3rd
SV2A	GST-SV2A [1-160]	S290D	1st
pSV2A pS42+S45+S47	CKKRVQDEYS*RRS*YS*RFEEEDDKK [residues 36 - 54 of human SV2A]	S287D	3rd

Table 2.1. In-house antibodies

Table 2.2 tabulates antibodies obtained from the indicated commercial sources. Antibodies were diluted in 5% skimmed milk in TBST or 5% BSA in TBST (which was filtered through 0.45µm filter) and used at the concentration recommended by the manufacturer.

Antibody	Cat No.	Company	Species
SV2A	ab32942	Abcam	rabbit
Synaptotagmin 1	ab7734	Abcam	mouse
SPTBN2	ab58234	Abcam	mouse
Flag	F3165	Sigma	mouse

Table 2.2. Commercial antibodies

2.1.4 cDNA constructs

The DSTT cloning team performed the cloning, subcloning and mutagenesis of the constructs described in this thesis.

TTBK2, CK1δ, SV2A and synaptotagmin 1 constructs are shown in Tables 2.3, 2.4 and 2.5 respectively. Most of the cDNA constructs were generated by Dr. Maria Deak, Dr. Mark Peggie and Mr. Thomas McCartney. The mammalian expression vector, pEBG6P, was generated by Dr M. Deak. This is a modified version of the pEBG2T vector (Sanchez et al., 1994) that allows the expression of proteins with an N-terminal GST tag followed by a PreScission cleavage site.

The rat Synaptotagmin1-pHluorin (Syt1-pH) construct (Table 2.6) was kindly provided by Professor Michael Cousin (University of Edinburgh) and mutagenesis was performed by Miss Simone Weidlich (DSTT cloning team). The SV2A-pHluorin construct was generated by inserting the superecliptic pHluorin into the first intravesicular loop of mouse SV2A.

Construct	Clone no.	Vector
GST-TTBK2-[1-450]^{WT}	DU17397	pEBG6P
GST-TTBK2-[1-450]^{KD}	DU19036	pEBG6P
GST-TTBK2-[1-316]^{WT}	DU38313	pGEX
GST-TTBK2-[1-316]^{KD}	DU38314	pGEX
GST-CK1δ-[1-294]^{WT}	DU19064	pGEX

Table 2.3. TTBK2 and CK1δ constructs

Expressed Protein	Plasmid	DU No.
GST-SV2A	pEBG6P-SV2A (synaptic vesicle glycoprotein 2A)	DU38471
GST-SV2A[1-160]	pGEX-6-SV2A-[1-160]	DU38732
GST-SV2A[1-160] S42A,S45A,S47A,S62A,S80A,S81A,T84A,S127A	pGEX-6- SV2A-[1-160] S42A,S45A,S47A,S62A,S80A,S81A,T84A,S127A	DU40838

Table 2.4. SV2A constructs

Expressed Protein	Plasmid	DU No.
SYT1-Flag	pCMV5 Syt1 C-Flag	DU41991
SYT1$^{[K327A]}$-Flag	pCMV5 Syt1 K327A C-Flag	DU44009
SYT1$^{[T329A]}$-Flag	pCMV5 Syt1 T329A C-Flag	DU44010
SYT1$^{[K327A+T329A]}$-Flag	pCMV5 Syt1 K327A,T329A C-Flag	DU44012

Table 2.5. Synaptotagmin 1 (Syt1) constructs

cDNA Construct	Plasmid	DU No.
Syt1-pH	pcDNA3-pHluorin rat SYT1	DU42404
Syt1$^{[K326A]}$-pH	pcDNA3-pHluorin rat SYT1 K326A	DU42411
Syt1$^{[T328A]}$-pH	pcDNA3-pHluorin rat SYT1 T328A	DU42412
Syt1$^{[K331A]}$-pH	pcDNA3-pHluorin rat SYT1 K331A	DU42420
Syt1$^{[K326A+T328A+K331A]}$-pH	pcDNA3-pHluorin rat SYT1 K326A+T328A+K331A	DU42421
SV2A-pH	pCMVmodified SV2A pHluorin (intra-luminal)	DU42855
SV2A^{S42A,S45A,S47A}-pH	pCMVmodified SV2A SV2A S42A,S45A,S47A pHluorin (intra-luminal)	DU42856
SV2A^{S80A,S81A,T84A} -pH	pCMVmodified SV2A SV2A S80A,S81A,T84A pHluorin (intra-luminal)	DU42857
SV2A^{6XA}-pH	pCMVmodified SV2A SV2A S42A,S45A,S47A,S80A,S81A,T84A pHluorin (intra-luminal)	DU42858

Table 2.6. Rat Synaptotagmin1-pHluorin (Syt1-pH) and mouse SV2A-pHluorin cDNA constructs

2.1.5 Buffers

Phosphate buffered saline (PBS): 137mM NaCl, 2.7mM KCl, 8.1mM di-sodium hydrogen phosphate, 1.5 mM potassium dihydrogen phosphate pH 7.4.

Lysis Buffer: 25mM HEPES-KOH pH 7.4, 1mM EGTA, 1mM EDTA, 0.3% (w/v) CHAPS (or 1% Triton X-100), 1mM sodium orthovanadate, 10mM sodium-ß-glycerophosphate, 50mM sodium fluoride, 5mM sodium pyrophosphate, 1µM microcystin-LR, 0.27M sucrose, 0.12M NaCl, 0.1% β-mercaptoethanol, 1mM benzamidine, 0.1mM phenylmethylsulphonylfluoride (PMSF) and cOmplete^{TM} protease inhibitor cocktail (one “mini” tablet per 10 ml buffer).

Lysis buffer ensures the immediate inhibition of proteases, protein kinases and phosphatases so that the phosphorylation states of proteins in lysates are fixed at the levels present in vivo, at the time of extraction. Benzamidine and PMSF or complete protease inhibitor tablets were included to prevent the action of metallo-, aspartic, cysteine and serine proteases. EGTA chelates Ca^{2+} ions while EDTA chelates Mg^{2+} ions, which are required for the phosphoryl transfer reaction carried out by protein kinases and hence leads to their inhibition. Sodium fluoride, sodium-β-

glycerophosphate and sodium pyrophosphate inhibit Ser/Thr protein phosphatases while sodium orthovanadate inhibits protein Tyr phosphatases. Sodium orthovanadate was prepared by several rounds of boiling, cooling to room temperature on ice and then adjusted to pH 10. This was repeated until the solution was stable at pH 10 and remained colourless. This procedure ensures that the majority of sodium orthovanadate is in the monomeric state that favours Tyr phosphatase inhibition (Gordon, 1991).

Substrate Lysis Buffer: 25mM HEPES-KOH pH 7.4, 1% Triton X-100, 0.27M sucrose, 0.12M NaCl, 0.1% β-mercaptoethanol, 1mM benzamidine, 0.1mM phenylmethylsulphonylfluoride (PMSF) and complete protease inhibitor cocktail (one "mini" tablet per 10 ml buffer).

Substrate Lysis buffer was used in experiments where the target protein to be purified from cells lysed with the buffer was going to be used as a phosphorylation substrate in subsequent *in vitro* kinase experiments. Omitting phosphatase inhibitors in this buffer ensures that endogenous phosphatases dephosphorylate the target protein to a large extent, favouring subsequent *in vitro* phosphorylation reactions.

Buffer A: 50mM Tris-HCl pH 7.5, 0.1mM EGTA, and 0.1% β-mercaptoethanol.

TBS-Tween buffer (TBST): 50mM Tris-HCl pH 7.5, 0.15M NaCl and 0.1% (v/v) Tween-20.

5X SDS-PAGE Sample Buffer: 5% SDS, 5% (v/v) β-mercaptoethanol, 250mM Tris-HCl pH 6.8, 32.5% (v/v) Glycerol, Bromophenol Blue.

SDS-PAGE Running Buffer: 25mM Tris-HCl pH 8.3, 192mM Glycine, 0.1% (w/v) SDS.

Western Blotting Transfer Buffer: 48mM Tris-HCl, 39mM Glycine, 20% (v/v) Methanol.

Coomassie staining solution: 45% (v/v) water, 45% (v/v) methanol, 10% (v/v) acetic acid, 0.25% (w/v) Brilliant Blue (G-250)

Coomassie destaining solution: 45% (v/v) water, 45% (v/v) methanol, 10% (v/v) acetic acid

ECL Solution 1: 0.1M Tris-HCl pH 8.5, 2.5mM Luminol, 0.4mM p-Coumaric acid

ECL Solution 2: 0.1M Tris-HCl pH 8.5, 5.6mM Hydrogen peroxide.

Colloidal blue fixing solution: 40% (v/v) water, 50% (v/v) methanol, 10% (v/v) acetic acid.

Colloidal blue staining solution: 55% (v/v) water, 20% (v/v) methanol, 20% (v/v) Invitrogen Stainer A, 5% Invitrogen Stainer B.

2.1.6 Cell lines

All cell lines were supplied by the MRC Protein Phosphorylation Unit and the Division of Signal Transduction Therapy (University of Dundee) with an original purchase from ATCC (American Type Culture Collection).

2.1.7 Instruments

The Procise 494C Sequenator was from Applied Biosystems (Foster City, USA). Centrifuge tubes, rotors and centrifuges were from Beckmann (Palo Alto, USA). Trans-Blot Cells, automatic western blot processors and gel dryer apparatus were from BioRad (Herts, UK). Speedvacs were from CHRIST (Osterode, Germany). HPLC system components were obtained from Dionex (Camberley, UK). Thermomixer IP shakers were purchased from Eppendorf (Cambridge, UK). The Biofuge microcentrifuge was from Haraeus Instruments (Osterode, Germany). pH meters and electrodes were from Horiba (Kyoto, Japan). X-Cell SureLock Mini-cell electrophoresis systems and X-Cell II Blot modules were from Invitrogen (Paisley, UK). The Polytron was from Kinematica (Brinkmann, CT, USA). X-omat autoradiography cassettes, with intensifying screens, were from Kodak (Liverpool, UK). The Konica automatic film processor was from Konica Corporation (Japan). The LiCOR odyssey infrared imaging system was from LiCOR biosciences (Cambridge, UK). CO_2 incubators were from Mackay and Lynn (Dundee, UK). Tissue culture class II safety cabinets were from Medical Air Technology (Oldham, UK). The PCR thermocycler (PTC-200) was from MJ Research. The 96-well Versamax plate reader was from Molecular Devices (Wokingham, UK). The Vydac 218TP54 C_{18} reverse phase HPLC column was from Separations group. The LTQ-

orbitrap mass spectrometer and Nanodrop was from Thermo Scientific. The VP-ITC machine was from MicroCal and the PheraStar plate reader was from BMG Labtech.

2.1.8 Animals and the generation of the TTBK2-knockin mouse

Animal studies were approved by the University of Dundee Ethics Committee and performed under a U.K. Home Office project license. Animals were obtained from Harlan and Taconic Artemis and maintained under specific pathogen-free conditions. The knockin mice were generated by Taconic Artemis on an inbred C57BL/6J background as described. Genotyping was performed by PCR on DNA extracted from ears or embryonic membranes. Primers 1 (5′-CATTTGTTGGCATTATTTCAAAGG-3′) and 2 (5′-AGTAGTAGTAGTAGTAGTAACATGG-3′) were used to detect the wild-type and knockin alleles. The PCR programme consisted of 2 min at 95 °C, 15 s at 95 °C, 30 s at 60 °C and 10 s at 72 °C for 35 cycles.

2.2 METHODS

2.2.1 Positional scanning peptide library screen (PSPL)

PSPL screening was performed as previously described (Mok et al., 2010). Briefly, peptides had the sequence Y-A-X-X-X-X-X-S/T-X-X-X-X-A-G-K-K-Biotin), where X is generally an equimolar mixture of the 17 amino acid residues excluding Cys, Ser and Thr. For each peptide in the set, a single X residue was fixed as one of the 20 unmodified amino acids, phosphothreonine or phosphotyrosine. Aliquots of peptides (0.6mM) were transferred from a 1536-well stock plate to a 1536-well reaction plate containing 2μl reaction buffer (50mM HEPES, pH 7.4, 1mM EGTA, 1mM DTT, 10mM $Mg(OAc)_2$, 0.1% Tween 20) in each well using a pin tool equipped with 200nl stainless steel slot pins. Kinase (75 μg of purified GST-TTBK2-$[1\text{-}450]^{WT}$ or GST-TTBK2-$[1\text{-}450]^{KD}$ and radiolabelled ATP (50μM, 0.33 μCi/μl [γ-^{32}P]ATP) were added together to each well using a strip of 200nl slot pins, and the plate was sealed and incubated at 30 °C for 2 h. Aliquots (200nl) were then transferred using a pin tool to a streptavidin membrane, which was washed twice with 0.1% SDS in TBS (10mM Tris, pH 7.5, 140mM NaCl), twice with 2M NaCl, and twice with 1% H_3PO_4 in 2M

NaCl. The membrane was then air dried and exposed to a phosphor storage screen to visualise radiolabel incorporation.

2.2.2 *In vitro* kinase assays using synthetic peptides as substrates

Quantification of peptide substrate phosphorylation was achieved by measuring the incorporation of radioactive ^{32}P from [$\gamma^{32}P$]-labelled ATP into a substrate peptide. Assays were carried out in a final volume of 50µl containing the purified protein kinase, the appropriate peptide substrate, 10mM $MgCl_2$ and 0.1mM [$\gamma^{32}P$]-labelled ATP. Control reactions contained either no purified kinase or kinase-inactive version of the kinase. Reactions were incubated on a Thermomixer at 30 ºC for the indicated times and terminated by spotting 40µl onto a 2cm square of P81 phosphocellulose paper. Paper squares were washed extensively in 75mM orthophosphoric acid to remove any ATP which was not incorporated into the substrate peptide and then washed in acetone and left to dry. Papers were transferred to 1.5ml eppendorf tubes and ^{32}P radioactivity measured by Cerenkov counting on a liquid scintillation counter. The protein kinase activity was expressed as specific activity (units of kinase activity per milligram of protein). One unit of protein kinase activity was the amount, which catalysed the incorporation of 1nmol phosphate into the substrate in 1min.

2.2.3 Transformation of chemically-competent *E.coli*

Calcium competent *E.coli* DH5α cells were provided by the DSTT using a previously described method (Inoue et al., 1990). For each transformation, approximately 10 ng DNA was added to 35 µl of competent cells and incubated on ice for 5min. Cells were then subjected to heat shock at 42 ºC for 90 sec in a water bath to induce the uptake of DNA and briefly placed back on ice. Bacteria were streaked onto LB agar plates containing 100 µg/ml ampicillin and plates incubated at 37 ºC overnight.

2.2.4 Purification of plasmids from *E.coli*

Transformed DH5α *E.coli* were cultured in 200ml LB containing 200 µg/ml ampicillin at 30-37°C while shaking at 200rpm overnight. Cells were pelleted by

centrifugation at 6000xg for 15min at 4 °C. Plasmid DNA was purified using the Qiagen plasmid Maxi kit according to the manufacturer's instructions.

2.2.5 Measurement of DNA concentration

DNA concentration was measured using NanoDrop instrument as per manufacturer's instructions. The absorbance at 280nm was also measured to allow the calculation of the 260nm:280nm ratio, an indicator of DNA purity. A 260:280 ratio greater than 1.6 is indicative of a highly pure sample.

2.2.6 Agarose gel electrophoresis

18 g of agarose was boiled in 180 ml of 1X TAE buffer. 10 µl of 10 mg/ml ethidium bromide were added after the boiled solution cooled to touchable temperature and then poured into a gel casting tray. Electrophoresis was carried out at 150V for 30-40min.

2.2.7 Site-directed mutagenesis

Site-directed mutagenesis was performed by the DSTT cloning team using QuikChange kit (Stratagene) and KOD polymerase (Novagen). All mutations were verified by DNA sequencing.

2.2.8 DNA sequencing

The sequencing was performed by DNA sequencing service (School of Life Sciences, University of Dundee) using DYEnamic ET terminator chemistry kit (Amersham Biosciences) on Applied Biosystems automated DNA sequencers.

2.2.9 Cell culture

All procedures were carried out in aseptic conditions meeting biological safety category 2 regulations. Cells were maintained at 37°C in a 5% CO_2 water-saturated

incubator and allowed to reach 80-90% confluency prior to passaging. For the passaging of cells, cells were washed once with sterile PBS and then incubated with sterile Trypsin/EDTA. Cells were then resuspended in pre- warmed culture medium and centrifuged at 800rpm for 5min. Media/trypsin was aspirated and cells resuspended in culture medium and transferred to flasks or dishes as required.

Human embryonic kidney 293 (HEK293) cells were grown in Dulbecco's modified eagle medium (DMEM) supplemented with 10% (v/v) foetal bovine serum (FBS), 2mM L-glutamine, 100 U/ml penicillin and 0.1mg/ml streptomycin. Mouse embryonic fibroblasts (MEFs) were grown in DMEM containing 10% (v/v) FBS, 2mM L-glutamine, 100U/ml penicillin and 0.1mg/ml streptomycin, 1X non-essential amino acids and 1mM sodium pyruvate.

2.2.10 Freezing/thawing cell lines

Cells in a confluent T-75 flask were trypsinised and centrifuged at 800rpm for 5min prior to resuspension in 3ml DMEM containing 45% FBS and 10% DMSO. 1ml aliquots were stored in cryovials in a polystyrene rack at -80°C prior to long-term storage in liquid nitrogen. When required, cells were rapidly thawed in a water bath at 37ºC and immediately transferred to a T-75 flask containing 15ml media.

2.2.11 Transfection of cells using PEI

HEK293 cells were cultured in 10cm dishes and transiently transfected using the polyethylenimine (PEI) method ((Durocher et al., 2002)). A stock solution of 1mg/ml PEI was prepared in 20mM HEPES (pH 7), passed through a 0.22µm filter and stored at -80°C. Cells were plated in 10cm dishes 24hrs prior to transfection. For transfection of one DNA plasmid, 5µg of DNA was mixed with 15µl 1mg/ml PEI and 1ml serum-free DMEM and left for 15min at room temperature before being added to cells dropwise. For co-transfections, 5µg of each DNA construct (10µg DNA in total) was mixed with 30µl PEI and 1ml DMEM. Following transfection, cells were left for 36hrs prior to harvesting.

2.2.12 Cell lysis

Cells were placed on ice, rinsed once with room temperature PBS and lysed using 0.5ml of Triton X-100-containing (for routine experiments) or CHAPS-containing (for some immunoprecipitation experiments) Lysis Buffer and plastic scrapers. Whole-cell lysates were clarified by centrifugation at 12,000rpm for 20min at 4°C, the supernatants removed and stored at -80 ºC until required.

2.2.13 Protein concentration estimation using Bradford assay

The protein concentration of cell lysates and purified proteins was determined using the Bradford method (Bradford, 1976). This is based on the fact that when Coomassie dye binds to protein in an acidic medium, there is a shift in the absorption maximum from 465nm to 595nm and a colour change from brown to blue. A standard curve was generated using BSA standards (0, 25, 125, 500, 750, 1500µg/ml). These were prepared in water and 5µl of each added to a 96-well plate in duplicate along with water as a blank control. 250µl Bradford reagent was added to each well, the mixture was allowed to stand for 5min at room temperature prior to measuring the absorbance at 595nm using a 96-well plate reader. A standard curve was produced by plotting the absorbance values against the BSA concentration. To determine the protein concentration, lysates were typically diluted 1:15 in water (purified proteins were not diluted) and 5µl added to the wells of a 96-well plate in triplicate along with 250µl Bradford reagent. The absorbance values were determined as above and using the standard curve, translated into protein concentration. For purified proteins, the purity of the sample was also verified by Coomassie staining of a polyacrylamide gel.

2.2.14 Affinity purification of GST-tagged or Flag-tagged proteins from HEK293 cells

HEK293 cells were transfected GST-tagged or flag-tagged constructs and harvested 48hrs post-transfection in Triton X-100 Lysis Buffer or in Substrate Lysis Buffer, if the target protein was going to be used as a substrate in the subsequent *in vitro* kinase reactions. 25ul of glutathione-sepharose or Flag-agarose beads were used per 5mg of cleared lysates to bind the target GST-tagged or Flag-tagged protein at 4°C for 2hrs

on a rotating platform. The beads were washed 4 times using Lysis Buffer (or Substrate Lysis Buffer) supplemented with NaCl for a final concentration of 0.5M and twice with Buffer A. GST-tagged proteins were eluted from the resin with an equal volume of Buffer A supplemented with 120mM NaCl, 0.27M sucrose and 40mM glutathione (pH 7.5-8) for 10min at room temperature on a rotating platform. Flag-tagged proteins were eluted from the resin with an equal volume of Buffer A supplemented with 120mM NaCl, 0.27M sucrose and 1 mg/ml Flag peptide for 10min at room temperature on a rotating platform. Elutions were filtered through a 0.22µm Spin-X column and 100 µl aliquots were snap-frozen in liquid nitrogen and stored at -80°C.

2.2.15 Covalent coupling of antibodies

Protein G, a protein isolated from Group G Streptococci, binds to the Fc region of antibodies and can be covalently attached to sepharose beads. This enables the immunoprecipitation of specific proteins. Protein G-sepharose was washed 5 times with PBS to remove traces of ethanol. The appropriate antibody and Protein G-sepharose were mixed in a ratio of 1µg antibody to 1µl resin and incubated on a rotating wheel at 4 °C for 1-2hrs. The resin was washed twice with PBS.

Antibodies were then covalently coupled to protein G-sepharose beads using dimethyl pimelimidate (DMP), a homo-bifunctional imidoester cross-linker that reacts with primary amine groups (Harlow, 1988). The resin was washed three times with 0.1M sodium tetraborate (pH 9.0). The resin was resuspended in sodium tetraborate containing 20mM DMP and incubated in the dark on a rotating wheel for 30min at room temperature. Fresh sodium tetraborate containing 20mM DMP was added for a further 30min.The resin was washed three times with 50mM glycine pH 2.5 to remove any non-covalently coupled antibody and glycine was neutralised with two washes of 0.2M Tris-HCl (pH 8.0). The resin was incubated with for 16 hrs with 0.2M Tris-HCl (pH 8.0) at 4°C on a rotating wheel to completely quench any residual DMP. The resin was rinsed twice with PBS and stored at 4ºC in PBS.

2.2.16 Immunoprecipitation of endogenous proteins

All procedures were carried out at 4 ºC. Typically 5 µg of antibody coupled to 5 µl of protein G Sepharose were used for each immunoprecipitation into a microcentrifuge tube. Lysate was added to the beads, the quantity depending on which protein was being immunoprecipitated. The protein of interest was immunoprecipitated by incubating the coupled antibody and lysate for 60 min at 4 ºC on a shaking platform. The mixture was centrifuged for 1 min at 13,000 rpm, the supernatant removed and the beads washed twice with 1 ml of lysis Buffer containing 0.5 M NaCl. This was followed by two washes with 1 ml Buffer A. The immunoprecipitate was then assayed for protein kinase activity or treated with LDS Sample Buffer and subjected to SDS/PAGE.

2.2.17 Immunoprecipitation of endogenous TTBK2 from mouse brain homogenate

The TTBK2 and pre-immune IgG antibodies were covalently coupled to protein G-Sepharose in a ratio of 1 mg of antibody to 1 ml of resin using a dimethyl pimelimidate cross-linking procedure (see 2.2.15). As a pre-clearing step, 50 mg of mouse lysate was incubated at 4 ºC for 20 min on a rolling shaker with 0.5 ml of protein G-Sepharose. The supernatant was then incubated at 4 ºC for 1h on a rolling shaker with 50µl of TTBK2 or IgG-protein G-Sepharose conjugated antibodies. The immunoprecipitates were washed four times with 10ml of Lysis Buffer containing 0.15M NaCl and lacking DTT and twice with 10ml of 10mM Tris-HCl pH 8, 0.1mM EGTA. The resin was resuspended in total volume of 0.1ml and 30µl of LDS Sample Buffer in the absence of 2-mercaptoethanol. The samples were filtered through a 0.44 µm Spin-X filter tube, DTT was added to the flow through to a final concentration of 10mM, then heated for 5 min at 70 ºC and concentrated by speed-vacuum centrifugation to 30µl. Samples were next alkylated for 30 min at room temperature using 50mM 4-vynilpyridine in 10mM NH_4HCO_3 then subjected to electrophoresis on a 4-12 % gel using MOPS as a running buffer and stained with Colloidal Blue Coomassie. The bands were excised, washed and digested with trypsin. Peptides were then analysed by mass spectrometry.

2.2.18 Lambda phosphatase treatment of SV2A immunoprecipitate

SV2A was immunoprecipitated from mouse brain lysate as described before. For λ-phosphatase treatment, immunoprecipitated proteins on beads were washed twice with lambda buffer (50 mM Tris-Cl pH 7.5, 100mM NaCl, 0.1mM EGTA, 2mM DTT, 0.01% Brij-35). The immunoprecipitate was then split into four aliquots: Aliquot 1 was left on ice, aliquot 2 was incubated for 60 min at 30 ºC in lambda buffer + 2.5mM $MnCl_2$ without λ -phosphatase, aliquot 3 was treated for 60 min at 30 °C with 100 U λ -phosphatase in lambda buffer + 2.5 mM $MnCl_2$ and aliquot 4 was treated for 60 min at 30 °C with 100 U λ-phosphatase that had been pre-incubated with 20mM EDTA, in lambda buffer + 2.5mM $MnCl_2$. After the 60 min incubations, the four pellets were washed three times in phosphatase buffer containing 150mM NaCl, then resuspended in SDS sample buffer and analysed by immunoblotting.

2.2.19 Resolution of proteins using SDS-PAGE

Sodium dodecyl sulphate polyacrylamide gel electrophoresis (SDS-PAGE) is used to separate proteins on the basis of their apparent molecular weight. The anionic detergents, sodium dodecyl sulphate (SDS) and lithium dodecyl sulphate (LDS), bind to proteins giving them a resulting negative charge that is proportional to their mass. As a result, the speed of migration of a protein through a constant gradient polyacrylamide gel matrix is a linear function of the logarithm of its molecular weight, with small proteins migrating faster than large proteins.

Separation gels were prepared containing 375mM Tris HCl pH 8.6, 0.1% SDS, 8-15% acrylamide (depending on the size of the protein) with N,N,N',N'-tetramethylethylenediamine (TEMED) and ammonium persulphate (APS) used to initiate polymerisation. Gels were allowed to polymerise for 30min under isopropanol. Stacking gels contained 125mM Tris HCl pH 6.8, 0.1% SDS, 4% acrylamide, TEMED and APS.

Cell lysates, immunoprecipitates and purified proteins were prepared in 1XLDS sample buffer containing 1X sample reducing agent (for use with pre-cast NuPAGE

4-12% Bis-Tris gels) or 1X SDS sample buffer (for use with home- made acrylamide gels) and heated to 70°C for 5min. Samples were loaded onto gels along with Precision plus protein standards which have apparent molecular weights of 250, 150, 100, 75, 50, 37, 25, 20, 15 and 10kDa. Electrophoresis was carried out at 90V for 30min prior to an increase of the voltage to 180V for a further 1hr and gels were either stained or transferred for immunoblotting.

2.2.20 Coomassie staining of polyacrylamide gels

Gels were incubated in Coomassie staining solution for 30 min before being washed in destaining solution overnight. Gels used for protein identification by mass spectrometry, were stained with Colloidal Coomassie according to the manufacturer's instructions.

2.2.21 Desiccation of polyacrylamide gels

Gels containing ^{32}P-labelled proteins were dried to improve the autoradiographic signal. Gels were transferred to water containing 5% glycerol and sandwiched between two sheets of cellophane. The gel was then dried in a GelAir™ Dryer.

2.2.22 Autoradiography

Coomassie stained gels were placed in an X-Omat autoradiography cassette and exposed to Hyperfilm™ for different lengths of time. Typically exposures were carried out for between 30min to 48hr in order to detect radioactively labelled proteins. For long exposures, the cassette was placed in a -80°C freezer to improve the autoradiographic signal. Films were developed using a Konica automatic developer.

2.2.23 Transfer of proteins onto nitrocellulose membranes

Gels that had been subjected to electrophoresis were assembled into a gel- membrane sandwich and loaded into a BioRad Mini Trans-blot electrophoretic transfer cell. Prior to assembly, nylon sponge pads, Whatman 3mm filter papers and nitrocellulose

membranes were soaked in transfer buffer containing 20% (v/v) methanol. The transfer cell was submerged in transfer buffer and electrotransfer carried out at 100V for 1.5hrs.

2.2.24 Immunoblotting

Nitrocellulose membranes were briefly stained with Ponceau-S, in order to ensure that proteins had been successfully transferred from the gel, before being washed in water. Membranes were then blocked for 30min in TBS-Tween buffer containing 5% (w/v) skimmed milk and incubated with the appropriate antibody at 4ºC overnight. Membranes were washed 6 times with TBS-T, incubated with horseradish peroxidase (HRP)-conjugated secondary antibodies for 1hr and washed another 6 times with TBS-T using an automatic western blot processor. Finally, membranes were incubated with the enhanced chemiluminescence reagent (either in-house or commercial reagents) and exposed to X-ray films for different lengths of time. As before, films were developed using a Konica automatic developer.

2.2.25 Processing protein bands for analysis by mass spectrometry

To minimise contamination with proteins such as keratin, sample preparation was carried out in a laminar flow hood. Gel pieces were cut into approximately 1mm cubes and washed for 10min in water, 50% acetonitrile/water, 0.1M NH_4HCO_3 and 50% acetonitrile/50mM NH_4HCO_3. Washes were carried out in a 0.5ml volume on a vibrax shaking platform for 10min and all liquid was removed between washes. The final step was repeated until the gel pieces were essentially colourless. Subsequently, 0.3ml acetonitrile was added and incubated for 15min before the supernatant was removed and gel pieces dried in a Speed-Vac. The gel pieces were incubated with 30µl 25mM Triethylammonium bicarbonate containing 5µg/ml Trypsin at 30°C overnight on a shaking platform. Subsequently, an equivalent volume of acetonitrile was added for 15min and the supernatant was collected in a clean tube and dried using a Speed-vac. Meanwhile 100µl 50% acetonitrile /2.5% formic acid was added to the gel pieces, incubated for 15min and the supernatant combined with the first dried extract. This was dried in a Speed Vac and stored at -20°C.

2.2.26 Mass spectrometry

LC-MS was performed by Dr D. Campbell and Mr R. Gourlay. Tryptic peptides were subjected to LC-MS on a Dionex 3000 nano liquid chromatography system coupled to an LTQ-orbitrap mass spectrometer. Results were searched against the IPI-human database using the Mascot algorithm (www.matrixscience.com) to identify tryptic peptides.

2.2.27 Phosphomapping using HPLC/Edman degradation

Proteins were phosphorylated in vitro using high-specific activity (~500,000cpm) [γ^{32}P]-labelled ATP and resolved on SDS-PAGE. Bands were processed for mass spectrometry analysis. Samples were then subjected to HPLC on a Vydac C_{18} column equilibrated in 0.1% (w/v) trifluoroacetic acid (TFA), with a linear acetonitrile gradient at a flow rate of 0.2 ml/minute. Fractions of 0.1 ml were collected and phosphopeptides were analysed by LC-MS/MS. Individual MS/MS spectra were inspected using XCalibur software. The phosphorylated residues were mapped by solid-phase Edman degradation. The ^{32}P-labelled peptide was coupled to a Sequelon-AA membrane and Edman sequencing carried out using an Applied Biosystems 494C sequencer. All HPLC and Edman degradation analyses were performed by Dr D. Campbell and Mr R. Gourlay.

2.3 Biophysical Techniques

2.3.1 Isothermal Titration Calorimetry (ITC)

Proteins and peptides for calorimetric analysis were dialysed against the same buffer: 20mM HEPES pH 7.5, 50mM NaCl. All protein solutions were filtered through a 0.22μm membrane and degassed thoroughly in a vacuum chamber before use.

ITC experiments were carried out on a Microcal VP-ITC (Milton Keynes, England). Figure 2.1 shows a diagram of the equipment used. A series of 30 x 4 μl injections of

buffered peptide were made into an isolated chamber containing 1.2 ml of buffered protein at various concentrations at a constant temperature of 25 °C. A space of 2 minutes was allowed between injections to ensure equilibration between reactants. The reaction cell was stirred at a constant speed of 300 rpm.

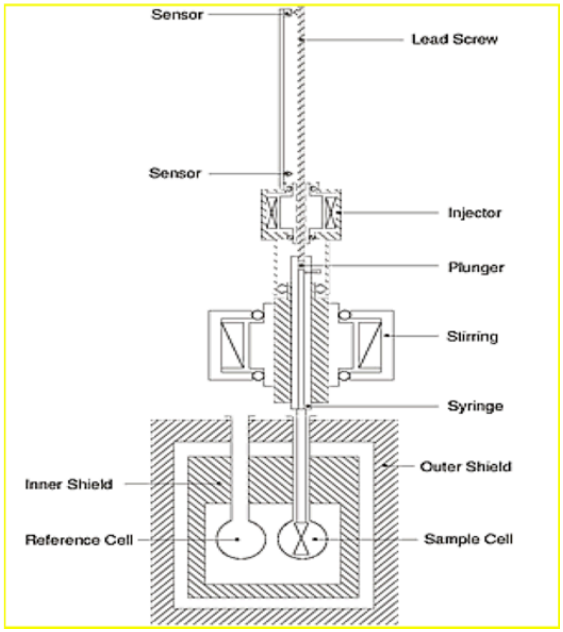

Figure 2.1. Diagram of the MicroCal VP-ITC. The protein for analysis is injected into the sample cell and the metal ligand drawn into the syringe. A small amount of sample buffer is then injected into the reference cell, in order to provide a reference temperature for the machine to equilibrate with after each injection. The chamber is shielded from the outside environment by a double casing. The syringe is then locked into place over the sample cell and set to stir the sample at 300rpm. After a period of time to allow the entire system to equilibrate, the plunger descends and releases a fixed amount of metal into the sample chamber. Any change in heat is then recorded and the system re-equilibrates in preparation for the next injection.

Heat changes within the cell were monitored during each injection of metal and recorded as the total heat change per second over time. A binding isotherm was then fitted to data and expressed as heat change per mole of metal against the metal to protein ratio. For each protein and for each condition, at least 2 runs were carried out to ensure reproducibility. Between each run, the chamber was thoroughly washed with at least 10 chamber volumes of MilliQ (Millipore, England) water and the syringe rinsed thoroughly again with at least 10 volumes of MilliQ water.

From the isothermic data, a regression model was used to predict the number of binding sites on the protein involved in the reaction, the dissociation constants of the binding (K_D) and the change in enthalpies (ΔH).

The choice of buffers was based on initial trials, which revealed that these buffers offered the minimum of background noise. Each experimental condition had a blank run with protein in the chamber replaced with buffer. This data was then subtracted from the run with protein present to take into account any energy of dilution or metal/buffer reaction.

2.3.2 Fluorescence Polarisation

Fluorescence polarisation (FP) or anisotropy can be used to measure protein–protein or protein–ligand interactions. Typically one binding partner is labelled with a fluorescence probe and the sample is excited with polarised light. The increase in the polarisation of the fluorescence upon binding of the labelled protein to its binding partner can be used to calculate the binding affinity (Owicki, 2000).

In broad terms, fluorescence polarisation is relevant where a small (tumbling), fluorescent molecule binds a larger target molecule. Thus the observation of small fluorescent ligands binding protein molecules are often experiments suitable for this type of detection. Fluorescence anisotropy is a method for measuring the binding interaction between two molecules, and can be used to measure the binding constant (or the inverse, the disassociation constant) for the interaction. The basic idea is that a fluorophore excited by polarised light (light whose "waves" only go one direction) will also emit polarised light. However, if a molecule is moving, it will tend to "scramble" the polarisation of the light by radiating at a different direction from the incident light. The "scrambling" effect is greatest with fluorophores freely tumbling in solution and decreases with decreased rates of tumbling. Protein interactions can be detected when one of the interacting partners is fused to a fluorophore: upon binding of the partner molecule a larger, more stable complex is formed, which will tumble more slowly (thus, increasing the polarisation of the emitted light and reducing the "scrambling" effect). This technique works best if a small molecule is fused to a fluorophore and binds to a larger partner (this maximises the difference in signal between bound and unbound states). Molecular interactions can thus be analysed using this approach where the smaller molecule is fluorescently labelled and the concentration of the larger binding partner is varied. An illustration depicting the concept of fluorescence anisotropy is shown in Figure 2.2 below.

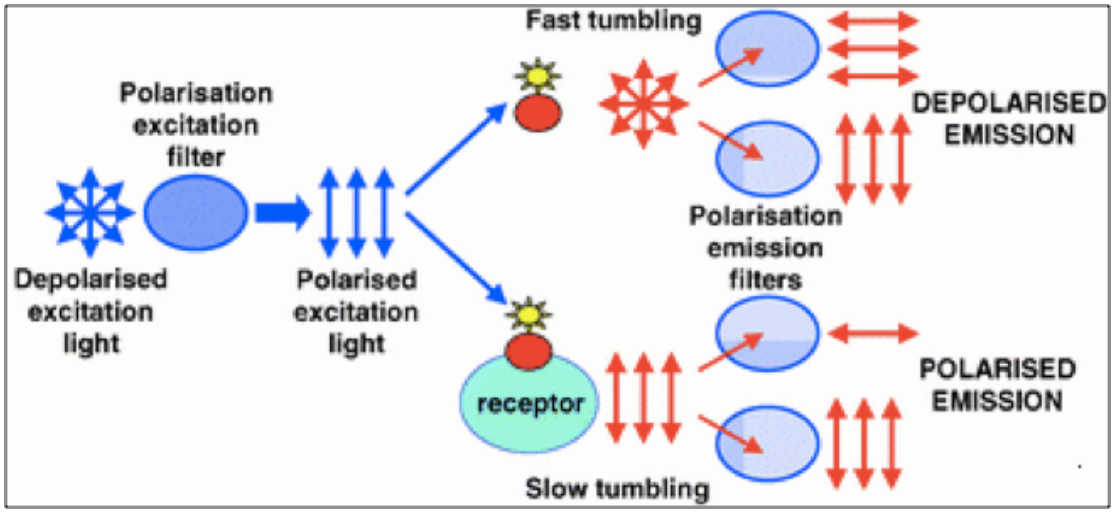

Figure 2.2. Illustration of the concept of fluorescence anisotropy. As molecules tumble in solution, the emitted light is depolarised. The depolarisation of the fluorescent molecule is dependent on the size and shape of the rotating molecule and also the viscosity of the solution. The smaller the molecule, the more rapidly it rotates and the more the light is depolarised and hence the lower the anisotropy. If a larger molecule interacts with the fluorescent molecule the rotation of the complex will be slower than of the unbound molecules and result in an increase in the fluorescence anisotropy.

2.3.2.1 Labelling peptides with FlAsH

Peptides were custom-synthesised with a N-terminal CCPGCCGG tetra-cysteine tag (Adams et al., 2002), where two glycine residues were added as a linker. This tag affords their labelling with FlAsH-EDT_2, an arsenic derivative of fluorescein. Labelling of N-terminally FlAsH-tagged (CCPGCC) peptides (Adams et al., 2002) was performed in 20mM HEPES (pH 7.5), 50mM NaCl and 5mM β-mercaptoethanol. 10 nmol of each FlAsH-tagged peptide was incubated with 5µl FlAsH-EDT_2 (Lumio Green) at room temperature for 2.0 h in the dark. Excess dye was removed by overnight dialysis into the above buffer.

2.3.2.2 Equilibrium fluorescence anisotropy measurements

All binding assays were performed by adding 100nM of labelled peptide to increasing concentrations of recombinant protein at room temperature. End point polarisation and anisotropy measurements were made using PheraStar plate reader (BMG Labtech) using a 485/520 nm fluorescence polarisation module. Data was analysed using GraphPad Prism 5 and mean fluorescence anisotropy values (2 measurements)

were plotted against protein concentration and the curves fitted to a single-site binding model to determine K_D values.

2.3.3 Sequence alignments

Sequence alignments were performed using the ClustalW algorithm for multiple sequence alignment and using JalView.

2.3.4 Statistical analysis

All the experiments presented in this thesis were repeated at least two or three times and similar results were obtained. Error bars always indicate the standard error of the mean (S.E.M.) and were calculated using GraphPad Prism.

2.4 The use of pHluorins for optical measurements of presynaptic acitivity

2.4.1 Hippocampal neuronal cultures and transfections

Dissociated primary hippocampal neuronal cultures were prepared from E17.5 from wild-type embryos of either sex by trituration of isolated hippocampi to obtain a single cell suspension, which was plated at a density of 5-10 $\times 10^6$ cells/coverslip on poly-D-lysine and laminin-coated 25 mm coverslips. Cultures were maintained in neurobasal media supplemented with B-27, 0.5 mM L-glutamine and 1% v/v penicillin/streptomycin. After 72 hours cultures were further supplemented with 1 μM cytosine β-d-arabinofuranoside to inhibit glial proliferation. Cells were transfected after 7 days in culture with Lipofectamine 2000 according to the manufacturer's instructions, with the following alterations: cells were preincubated in 2ml MEM at 5% CO2 for 30 min at 37°C, and then incubated for 2 hours with 2μl lipofectamine and 1 μg DNA construct/well. Cells were subsequently washed with MEM before replacement of conditioned neurobasal media. Cells were imaged after 14-21 days in culture.

2.4.2 Fluorescent imaging protocols for pHluorin reporters

Hippocampal cultures were mounted in a Warner imaging chamber with embedded parallel platinum wires (RC-21BRFS) and placed on the stage of a Zeiss (Germany) Axio Observer D1 epifluorescence microscope. Neurons transfected with pHluorin reporters were visualised at 500 nm (all >525 nm emission). In all experiments cultures were stimulated with a train of 200 action potentials delivered at 10 Hz (100 mA, 1 ms pulse width). Cultures were subjected to continuous perfusion with imaging buffer (in mM: 136 NaCl, 2.5 KCl, 2 $CaCl_2$, 1.3 $MgCl_2$, 10 glucose, 10 HEPES, pH 7.4). Fluorescent images were captured at 4 s intervals using a Hamamatsu Orca-ER digital camera (Hamamatsu City, Japan) and processed offline using Image J 1.43 software (NIH, USA). Regions of interest of identical size were placed over nerve terminals that displayed an increase on stimulation and the total fluorescence intensity was monitored over time. All statistical analyses were performed using Microsoft Excel and GraphPad Prism (La Jolla, CA) software. The pHluorin fluorescence change was calculated as $\Delta F/F_0$ in all cases.

Estimation of surface Syt1-pHluorin and SV2A-pHluorin was performed by perfusing acidic imaging buffer (substituting 20mM MES for HEPES, pH 5.5) over cultures for 30 seconds (to quench surface Syt1-pHluorin) followed by a 1 min perfusion with standard imaging buffer (pH 7.4). Cultures were then subjected to alkaline imaging buffer (50mM NH_4Cl substituted for 50mM NaCl) for 30 seconds to reveal total Syt1-pHluorin. The surface fraction of Syt1-pHluorin as a percentage of total was estimated using the following equation ((neutral fluorescence – acidic fluorescence / alkali fluorescence – acidic fluorescence) × 100).

3 Substrate specificity of TTBK2

Since its discovery by Japanese scientists in 1995, considerable work has been invested in examining TTBK2's relationship with tau phosphorylation and neurodegeneration. However, the validity of these studies has never been substantiated *in vivo*. In 2007, the identification of TTBK2 truncating mutations, as the cause of spinocerebellar ataxia type 11 (SCA11), reemphasised that TTBK2 has a prominent physiological role in the brain.

Before tackling the pertinent questions regarding TTBK2's physiological function, basic biochemical investigations would require an appropriate tool: an *in vitro* peptide substrate to assay TTBK2's intrinsic activity. However, a basic biochemical characterisation of TTBK2 was never performed before I started my PhD and thus nothing was known about TTBK2 substrate selectivity and specificity. In this chapter, I present an initial biochemical characterisation of TTBK2. To better understand the substrate specificity of TTBK2, I have used a degenerate peptide library approach that provides an unbiased evaluation of the importance of the residues surrounding the site of phosphorylation for an optimal substrate. This initial analysis of TTBK2 substrate specificity has shown that it has a conspicuous preference for a phosphotyrosine residue at the +2 position relative to the phosphorylation site. This information was used to develop an optimised peptide substrate, TTBKtide, to assess TTBK2 catalytic activity.

TTBKtide was subsequently used to evaluate how SCA11 truncating mutations affect kinase activity. SCA11 truncating mutations markedly enhance TTBK2 protein expression but, however, lead to inhibition of TTBK2 kinase activity. TTBK2-knockin mice expressing an SCA11 disease-causing mutation were generated and the inhibition of endogenous protein kinase activity by the SCA11 truncating mutation was confirmed. Also, homozygosity of the SCA11 mutation causes embryonic lethality. These findings will provide the tools and the platform for further investigations into the function and regulation of TTBK2, as well as its role in SCA11.

3.1 Expression and purification of GST-TTBK2-[1-450]WT and GST-TTBK2-[1-450]D163A (kinase inactive).

To explore TTBK2's substrate selectivity, recombinant TTBK2 was expressed in mammalian cells. HEK293 cells were transfected with GST-tagged constructs expressing TTBK2-[1-450]^{WT} and kinase-inactive TTBK2-[1-450]^{D163A}. 36hrs post-transfection, cells were lysed and GST purifications carried out. Purified proteins were subjected to SDS-PAGE and the protein bands visualised using Coomassie staining (Figure 3.1).

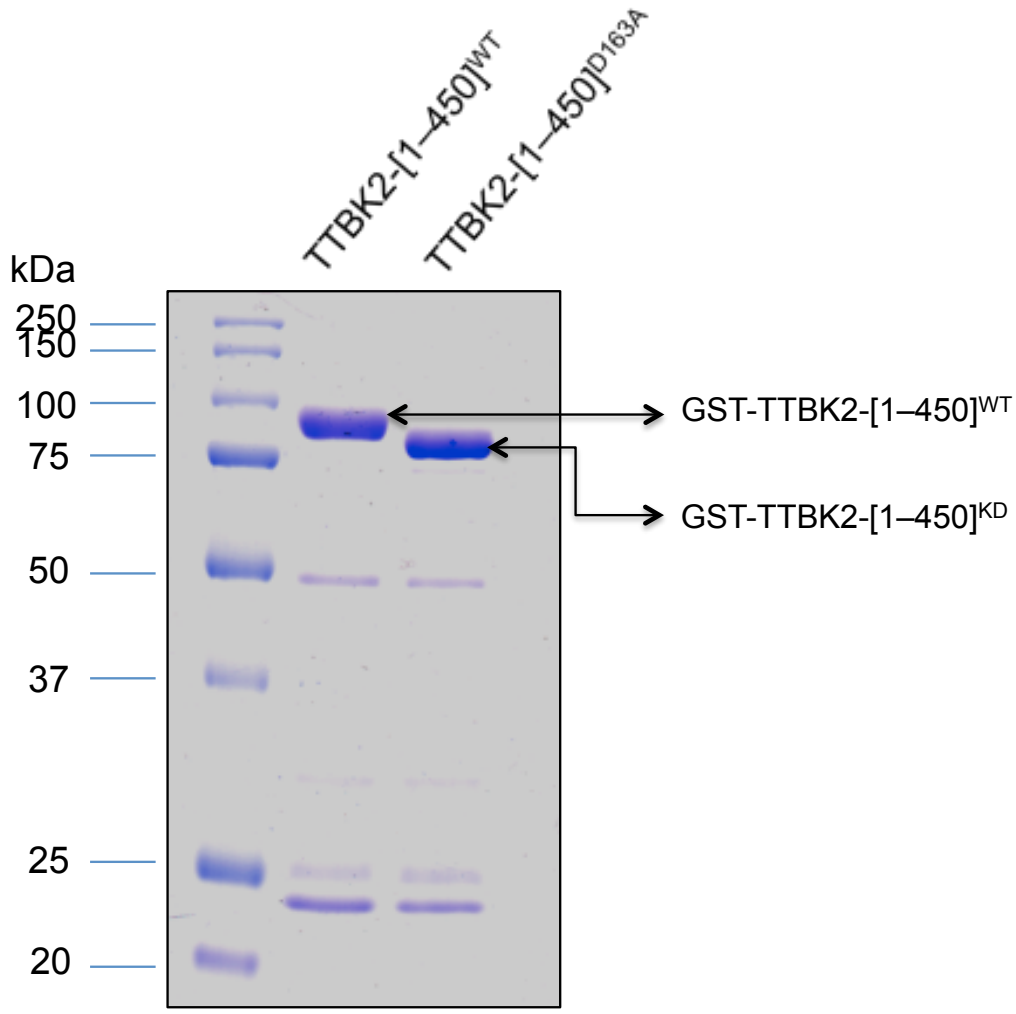

Figure 3.1. Expression and purification of GST-TTBK2-[1-450]^{WT} and GST-TTBK2-[1-450]^{D163A} (kinase inactive). HEK293 cells were transfected with GST-tagged constructs expressing TTBK2-[1-450]^{WT} and kinase-inactive TTBK2-[1-450]^{D163A}. 36hrs post-transfection, cells were lysed and GST purifications carried out. Purified proteins were subjected to SDS-PAGE and the protein bands visualised using Coomassie staining.

Adequate expression of both GST-TTBK2-[1-450]^{WT} and kinase-inactive GST-TTBK2-[1-450]^{D163A} was observed as seen in Figure 3.1. The band shift displayed by

the wild-type protein compared to the kinase-inactive version is due to auto-phosphorylation of the active kinase as ascertained by mass spectrometry (data not shown).

3.2 Analysis of the substrate specificity of TTBK2 by a positional scanning peptide library approach

An unbiased positional scanning peptide library (Hutti et al., 2004, Turk et al., 2006) approach was initially used to probe the substrate specificity preferences of TTBK2. In collaboration with Dr. Lewis Cantley's laboratory (Harvard Medical School), a 'Positional Scanning Peptide Library' was performed. This assay employs 198 biotinylated peptide libraries that each contain a 1:1 mixture of serine and threonine at the central position and one additional position fixed to one of the 20 amino acids, as well as phosphothreonine or phosphotyrosine. Phosphothreonine and phosphotyrosine were included to allow substrate specificity analysis of kinases such as CK1, to which TTBK2 is related, that have preferences for priming phosphorylation sites. All other positions contained an equimolar degenerate mixture of natural amino acids (except serine, threonine and cysteine).

The 198 libraries were screened using [γ-^{32}P] ATP and recombinant TTBK2-[1–450]^{WT} or kinase-inactive TTBK2-[1–450]^{D163A} expressed in HEK-293 cells. Biotinylated peptides were then captured on a streptavidin-coated membrane. The relative amino acid preference at each position was determined by quantifying ^{32}P-radioactivity incorporation following phosphoimaging (Figure 3.2).

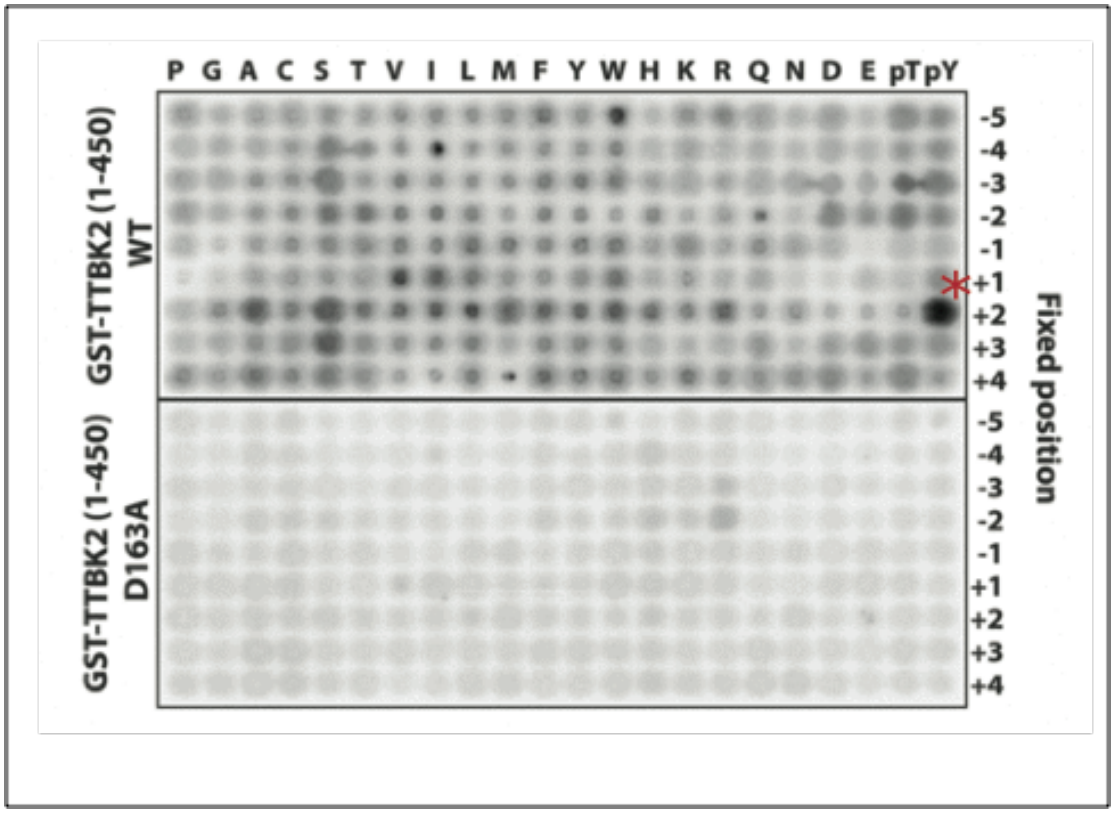

Figure 3.2. Positional scanning peptide library screen. Recombinant HEK-293 purified GST–TTBK2-[1–450]^{WT} (wild-type) and catalytically inactive GST–TTBK2-[1–450]^{D163A} were used to screen a positional scanning peptide library consisting of 198 biotinylated peptide libraries in individual kinase assays. Reaction products were bound to streptavidin-coated membrane and, after washing, phosphorylation was visualised by phospho-imaging. TTBK2 displayed a conspicuous preference for a phosphotyrosine residue at the +2 position, indicated by a red asterisk.

The most salient observation from this peptide library screen was that GST–TTBK2-[1–450]^{WT} has a conspicuous preference for a phosphotyrosine residue at the +2 position downstream from the site of phosphorylation (indicated by a red asterisk in Figure 3.2). This finding was consistently observed in two independent experiments.

Apart from the marked incorporation of radioactive ATP for the +2 phosphotyrosine peptide library, low levels of phosphorylation were detected in a few other libraries e.g. library with serine at -3. However the levels of ATP incorporation in those libraries were not as high as in the +2 phosphotyrosine library. For the screen undertaken with the kinase-inactive GST–TTBK2-[1–450]^{D163A} overall levels of phosphorylation observed were considerably low, and crucially no preference for a +2 phosphotyrosine was detected.

3.3 Elaboration of an optimal TTBK2 peptide substrate, TTBKtide.

TTBK2 is a member of the CK1 family of kinases and it was established that it could phosphorylate a model peptide substrate termed CK1tide that is frequently employed to assess CK1 isoform activity (Marin et al., 1994). CK1δ phosphorylates CK1tide (RRKDLHDDEEDEAMS*ITA) at the serine residue marked with an asterisk (Marin et al., 1994), and Dr. Michale Bouskila (former postdoc in the lab) confirmed that TTBK2-[1–450]^{WT} also phosphorylates CK1tide specifically at this serine residue by solid-phase sequencing (data not shown).

To further delineate the substrate selectivity of TTBK2 and to define the optimal phosphorylation motif for TTBK2, I sought to analyse the kinetics of phosphorylation reactions using a number of different synthetic peptides with variations on the CK1tide sequence. A number of peptides were carefully designed, synthesised and assayed with recombinant GST-TTBK2 [1-450]^{WT} and GST-TTBK2 [1-450]^{KD}.

Firstly, to test the contribution of the residue at the +2 position to TTBK2 substrate recognition and the importance of a phosphotyrosine at this position, three different peptides with variations at the critical +2 position in the CK1tide sequence were generated:

- RRKDLHDDEEDEAMSITA (CK1tide)
- RRKDLHDDEEDEAMSIYA (+2Y peptide)
- RRKDLHDDEEDEAMSIY^{P}A (+2Y^{P} peptide)
- RRKDLHDDEEDEAMSIT^{P}A (+2T^{P} peptide)

Those three peptides and CK1tide were assayed with recombinant GST-TTBK2-[1-450]^{WT} and detailed kinetic analysis to study the relative phosphorylation kinetics of each peptide were carried out and are shown in (Figure 3.3) on the next page.

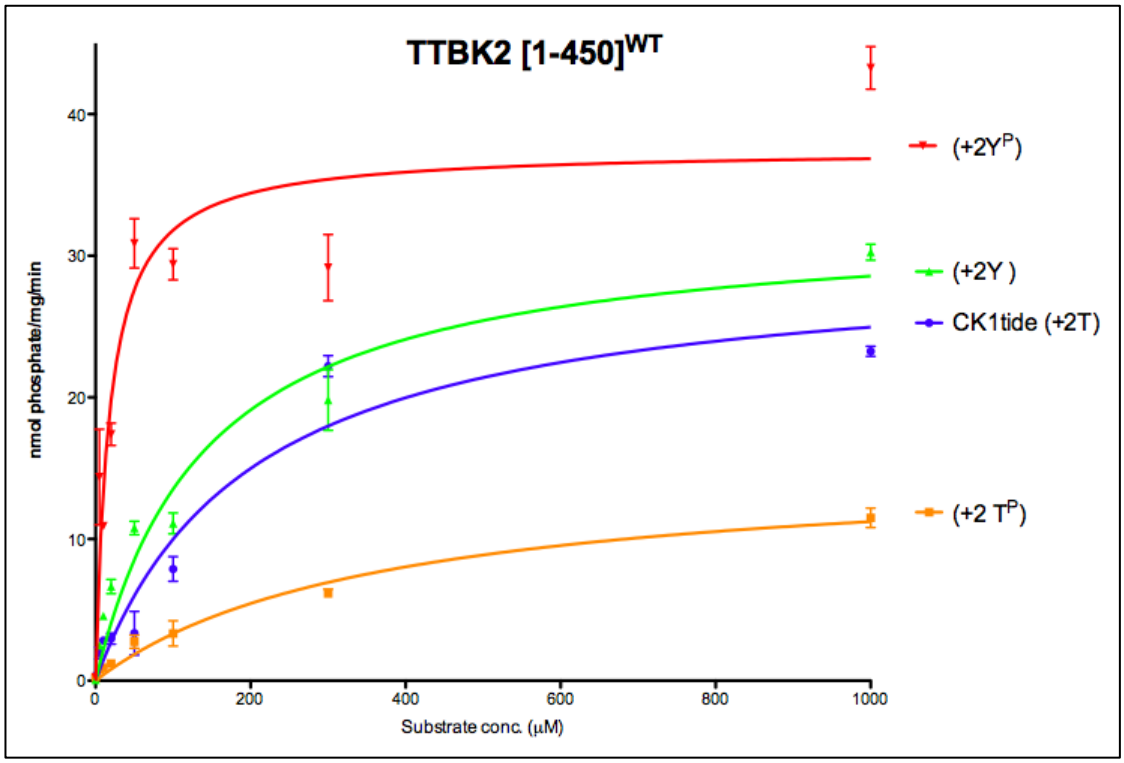

	RRKDLHDDEEDEAMSITA (CK1tide)	RRKDLHDDEEDEAMSIT^{P}A (+2T^{P})	RRKDLHDDEEDEAMSIYA (+2Y)	RRKDLHDDEEDEAMSIY^{P}A (+2Y^{P})
V_{max} (nmol/mg/min)	30.0	15.3	32.6	**37.5**
K_m (μM)	200.0	361.1	141.2	**18.0**

Figure 3.3. Phosphorylation kinetics of synthetic peptides by TTBK2. Three CK1tide variants with with a phosphothreonine, tyrosine and phosphotyrosine at the +2 position were synthesised, and the kinetics of their phosphorylation by GST–TTBK2 [1-450]^{WT} was analysed. K_m and V_{max} values were derived by non-linear regression analysis. Results shown are means±S.D. for three independent experiments.

Replacement of the +2 threonine residue of CK1tide with a tyrosine did not improve the kinetic constants. However, assay of the peptide with a phosphotyrosine at this position produced a substantial improvement in the K_m value. The K_m value of TTBK2 with RRKDLHDDEEDEAMSIY^{P}A as the substrate compared to RRKDLHDDEEDEAMSIYA was 8-fold lower (141.2 μM compared to 18.0 μM) (see table in Figure 3.3) while the V_{max} was only marginally enhanced. A phosphotyrosine residue at the +2 position was therefore a positive determinant for

TTBK2 recognition, and this observation corroborates the finding from the peptide library screen.

The peptide RRKDLHDDEEDEAMSIT^{P}A gave a lower V_{max} and a significantly higher K_m compared to CK1tide. Thus, introducing a phosphothreonine rather than a phosphotyrosine residue at the +2 position failed to enhance TTBK2 activity (Figure 3.3) indicating the specificity of a phosphotyrosine residue at the +2 position as a positive determinant for TTBK2 recognition.

3.3.1 Specificity of the +2 position relative to the phosphorylation site

To establish the importance of having a phosphotyrosine residue at the +2 position relative to other positions, eight further CK1tide derivatives with varying positions of the phosphotyrosine from +4 to -5 relative to the phosphorylatable serine were generated. The peptide sequences were as follows:

- RRKDLHDDEEDEAMSITAY^{P}
- RRKDLHDDEEDEAMSITY^{P}
- RRKDLHDDEEDEAMSIY^{P}A
- RRKDLHDDEEDEAMSY^{P}TA
- RRKDLHDDEEDEAY^{P}SITA
- RRKDLHDDEEDEY^{P}MSITA
- RRKDLHDDEEDY^{P}AMSITA
- RRKDLHDDEEY^{P}EAMSITA
- RRKDLHDDEY^{P}DEAMSITA

TTBK2 assays of those peptides are shown on the next page.

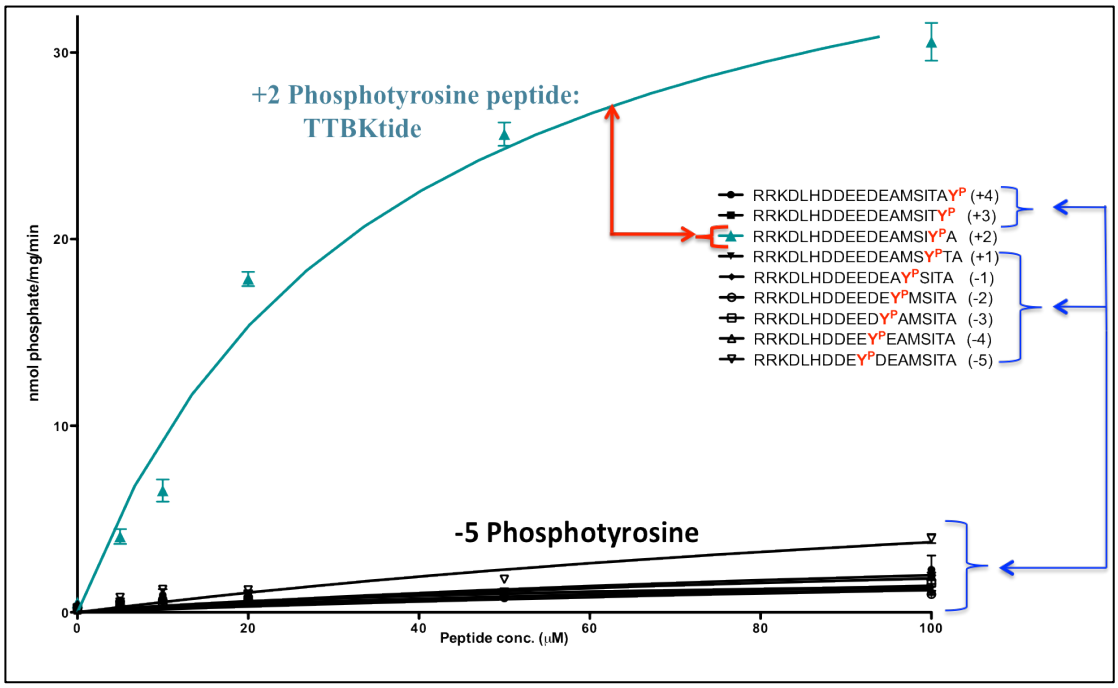

Figure 3.4. Potentiation by phosphotyrosine at +2. Peptides with various positions of the phosphotyrosine residue from +4 to −5 relative to the phosphorylated serine residue were synthesised and analysed for their ability to phosphorylate GST–TTBK2 [1–450]^{WT} purified from HEK-293 cells. K_m and V_{max} values were derived by non-linear regression analysis as described in the Materials and methods section. Results shown are means±S.D. for three independent experiments.

Assays of TTBK2 with those nine peptides showed that the rates of phosphorylation of those peptides were noticeably lower compared to the peptide with a phosphotyrosine at the +2 position (Figure 3.4). This further substantiated the findings of the positional scanning peptide library approach, revealing that introducing a phosphotyrosine residue at only the +2 position, but not at any other position, strongly enhanced peptide phosphorylation.

Collectively, the results of those peptide assays support the view that the substrate recognition of TTBK2 is substantially enhanced by the presence of a phosphotyrosine residue and this recognition is exceptionally specific for a phosphotyrosine at the +2 position. Consequently, the CK1tide peptide with a phosphotyrosine residue at the +2 position was chosen as the optimal peptide to perform TTBK2 activity assays and henceforth named TTBKtide (RRKDLHDDEEDEAMSIY^{P}A).

3.4 Residues phosphorylated by TTBK2

To compare the efficiency with which TTBK2 phosphorylates the serine, threonine or tyrosine residues, I compared the phosphorylation of three variants of TTBKtide in which the phosphorylated residue was either serine or threonine or tyrosine at the phosphoacceptor site. The amino acid sequence of the three peptides assayed were as follows:

- RRKDLHDDEEDEAMSIY^{P}A
- RRKDLHDDEEDEAMTIY^{P}A
- RRKDLHDDEEDEAMYIY^{P}A

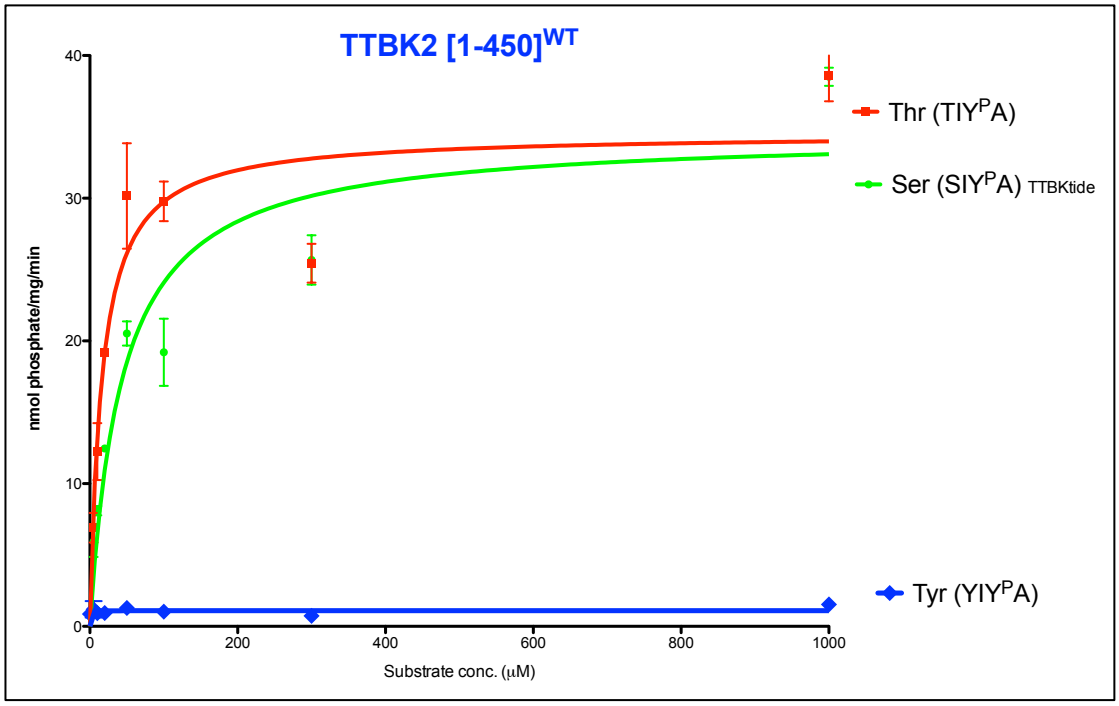

	RRKDLHDDEEDEAMSIY^{P}A (TTBKtide)	RRKDLHDDEEDEAMTIY^{P}A	RRKDLHDDEEDEAMYIY^{P}A
V_{max} (nmol/mg/min)	**37.5**	38.5	NP
K_m (μM)	**18.0**	16.0	NP

Figure 3.5. Phosphorylation of TTBKtide variants with threonine and tyrosine as the phosphoacceptor. Three TTBKtide variants with serine, threonine and tyrosine residues at the phospho-acceptor position were synthesised, and the kinetics of their phosphorylation by GST–TTBK2-[1-450]^{WT} was analysed. K_m and V_{max} values were derived by non-linear regression analysis. NP* denotes that the peptide was phosphorylated too poorly to undertake accurate kinetic analysis. Results shown are means±S.D. for three independent experiments.

Substituting the phosphoacceptor serine with a threonine residue did not alter the efficacy of the peptide as a TTBK2 substrate, with similar K_m and V_{max} values (see

table in Figure 3.5). However, replacement of the phosphoacceptor site with a tyrosine residue resulted in a peptide that no longer served as a TTBK2 substrate (Figure 3.5). Thus, TTBK2 showed no preference for serine or threonine residues as the phosphoacceptor whereas tyrosine residues are not phosphorylated by TTBK2. This result is consistent with the classification of TTBK2 as a serine/threonine kinase.

3.5 Substrate selectivity of CK1 superfamily enzymes

Since TTBK2 is a member of the CK1 superfamily of kinases. I evaluated whether other CK1 family enzymes exhibited the same preference for a phosphotyrosine at +2. To this end, CK1delta (CK1δ) was assayed against CK1tide, unphosphorylated TTBKtide and TTBKtide. The three peptides used were as follows:

- RRKDLHDDEEDEAMSITA
- RRKDLHDDEEDEAMSIYA
- RRKDLHDDEEDEAMSIY^{P}A

The three above peptides were assayed with GST-CK1δ-[1-294] expressed in bacteria and the kinetics are detailed in Figure 3.6 below.

Assays of those peptides with CK1δ showed that it displayed a higher affinity for TTBKtide than for its unphosphorylated derivative; attested by a 2-fold lower K_m (74.1 μM compared to 172.4 μM). The difference in V_{max} between the two peptides was clear: a 3-fold higher V_{max} was observed for TTBKtide when compared to unphosphorylated TTBKtide (563.5 Units/mg compared to 187.2 Units/mg, where 1 unit is the incorporation of 1 nmol of phosphate per minute).

Importantly, CK1tide was a poorer substrate compared to the other two peptides. TTBKtide produced an almost 10-fold higher V_{max} (563.5 U/mg compared to 58.1 U/mg) and a marginally lower K_m (74.1 U/mg compared to 103.1 U/mg) than CK1tide. Similar kinetics were observed with other CK1 isoforms, CK1α, CK1γ and CK1ε (data not shown). These findings support the notion that a phosphotyrosine at +2 may be also be a determinant of substrate recognition by CK1 isoforms.

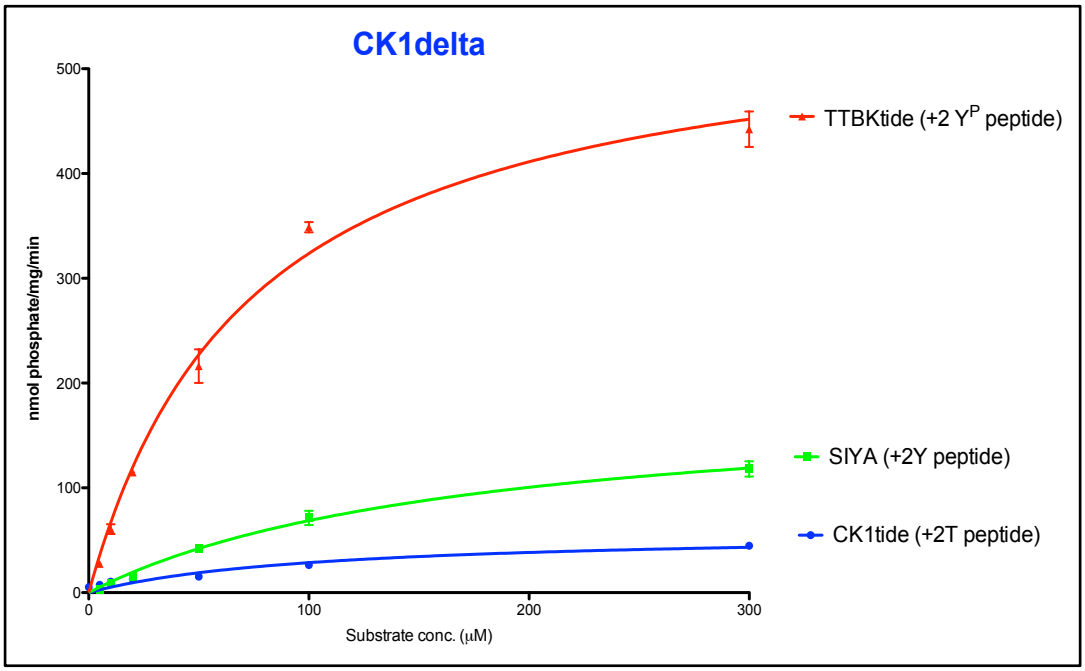

	RRKDLHDDEEDEAMSITA	RRKDLHDDEEDEAMSIYA	RRKDLHDDEEDEAMSIY^{P}A
V_{max} (nmol/mg/min)	58.1	187.2	563.5
K_m (μM)	103.1	172.4	74.1

Figure 3.6. Phosphorylation of CK1tide, unphosphorylated TTBKtide and TTBKtide by CK1 delta. The kinetics of the phosphorylation of the three peptides by GST–CK1δ-[1-294]^{WT} was analysed. K_m and V_{max} values were derived by non-linear regression analysis. Results shown are means±S.D. for three independent experiments.

The importance of a phosphotyrosine at +2 had not been previously recognised. Historically, CK1tide has been used as the standard peptide used to assay CK1 activity. TTBKtide is therefore a better *in vitro* peptide substrate to assay intrinsic CK1 activity.

3.6 CK1 consensus phosphorylation motif

Studies utilising peptides based on the amino acid sequence of glycogen synthase showed that CK1 preferentially phosphorylates peptides containing a phosphoserine residue N-terminal to the Ser/Thr targeted for phosphorylation (Nakielny et al., 1991). Other studies using synthetic peptides defined a minimal recognition motif: S^{P}-X-X-S/T (Kuret et al., 1985, Flotow et al., 1990, Flotow and Roach, 1991).

This recognition motif indicates that the phosphorylation of serine and threonine residues by CK1 requires the preceding phosphorylation of amino acid residues N-terminal to the target site. This requirement of a priming phosphorylation of amino acid by another kinase restricted CK1 to a function in the hierarchical phosphorylation of substrates. However, further studies revealed that a cluster of acidic amino acids N-terminal of the target serine/threonine and an acidic amino acid in position n-3 could substitute for the phosphoamino acid effectively (Flotow and Roach, 1991).

3.6.1 Impact of a phosphoserine residue at -3 on substrate recognition by TTBK2 and CK1δ

To compare the requirement for an N-terminal -3 phosphoserine to that of a +2 phosphotyrosine, four more TTBKtide (RRKDLHDDEEDEAMSIY^{P}A) variants with substitutions at the -3 position were designed and assayed. The peptides sequences were as follows:

- RRKDLHDDEEDSAMSIYA
- RRKDLHDDEEDSAMSIY^{P}A
- RRKDLHDDEEDS^{P}AMSIYA
- RRKDLHDDEEDS^{P}AMSIY^{P}A

Assays of those above four peptides with TTBK2 are shown on the next page.

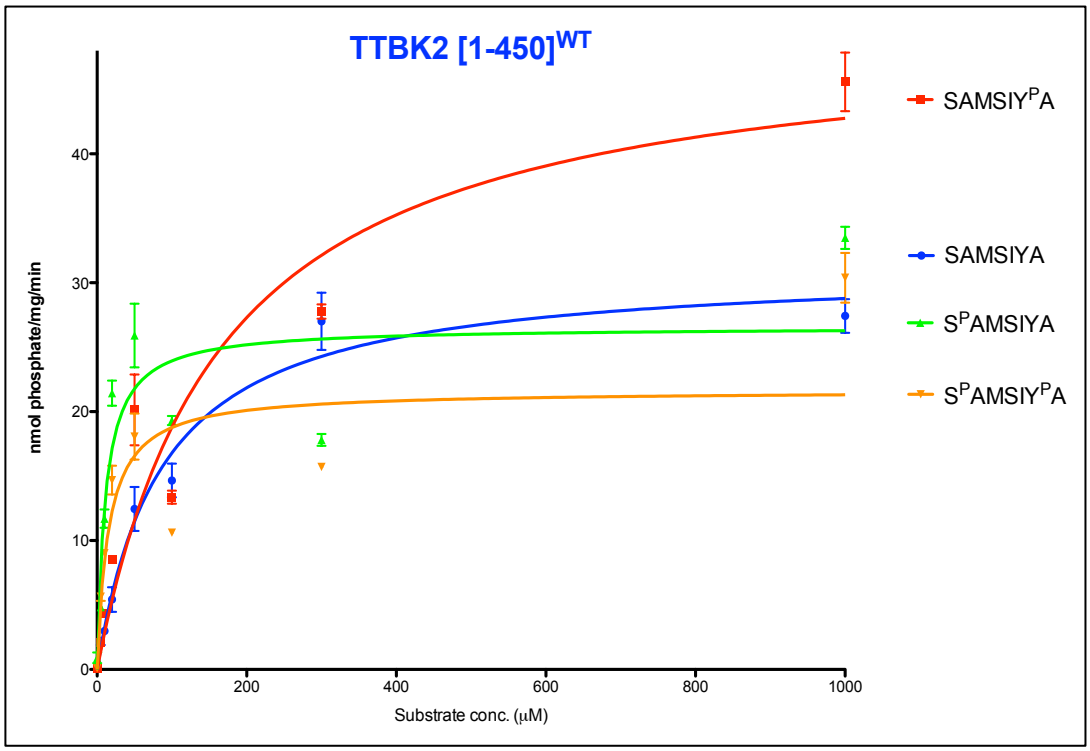

	RRKDLHDDEEDSAMSIYA	RRKDLHDDEEDSAMSIY^{P}A	RRKDLHDDEEDS^{P}AMSIYA	RRKDLHDDEEDS^{P}AMSIY^{P}A
V_{max} (nmol/mg/min)	**31.3**	**49.8**	**26.6**	**21.6**
K_m (μM)	**86.1**	**65.0**	**11.0**	**15.3**

Figure 3.7. Phosphorylation of CK1tide variants with serine/phosphoserine at -3 and tyrosine/phosphotyrosine at +2 by TTBK2. Four CK1tide variants with serine/phosphoserine at -3 and tyrosine/phosphotyrosine at +2 were synthesised, and the kinetics of their phosphorylation by GST-TTBK2-[1-450]^{WT} was analysed. K_m and V_{max} values were derived by non-linear regression analysis. Results shown are means±S.D. for three independent experiments.

The K_m of the peptide RRKDLHDDEEDSAMSIY^{P}A was similar to that of the peptide RRKDLHDDEEDSAMSIYA (65.0 μM compared to 86.1 μM) and the change in V_{max} values between the two peptides is approximately 1.5-fold. This indicates that the presence of a serine residue at -3 (instead of glutamic acid in the TTBKtide sequence) weakens the recognition of the +2 phosphotyrosine by TTBK2.

The two peptides with phosphoserine at -3 yielded lower V_{max} values than the peptides with serine at -3. However, the K_m values of those two peptides are significantly lower than the peptides with serine at -3 (11.0 μM and 15.3 μM for the peptides with phosphoserine at -3 compared to 86.1 μM and 65.0 μM for the peptides

with serine at -3). This suggests that the residue at the -3 position influences the recognition of the +2 phosphotyrosine.

It is known that a phosphoserine at the -3 position is a critical determinant for substrate recognition by CK1 enzymes. To evaluate the impact of a tyrosine/phosphotyrosine at +2 on the substrate recognition of CK1, those four peptides were also assayed with CK1δ and the results are shown in Figure 3.8 below.

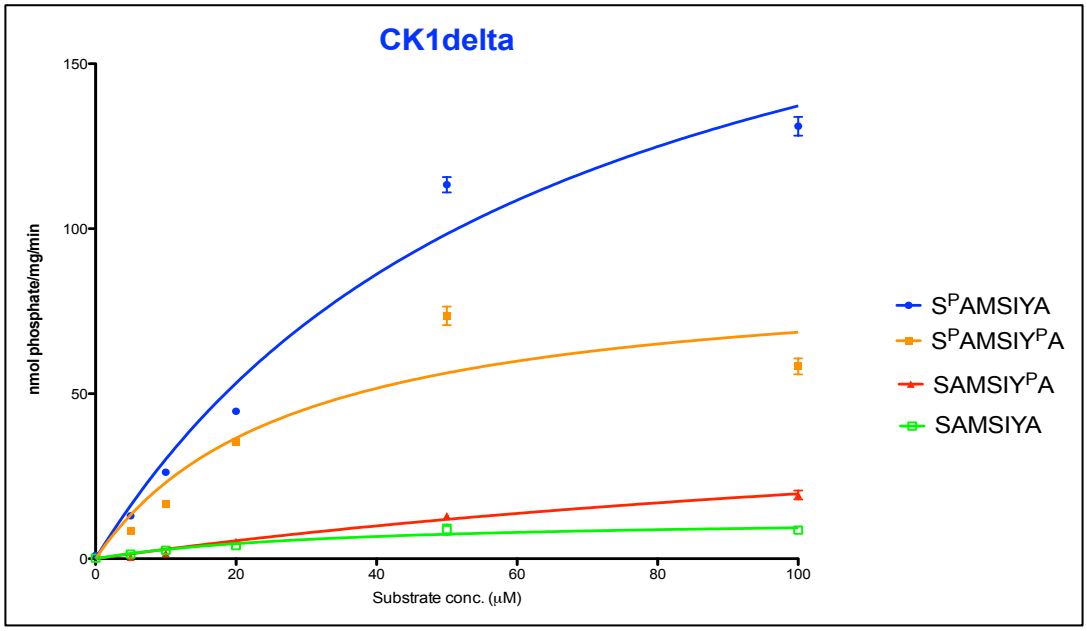

	RRKDLHDDEEDSAMSIYA	RRKDLHDDEEDSAMSIYPA	RRKDLHDDEEDSPAMSIYA	RRKDLHDDEEDSPAMSIYPA
V_{max} (nmol/mg/min)	**12.7**	**56.6**	**226.7**	**87.9**
K_m (μM)	**ND**	**187.3**	**65.2**	**28.1**

Figure 3.8. Phosphorylation of CK1tide variants with serine/phosphoserine at -3 and tyrosine/phosphotyrosine at +2 by CK1δ. Four CK1tide variants with serine/phosphoserine at -3 and tyrosine/phosphotyrosine at +2 were synthesised, and the kinetics of their phosphorylation by GST–CK1δ-$[1\text{-}294]^{WT}$ was analysed. K_m and V_{max} values were derived by non-linear regression analysis. Results shown are means±S.D. for three independent experiments. ND: not determined.

With CK1δ, the K_m of the peptide RRKDLHDDEEDSAMSIY^{P}A was 5-fold higher than that of the peptide RRKDLHDDEEDSAMSIYA (187.3 μM compared to 35.4 μM), which reflects the discrepancy in V_{max} values between the two peptides: approximately 5-fold (56.6 U/mg compared to 12.7 U/mg). Remarkably, the two peptides with phosphoserine at -3 yielded considerably higher V_{max} values than the

peptides with serine at -3 position. The peptide RRKDLHDDEEDS^{P}AMSIYA had the highest V_{max} (226.7 U/mg) while the peptide with two phosphorylated residues (RRKDLHDDEEDS^{P}AMSIY^{P}A) had an approximately 3-fold lower V_{max} (87.9 U/mg). The difference in K_m values between these two peptides is approximately two-fold (65.2 μM compared to 28.1 μM).

While CK1δ showed a similar preference for a +2 phosphotyrosine, the impact on its recognition may vary depending on the residue at the -3 position. The requirement for a priming phosphorylation at -3 is known for CK1 kinases and these data suggest that a +2 phosphotyrosine may also act as an alternative priming site for substrate recognition.

3.7 Molecular basis for phosphate priming

CK1 isoforms possess a well-known requirement for priming phosphorylation (Flotow et al., 1990, Flotow and Roach, 1991, Nakielny et al., 1991). The crystal structures of yeast CK1 (Xu et al., 1995) (PDB code 1EH4) and human CK1δ (Longenecker et al., 1996) (PDB code 1CKI) reveal the presence of a sulphate-binding groove on the small lobe of the kinase domain, predicted to function as the phosphate-priming site (Figure 3.9A). This pocket consists of four highly conserved basic lysine and arginine residues on CK1 isoforms and form ionic interactions with the sulfate residue (Figure 3.9A). In CK1 those residues are Lys38 (site A), Lys130 (site B), Arg168 (site C) and Lys171 (site D). Sequence alignments show that three of these residues are conserved in TTBK1 and TTBK2 (Lys50, Lys143 and Arg181 in the TTBK2 protein sequence). The fourth residue is an alanine in TTBK2 (Ala184) as well as in TTBK1 (Figure 3.9B).

To verify whether these residues on TTBK2 could be involved in enhancing the recognition and phosphorylation of +2-phosphotyrosine-containing substrates, the effect of mutations of Lys50, Lys143, Arg181 and Ala184 on the phosphorylation of TTBKtide and its unphosphorylated counterpart was investigated. Mutation of Lys50 or Lys143 to either glutamic acid or alanine inactivated/destabilised TTBK2 (Figure 3.10A) and equivalent mutations in CK1δ had similar effects (Figure 3.10B).

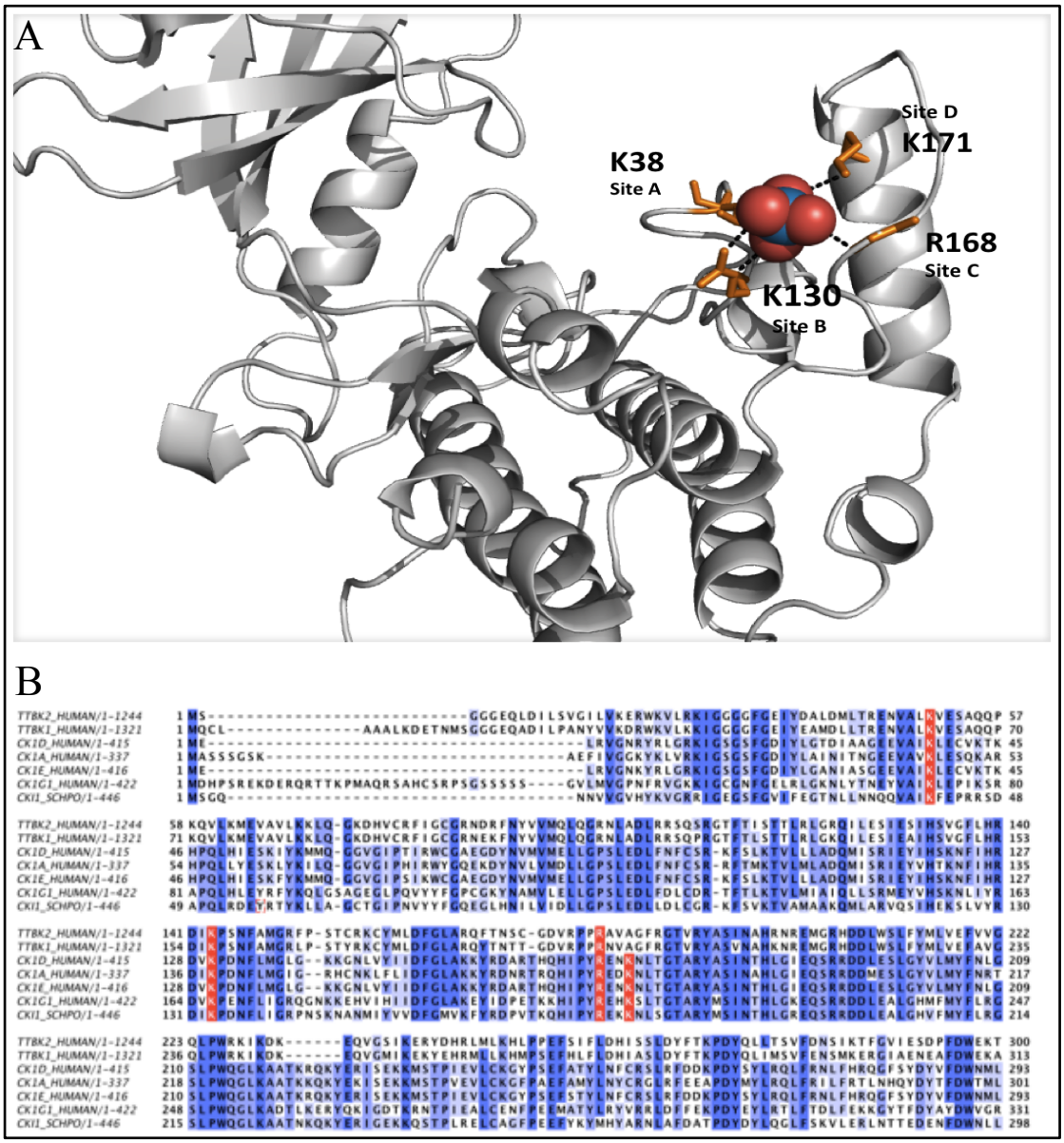

Figure 3.9. Molecular basis for phosphate priming. (A) High-resolution structure of CK1δ protein (from The PyMOL Molecular Graphics System, Version 1.5.0.4 Schrödinger, LLC.) showing the sulphate-binding site on the C-lobe of the kinase domain predicted to function as the phosphate-priming region (Longenecker et al., 1996). Lys38 (site A), Lys130 (site B), Arg168 (site C) and Lys171 (site D) form ionic interactions with the sulphate molecule and are shown in orange. (B) Sequence alignment of the indicated species of TTBK1, TTBK2 and CK1 family enzymes showing the sequence conservation of the sulphate-binding residues (highlighted in red).

In contrast, mutation of Arg181 or Ala184 did not affect stability (Figure 3.10A) or the intrinsic TTBK2 kinase activity as judged by the ability of these mutants to phosphorylate a peptide lacking the +2 phosphotyrosine residue (Figure 3.10A). However, the ability of TTBK2 [R181A or R181E] or TTBK2 [A184G or A184E] mutants to phosphorylate tyrosine-phosphorylated TTBKtide was markedly impaired (K_m values of 100-150 μM compared with 18 μM for wild-type TTBK2) (Figure 3.11). Assays of the corresponding CK1 delta mutants yielded similar results (Figure

3.10B). These results suggest that TTBK2 possesses a phosphate-priming groove similar to CK1, and that it recognises +2 phosphotyrosine residues as well as N-terminal phosphoserine/phosphothreonine at -3.

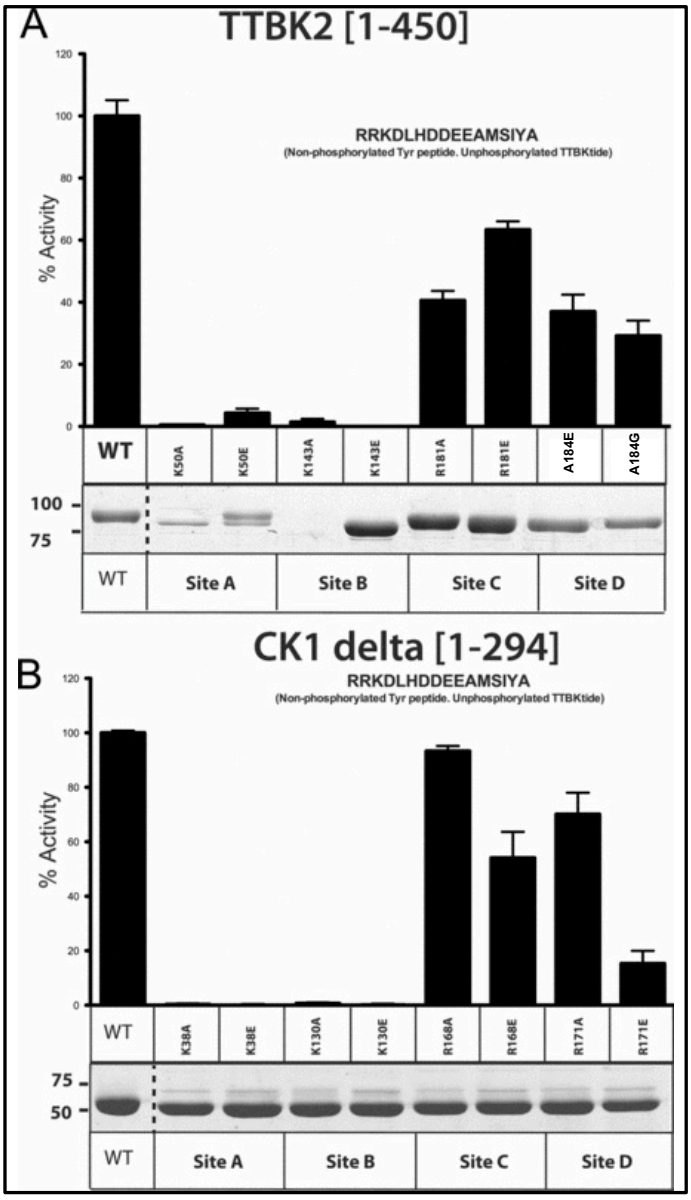

Figure 3.10. Expression and activity of phosphate-binding groove mutants of TTBK2 and CK1δ. (A) HEK-293 cells were transiently transfected with the indicated forms of GST-tagged TTBK2. After 36 h of transfection, cells were lysed and the GST-TTBK2 proteins affinity purified on glutathione–sepharose. Equivalent volumes of GST-TTBK2 [corresponding to 50 ng of wildtype (WT) protein] were subjected to a kinase assay employing the indicated dephosphorylated peptide. Results are means for triplicate experiments repeated twice with similar results. Equivalent volumes of GST-TTBK2 (corresponding to 500 ng of wild-type) were subjected to SDS/PAGE and the gels stained with Coomassie Blue. The wild-type controls were run on the same gel, but as a space was left in the adjacent lane the image was cut, indicated by the dotted line. (B) As in (A) except that CK1δ was purified from *E. coli*.

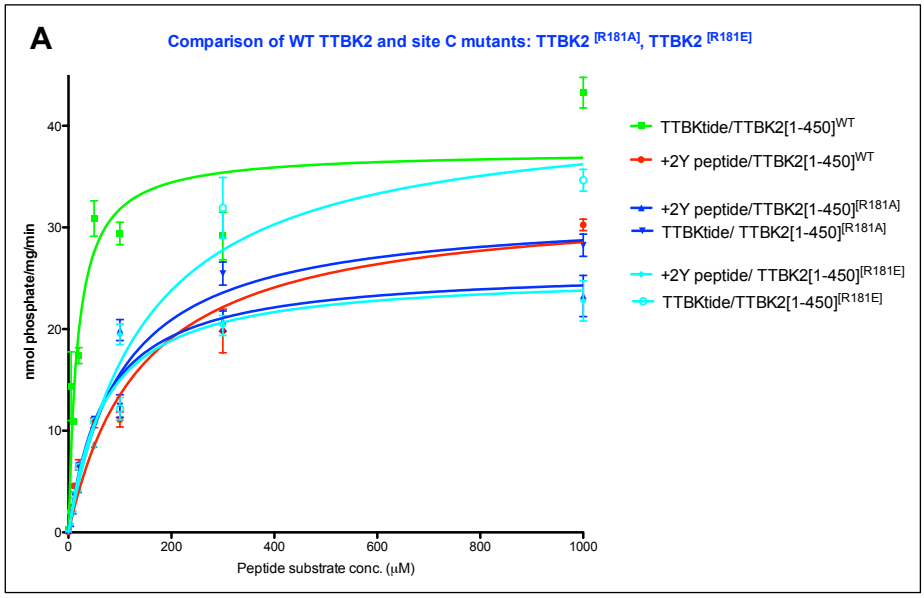

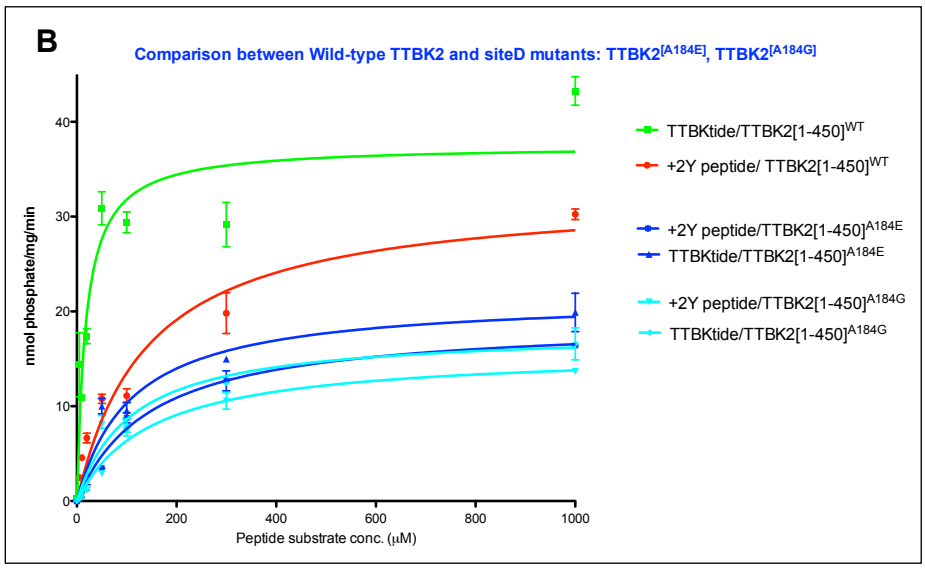

C		RRKDLHDDEEDSAMSIYA (non-Phosphorylated TTBKtide or +2Y peptide)		RRKDLHDDEEDSAMSIY^{P}A (TTBKtide)	
		K_m (μM)	V_{max} (U/mg)	K_m (μM)	V_{max} (U/mg)
TTBK2 WT	WT	141	33	18	38
TTBK2 Site C mutants	R181A	70	26	103	32
	R181E	70	26	150	42
TTBK2 Site D mutants	A184G	149	19	108	22
	A184E	149	16	108	18

Figure 3.11. The indicated GST–TTBK2-[1–450] mutant proteins expressed in Figure 3.10A were tested for their ability to phosphorylate TTBKtide (RRKDLHDDEEDEAMSIY^{P}A) and a variant of TTBKtide (RRKDLHDDEEDEAMSIYA) where the tyrosine at the +2 position was not phosphorylated. A) Kinetic data from TTBK2 site C mutants; B) Kinetic data from TTBK2 site D mutants; C) Table summarising kinetic constants. K_m and V_{max} values were derived by non-linear regression analysis.

3.8 Generation of TTBK2-[family-1 mutation]-knockin mice

Knockin mice that precisely mimic the one-base insertion of adenosine in exon 13 at nucleotide 1329, observed in SCA11 family 1, were generated by the TaconicArtemis company (Bouskila et al., 2011). Heterozygous TTBK2$^{fmly1/+}$ (where fmly1 is family 1) mice were viable and fertile. The oldest TTBK2$^{fmly1/+}$ mice analysed were ~1 year of age and display no overt phenotype. Anatomical dissection of 1-year-old mouse brains also revealed no discernable abnormality. Breeding of heterozygous TTBK2$^{fmly1/+}$ mice resulted in no homozygous TTBK2$^{fmly1/fmly1}$ mice being born, indicating that the homozygous mutation resulted in embryonic lethality.

Dissection of embryos at different stages of development showed that at E10 (embryonic day 10) TTBK2$^{fmly1/fmly1}$ embryos were detected at the expected Mendelian frequency (Figure 3.12A), but displayed major abnormalities compared with littermate TTBK2$^{fmly1/+}$ or TTBK2$^{+/+}$ embryos. By stage E11, no homozygous TTBK2$^{fmly1/fmly1}$ embryos were observed, suggesting that these embryos perished before this stage. Homozygous E10-TTBK2$^{fmly1/fmly1}$ embryos were developmentally delayed, lacking prominent subdivisions of the developing brain, and were smaller than wild-type littermates (Figure 3.12B). These embryos failed to complete embryonic turning movements or undergo normal caudal extension of the body; in several cases the rudimentary caudal body, which contained some somites (future vertebrae, muscle and dermis) and spinal cord, remained folded back on more rostral tissues. This distortion and underdevelopment of the main body axis (Figure 3.12B) are the probable causes of embryonic lethality.

3.9 Expression and activity of mutant TTBK2 in tissues and fibroblasts derived from knockin mice

Endogenous TTBK2 expression and activity in various mouse tissues was analysed. This revealed significantly higher levels of TTBK2 protein and activity in brain and testes than other tissues investigated (Figure 3.13A). In wild-type TTBK2$^{+/+}$ brain and testes, TTBK2 migrated on an SDS/PAGE gel at the expected ~150 kDa size. As predicted, in tissues of the heterozygous TTBK2$^{fmly1/+}$ mice, the level of full-length

TTBK2 was reduced by ~50% and a truncated form of TTBK2 migrating at ~50 kDa that was not seen in the wild-type mice was observed (Figure 3.13B).

A

Genotype	+/+	+/-	-/-	Total
Pups number	54	62	0	116

B

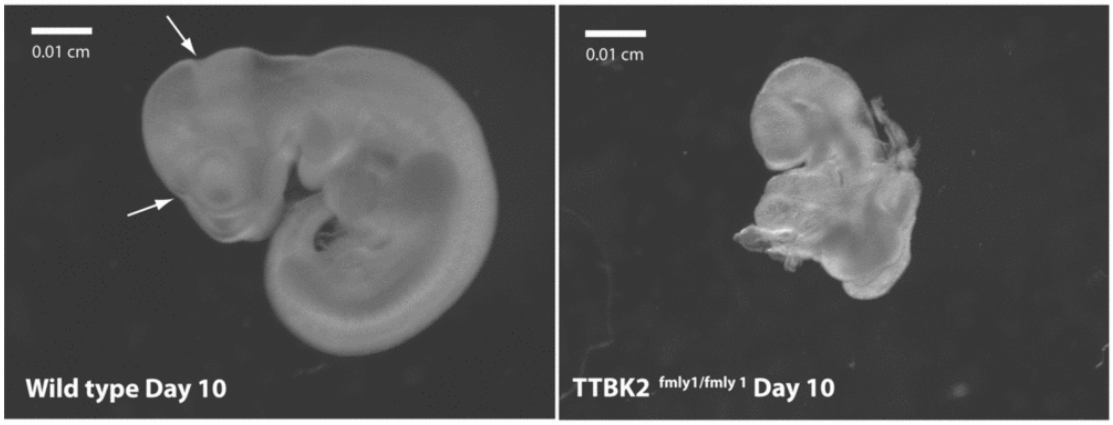

Figure 3.12. Generation of TTBK2-(family-1 mutation)-knockin mice. (A) TTBK2$^{fmly1/+}$ mice were mated and the progeny genotyped. The number of mice obtained is indicated for each genotype. (B) Wild-type and homozygous TTBK2$^{fmly1/fmly1}$ embryos at E10 were detected at the expected Mendelian frequency. Mutant embryos are smaller and developmentally delayed, lacking prominent subdivisions of the brain (arrows on the wild-type embryo). Incomplete embryonic turning movements may result in failure to extend the body axis. A total of 27 separate E10 TTBK2$^{fmly1/fmly1}$ embryos were analysed and similar phenotypes were observed.

Endogenous TTBK2 catalytic activity after immunoprecipitation from brain and testes extracts was assayed against the TTBKtide peptide substrate. These experiments revealed that TTBK2 activity was reduced ~40–50% in tissues derived from heterozygous TTBK2$^{fmly1/+}$ compared with wild-type littermate animals, consistent with the view that the truncating mutation suppresses TTBK2 catalytic activity (Figure 3.13B).

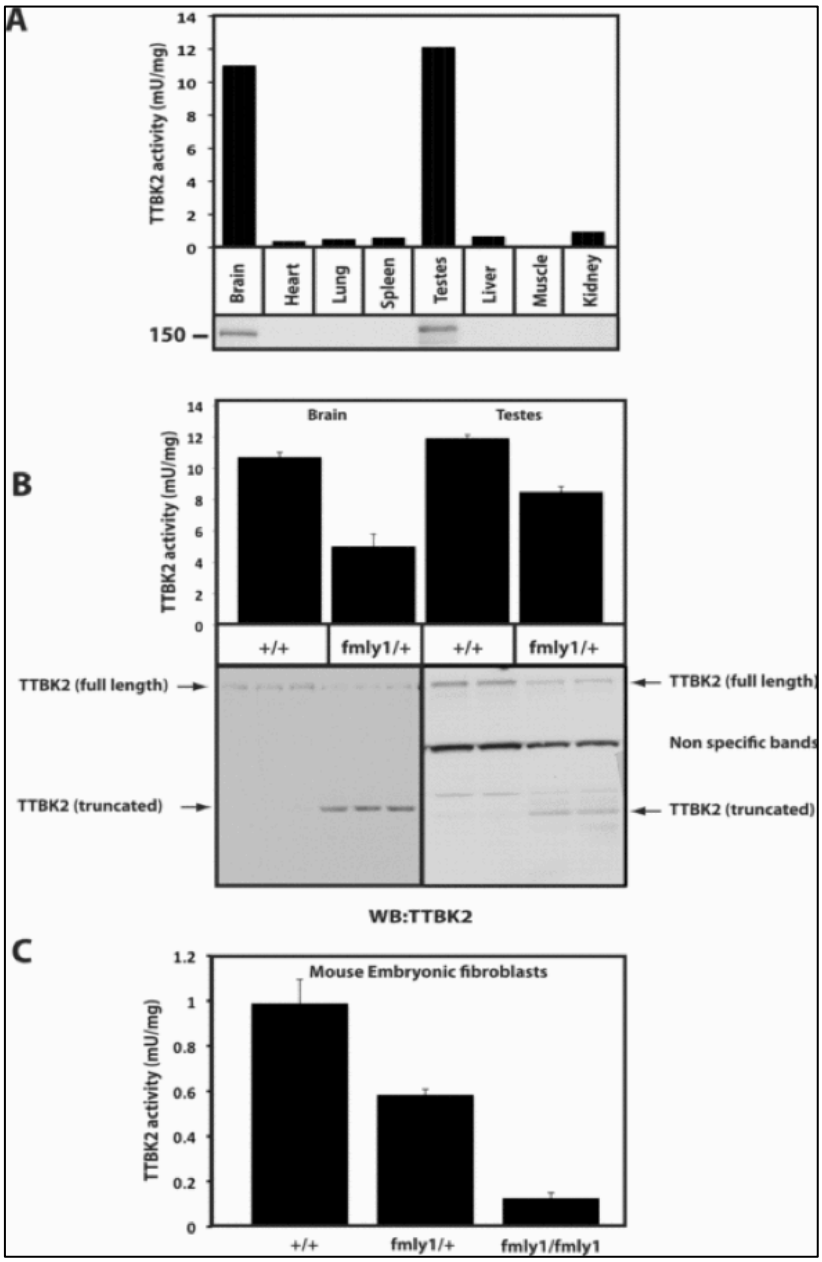

Figure 3.13. Study of TTBK2 in wild-type and TTBK2$^{fmly1/+}$ knockin mice. (A) The indicated tissue extracts were generated from wild-type mice. Extracts were immunoblotted for TTBK2 (lower panel) or TTBK2 was immunoprecipitated and subjected to a TTBK2 kinase assay employing TTBKtide as the peptide substrate (upper panel). Results are means of duplicate experiments that were repeated four separate times with similar results. (B) Brain and testes lysates were generated from TTBK2$^{+/+}$ and TTBK2$^{fmly1/+}$ mice and subjected to immunoblot or TTBK2 kinase assay analysis, as in (A). (C) MEFs were generated from TTBK2$^{+/+}$, TTBK2$^{fmly1/+}$ and TTBK2$^{fmly1/fmly1}$ E10 embryos. TTBK2 activity was assessed following immunoprecipitation as in (A). Owing to the low levels of TTBK2 protein expressed in MEFs and high antibody background in immunoprecipitates, we were unable to detect expression of TTBK2 by immunoblot analysis. Results in (B) and (C) are means±S.D.

TTBK2 activity in mouse embryonic fibroblasts (MEFs) derived from wild-type TTBK2$^{+/+}$, heterozygous TTBK2$^{fmly1/+}$ and homozygous TTBK2$^{fmly1/fmly1}$ littermate stage-E10 embryos was also assessed. TTBK2 activity derived from homozygous

TTBK2$^{fmly1/fmly1}$ cells was ~90% lower than activity observed in wild-type TTBK2$^{+/+}$ fibroblasts (Figure 3.13C). The heterozygous TTBK2$^{fmly1/+}$ displayed intermediate TTBK2 activity.

3.10 Discussion

I have undertaken the first characterisation of TTBK2 catalytic activity and substrate specificity, and found that it possesses a marked preference for a phosphotyrosine residue at the +2 position from the site of phosphorylation (Figure 3.3). The substrate selectivity of CK1 superfamily kinases is known to be directed towards phosphate groups and one of the most-studied consensus phosphorylation sites for CK1 isoforms is S^P/T^P-X-X-S/T, where S^P/T^P refers to a phosphoserine or phosphothreonine, X refers to any amino acid and the underlined residue refers to the target site (Flotow et al., 1990, Flotow and Roach, 1991, Nakielny et al., 1991). In the case of CK1 isoforms, the priming phosphorylation site is at the -3 position rather than at the +2 position for TTBK2. If both TTBK2 and CK1 use a similar phosphate-binding site within their catalytic domain, there would need to be marked differences in the mechanism and orientation at which primed phosphorylated substrates interact with CK1 and TTBK2.

Sequence comparisons with CK1 isoforms indicate that TTBK2 possesses a phosphate-priming binding site in its catalytic domain equivalent to that in the related CK1 isoforms. Mutating two key conserved residues within this putative phosphate-binding groove (Arg181 or Ala184) did not affect the ability of TTBK2 to phosphorylate a non-tyrosine-phosphorylated peptide, but inhibited phosphorylation of a tyrosine-phosphorylated peptide (Figure 3.9). The residues making up this putative phosphate-binding pocket are conserved on TTBK1, suggesting that this isoform may also possess a preference for +2-residue phosphotyrosine priming. The key difference in the putative phosphate-binding groove between CK1 and TTBK1/TTBK2 is the presence of a non-basic alanine residue in TTBK1 and TTBK2 rather than a basic lysine residue in all CK1 isoforms. It would be interesting to explore whether this contributes towards the preference of TTBK2 for phosphotyrosine rather than phosphoserine/phosphothreonine priming in CK1 isoforms.

In future work, it would be interesting to co-crystallise the catalytic domain of TTBK2 with a +2-tyrosine-phosphorylated peptide to define the molecular mechanism by which TTBK2 interacts with such substrates and establish whether this putative phosphate-binding groove is involved. The structure of CK1 bound to an S^P/T^P-X-X-S/T-motif-containing peptide has not been reported, but would be of interest to compare it with that of TTBK2. It would also be important to mine phosphorylation-site databases for proteins phosphorylated on S/T-X-Y^P motifs and determine whether any of these proteins might comprise physiological substrates for TTBK2.

The optimal phosphorylation motif for TTBK2 was determined by oriented peptide library screening and the results were corroborated by a detailed kinetic analysis of individual peptides containing substitutions at crucial positions. This has enabled the elaboration of an optimal peptide substrate for assessing TTBK2 activity (TTBKtide: RRKDLHDDEEDEAMSIY^{P}A) that is phosphorylated with a K_m of 18μM and a V_{max} of 38 units/mg.

3.10.1 Disease-causing TTBK2 mutations markedly increase protein expression and inhibit kinase activity

TTBKtide was used to assay intrinsic TTBK2 activity to determine the effect of SCA11 truncating mutations on TTBK2 activity. These activity assays showed that two familial SCA11 mutations analysed induce a reduction in TTBK2 protein kinase activity. Truncation of TTBK2 at residue 450, in close proximity to where the familial TTBK2 truncating mutations occur, suppressed TTBK2 activity. The observations that TTBK2 immunoprecipitated from TTBK2$^{fmly1/+}$ mice possessed ~40% less activity (Figure 3.13B) and TTBK2 immunoprecipitated from TTBK2$^{fmly1/fmly1}$ MEFs (Figure 3.13C) had ~10-fold lower activity also support the notion that SCA11 mutations drastically reduce endogenous TTBK2 activity. Thus these findings indicate that loss of TTBK2 activity could underpin the development of SCA11 in patients.

The developmental delay and small size of homozygous TTBK2$^{fmly1/fmly1}$ embryos are consistent with a role for TTBK2 activity in the regulation of fundamental cellular processes, such as cell proliferation. The failure of embryonic turning and underdevelopment of the body axis might also lead to a poor placental connection and hence embryonic lethality.

3.10.2 Signalling specificity of Ser/Thr kinases

As key signalling enzymes, protein kinases participate in the regulation of multiple cellular responses and have evolved two properties that are essential for their function: sensitive means of regulation and high specificity for substrates. Although protein kinase active sites do possess preferred target phosphorylation sequences, this stereochemical complementarity is not stringent enough; often they cannot entirely explain the *in vivo* specificity of kinases.

Many protein kinases display clear preferences for the amino acid sequence immediately surrounding the phosphorylated residue in the substrate (Kemp et al., 1975). However, in many cases, these substrate motif preferences are not sufficient to predict functional connectivity of kinases: Some ideal motifs do not appear to be endogenous substrates, and conversely, some known endogenous substrates do not match ideal profiles (Miller, 2003, Biondi and Nebreda, 2003). In addition, certain kinases appear to be quite promiscuous for minimal peptide substrates (Biondi and Nebreda, 2003).

Protein kinases have evolved several biochemical mechanisms, through which specificity is generated during signal transduction. These include subcellular co-localisation, interaction with substrates via a scaffolding protein, modular docking interactions and specific protein kinase-substrate docking mechanisms (Pawson and Nash, 2000).

3.10.3 Use of distributed surfaces for recognition

The use of docking site interactions has emerged as a common mechanism used by certain Ser/Thr kinases to achieve both selectivity and regulation (Biondi and Nebreda, 2003, Holland and Cooper, 1999). Docking interactions involve a docking groove on the kinase that is distinct from the active site. The docking groove recognises a peptide docking motif, which is distinct from the actual phosphoacceptor substrate motif but on the same molecule. Docking interactions appear to function as extended recognition surfaces that can increase enzyme-substrate encounters (reduce K_m) and confer higher specificity than can be achieved by interactions between the active site and substrate motif alone. Moreover, such increases in efficiency and specificity can be achieved without altering or compromising the function of the active site.

Docking grooves are found in several Ser/Thr kinase families, including CK1 isoforms and the mitogen-activated protein kinases (MAPKs) (Sharrocks et al., 2000, Tanoue et al., 2000). The best-characterised MAPK docking motif is referred to as the d-box, which is recognised by a conserved groove on the MAPK (Chang et al., 2002). The structures of several d-box docking complexes have been solved (Jacobs et al., 1999, Remenyi et al., 2005), revealing the docking groove is on the opposite surface from the active site. Mutation of either the docking groove on MAPKs or of the docking motif on substrates disrupts proper signal transmission (Remenyi et al., 2005, Grewal et al., 2006).

Many of these kinases show distinct motif-sequence preferences (Remenyi et al., 2005, Barsyte-Lovejoy et al., 2002). Presumably, the distinct docking and active site specificities work together to increase overall selectivity of kinase-substrate interactions.

Docking grooves have been identified in several families of Ser/Thr kinases, in addition to MAPKs (Biondi and Nebreda, 2003). These docking grooves are distributed across the surface of the kinase domain illustrating how much of the kinase surface can potentially be tapped for this type of additional recognition function. The spatial relationship between the docking groove and active site on the

kinase may set the distance constraints between the docking and phosphoacceptor sites in substrates.

3.10.4 Regulation via docking interactions

In most cases, docking interactions appear to play a relatively passive role as modular specificity control elements: They presumably increase the likelihood of enzyme-substrate encounter. However, in some cases, these interactions appear to regulate kinase function directly. For example, there are now several reported cases in which peptide binding at the docking groove can allosterically activate kinase function. Certain d-box docking site peptides can stimulate MAPK catalytic activity or autophosphorylation (Jacobs et al., 1999), whereas others may inhibit activity (Heo et al., 2004). FxFP motif binding to ERK appears to be coupled to the positioning of the ERK activation loop (Lee et al., 2004). In addition, 3-phosphoinositide-dependent kinase-1 (PDK1) interacts with downstream substrate kinases that contain a conserved docking motif known as the PDK1 interaction fragment (PIF). Binding of PIF motifs to PDK1 increases kinase activity (Biondi et al., 2000).

Another way in which docking motifs can act as regulatory elements is when the docking interactions are themselves phosphorylation-dependent. For example, PIF motifs must be phosphorylated before they bind effectively to the PIF pocket and activate PDK1 (PIF motif: Phe-X-X-Phe-pSer/pThr-Phe/Tyr). Thus, downstream substrates must be subjected to a priming phosphorylation prior to the interaction with and phosphorylation by PDK1 (Biondi et al., 2002).

A similar priming event is required for phosphorylation of some substrates by glycogen synthase kinase-3 (GSK3), which is part of the insulin signalling pathway. GSK3 substrates must be phosphorylated on a residue that is C-terminal to the Ser/Thr site to be modified by GSK3 (Fiol et al., 1988). This priming phosphorylation motif binds to a phospho-recognition docking groove adjacent to the active site (Dajani et al., 2001). The priming phosphorylation scheme observed in GSK3 and PDK1 pathways provides a mechanism for making signal processing dependent on a

sequence of catalytically distinct phosphorylation events, thereby increasing the specificity and complexity of control.

3.10.5 Substrate selectivity of TTBK2/CK1 conferred by a phosphorylation-dependent docking mechanism

The structure of CK1δ provides an explanation for the preference of CK1 kinases for substrates with -3 priming phosphorylation. Coupled with the observations that peptides with a +2 phosphotyrosine or a -3 phosphoserine enhance substrate recognition and enzymatic activity, a model analogous to the phosphate-docking interactions of GSK3 and PDK1, for the mechanism of substrate recognition by TTBK2 (and other CK1 superfamily kinases) emerges.

TTBK2 recognises a primed phosphorylation motif, which binds to a phospho-recognition docking groove adjacent to the active site (Figure 3.14).

3.10.6 Evolution of kinase circuits using docking interactions

The development of substrate recognition sites distinct from the actual phosphoacceptor sequence dramatically increases the modularity of kinase interactions and connectivities. Related kinases can develop slightly different docking grooves, thus allowing them to have distinct specificities without evolutionarily taxing the structure and efficiency of the active site.

Nonetheless, docking motifs are limited in their degree of modularity and evolvability. The docking grooves are intimately tied to the core catalytic module, in this case the catalytic Ser/Thr kinase domain. Thus, although docking motifs can be easily transferred to new substrates, the docking grooves cannot be dramatically altered or transferred to unrelated catalytic activities. Docking grooves are a step toward the separation of recognition and catalysis, but they do not employ generic interactions that could be transferred to new functions. Thus, docking grooves may represent a more ancestral solution to achieving modular connectivities. Interestingly,

although docking interactions are prevalent in many serine/threonine kinases (the more ancient eukaryotic protein kinases), similar docking interactions have not been identified in the more recently evolved tyrosine kinases.

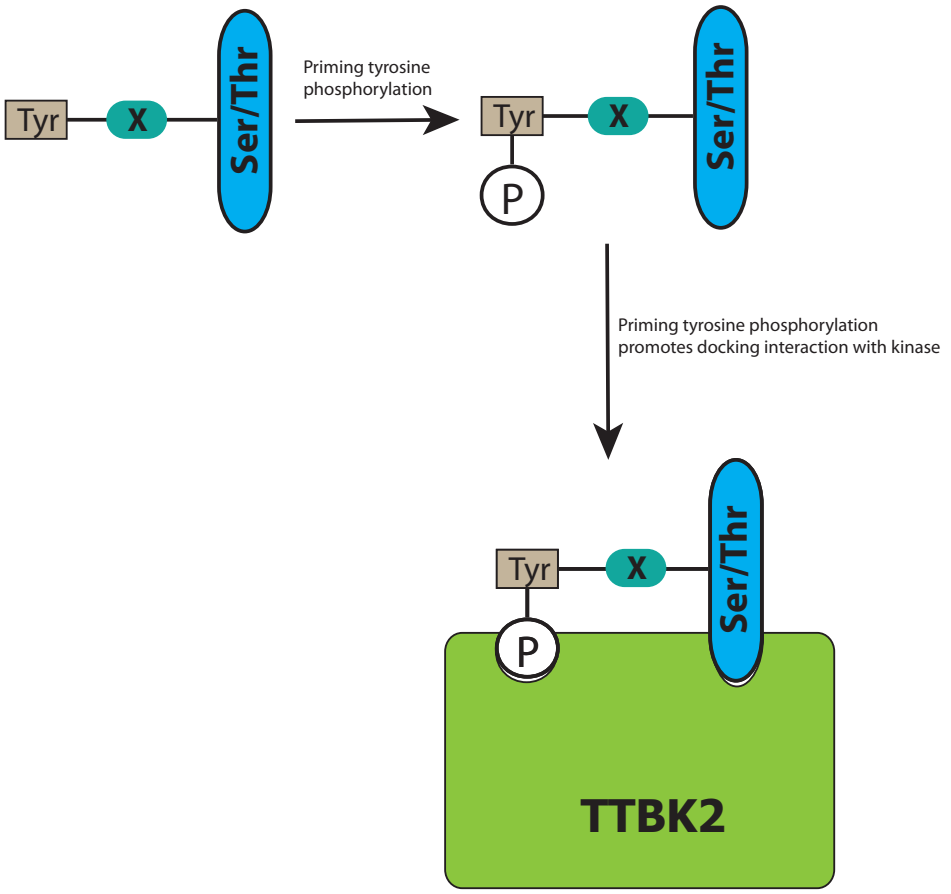

Figure 3.14. Schematic illustration of phosphorylation-dependent substrate interaction with TTBK2. TTBK2 possesses a phosphate-binding pocket that is distinct from the active site. This pocket acts as a docking groove that recognises a peptide-docking motif, which is distinct from the actual phosphoacceptor substrate motif. The docking groove recognises a phosphotyrosine two postions from the phosphoacceptor serine or threonine. X: any amino acid.

3.11 Conclusions

In conclusion, this initial work provides some initial insights into substrate specificity of TTBK2 and how SCA11-causing mutations affect kinase activity. In further studies, it will be crucial to define the substrates that TTBK2 phosphorylates physiologically and subsequently investigate whether aberrantly reduced phosphorylation of these targets contributes to the pathogenesis of SCA11. In

particular, it would be interesting to determine whether physiological TTBK2 substrates are primed with a +2 phosphotyrosine and how regulation of tyrosine phosphorylation is coupled to the control of these TTBK2 targets. Identifying the key targets of TTBK2 could provide vital new insights into the molecular mechanism underpinning the development of spinocerebellar ataxia.

4 Deciphering the physiological role of TTBK2

At the physiological and biochemical level, proteins rarely act alone; rather, they interact with other proteins to perform particular cellular tasks. To assign cellular functions to the TTBK2 protein, and to understand the physiological context in which it operates, the identification and analysis of proteins that specifically interact with TTBK2 is essential.

Co-immunoprecipitation (co-IP) combined with mass spectrometry (MS) has become the method of choice for identifying protein-protein interactions (Free et al., 2009). In this experimental strategy, mouse brain tissue was homogenised under non-denaturing conditions so that the protein interactions within the cells are not disrupted in the cell extract. When the target protein, TTBK2, is captured (immunoprecipitated) with a specific antibody bound to protein G sepharose beads, interacting partners of this protein may also precipitate. After removing non-specifically bound proteins by repeated washing, co-immunoprecipitated interacting partners were eluted from the beads using Laemmli buffer, separated by SDS-polyacrylamide gel electrophoresis (SDS-PAGE), digested in-gel using proteases, and identified by tandem mass spectrometry.

4.1 Immunoprecipitation of endogenous TTBK2 from mouse brain homogenates

To unequivocally identify proteins that specifically interact with TTBK2 physiologically, endogenous TTBK2 was immunoprecipitated from mouse brain homogenate using two different anti-TTBK2 antibodies and, in a parallel experiment; a control immunoprecipitation using a pre-immune (IgG) antibody was performed. The three immunoprecipitates samples were subjected to SDS/PAGE, which was then stained with colloidal Coomassie (Figure 4.1). The identity of the major bands in the TTBK2 and the control immunoprecipitations was established by tryptic-peptide MS fingerprinting analysis.

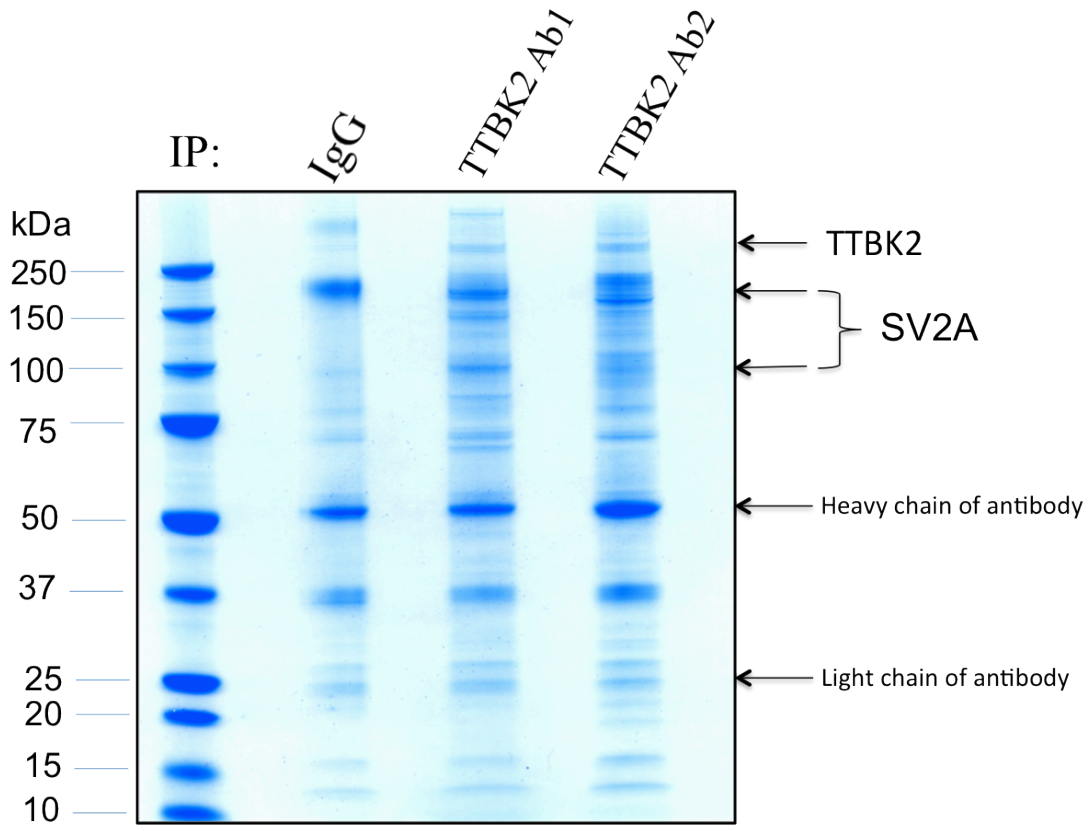

Figure 4.1. Immunoprecipitation of endogenous TTBK2. Mouse brain homogenate was subjected to immunoprecipitation with a pre-immune antibody (IgG) and two different TTBK2 antibodies. The immunoprecipitates were subjected to SDS-PAGE and the protein bands visualised following colloidal Coomassie blue staining. The indicated bands were excised, digested with trypsin and identities determined by mass spectrometry. The identity of the major bands observed in the TTBK2 are indicated on the right hand side.

4.2 Mass spectrometry data analysis

An important issue in the MS-based co-IP approach is how to distinguish the *bona fide* interacting proteins from a large pool of non-specifically bound proteins. Because of the significant improvement in detection capability of mass spectrometry, many proteins could be detected in a co-IP sample even after the most stringent purification processes (Walther and Mann, 2010). Some identified proteins may, however, be non-specifically bound proteins. These background proteins often include abundant proteins such as actin and heat shock proteins. In addition, some proteins may bind non-specifically to the protein G beads or the antibody. To distinguish these irrelevant background proteins, a negative control using serum IgG with the same concentration as that of TTBK2 antibody was used in the experiment. Because identical amount of IgG was immobilised to G sepharose beads, the negative control provided a similar

affinity matrix to which background proteins bound. Also, the comparison of the two different immunoprecipitations by the TTBK2 antibodies improved the level of confidence of the identified interactors as proteins that were not reproduced by the two different antibodies in two independent experiments were filtered out.

Using the database-searching tool MASCOT, a primary dataset of high-scoring peptides present in the three different immunoprecipitates was generated. Non-specific contaminants were then filtered out using stringent criteria in a manner similar to that reported previously (Amoresano et al., 2010). First, the protein identification results between the samples and the negative IgG control using the in-built OLMAT tool of the ProteinGuru online software (www.proteinguru.com) was compared. Common non-specific binding proteins such as actin, tubulin, and heat shock proteins were identified in all immunoprecipitates, and thus were considered background proteins. Secondly, the proteins that were not present in both TTBK2 immunoprecipitates were filtered out. Thirdly, MASCOT protein scores of a value of >24 were considered significant ($p<0.05$).

Thus, an unequivocal list of proteins coprecipitated in the TTBK2-specific pull-down was compiled. The number of peptides sequenced by MS, protein sequence coverage and accession numbers for each protein identified are indicated in Table 4.1.

.

		TTBK2 Ab1			TTBK2 Ab2				
Accession Number	MW(Da)	MASCOT Score	Peptide Hits	Sequence Coverage	MASCOT Score	Peptide Hits	Sequence Coverage	Gene	Protein Name
Q9JIS5	83392	2107	91	36%	1672	71	25%	**SV2A**	Synaptic vesicle glycoprotein 2A
P46096	47730	1923	103	54%	227	17	21%	**Syt1**	Synaptotagmin-1
Q6PIC6	113045	1429	78	45%	1720	97	46%	**ATP1A3**	Sodium/potassium-transporting ATPase subunit alpha-3
Q3UVR3	137598	636	48	25%	876	70	35%	**TTBK2***	Tau-tubulin kinase 2
Q3UVR3	137598	415	24	15%	200	17	10%	**TTBK2***	Tau-tubulin kinase 2
Q3UVR3	137598	250	12	7%	133	14	8%	**TTBK2***	Tau-tubulin kinase 2
Q62277	34288	1089	128	20%	354	41	18%	**SYP**	Synaptophysin
O54724	43927	1377	54	36%	272	22	28%	**PTRF**	Polymerase I and transcript release factor
Q6PIE5	113457	978	42	19%	865	51	22%	**ATP1A2**	Sodium/potassium-transporting ATPase subunit alpha-2
P17427	104017	737	76	39%	773	83	36%	**AP2a1**	AP2 complex subunit alpha
Q9DBG3	104583	814	61	42%	424	58	33%	**AP2b1**	AP2 complex subunit beta
Q8BVE3	56275	747	44	46%	1313	96	34%	**ATP6V1h**	V-type proton ATPase subunit H (VPP1)
P84091	49655	30	3	6%	37	12	25%	**AP2m1**	AP2 complex subunit mu-2
Q9Z0J4	161740	1281	93	34%	60	18	9%	**NOS1**	Nitric oxide synthase, brain
P08551	61528	675	36	37%	248	19	20%	**NEFLl**	Neurofilament light polypeptide
Q8R191	24774	655	38	23%	253	11	23%	**Syngr3**	Synaptogyrin-3
O35633	58313	646	43	37%	495	24	31%	**SLC32A1**	Vesicular inhibitory amino acid transporter
Q3TXX4	62312	124	18	13%	104	10	7%	**SLC17a7**	Vesicular glutamate transporter 1 (VGLUT1)
Q5SSM3	89564	324	20	21%	26	2	2%	**Arhgap44**	Rho GTPase-activating protein 44
P61264	33452	255	24	46%	214	6	14%	**STX1b**	Syntaxin-1B
O35954	135996	511	42	27%	195	25	13%	**PITPNM1**	Membrane-associated phosphatidylinositol transfer protein 1
P60879	23528	502	28	43%	579	24	30%	**SNAP25**	Synaptosomal-associated protein 25
Q9EP53	129692	495	51	35%	137	14	10%	**Tsc1**	Hamartin
O35609	38772	485	17	22%	107	3	8%	**SCAMP3**	Secretory carrier-associated membrane protein 3
Q9D0J4	21022	1270	40	77%	259	9	43%	**Arl2**	ADP-ribosylation factor-like protein 2
P70704	130938	236	21	14%	27	3	1%	**ATP8A1**	Probable phospholipid-transporting ATPase IA

Table 4.1.-(part 1). Summary of MS data: Proteins co-immunoprecipitating with TTBK2 from mouse brain homogenate. Interacting proteins are listed in decreasing order of

		TTBK2 Ab1			TTBK2 Ab2				
Accession Number	MW(Da)	MASCOT Score	Peptide Hits	Sequence Coverage	MASCOT Score	Peptide Hits	Sequence Coverage	Gene	Protein Name
O35643	104768	344	31	21%	262	29	17%	**AP1b1**	AP-1 complex subunit beta-1
Q61037	204395	305	20	11%	367	26	9%	**Tsc2**	Tuberin
Q8R361	69853	943	19	25%	34	12	16%	**Rab11FIP5**	Rab11 family-interacting protein 5
Q68FF6	86046	288	35	34%	27	5	5%	**Git1**	ARF GTPase-activating protein GIT1
P61264	33452	255	24	46%	122	7	27%	**Stx1b**	Syntaxin-1B
Q5SX79	90410	194	15	16%	90	5	6%	**Shroom1**	Protein Shroom1
Q8C996	31344	168	5	18%	233	10	23%	**Tmem163**	Transmembrane protein 163
O88935	74223	164	10	18%	35	3	5%	**Syn1**	Synapsin-1
P08553	95973	150	20	24%	164	33	22%	**NEFM**	Neurofilament medium polypeptide

Table 4.1 – (part II). Summary of MS data: Proteins co-immunoprecipitating with TTBK2 from mouse brain homogenate. Interacting proteins are listed in decreasing order of MASCOT scores obtained from TTBK2 Ab1 immunoprecipitation. Mascot protein score where a value of >24 was considered significant ($p<0.05$), number of peptides sequenced by LC MS/MS, percentage of protein sequence covered (%), accession numbers and molecular weight for each protein identified are indicated. TTBK2, the bait protein is shaded in blue and synaptic vesicle membrane proteins are shaded in yellow. *TTBK2, the bait protein was detected by MS in three different gel pieces and the MASCOT scores, peptides detected and sequence coverage are indicated for each.

4.3 Results of TTBK2 co-immunoprecipitation

Endogenous TTBK2, the bait protein, was predictably detected in three different gel pieces with 25%, 15% and 7% sequence coverage with a MASCOT scores of 636, 415 and 250 with TTBK2 antibody 1 (Ab1). With TTBK2 antibody 2 (Ab2), TTBK2 was detected with 35%, 10% and 8% sequence coverage with a MASCOT scores of 876, 200 and 133.

The number of TTBK2-binding proteins from mouse brain homogenates was high, exposed by the number of protein bands visible on the colloidal Coomassie blue-stained gel of the immunoprecipitates (Figure 4.1). Two high scoring peptide matches were (the two proteins with high MASCOT scores) synaptic vesicle glycoprotein 2A (SV2A) and synaptotagmin 1. This finding was reproducible by both TTBK2 antibodies used for immunoprecipitations in two independent experiments. SV2A is an integral membrane glycoprotein present in all synaptic vesicles (Bajjalieh et al., 1992). Synaptotagmin 1 is a calcium-sensing protein, which is also found in the membrane of synaptic vesicles (Geppert et al., 1994). This observation may indicate that TTBK2 is part of a protein complex that includes SV2A and synaptotagmin 1.

Intriguingly, further evaluation of the list of TTBK2 interactors exposed the presence of proteins such as synaptophysin, ATP6V1h (V-type proton ATPase subunit H), synaptogyrin 1, synaptogyrin 3, SNAP25 (Synaptosomal-associated protein 25), SCAMP1 (Secretory carrier-associated membrane protein 1), Syntaxin-1B, Synapsin 1, vesicular glutamate transporter (VGLUT1) and Rab proteins, which are all members of the unique collection of membrane proteins that typify the synaptic vesicle (SV) (shaded in yellow in Table 4.1). Indeed, 12 out of 19 major integral synaptic vesicle membrane proteins were identified by mass spectrometry (those marked with a red tick in Figure 4.2) as TTBK2 co-immunoprecipitants.

Another notable group of proteins that co-immunoprecipitated with TTBK2 were ATP1A1, ATP1A2 and ATP1A3. These are Na^+/K^+-ATPases (sodium/potassium pumps) and belong to the P-type ATPase group and their function is to establish and maintain an electrochemical gradient of sodium and potassium ions across the plasma membrane at neuronal synapses (de Carvalho Aguiar et al., 2004).

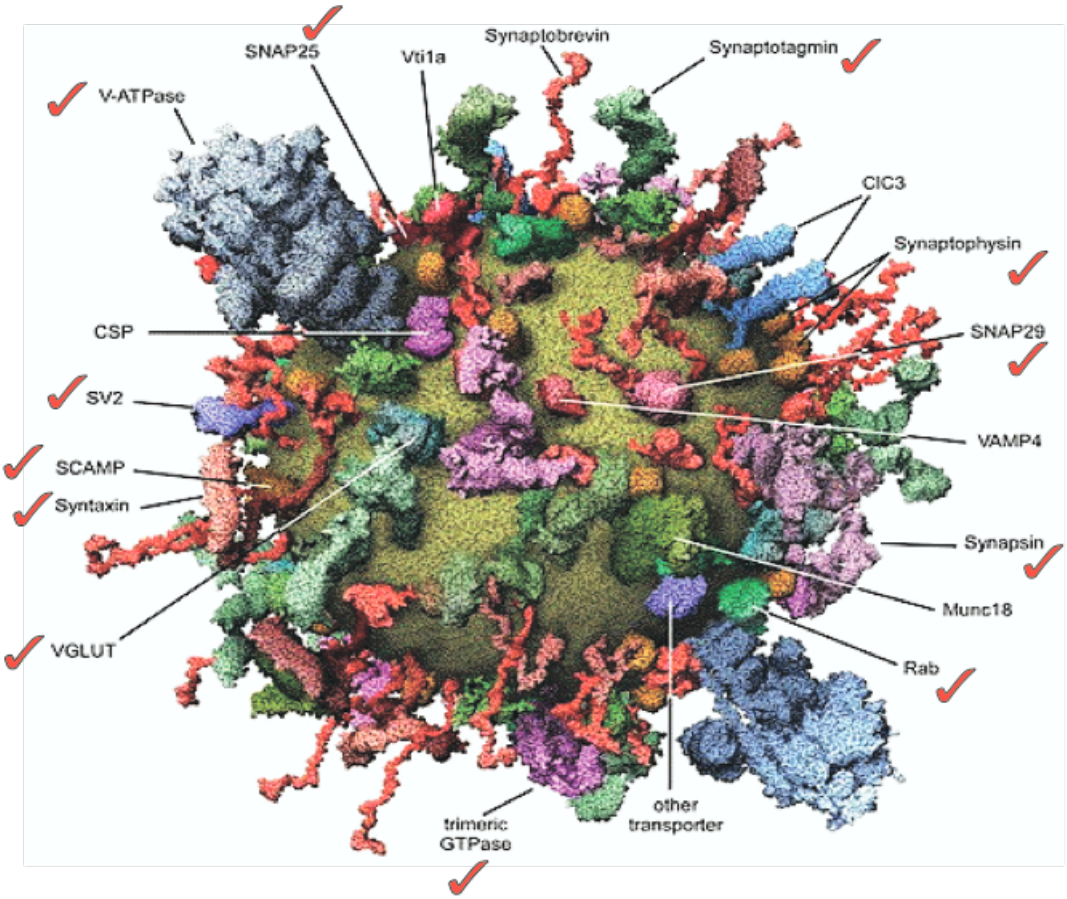

Figure 4.2. A molecular model of a prototypic synaptic vesicle (SV). Takamori et al. (2006) have determined the protein and lipid composition; measured vesicle size, density, and mass; calculated the average protein and lipid mass per vesicle; and determined the copy number of more than a dozen major constituents. The authors constructed this model that integrates all quantitative data and includes structural models of abundant proteins. Synaptic vesicles are dominated by proteins, possess a surprising diversity of trafficking proteins, and, with the exception of the V-ATPase that is present in only one to two copies, contain numerous copies of proteins essential for membrane traffic and neurotransmitter uptake. SV proteins marked with red ticks co-immunoprecipitated with TTBK2. [Adapted from (Takamori et al., 2006)].

The TTBK2 immunoprecipitates also contained proteins involved in clathrin-mediated endocytosis, in particular, the components of the AP2 complex (Adaptor-related protein complex 2): AP2α2, AP2β2, AP2μ2 and AP2σ2. Synaptic vesicles are known to recycle via clathrin-mediated endocytosis (Maycox et al., 1992) and evidence for this is provided by the fact that many SV proteins were detected in a proteome analysis of brain clathrin-coated vesicles (Blondeau et al., 2004).

In addition, many other proteins that have been reported to be associated with synaptic vesicles e.g., calcium-calmodulin-dependent protein kinase II, MAP6

(microtubule-associated protein 6) and amphiphysin were also detected. Some of these proteins transiently associate with a subset of vesicles. They are not, however, requisite components of all synaptic vesicles. While some of these proteins may participate in SV function, such as cytoskeletal proteins (vesicle transport), others may be only loosely associated with the vesicle membrane and have crucial roles in the trafficking of SVs.

Viewed collectively, the list of TTBK2 interactors combined was not a random collection of proteins. Rather, these proteins all belong to the unique collection of membrane proteins that epitomise the synaptic vesicle and other accessory proteins involved in their trafficking. Thus, the unifying theme that connects all the TTBK2-interacting proteins identified by the co-immunoprecipitation of endogenous TTBK2 from mouse brain homogenate is SV trafficking.

The salient aspect of the TTBK2 interactors identified is that TTBK2 interacts physiologically with a set of genuine SV membrane residents and SV ancillary proteins at neuronal synapses. This strongly suggests that TTBK2 participates in the protein network regulating synaptic vesicle trafficking and hence a tantalising physiological role for TTBK2 at the synapse regulating certain step(s) of the SV cycle remains to be uncovered.

4.4 The synaptic vesicle cycle

The key event of the synaptic vesicle (SV) cycle is the fusion of the membrane of synaptic vesicles with the presynaptic plasma membrane, a process that is tightly regulated by calcium. After exocytosis, vesicles are endocytosed and recycle. As a result, synaptic vesicles undergo a cycle of membrane traffic composed of exocytosis, endocytosis and recycling (Figure 4.3). More recent studies have further delineated the various stages of the synaptic vesicle cycle, including attachment (also called docking), prefusion (priming), triggering, recycling and reloading of the vesicles with transmitter.

The synaptic vesicle cycle can be envisioned to start with the uptake of neurotransmitters into synaptic vesicles by an energy-dependent step that requires

ATP (step 1 in Figure 4.3). Specialised transporter proteins in the synaptic vesicle membrane mediate this process.

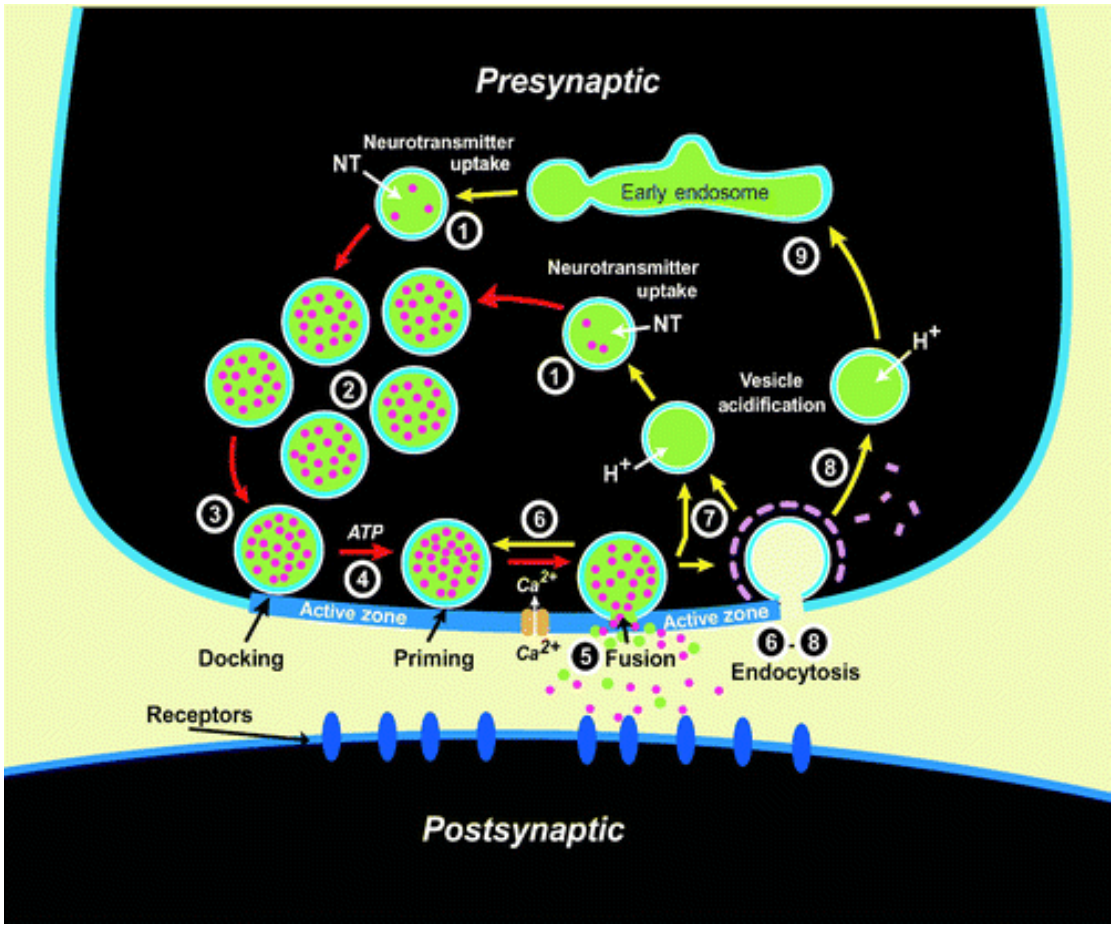

Figure 4.3. The synaptic vesicle cycle. Synaptic vesicles are filled with neurotransmitters by active transport (step 1) and form the vesicle cluster that may represent the reserve pool (step 2). Filled vesicles dock at the active zone (step 3), where they undergo a priming reaction (step 4) that makes them competent for Ca^{2+} triggered fusion-pore opening (step 5). After fusion-pore opening, synaptic vesicles undergo endocytosis and recycle via several routes: local reuse (step 6), fast recycling without an endosomal intermediate (step 7), or clathrin-mediated endocytosis (step 8) with recycling via endosomes (step 9). Steps in exocytosis are indicated by red arrows and steps in endocytosis and recycling by yellow arrows. [Adapted from (Sudhof, 2004)].

Synaptic vesicles filled with neurotransmitters move to the active zone of the presynaptic plasma membrane in a translocation process that probably occurs by diffusion, although the participation of molecular motors has not been excluded (step 2). At the active zone the vesicles become attached to the plasma membrane (step 3). Attachement (or docking) of the vesicles involves a specific interaction between vesicles and the active zone; the vesicles do not attach to any other part of the presynaptic plasma membrane except for the active zone. Attached vesicles undergo

an ATP-dependent prefusion reaction(s) that primes them for calcium-dependent release and may involve a partial fusion process (step 4). Calcium then triggers the completion of fusion in a rapid reaction that can occur in less than 0.1 milliseconds (Sabatini and Regehr, 1999). Calcium triggering of release involves the binding of multiple calcium ions at a calcium-binding site (step 5).

The synaptic vesicle cycle contains many independent steps, all of which involve protein-protein interactions. Vesicle transport, target recognition, docking, and fusion each involve the ordered and sequential recruitment of protein complexes from the cytoplasm. The membrane constituents SVs are ultimately responsible for orchestrating the association of the complex, task execution, and complex disassembly.

4.4.1 Medicine Nobel Prize 2013 awarded to discoverers of vesicle trafficking system

In October 2013, the Nobel committee recognised the achievements of three researchers for their discoveries of machinery regulating vesicle traffic. James Rothman of Yale University in New Haven, Connecticut; Randy Schekman at the University of California, Berkeley; and Thomas Südhof of Stanford University were jointly awarded the Nobel prize for physiology or medicine for 2013. The groundbreaking work of these laureates has revolutionised our understanding of a basic cellular function - protein and neurotransmitter secretion.

The laboratories of Schekman and Rothman worked out the basic mechanisms of vesicle fusion, in which proteins embedded in the membranes of vesicles recognise proteins on the membranes of their destination through a lock-and-key mechanism that is still being worked out.

Thomas Südhof's work focused on vesicle fusion in neurons. He identified and characterised numerous key components of the synaptic-vesicle fusion apparatus and the parallel regulatory machinery that makes synaptic secretion so fast. Of greatest importance, he identified the synaptic vesicle protein synaptotagmin, and showed that

this protein is the enigmatic calcium sensor that 'turbocharges' synaptic-vesicle secretion.

4.5 Synaptic vesicles: Molecular anatomy of an organelle.

A fruitful approach to understanding the molecular mechanisms of the synaptic vesicle cycle and neurotransmitter release was the characterisation of the proteins associated with synaptic vesicles (Sudhof, 1995). Synaptic vesicles are homogeneous in size and density, making it relatively easy to isolate large amounts of pure vesicles by a combination of density-gradient and size fractionation techniques. The characterisation of the proteins localised to synaptic vesicles has opened the door to genetic, physiological, and biochemical studies of their functions (Fernandez-Chacon and Sudhof, 1999). Through this set of diverse approaches, elaborate and testable biochemical models of vesicle attachment and fusion at the nerve terminal are now available.

As judged by electron microscopy, synaptic vesicles are electron-lucent organelles that are about 35 nanometres in diameter and may be slightly larger in native conditions. Because they are relatively small, synaptic vesicles can accommodate a limited number of lipids and proteins. Calculations suggest that each synaptic vesicle is composed of approximately 10, 000 molecules of phospholipids and of proteins with a combined approximate molecular weight of 5-10 x 10^3 kDa (Jahn and Sudhof, 1993). Since an average protein has a molecular weight of around 50 kDa, synaptic vesicles contain approximately 200 protein molecules (Sudhof, 2004). The only function of synaptic vesicles is their role in uptake and release of neurotransmitters; thus they are functionally relatively simple. In principle, the limited number of functions and proteins associated with synaptic vesicles should make it possible to obtain a complete molecular dissection of these organelles. Indeed, as a result of intensive biochemical studies, synaptic vesicles are possibly the best described of all organelles. We now know the structures of most vesicle proteins; the functions of some of them have been deduced and testable ideas about the functions of others have been formulated.

Synaptic vesicle proteins can be conceptually divided into two functional classes: transport proteins, which mediate the uptake of neurotransmitters and other components into synaptic vesicles (step 1 of the vesicle cycle; Figure 4.3), and trafficking proteins that participate in synaptic vesicle exo- and endocytosis and recycling (steps 2–9 in Figure 4.3).

The most prominent transport protein of synaptic vesicles is the proton pump (V-ATPase), which generates the electrochemical transmembrane gradient that fuels neurotransmitter uptake and neurotransmitter transporters that mediate the actual uptake. A single copy of the proton pump per vesicle is probably sufficient to drive neurotransmitter uptake; because of its large size, a single copy would account for approximately 10% of the total vesicle protein. One of the determinants of the transmitter type that is used by a particular synapse is the class of neurotransmitter transporter present in the vesicle. For example, as the neurotransmitter glutamate is a universal component of the cytosol, any synaptic vesicle that transports glutamate will make the corresponding nerve terminal glutamatergic. In addition to the proton pump and neurotransmitter transporters, synaptic vesicles contain ancillary transport proteins that mediate zinc transport, chloride flux, and possibly other transport activities; which have not yet been identified.

The trafficking proteome of synaptic vesicles is complex. It includes intrinsic membrane proteins; proteins associated via posttranslational lipid modifications, and peripherally bound proteins (Figure 4.4). These proteins do not share a characteristic that would make them identifiable as synaptic vesicle proteins, and little is known about how these proteins are specifically deposited into synaptic vesicles. As summarised in Figure 4.4, many but not the entire collection of known synaptic vesicle proteins interact with non-vesicular proteins and are linked to specific functions.

There are currently nine families of synaptic vesicle proteins that appear to be involved in membrane traffic (Figure 4.4). It is possible that additional proteins of synaptic vesicles remain to be identified, but it is unlikely that many proteins are missing. In addition to the known proteins, many other proteins have been reported to be associated with synaptic vesicles (e.g., calcium-calmodulin-dependent protein kinase II, actin, SNAPIN, and dynein). However, these proteins have only rarely been

found in highly purified vesicles, and, when present, they were such low abundance in the purified vesicles that they cannot be stoichiometric components of all vesicles. Although we cannot currently exclude the possibility that some of these proteins transiently associate with a subset of vesicles, they are requisite components of all synaptic vesicles.

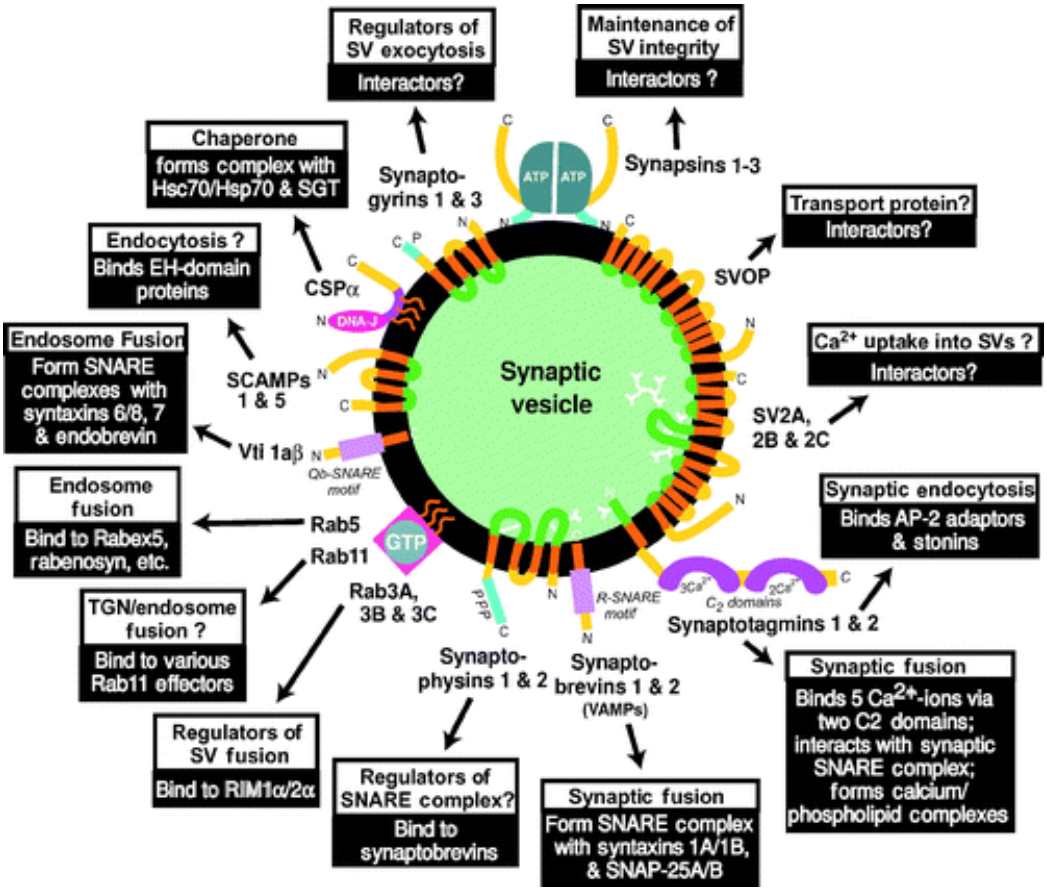

Figure 4.4. Structures, proposed interactions, and putative functions of synaptic vesicle trafficking proteins. Proteins are shown schematically (green, intravesicular sequences; orange, transmembrane regions; blue, phosphorylation domains; pink, SNARE motifs; red and gray, folded domains; yellow, other sequences). The white connecting lines in the intravesicular space identify disulfide bonds, and the branched white lines indicate sugar residues. In the boxes corresponding to the individual proteins, proposed functions are shown on a white background and purported interactions on a black background [adapted from (Sudhof, 2004)].

As illustrated in Figure 4.4, synaptic vesicle proteins share no common structural theme but consist of all types of membrane proteins. The proteins include peripheral membrane proteins (e.g., synapsins and rabphilin) and proteins that are attached to the vesicles by a post-translational lipid modification (CSP: Cysteine string protein, rab proteins) in addition to transmembrane proteins with single (synaptotagmins, VAMP/synaptobrevins) or multiple (synaptophysins, synaptogyrins, SV2s,

SCAMPs) transmembrane regions. Interestingly, synaptic vesicles contain three families of proteins with 4 transmembrane regions arranged in the same topology (synaptophysins, synaptogyrins, SCAMPs) and two families of proteins with 12 transmembrane regions (SV2s and SVOP) but only a single family of each type I and type II transmembrane proteins (synaptotagmin and VAMP/synaptobrevin, respectively).

VAMP/synaptobrevin, syntaxin and SNAP-25 are the founding members of a large family of membrane fusion proteins referred to as SNAREs (an acronym derived from "**SNA**P (Soluble NSF Attachment Protein) **RE**ceptor"). SNAREs can be divided into two categories: vesicle or v-SNAREs, which are incorporated into the membranes of transport vesicles during budding, and target or t-SNAREs, which are located in the membranes of target compartments (Sudhof et al., 1993).

The primary role of SNARE proteins is to mediate vesicle fusion that mediate docking of synaptic vesicles with the presynaptic membrane. These SNAREs are the targets of the bacterial neurotoxins responsible for botulism and tetanus. Botulinum and tetanus toxins enter nerve terminals and irreversibly inhibit SV exocytosis, thereby incapacitating the victim. The toxins are proteases, each of which cleaves a single target at a single site (Schiavo et al., 1994).

Most synaptic vesicle trafficking proteins are members of gene families composed of closely related isoforms that are on synaptic vesicles. However, the evolutionary history of the different vesicle proteins is quite distinct. Some proteins are evolutionarily conserved to a high degree (e.g. VAMP/synaptobrevin, synaptotagmin). For other proteins (e.g. synapsins and synaptophysin) only distantly-related homologues can be found in invertebrates, and some proteins such as SV2 are absent from invertebrates. These differences in evolutionary conservation indicate that some proteins may be components of the basic machinery for release, whereas others may have more peripheral regulatory functions that are important in complex nervous systems but not in simpler organisms.

Taken together, synaptic vesicle proteins are characterised by a great variety of structures and topologies (Figure 4.4). The only characteristic that all vesicle proteins share is that they lack cleaved signal peptide, usually the most common mechanism of membrane protein insertion. Although most transmembrane proteins of synaptic vesicles probably include internal signal peptides, the VAMP/synaptobrevins contain a C-terminal membrane anchor. As a result protein synthesis is completed before the translocation machinery would recognise the hydrophobic sequence. Thus, as expected, the transmembrane regions of these proteins are probably inserted into lipid bilayers posttranslationally, independent of the translocation apparatus (Kutay et al., 1995). In spite of this unconventional membrane insertion, the site of the initial membrane association of VAMP/synaptobrevins appears to be the endoplasmic reticulum; the proteins then flow through the secretory pathway in a normal fashion.

Although most vesicle proteins are highly concentrated in presynaptic nerve terminals, lower levels of these molecules can be found throughout the cell. In immature neurons or cells in culture, a considerable concentration of the vesicle proteins is found in the Golgi apparatus. Following exit from the trans-Golgi network, synaptic vesicle membrane proteins have been proposed to follow constitutive vesicular trafficking pathways to the plasma membrane. From the plasma membrane, the proteins may be internalised and sorted from other proteins within the endosomal system (Johnston et al., 1989). Vesicle proteins travel via fast anterograde axonal transport to synaptic sites, assisted by a diverse array of motor proteins. The final assembly of a fully mature synaptic vesicle may not occur until further rounds of exo- and endocytosis at or close to the synapse, but the exact mechansisms involved are obscure.

Despite a large body of work, the functions of most synaptic vesicle proteins remain unknown. For several proteins, a point of action has been identified, but it is unclear what exactly these proteins do at that point. A further complicating factor is that the relative simplicity of the protein composition of synaptic vesicles suggests that many vesicle proteins must have multiple functions. The synaptic vesicle cycle contains many independent steps (Figure 4.3), all of which are likely to involve protein-protein interactions. These protein-protein interactions must ultimately target synaptic vesicle proteins. Since there are only 9 different families of putative trafficking proteins,

many proteins must have multiple functions in order to account for all the steps in the vesicle cycle.

Many SV proteins are known to be phosphoproteins, which suggests that their functional role is modified by phosphorylation. Modulation of neurotransmitter release is brought about by changes in intracellular second messengers that activate protein kinases (Greengard et al., 1993). The resultant phosphorylation of synaptic vesicle-associated proteins appears to play a key role in regulating neurotransmission. The importance of phosphorylation of SV proteins in synaptic membrane traffic is well-established. The cycle of synaptic vesicle exo- and endocytosis requires the carefully orchestrated formation and dissociation of protein complexes. Regulation of the binding affinity through phosphorylation is likely to mediate changes in secretory efficiency that contributes to the modulation of synaptic transmission and synaptic plasticity (Sudhof, 1995).

4.6 Identification of Synaptic Vesicle glycoprotein 2A (SV2A) as a TTBK2 substrate.

To investigate whether any of the identified interacting SV proteins is a putative substrate for TTBK2, *in vitro* phosphorylation assays were performed. For this purpose, I elected to bacterially express an N-terminal fragment of human TTBK2, encompassing residues 1–316, which is a catalytically active proteolytic fragment of TTBK2 that has been detected in mouse brain extracts by the discoverers of TTBK2 as a 36 kDa species and displays *in vitro* kinase activity towards Tau and Tubulin (Takahashi et al., 1995, Tomizawa et al., 2001). A kinase-dead (KD) mutant (D163A) of TTBK2 was also purified in parallel, in order to rule out in vitro phosphorylation by contaminating kinases co-purifying with TTBK2.

Similarly, several TTBK2-interacting proteins identified in the co-immunoprecipitation assays were expressed as GST fusion proteins in *E.coli* or HEK293 cells. GST fusion proteins, thus expressed and purified, were incubated with GST-TTBK2 $[1\text{-}316]^{WT}$ and GST-TTBK2 $[1\text{-}316]^{KD}$ in the presence of 100 μM [γ-^{32}P] ATP for 30 min at 30°C. The reaction mixtures were subjected to SDS-PAGE, and phosphorylated proteins were imaged by autoradiography.

All the proteins tested as substrates showed no phosphorylation at all, except one. Only SV2A (Synaptic Vesicle glycoprotein 2A) displayed substantial phosphorylation by TTBK2 *in vitro* (Table 4.2). SV2A was significantly phosphorylated by TTBK2 *in vitro* (Figure 4.5), with an incorporation of more than 4.0 moles phosphate per mole of SV2A, indicating multiple phosphorylation sites.

Gene	Protein name	*In vitro* Phosphorylation by TTBK2
SV2A	**Synaptic vesicle glycoprotein 2A**	**Substantial Phosphorylation**
Syt1	**Synaptotagmin-1**	No Phosphorylation
ATP1A3	**Sodium/potassium-transporting ATPase subunit alpha-3**	No Phosphorylation
SYP	**Synaptophysin**	No Phosphorylation
ATP6V1h	**V-type proton ATPase subunit H**	No Phosphorylation
NSF	**N-ethylmaleimide sensitive factor**	No Phosphorylation
SLC32A1	**Vesicular inhibitory amino acid transporter**	No Phosphorylation
SNAP25	**Synaptosomal-associated protein 25**	No Phosphorylation
SCAMP3	**Secretory carrier-associated membrane protein 3**	No Phosphorylation
STX1b	**Syntaxin-1B**	No Phosphorylation

Table 4.2. Table listing the synaptic proteins tested as a TTBK2 substrate.

The generic 26 kDa substrate histone H1 was used as a positive control for the kinase reaction. Histone H1 was well phosphorylated by TTBK2 indicating that reaction conditions used were permissive to kinase reactions. On SDS-PAGE, GST-TTBK2 [1-316] migrates like a protein of about 70 kDa and thus the phosphorylation detected in the wild-type kinase reactions below the 75 kDa mark corresponds to autophosphorylation of the TTBK2 kinase.

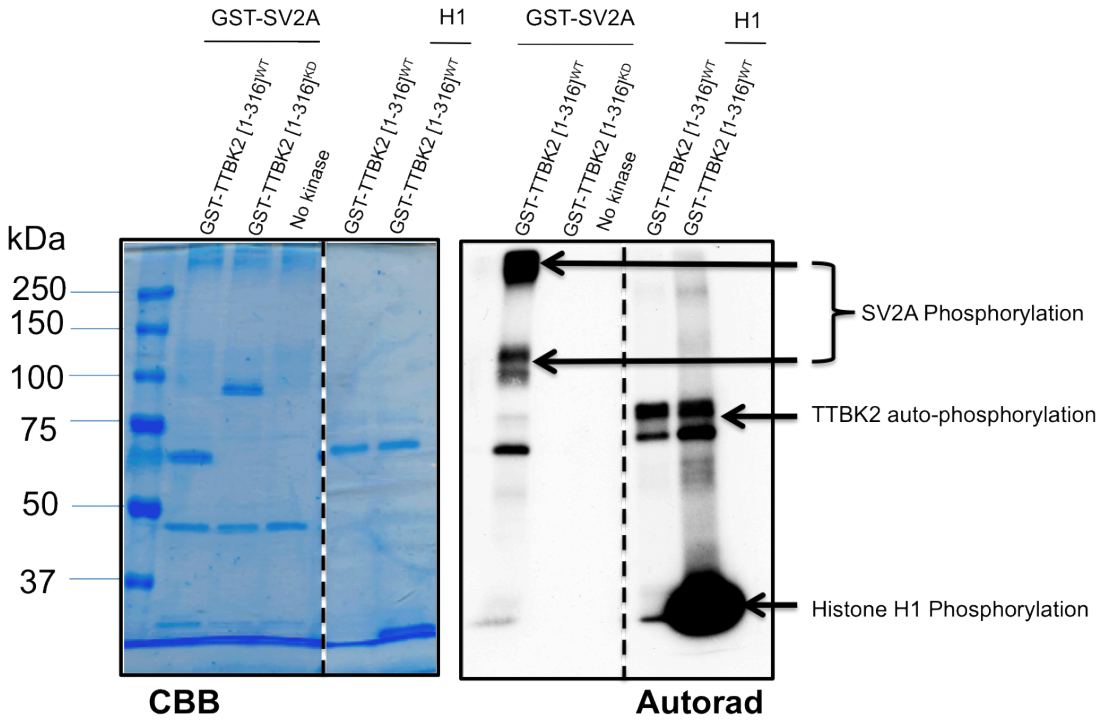

Figure 4.5. SV2A is an *in vitro* TTBK2 substrate. *In vitro* phosphorylation of recombinant GST-SV2A by either GST-TTBK2 [1-316]^{WT} or GST-TTBK2 [1-316]^{KD} or kinase buffer alone. The left panel shows the CBB staining of the SDS-PAGE gel and the right panel shows the result of autoradiography. The autoradiogram (right) shows two diffuse bands running at 100 and above 250 kDa, corresponding to two different forms of SV2A. Diffuse bands are observed due to the glycosylation of SV2A. SV2A migrates in two different forms of distinctive molecular weights. The lower band corresponds to GST-SV2A and the upper band matches to GST-SV2A complexed with laminin proteins. Arrows indicate SV2A bands, autophosphorylation of TTBK2 and histone H1. Histone H1 was used as a positive control for the kinase reaction.

As shown in Figure 4.5 above GST-SV2A was profusely phosphorylated by GST-TTBK2 [1-316]^{WT} but not by GST-TTBK2 [1-316]^{KD}. The autoradiogram shows two distinct diffuse bands running at 100 and above 250 kDa, typical of SV2A (Figure 4.5). The diffuse appearance of the bands is possibly due to the glycosylation of SV2A. SV2A migrates in two different forms of distinctive molecular weights. The lower band corresponds to GST-SV2A and the upper band matches to GST-SV2A complexed with laminin (Son et al., 2000), an extracellular matrix protein. The interaction of SV2A with laminin is strong in that it resists dissociation by high pH and detergents (Son et al., 2000). No phosphorylation was detected in the kinase-dead reactions.

4.7 Initial discovery of SV2A

Synaptic vesicle protein 2 (SV2) was discovered with a monoclonal antibody prepared against cholinergic vesicles from the electric organ of the marine electric ray *Discopyge ommata* (Buckley and Kelly, 1985). Immunolocalisation by electron microscopy revealed that this antibody recognised an epitope on the cytoplasmic face of synaptic vesicles. Biochemical evidence suggested that SV2 is a membrane-associated glycoprotein of approximately 80 kDa. The SV2 epitope was present in fish, amphibians, and mammals and is specifically localised to neural and endocrine cells. Immunohistochemical studies demonstrated that the SV2 epitope was not limited to neurons that contain a specific neurotransmitter but was detected in all neuronal and endocrine cells surveyed (Buckley and Kelly, 1985, Floor and Feist, 1989, Lowe et al., 1988). Its presence across a wide range of species, from elasmobranchs to mammals, suggests that it plays a critical role in vesicle functioning.

cDNAs encoding SV2 were cloned by screening a rat brain library with DNA probes based on amino acid sequence (Bajjalieh et al., 1992) and by screening for immunoreactivity in cells transfected with the cDNA (Feany et al., 1992). Computational analyses of the predicted protein sequence revealed that SV2 has 12 putative membrane-spanning domains.

SV2 (Synaptic Vesicle Protein 2) was found to be a family of membrane glycoproteins specific to the secretory vesicles of neurons and endocrine cells in vertebrates (Buckley and Kelly, 1985). Mammals have three SV2 genes that encode the three isoforms SV2A, SV2B, and SV2C (Bajjalieh et al., 1993, Bajjalieh et al., 1992, Feany et al., 1992, Janz et al., 1998). Of these, SV2A is the most broadly expressed, and is present in essentially all neurons (Bajjalieh et al., 1994). Notably, it is the only isoform expressed in many inhibitory, GABAergic neurons (Bajjalieh et al., 1994, Gronborg et al., 2010).

4.7.1 SV2A domain architecture

All SV2 proteins contain 12 transmembrane regions (TMRs) with N- and C-terminal cytoplasmic sequences and a large intravesicular loop that is *N*-glycosylated (Figure 4.6). Comparisons of different SV2 isoforms show that the TMRs and cytoplasmic loops are highly conserved, while the intravesicular loop, although *N*-glycosylated in all SV2 isoforms, exhibits little homology (Janz and Sudhof, 1999). While SV2A is expressed ubiquitously, SV2B is present in a more restricted forebrain pattern (Bajjalieh et al., 1994), and SV2C is concentrated in caudal brain regions (Janz and Sudhof, 1999). A distantly related synaptic vesicle protein called SVOP (SVtwo-related protein) contains a similar transmembrane structure as SV2, but lacks its long cytoplasmic and highly glycosylated intravesicular loops (Janz et al., 1998).

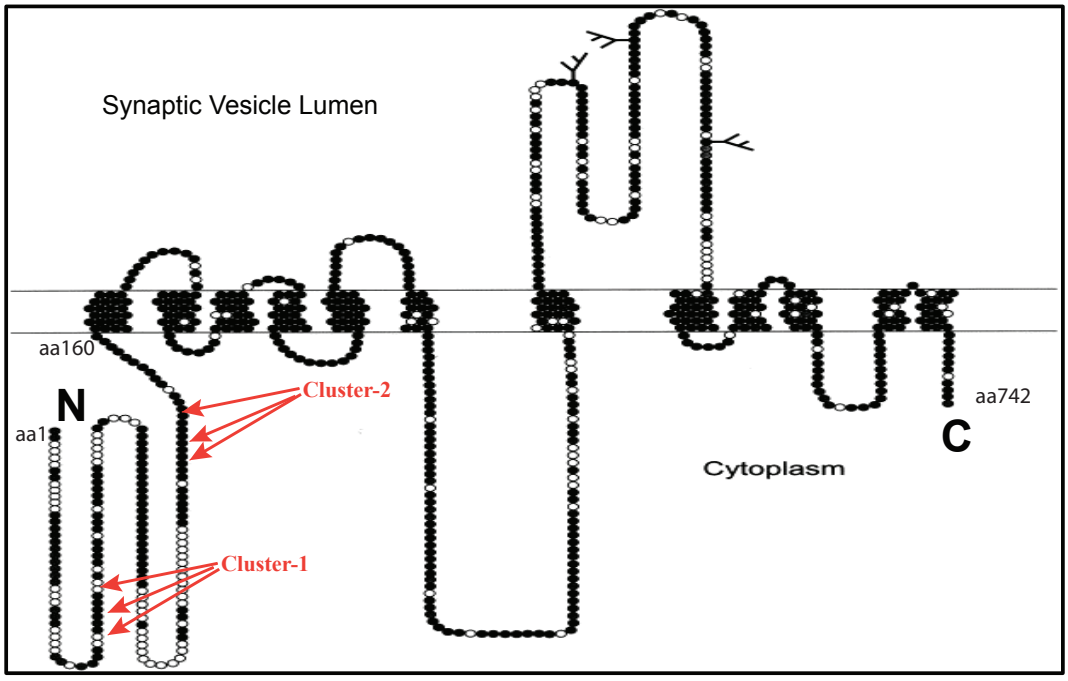

Figure 4.6. Domain structure of SV2A. Schematic diagram of the structure of the SV2A protein. Amino acids residues in the primary sequence of SV2A are indicated by circles, with 12 potential transmembrane regions (TMRs). Branched lines show positions of N-linked carbohydrates. N and C termini are identified by letters.

SV2s share significant sequence homology to a large family of transport proteins. Included in this family are bacterial and fungal proteins that co-transport protons with sugars, citrate, and drugs, and mammalian facilitative glucose transporters

(Henderson and Maiden, 1990, Maiden et al., 1987). This similarity to a large class of transport proteins suggested that SV2 might be a transporter specific to synaptic vesicles and initially investigators thought that SV2A may be a neurotransmitter transporter, but its presence in nerve terminals with distinct neurotransmitters dispelled this idea (Bajjalieh et al., 1994).

Despite many hypotheses, SV2A has no validated function as a transporter or otherwise. Much of the data regarding the function of SV2A comes from studies using SV2A and SV2A/B knockout mice. SV2A is indispensable for survival in mice. Mice with knock out of one allele of SV2A have an elevated incidence of epileptic seizures, and mice with both copies knocked out have very severe epileptic seizures after the first postnatal week and die by the third week (Crowder et al., 1999), primarily because of fulminant epilepsy. SV2B knock out (KO) mice, however, are phenotypically unremarkable and SV2C KO mice have not been reported yet.

4.8 Mapping of TTBK2 phosphorylation sites on SV2A

To map TTBK2 phosphorylation sites, GST-SV2A [1-160] was maximally phosphorylated with either TTBK2 $[1\text{-}316]^{WT}$ or TTBK2 $[1\text{-}316]^{KD}$. Five reactions were set up in a 40 µl volume of Buffer A containing 1 µg GST–TTBK2 [1–316], 1 µg GST-SV2A (full-length), 10 mM $MgCl_2$, 0.1 µM [γ-^{32}P] ATP. After incubation for 60 min at 30 °C, incorporation of phosphate was determined after electrophoresis of samples on a NuPAGE® Bis-Tris 10%-polyacrylamide gel and autoradiography of Coomassie Blue-stained gels. The protein bands corresponding to SV2A were excised, and phosphate incorporation was quantified on a scintillation counter. After tryptic digestion, more than 86% of the ^{32}P radioactivity incorporated into the gel band was recovered and the samples were chromatographed on a reverse-phase Vydac 218TP5215 C_{18} HPLC column to isolate ^{32}P-labelled phosphopeptides. The HPLC trace obtained is shown in Figure 4.7. Under the conditions employed, SV2A was phosphorylated by wild-type TTBK2 to ~ 4.0 mol of phosphate/mol of SV2A, indicating multiple phosphorylation sites.

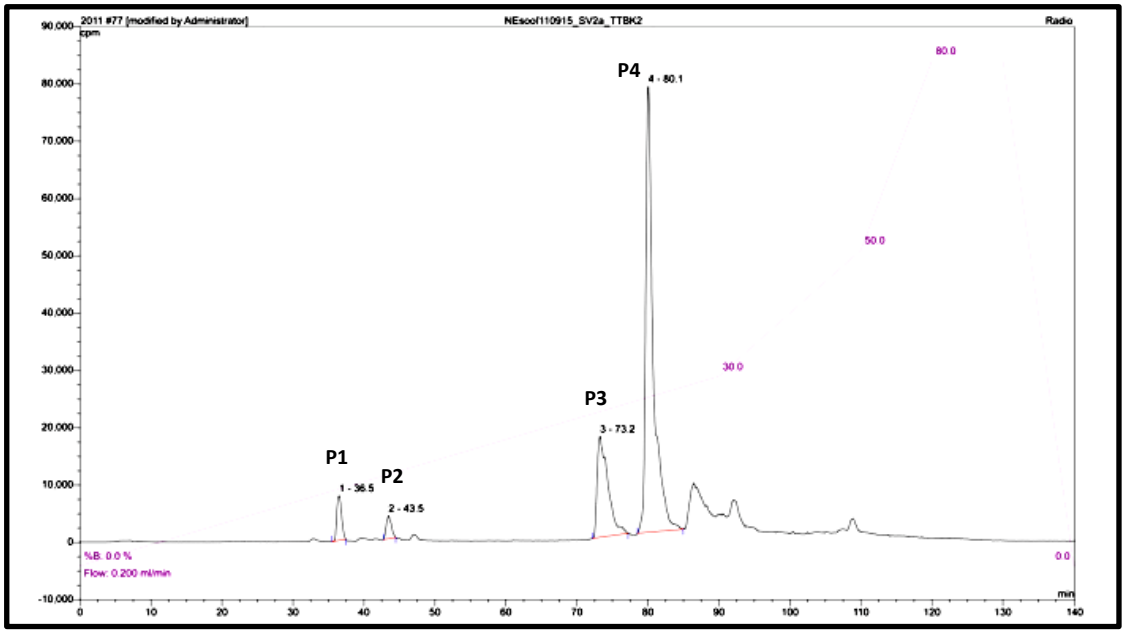

Figure 4.7. Full-length SV2A was phosphorylated by TTBK2 [1-316]^{WT} for 60 minutes. The ^{32}P-labelled SV2A was isolated by SDS-PAGE, digested with trypsin and the resulting peptides were chromatographed on a C_{18} column. Fractions containing the major ^{32}P-labelled peptides are marked (P1-P4).

Peptide analysis of the fractions corresponding to the major ^{32}P-containing peaks was performed using an Applied Biosystems 4700 Proteomics Analyser (MALDI-TOF/TOF) and solid-phase Edman degradation on an Applied Biosystems 494C sequenator of the peptide coupled to Sequelon-AA membrane. ^{32}P radioactivity was measured after each cycle of Edman degradation and the deduced amino acid sequences of peptides P1, P2, P3 and P4 are shown below in Table 4.3.

Sample ID	Phosphopeptide	Cycle of ^{32}P release	Phosphorylation site
P1	VQDEY**S**RR	**6**	**S42**
P2	GGL**S**DGEGPPGGR	**4**	**S127**
P3	SY**S**RFEEEDDDDDF	**3**	**S47**
P4	VQDEY**S**RR**S**Y**S**RFEEEDDDDDFPAP**S**DGY	**6,9,11, 26**	**S42,S45,S47 S62**
P4	GEGTQDEEEGGA**SS**DA**T**EGHDEDDEIYEGEYQGIPR	**13,14, 17**	**S80,S81,T84**

Table 4.3.The indicated peptides were analysed by MALDI-TOF/TOF MS. The phosphorylated residues in each peptide were determined by solid-phase Edman sequencing in which ^{32}P radioactivity was released is indicated. The deduced amino acid sequences of peptides P1, P2, P3, and P4 are indicated; the phosphorylated residues are underlined.

Eight potential phosphosites were identified: Ser42, Ser45, Ser47, Ser62 and Ser127. Ser42 and Ser45 theoretically comprise the canonical CK1 consensus sequence (S^P/T^P-X-X-S/T). Notably, all the identified TTBK2 phosphosites on SV2A are all located on the cytosolic N-terminus of the protein, corresponding to amino acids 1 to 160 (Figure 4.6).

4.9 Expression and phosphorylation of the cytosolic N-terminal fragments of SV2A, SV2B and SV2C.

As previously mentioned, the TTBK2 phosphosites on SV2A are all located on the cytosolic N-terminus of the protein. Since very low levels of expression of full-length recombinant SV2A were observed, the cytosolic amino terminus of SV2A (amino acids 1-160) was subcloned and expressed in bacterial cells. The corresponding regions of SV2B and SV2C: SV2B [1-103] and SV2C [1-146] (see alignment in Figure 4.8 on next page), were also cloned and expressed.

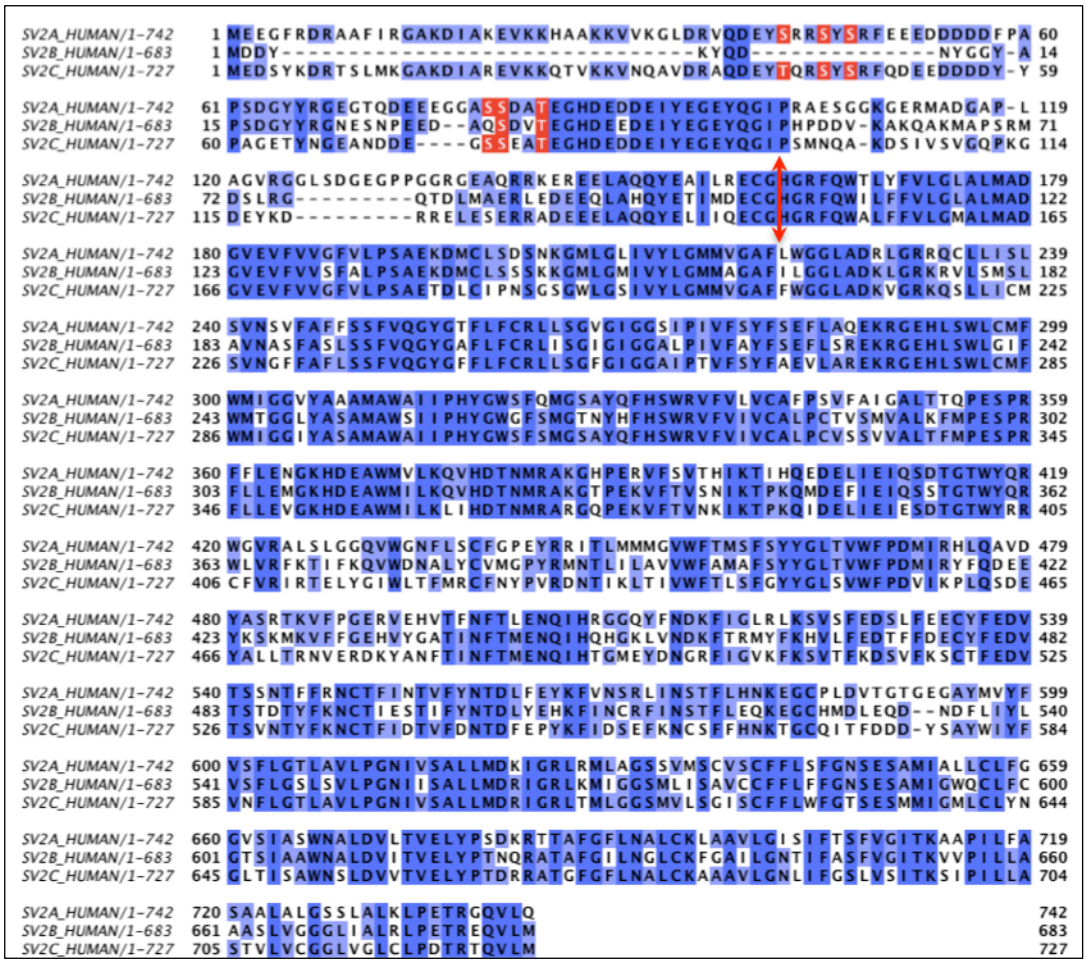

Figure 4.8. Multiple sequence alignment of the human SV2A, SV2B and SV2C. The amino terminal sequences of the SV2 isoforms illustrating the similarity between SV2A and SV2C, and the divergence of SV2B. Conserved phosphorylation sites are highlighted in red. Red arrowed line indicates the boundary between the cytosolic portion of the proteins and the first membrane-spanning domain, corresponding to residues 160 for SV2A, 103 for SV2B and 146 for SV2C.

The *in vitro* phosphorylation of the N-terminal fragments; SV2A [1-160] and SV2B [1-103] and SV2C [1-146] by TTBK2 was evaluated by autoradiography and the resulting autoradiogram is shown below (Figure 4.9). All three SV2 isoforms were profusely phosphorylated by TTBK2 with similar stoichiometry.

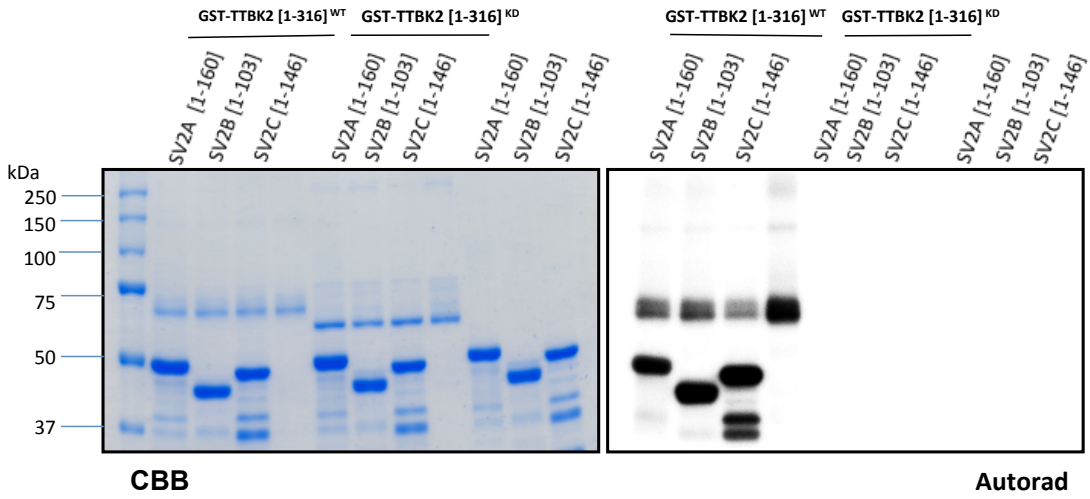

Figure 4.9. Phosphorylation of SV2 isoforms was determined after SDS-PAGE and autoradiography (right panel) of the Coomassie Blue-stained bands (left panel). TTBK2-[1–316]^{WT} or kinase-dead (KD) [D163A] TTBK2-[1–316]^{KD} was incubated with the indicated proteins SV2A-[1-160], SV2B-[1-103], SV2C-[1-146] in the presence of Mg^{2+} and [γ-^{32}P] ATP.

4.10 Mapping TTBK2 phosphorylation sites on SV2A, SV2B and SV2C.

SV2A [1-160], SV2B [1-103] and SV2C [1-146] were found to be very potent *in vitro* substrates for TTBK2 and phosphosite mapping was performed on those N-terminal fragments of SV2A, SV2B and SV2C.

To map the TTBK2 phosphorylation sites in SV2A-[1-160], SV2B-[1-103], and SV2C-[1-146], the three SV2 isoforms were phosphorylated by TTBK2-[1–316]^{WT} and TTBK2 [1-316]^{KD} as a control as described previously. Under these conditions, SV2A, SV2B and SV2C were phosphorylated with similar stoichiometries.

HPLC, peptide analysis and Edman degradation was carried out as described previously. The HPLC traces, resulting peptide analyses and Edman sequencing results for SV2A-[1-160], SV2B-[1-103] and SV2C-[1-146] are detailed below.

4.10.1 TTBK2 phosphosite mapping of SV2A[1-160]

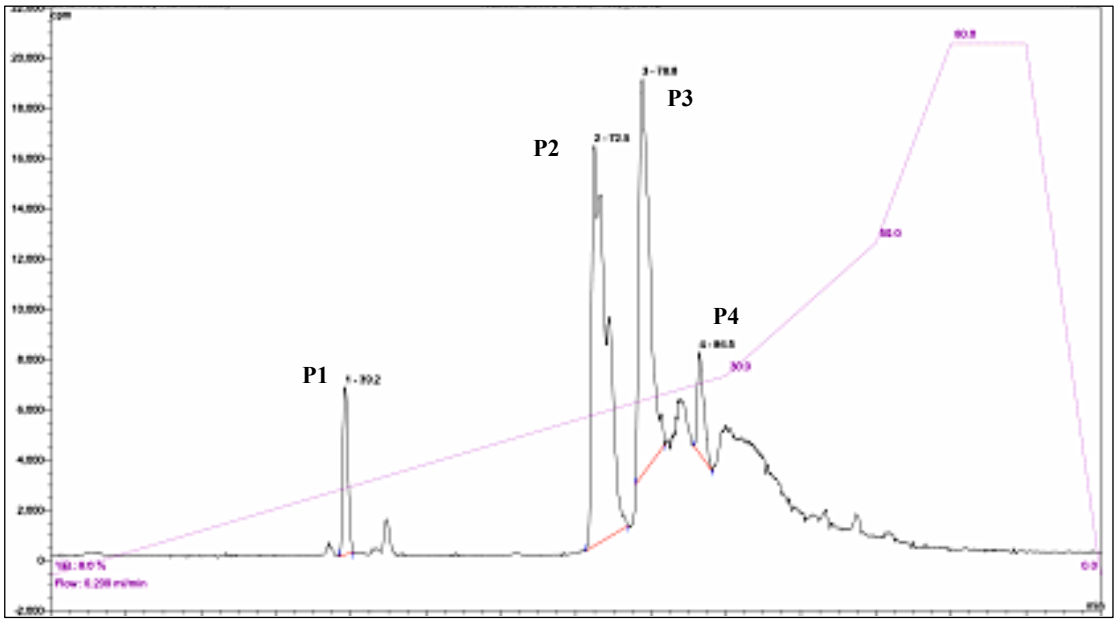

Figure 4.10. SV2A-[1-160] was phosphorylated by TTBK2-[1-316]^{WT} for 60 minutes. The ^{32}P-labelled SV2A was isolated by PAGE, digested with Asp-N and the resulting peptides were chromatographed on a C_{18} column. Fractions containing the major ^{32}P-labelled peptides are marked.

Edman sequencing of the phosphopeptides P1, P2, P3 and P4 (Figure 4.10) are summarised in Table 4.4.

Sample ID	Phosphopeptide	Cycle of ^{32}P release	Phosphorylation site(s)
P1	VQDEY**S**RR	**6**	**S42**
P2	GEGTQDEEEGGA**SS**DA**T**EGHDEDD	**13,14,17**	**S80,S81,T84**
P3	GEGTQDEEEGGA**SS**DA**T**EGHDEDD	**13,14,17**	**S80,S81,T84**
P4	**S**Y**S**RFEEEDDDDDFPAPSDGYYR	**1,3**	**S45,47**

Table 4.4. The indicated peptides were analysed by MALDI-TOF/TOF MS. The phosphorylated residues in each peptide were determined by solid-phase Edman sequencing in which ^{32}P radioactivity was released is indicated. The deduced amino acid sequences of peptides P1, P2, P3, and P4 are indicated; the phosphorylated residues are underlined.

There is significant overlap between the two phosphomapping datasets (full-length SV2A and SV2A[1-160]. All the phosphosites identified previously on full-length SV2A: Ser42, Ser45, Ser47, Ser80, Ser81 and Thr84 were exposed on the N-terminal

fragment SV2A [1-160]. However, Ser62 and Ser127 were not detected on SV2A [1-160].

Cumulatively, the mapping of TTBK2 phosphosites on SV2A revealed eight potential phosphorylation sites: Serines 42, 45, 47, 62, 80, 81, 127 and Threonine 84.

4.10.2 TTBK2 phosphosite mapping of SV2B[1-103]

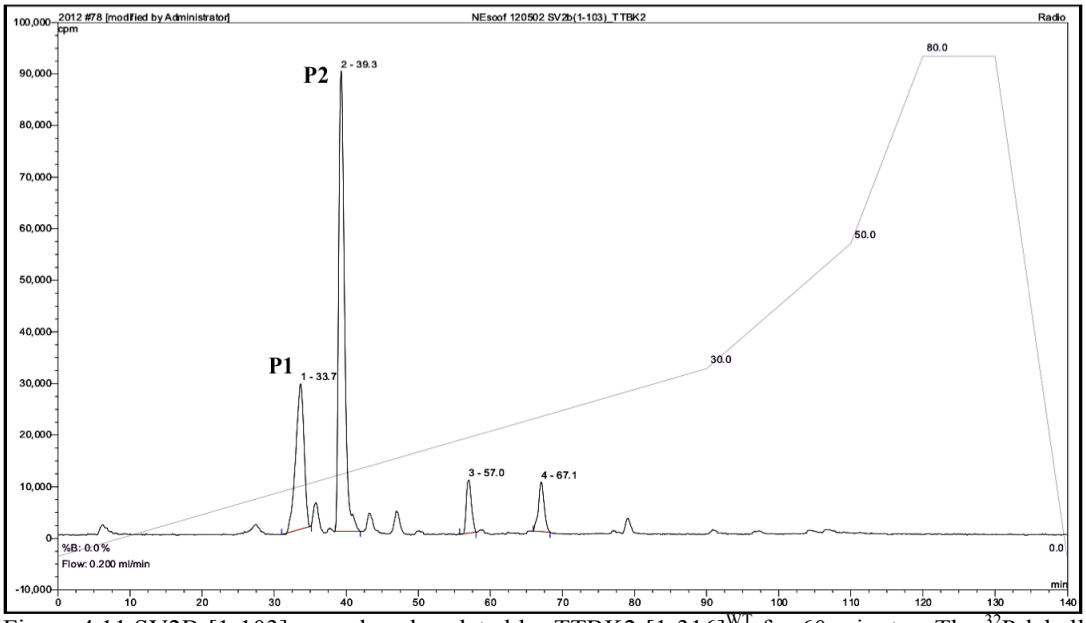

Figure 4.11.SV2B-[1-103] was phosphorylated by TTBK2-[1-316]^{WT} for 60 minutes. The ^{32}P-labelled SV2B was isolated by PAGE, digested with Asp-N and the resulting peptides were chromatographed on a C_{18} column. Fractions containing the major ^{32}P-labelled peptides are marked P1 and P2.

Edman sequencing of the phosphopeptides P1 and P2 (Figure 4.11) are summarised in Table 4.5.

Sample ID	Phosphopeptide	Cycle of ^{32}P release	Phosphorylation site(s)
P1	DAQ**S**DV**T**EGH	**4,7**	**S33, T36**
P2	DAQ**S**DV**T**EGH	**4,7**	**S33, T36**

Table 4.5. The indicated peptides were analysed by MALDI-TOF/TOF MS. The phosphorylated residues in each peptide were determined by solid-phase Edman sequencing in which ^{32}P radioactivity was released is indicated. The deduced amino acid sequences of peptides P1 and P2 are indicated; the phosphorylated residues are underlined.

The two peptides sequenced for SV2B were identical. Two phosphorylation sites were identified for SV2B: Ser33 and Thr36.

4.10.3 TTBK2 phosphosite mapping of SV2C[1-146]

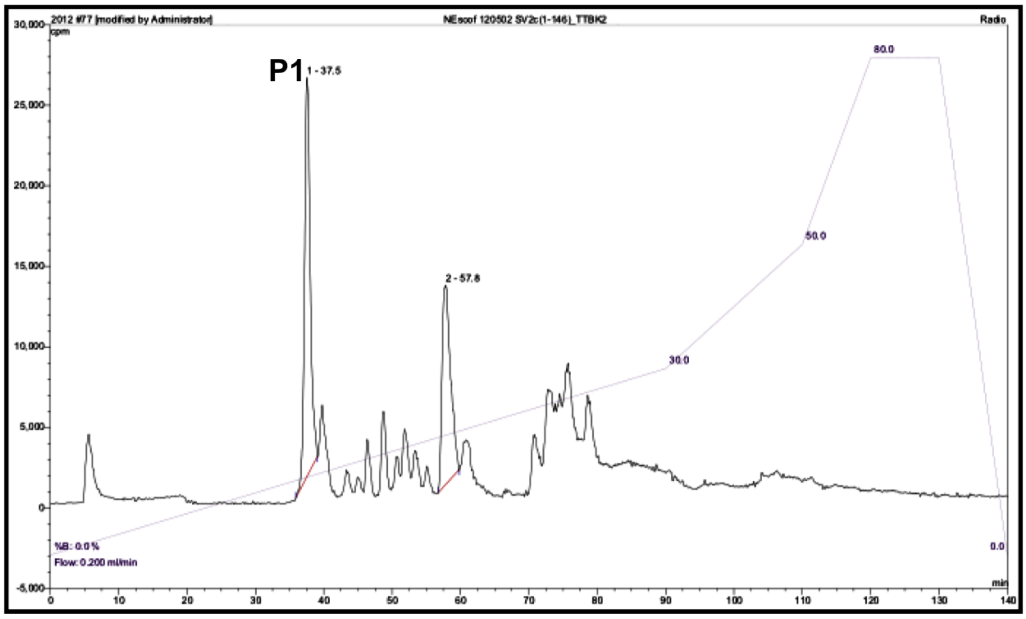

Figure 4.12.SV2C-[1-146] was phosphorylated by TTBK2-[1-316]^{WT} for 60 minutes. The ^{32}P-labelled SV2c was isolated by PAGE, digested with Asp-N and the resulting peptides were chromatographed on a C_{18} column. Fractions containing the major ^{32}P-labelled peptides are marked.

Edman sequencing of the phosphopeptide P1 (Figure 4.12) are summarised in Table 4.6.

Sample ID	Phosphopeptide	Cycle of ^{32}P release	Phosphorylation site(s)
P1	DEY**T**QRSY**S**RFQ	**4,9**	**T42, S47**

Table 4.6. The indicated peptide was analysed by MALDI-TOF/TOF MS. The phosphorylated residues in the peptide were determined by solid-phase Edman sequencing in which ^{32}P radioactivity was released is indicated. The deduced amino acid sequences of peptide P1 is indicated; the phosphorylated residues are underlined.

The sequence of only one peptide was obtained for SV2C and revealed two phosphorylation sites: Thr42 and Ser47.

4.11 Confirmation of accuracy of SV2A phosphomapping

I next assessed how mutation of these eight residues affected the phosphorylation of SV2A [1-160]. I compared phosphorylation of SV2A [1-160]^{WT} and

SV2A [1-160]^{8XA}, which is an SV2A mutant in which Ser42, Ser45, Ser47, Ser62, Ser80, Ser81, Thr84 and Ser127 are mutated to alanines by TTBK2 [1-316]^{WT} and TTBK2 [1-316]^{KD} using autoradiography (Figure 4.13).

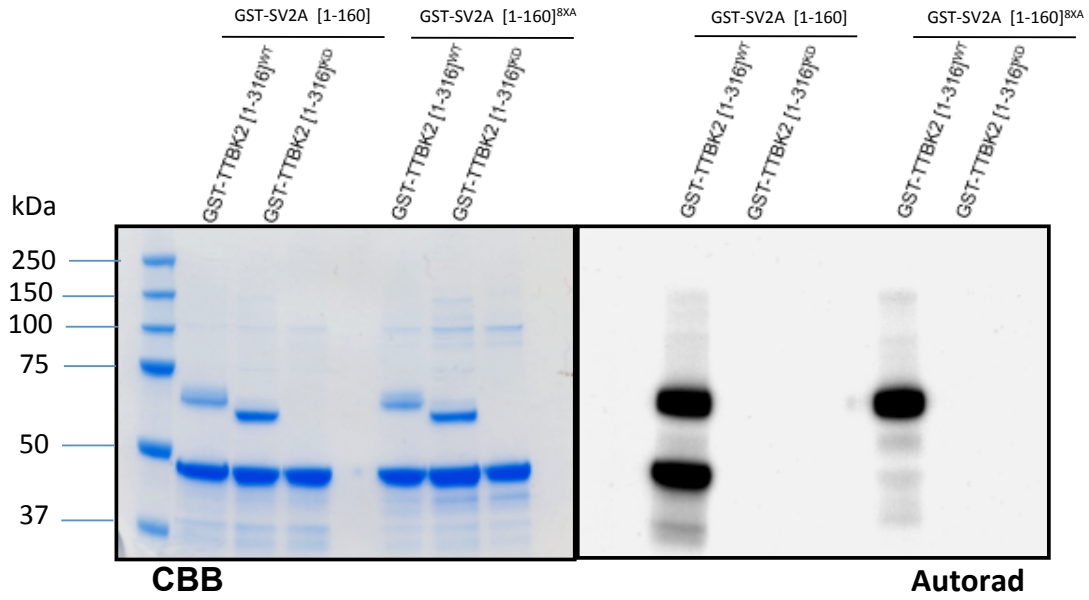

Figure 4.13. Autoradiogram comparing the phosphorylation of SV2A-[1-160]^{WT} and SV2A[1-160]^{8XA} by TTBK2-[1-316]^{WT} and TTBK2-[1-316]^{KD}. GST-SV2A-[1-160]^{WT} and GST-SV2A-[1-160]^{8XA} were incubated with recombinant either GST-TTBK2-[1-316]^{WT} or GST-TTBK2-[1-316]^{KD} and Mg^{2+}-[γ-^{32}P]ATP for 30 mins and subjected to SDS-PAGE and autoradiography.

As shown by the autoradiogram in Figure 4.13, TTBK2-[1-316]^{WT} autophosphorylates and phosphorylates SV2A-[1-160]^{WT}. Mutations of Ser42, Ser45, Ser47, Ser62, Ser80, Ser81, Thr84 and Ser127 to alanines completely abolished phosphorylation of SV2A by TTBK2 (Figure 4.13), while the level of TTBK2 autophosphorylation detected remains identical. This adds further support to the view that all prospective phosphosites have been accurately mapped.

4.12 Conservation of phosphosites between SV2 isoforms

The three SV2 proteins are differentially expressed in brain. SV2A is present in almost all neurons, SV2B exhibits a more restricted distribution in retinal photoreceptors (Bajjalieh et al., 1994), and SV2C is present only in a small subset of neurons in the basal forebrain and caudal brain regions (Janz and Sudhof, 1999). SV2A is by far the most widely expressed isoform.

SV2A and SV2C are larger proteins than SV2B (742, 727 and 683 amino acids respectively) and the residues preceding the first transmembrane domain constitute the most divergent region between isoforms (Figure 4.8). Whereas the membrane spanning domains are 73% identical in SV2A and SV2B, the amino termini are only 34 % identical. SV2A and SV2C are more similar, sharing 50% identity in the amino terminal region. The most striking difference between SV2A/C and SV2B are the 49 amino acids present at the very amino terminus of SV2A/C, a region that contains multiple stretches of identical residues.

Accordingly, SV2A and SV2C share similar phosphorylation sites. The corresponding residues of SV2A Ser42, Ser45 and Ser47 in SV2C are Thr42, Ser45 and Ser47. Our phosphomapping, however, did not show phosphorylation of SV2C Ser45. This may be due to a miscleavage of the phosphopeptide. SV2B does not possess equivalent residues (Figure 4.8).

The other notable phosphosites identified on SV2A were Ser80, Ser81 and Ser84; which correspond to SV2C Ser75, Ser76 and Thr79. These phosphosites were not detected on SV2C due to poor detection of phosphopeptides by mass spectrometry. SV2B, on the other hand, possesses phosphosites Ser33 and Thr36; which parallel Ser81 and Thr84 of SV2A (Figure 4.8). The conservation of certain phosphosites between SV2 isoforms may point to common generic regulatory mechanisms modulated by those sites.

Ser62 is shared between SV2A and SV2B but is not present in the SV2C sequence. Ser127 is only present in SV2A and not in SV2B or SV2C. The dearth of

conservation of those two sites suggests that they may not be important for SV2 function.

4.13 Conservation of SV2A phosphosites in SV2A orthologues

To identify which of the identified human phosphosites are conserved in distantly related model organisms and thereby likely to be essential for fundamental cellular activities, I investigated the conservation of protein phosphorylation events i.e. sites that are conserved at similar positions in orthologous proteins between human, mouse, rat, cow and Xenopus (Figure 4.14). Assessment of conservation showed that Ser62 is not conserved at all in other species, while Ser127 was conserved in human, mouse and rat orthologues but not in lower species (highlighted in green in Figure 4.14).

The six remaining phosphorylation sites (Ser42, Ser45, Ser47, Ser80, Ser81 and Thr84) identified in human SV2A are well conserved in not only the human and mouse proteins, but also in lower organisms including *Xenopus Tropicalis* (highlighted in red in Figure 4.14). The degree of conservation of those phosphosites implies that they are vital for the function of SV2A.

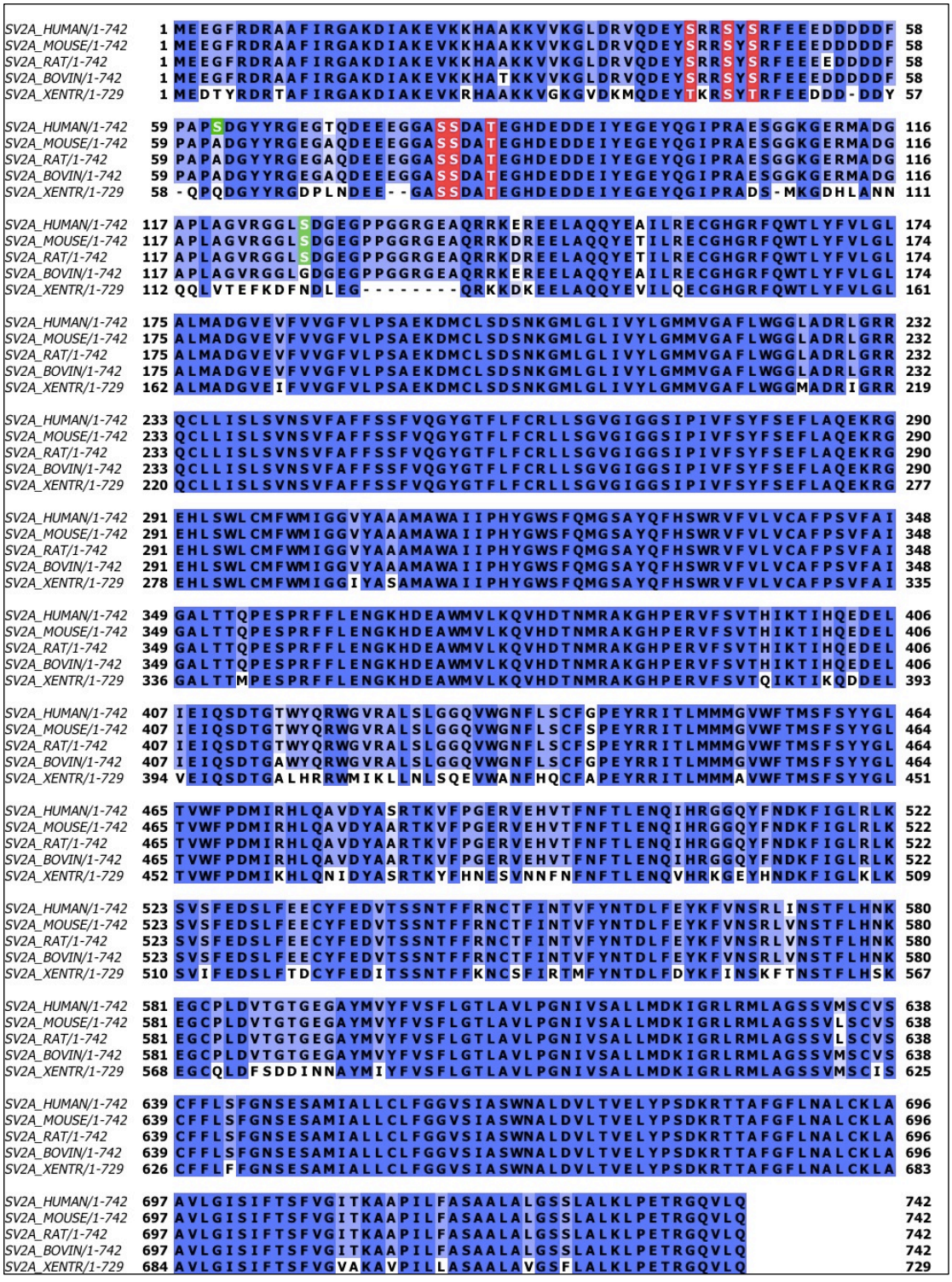

Figure 4.14. Multiple sequence alignment of human SV2A and SV2A from selected species. Ser62 and Ser127 are highlighted in green; Ser62 is not conserved among other species, while Ser127 was conserved in human, mouse and rat but not in lower species. Ser42, Ser45 and Ser47 were collectively referred to as cluster-1. Similarly, Ser80, Ser81 and Thr84 were jointly designated as cluster-2. Cluster-1 and cluster-2 residues are highlighted in red, emphasising their inter-species conservation.

The positions of those phosphosites on the cytoplasmic N-terminus of SV2A showed that they were clustered within two motifs of six and five amino acids respectively.

The three phosphosites: Ser42, Ser45 and Ser47 were henceforth collectively referred to as cluster-1. Similarly, Ser80, Ser81 and Thr84 were jointly designated as cluster-2.

4.14 Functional importance of phosphorylation sites

The synaptic vesicle cycle at the nerve terminal consists of vesicle exocytosis with neurotransmitter release, endocytosis of empty vesicles, and regeneration of fresh vesicles. Of all the cellular transport pathways, the synaptic vesicle cycle is the fastest and the most tightly regulated. The cycle of synaptic vesicle exo- and endocytosis requires the carefully orchestrated formation and dissociation of protein complexes. Vesicle transport, target recognition, docking, and fusion each involve the ordered and sequential recruitment of protein complexes from the cytoplasm. Much of this temporal and spatial control is achieved through phosphorylation-dependent protein-protein interactions, allowing the formation and dissociation of complexes to be regulated through the action of kinases and phosphatases.

I hypothesised that the cytoplasmic N-terminus of SV2A constitutes a domain that participates in phosphorylation state-dependent protein-protein interactions intrinsic to its physiological function in the synaptic vesicle trafficking cycle. The identification of protein-protein interactions of SV2A that depend on the phosphorylation state of SV2A at cluster-1 or cluster-2 is likely to shed light on the normal physiological function of SV2A phosphorylation as well as identify potential roles for SV2A in the SV cycle.

To identify protein-protein interactions that are potentially regulated by the SV2A phosphorylation sites at cluster-1 and cluster-2, I undertook a mass spectrometric analysis of brain protein complexes that could be pulled down *in vitro* by peptides encoding the phosphorylated motifs, cluster-1 and cluster-2 of SV2A.

Mass spectrometric analysis of protein-protein interactions offers a uniquely unbiased tool for elucidating the components of protein complexes. This targeted mass spectrometry-based functional proteomics approach was used to identify and compare qualitative and relative quantitative differences in protein-protein interactions of non-phosphorylated, singly-phosphorylated, doubly-phosphorylated and triply-phosphorylated peptides encompassing the amino acid sequences spanning the

cluster-1 and cluster-2 motifs and flanking sequences (Table 4.7 and Figure 4.6). Those biotinylated peptides were employed in pull-down experiments from mouse brain homogenates to identify protein interactors by mass spectrometry and to assess the phosphorylation-dependence of those interactions.

4.15 Quantitative analysis of proteins pulled-down by differentially phosphorylated SV2A cluster-1 peptides

Eight biotinylated peptides (Table 4.7) corresponding to residues 28 to 61 of human SV2A, plus 4 Arginine residues added to the C-terminus to promote solubility, were custom-made by GL Biochem (Shanghai, China). The identity, purity and phosphorylation status of the peptides were ascertained by mass spectrometry.

	Cluster-1 peptides
Phosphorylation status	Peptide Sequence
NPCluster-1	BIOTIN-KKVVKGLDRVQDEYSRRSYSRFEEEDDDDDFPAPRRRR
SV2A pS42	BIOTIN-KKVVKGLDRVQDEY**S^{P}**RRSYSRFEEEDDDDDFPAPRRRR
SV2A pS45	BIOTIN-KKVVKGLDRVQDEYSRR**S^{P}**YSRFEEEDDDDDFPAPRRRR
SV2A pS47	BIOTIN-KKVVKGLDRVQDEYSRRSY**S^{P}**RFEEEDDDDDFPAPRRRR
SV2A pS42+pS45	BIOTIN-KKVVKGLDRVQDEY**S^{P}**RR**S^{P}**YSRFEEEDDDDDFPAPRRRR
SV2A pS42+pS47	BIOTIN-KKVVKGLDRVQDEYSRR**S^{P}**Y**S^{P}**RFEEEDDDDDFPAPRRRR
SV2A pS45+pS47	BIOTIN-KKVVKGLDRVQDEY**S^{P}**RR**S^{P}**YSRFEEEDDDDDFPAPRRRR
SV2A pS42+pS45+pS47	BIOTIN-KKVVKGLDRVQDEY**S^{P}**RR**S^{P}**Y**S^{P}**RFEEEDDDDDFPAPRRRR

Table 4.7. Cluster-1 peptides used in pull-down experiments. Cluster-1 biotinylated peptides correspond to residues 28 to 61 of human SV2A; 4 Arginine residues have been added to the C-terminus to promote solubility. Each of the 8 peptides has a different phosphorylation status, indicated in the first column of the table. Phosphorylated residues are highlighted in red.

For Cluster-1, bait peptides consisted of amino-terminally tagged biotinylated peptides (GL Biochem, Shanghai, China) (Table 4.7). The peptides used were as

follows: the non-phosphorylated amino acids corresponding to residues 28 to 61 of human SV2A, plus 4 Arginine residues added to the C-terminus to promote solubility (NP1); the NP1 peptide phosphorylated either at Ser42 (pS42) or at Ser45 (pS45) or at Ser47 (pS47), respectively; the NP1 peptide phosphorylated either at Ser42 and at Ser45 (pS42+45), or at Ser42 and at Ser47 (pS42+47), or at Ser45 and at Ser47 (pS45+47); and the NP1 peptide phosphorylated at Ser42, Ser45 and Ser47 (pS42+45+47).

For each affinity peptide pull-down, 10 mg of mouse brain homogenate in CHAPS lysis buffer was pre-cleared five times with 10µl of streptavidin sepharose beads to eliminate proteins that bind non-specifically to the resin. 3µg of each peptide was then incubated to 10 mg of pre-cleared mouse brain lysate for 10 minutes at 4 ^{0}C. 20µl of 1:1 streptavidin bead slurry was then added to each mixture for 5 minutes. Samples were washed three times in lysis buffer containing 0.15 M NaCl. Bound proteins were eluted from the immobilised peptides with 1 % Rapigest and processed for mass spectrometry analysis.

Mass spectrometry data for each peptide pull-down was then analysed to distinguish proteins binding with different affinities to each peptide. Relative protein quantification was determined using peptide hits quantification and MASCOT scores are shown in Table 4.8. I applied stringent thresholds to decide on the inclusion of proteins. Firstly, only proteins binding with high affinity with a MASCOT score of higher than 100 were included. Secondly, for the affinity to be preferential, it was essential that there were more peptide hits and higher MASCOT scores depending on the phosphorylation status of the peptide. The number of peptide hits, sequence coverage and MASCOT scores were all considered for confirmation of preferential affinity.

Enrichment or depletion of a particular protein in a pull-down with either the phosphorylated or non-phosphorylated bait peptides was assessed using the ratio of normalised peptide hits for the peptides of that protein obtained using the bait peptides. Enrichment was arbitrarily defined as a 2-fold greater number of normalised peptide hits or normalised ion currents for the phosphorylated versus non-phosphorylated bait peptide or vice versa.

4.15.1 Results of cluster-1 peptide pull-downs

For cluster-1, there were several proteins that showed different binding affinities in pull-downs depending on the phosphorylation status of the peptide used as bait. To tease out which of the interactions were phosphorylation-dependent, I stratified the highest-scoring proteins into discrete functional groupings and analysed the number of peptides hits, sequence coverage and MASCOT scores for those proteins in each peptide pull-down (Table 4.7).

A major class of proteins that were pulled down by the cluster-1 peptides was all four subunits of the clathrin adaptor AP2 complex (adaptor-related protein complex 2). AP2 is the best-characterised member of the family of heterotetrameric clathrin adaptor complexes that play pivotal roles in many vesicle trafficking pathways within the cell. The AP2 adaptor complex works on the plasma membrane to internalise cargo in clathrin-mediated endocytosis (Pearse et al., 2000). AP2 is a heterotetrameric protein, which is made up of four different subunits. Each subunit is called an adaptin, and each adaptin is named after a Greek letter—α, β, μ, and σ adaptin subunits (Figure 4.15) (Collins et al., 2002). The AP2 complexes which function both as a linker between the plasma membrane and the clathrin lattice and as a sorter for some proteins to be internalised, comprise two large subunits of 100–130 kDa (α and β2), a medium subunit of ~50 kDa (μ2), and a small subunit of 17–20 kDa (σ2) (Kirchhausen, 1999).

One striking finding was that all four subunits of the AP2 complex (AP2α, AP2β2, AP2μ2 and AP2σ2) (Table 4.8) were present in all 8 peptide pull-downs. However, the comparison of the number of peptide hits, sequence coverage and MASCOT scores for each subunit indicated that the affinity was dependent on the phosphorylation status of the peptide used as bait. Intriguingly, the affinity of the AP2 complex appeared to decrease upon phosphorylation of cluster-1. The highest number of peptide hits and MASCOT scores for AP2 subunits were seen with the dephosphorylated cluster-1 peptide (NP1).

SV2A Cluster-1 peptide pull-downs										
			MASCOT scores (number of peptide hits)							
			Peptide pull-down							
UniProtKB/Swiss-Prot entry name	Primary accession number	Gene name	NP1	pS42	pS45	pS47	pS42+pS45	pS42+pS47	pS45+pS47	pS42+pS45+pS47
Spectrin β chain, brain 2	Q68FG2	SPTBN2	45 (10)	-	140 (17)	27 (16)	-	-	56 (8)	1376 (42)
AP2 complex subunit α1	P17426	AP2A1	848 (33)	1191 (56)	854 (40)	151 (17)	606 (36)	268 (17)	904 (41)	737 (24)
AP2 complex subunit α2	P17427	AP2A2	291 (16)	1026 (51)	442 (29)	101 (13)	659 (36)	222 (15)	757 (41)	416 (21)
AP2 complex subunit β-2	Q9DBG3	AP2B1	310 (29)	819 (46)	435 (24)	76 (11)	549 (32)	207 (27)	522 (34)	172 (11)
AP2 complex subunit μ-2	P84091	AP2M1	783 (37)	1068 (71)	709 (43)	133 (22)	377 (34)	416 (34)	456 (29)	343 (20)
AP2 complex subunit σ-2	P62743	AP2S1	-	36 (5)	-	-	52 (6)	-	26 (6)	28 (3)
Na/K-transporting ATPase subunit alpha-3	Q6PIC6	ATP1A3	133 (10)	37 (6)	355 (16)	712 (42)	-	220 (5)	310 (20)	682 (21)
Actin, α1	P62737	ACTA1	-	-	677 (31)	642 (32)	-	428 (23)	-	-
β-actin	P60710	ACTB	657 (31)	807 (35)	1244 (61)	1463 (69)	334 (16)	876 (46)	-	2273 (89)
CaM kinase II α chain	P11798	Camk2a	897 (39)	846 (28)	559 (25)	884 (42)	400 (18)	687 (26)	420 (21)	235 (18)

Table 4.8. Proteins with differential affinities for SV2A cluster-1 depending on its phosphorylation status. Comparisons are shown only for proteins identified with a MASCOT score of 100 or more. The MASCOT scores for each protein for each peptide pull-down are shown. The number of peptide hits for each protein is shown between parentheses.

Lower scores were observed with the singly-phosphorylated and doubly-phosphorylated peptides and the lowest scores was seen with the triply-phosphorylated peptide (Table 4.8), indicating that phosphorylation of cluster-1 impedes the interaction of SV2A with the AP2 complex.

4.15.1 The clathrin adaptor AP2 complex

The AP2 complex is a stable complex of four subunits called adaptins which give rise to a structure that has a core domain and two appendage domains attached to the core domain by polypeptide linkers (Figure 4.15). These appendage domains are sometimes called 'ears'. The core domain binds to the membrane and to cargo destined for internalisation. The alpha and beta appendage domains bind to accessory proteins and to clathrin. Their interactions allow the temporal and spatial regulation of the assembly of clathrin-coated vesicles and their endocytosis.

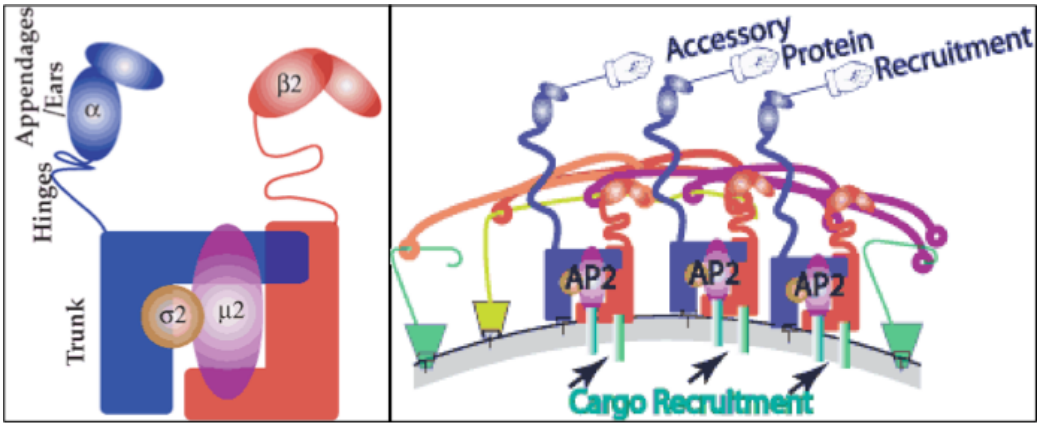

Figure 4.15. The AP2 adaptor complex.

Left Panel: **The structure of the free AP2 complex.** There are 4 different subunits (as illustrated in the model above based on the crystal structure) and thus they are sometimes called polymeric or hetrotetrameric adaptors. The trunk domain binds to membranes and to cargo via the μ and β subunits. The appendage domains (sometimes called 'ears') bind to accessory proteins. Structures of a number of appendage domains have been solved and binding motifs and partners characterised. The hinge domains bind to clathrin terminal domains. Right Panel: **structure of AP2 as bound to a vesicle.** The AP2 adaptor complex works on the plasma membrane to internalise cargo. In the above picture the beta-appendage is bound to the clathrin cage while the alpha-appendage is free to recruit accessory proteins. The AP2 complex is critical in synaptic vesicle recycling. (adapted from www.endocytosis.org).

AP2 was previously reported to interact with the amino-terminus of SV2A (Yao et al., 2010). SV2A has been shown to serve as a receptor for clathrin adaptor proteins via a

tyrosine-based endocytosis motif (Yao et al., 2010). SV2A contains two tyrosine-based endocytosis motifs, termed YXXΦ motifs, where Y denotes tyrosine, X denotes any amino acid, and Φ denotes a hydrophobic amino acids. The first endocytosis motif is at amino acids 46-49 with sequence $Y^{46}S^{47}RF$, which is in SV2A's cytoplasmic amino terminus. The serine residue, Ser47, in the endocytic motif is a major site of phosphorylation and so are two other adjacent serine residues, Ser42 and Ser45. Those three phosphosites were collectively grouped as cluster-1. Importantly, Tyr46 appeared to be a major determinant of the interaction because binding was substantially lost upon mutagenesis of this residue to alanine (Yao et al., 2010). The endocytosis motif of SV2A thus has the highest affinity for endocytosis-related proteins, particularly the clathrin adaptor complex AP2 (Yao et al., 2010). This high affinity binding to AP2 is consistent with SV2A acting at the point of cargo recognition that ensures synaptic vesicle retrieval by endocytosis.

All the four subunits of the AP2 complex were also detected in TTBK2 co-immunoprecipitations from mouse brain homogenate (Table 4.1), indicating their physiological association with SV2A and possibly other SV proteins. Phosphorylation of the serine residues of cluster-1 adjacent to Tyr46 is likely to act as additional specificity determinants of this interaction.

4.15.2 Spectrin B2

Another major group of proteins enriched in pull-downs with certain phosphorylated SV2A cluster-1 peptides were a number of presynaptic cytoskeletal elements, particularly the brain-specific βIII spectrin (SPTBN2) when SV2A was phosphorylated at cluster-1. Enrichment for α-actin and β-actin was also observed. These proteins are present in the presynaptic portion of neurons and form a dense presynaptic cytoskeletal structure known as the presynaptic particle web involved in the stabilisation of the synapse (Phillips et al., 2001).

SPTBN2 was not present in pull-downs with NP1 or singly-phosphorylated peptides. It was only observed in pull-downs with three peptides as bait: two doubly-phosphorylated peptides (pS42+45 and pS42+47) and the triply-phosphorylated peptide. Comparison of the number of peptide hits, sequence coverage and MASCOT

scores revealed that SPTBN2 binding was significantly enhanced by the triply-phosphorylated peptide (Table 4.8), indicating that phosphorylation of cluster-1 may induce SPTBN2 binding to SV2A.

4.15.3 ATP1A3 and Camk2a

Two other proteins were observed consistently in these peptide pull-downs, but their binding affinities were independent of the phosphorylation status of the bait peptide. These two proteins were ATP1A3 and CamK2a (Calcium/Calmodulin-Dependent Protein Kinase II Alpha).

ATP1A3 is an α subunit of the Na^+/K^+ ATPase pump that is partly responsible for establishing and maintaining electrochemical gradients of sodium and potassium ions across the plasma membrane of neurons (de Carvalho Aguiar et al., 2004). Mutations in ATP1A3 have been shown to cause rapid-onset dystonia-parkinsonism (DYT12) (Blanco-Arias et al., 2009). More recently, *de novo* ATP1A3 mutations have been identified as the primary cause of alternating hemiplegia of childhood (AHC) thus expanding the spectrum of phenotypes associated with mutations in ATP1A3.

CamK2a belongs to the serine/threonine protein kinases family, and to the Ca^{2+}/calmodulin-dependent protein kinases subfamily. CamK2a is crucial for calcium signalling in several aspects of plasticity at glutamatergic synapses. Both Camk2a and ATP1A3 also co-immunoprecipitate with endogenous TTBK2 from mouse brain homogenate, indicating that they may in a protein complex with SV2A in the brain. However, comparison of the MASCOT scores from the peptide pull-downs indicates that the associations of SV2A cluster-1 to these two proteins are not phospho-dependent.

4.16 Quantitative analysis of proteins pulled-down by differentially-phosphorylated SV2A cluster-2 peptides

Similarly, eight cluster-2 peptides (Table 4.9) corresponding to residues 67 to 98 of human SV2A in which 4 Arg residues have been added to the C-terminus to promote

solubility were used to assess phosphorylation-dependent binding to Cluster-2.

For Cluster-2, the peptides used were as follows. The non-phosphorylated amino acids corresponding to residues 67 to 98 of human SV2A, plus 4 Arginine residues added to the C-terminus to promote solubility (NP2 peptide); the NP2 peptide phosphorylated either at Ser80 (pS80) or at Ser81 (pS81) or at Thr84 (pT84), respectively; the NP2 peptide phosphorylated either at Ser80 and at Ser81 (pS80+pS81), or at Ser80 and at Thr84 (pS80+pT84), or at Ser81 and at Thr84 (pS81+pT84); and the NP2 peptide phosphorylated at Ser80, Ser81 and Thr84 (pS80+pS81+pT84). The identity, purity and phosphorylation status of the peptides were verified by mass spectrometry.

	Cluster-2 peptides
Phosphorylation status	Peptide Sequence
NP2	Biotin—RGEGAQDEEEGGASSDATEGHDEDDEIYEGEYRRRR
SV2A pS80	Biotin—RGEGAQDEEEGGA**S^{P}**SDATEGHDEDDEIYEGEYRRRR
SV2A pS81	Biotin—RGEGAQDEEEGGAS**S^{P}**DATEGHDEDDEIYEGEYRRRR
SV2A pT84	Biotin—RGEGAQDEEEGGASSDA**T^{P}**EGHDEDDEIYEGEYRRRR
SV2A pS80+81	Biotin—RGEGAQDEEEGGA**S^{P}S^{P}**DATEGHDEDDEIYEGEYRRRR
SV2A pS80+pT84	Biotin—RGEGAQDEEEGGA**S^{P}**SDA**T^{P}**EGHDEDDEIYEGEYRRRR
SV2A pS81+pT84	Biotin—RGEGAQDEEEGGAS**S^{P}**DA**T^{P}**EGHDEDDEIYEGEYRRRR
SV2A pS80+pS81+pT84	Biotin—RGEGAQDEEEGGA**S^{P}S^{P}**DA**T^{P}**EGHDEDDEIYEGEYRRRR

Table 4.9. Cluster-2 peptides used in pull-down experiments. Cluster-2 biotinylated peptides correspond to residues 67 to 98 of human SV2A plus 4 Arginine residues have been added to the C-terminus to promote solubility. Each of the 8 peptides has a different phosphorylation status, indicated in the first column of the table. Phosphorylated residues are highlighted in red.

The dataset for the Cluster-2 peptides was analysed using the same stringent criteria used for the analysis of cluster-1 peptide pull-downs. The data is summarised in Table 4.10 (on the next page). Several presynaptic cytoskeletal elements were seen to bind to the cluster 2 peptides. γ-actin, WDR11 (WD repeat-containing protein 11) and neurofilament medium polypeptide (NEFM) were observed with all 8 cluster-2 peptides. However, similar number of peptide matches and MASCOT scores were

observed for those proteins in all 8 peptide pull-downs signifying that the binding affinities were independent of the phosphorylation status of the bait peptides. Whilst the interaction of SV2A with those cytoskeletal elements may be critical for SV2A's function in the SV cycle, they are not regulated by phosphorylation of cluster-2.

Nevertheless, further inspection of these pull-downs revealed that synaptotagmin 1 (Syt1), another SV membrane protein, binds to the triply-phosphorylated cluster-2 peptide with very high affinity and was conspicuously not retrieved by the rest of the peptides from mouse brain homogenate. This finding strongly suggests that phosphorylation of SV2A at Ser80, Ser81 and Thr84 may regulate the interaction of SV2A with Syt1. Synaptotagmins are SV proteins present in multiple isoforms (Li et al., 1995). Syt1 is one of the most abundant SV proteins. A typical SV contains 15 synaptotagmin 1s, accounting for ≈7% of the total SV protein content (Takamori et al., 2006).

SV2A Cluster-2 peptide pull-downs										
			MASCOT scores (number of peptide hits)							
			Peptide pull-down							
UniProtKB/Swiss-Prot entry name	Primary accession number	Gene name	NP2	pS80	pS81	pT84	pS80+pS81	pS80+pT84	pS81+pT84	pS80+pS81+pT84
actin	P68033	ACTC	1267 (56)	1098 (40)	1078 (46)	1276 (57)	1238 (54)	822 (45)	845 (44)	820 (41)
Neurofilament medium polypeptide	P08553	NEFM	33 (14)	355 (36)	253 (26)	144 (19)	166 (28)	156 (22)	191 (23)	147 (17)
Vacuolar protein sorting-associated protein 13C	Q8BX70	VPS13C	486 (56)	1540 (94)	861 (59)	368 (51)	944 (71)	1731 (16)	1061 (79)	1259 (102)
WD repeat-containing protein 11	Q8K1X1	WDR11	124 (9)	22 (1)	66 (6)	36 (5)	198 (11)	-	288 (11)	606 (36)
Synaptotagmin 1	P46096	**Syt 1**	-	-	-	-	-	-	-	**157 (12)**

Table 4.10. Proteins with differential affinities for SV2A cluster-2 depending on its phosphorylation status. Comparisons are shown only for proteins identified with a MASCOT score of 100 or more. The MASCOT scores for each protein for each peptide pull-down are shown. The number of peptide hits for each protein is shown between parentheses

4.17 Confirmation of quantitative mass spectroscopy by immunoblotting

I used immunoblotting of the mixture of proteins pulled down by all 16 bait peptides as an independent method of assessing the validity of the mass spectrometry results. As shown in Figure 4.16, SPTBN2 did not bind NP1 or any of the singly-phosphorylated cluster-1 peptides. Low-level binding to the two of the doubly-phosphorylated peptides (pS42+pS45 and pS45+pS47) was detected by immunoblotting. The triply-phosphorylated cluster-1 peptide was able to bind SPTBN2 with higher affinity than the other two peptides as shown in Figure 4.16. None of the cluster-2 peptides bound SPTBN2. This pattern of enrichment of SPTBN2 was in complete agreement with the mass spectrometric analysis.

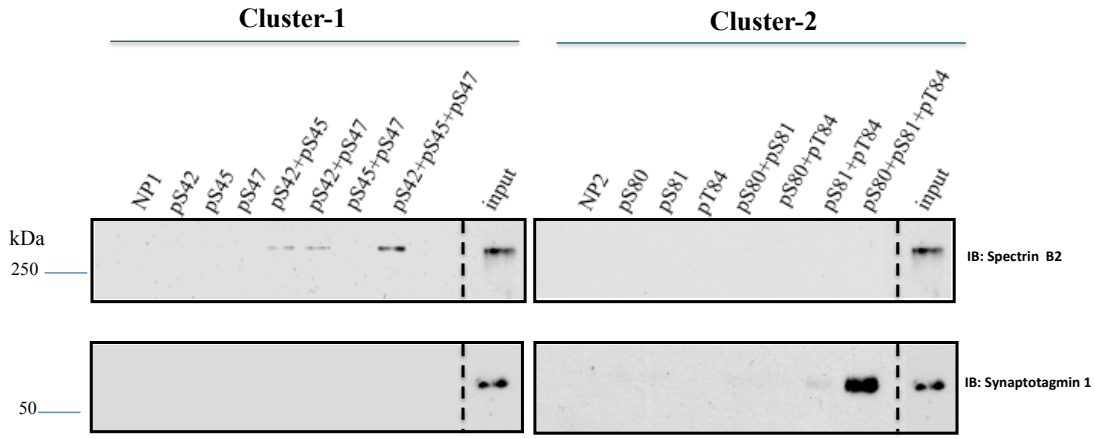

Figure 4.16. Composite of immunoblots confirming peptide pull-down mass spectroscopy data. Each lane is labelled with a bait peptide with different phosphorylation status that was used in pull-down experiments. Eluted proteins bound to each peptide were separated by SDS-PAGE and immunoblot analysis was performed with antibodies against SPTBN2 and Syt1.

Immunoblotting all the peptide pull-downs for Syt1 corroborates the previous observation that only the SV2A cluster-2 triply-phosphorylated peptide binds Syt1 with very high affinity Figure 4.16, while none of the other peptides retrieved Syt1 from mouse brain lysate. This observation adds further support to the notion that the phosphorylation of the three cluster-2 residues modulates the binding of SV2A to Syt1.

4.18 Validation of phosphorylation-dependence of interactions

These observations suggest that a phosphorylation-dependent mechanism modulates the association of SPTBN2 and Syt1 to the amino-terminus of SV2 via cluster-1 and cluster-2 respectively. To test the phosphorylation-dependence of those interactions *in vivo*, I carried out a λ-phosphatase treatment on endogenous SV2A immunoprecipitates.

SV2A was immunoprecipitated from mouse brain lysate as described before. For λ-phosphatase treatment, immunoprecipitated proteins on beads were washed twice with lambda buffer (50mM Tris-Cl pH 7.5, 100mM NaCl, 0.1mM EGTA, 2mM DTT, 0.01% Brij-35). The immunoprecipitate was then split into four aliquots (Figure 4.17A): Aliquot 1 was left on ice, aliquot 2 was incubated for 60 min at 30 ºC in lambda buffer + 2.5mM $MnCl_2$ without λ -phosphatase, aliquot 3 was treated for 60 min at 30 °C with 100 U λ -phosphatase in lambda buffer + 2.5mM $MnCl_2$ and aliquot 4 was treated for 60 min at 30 °C with 100 U λ-phosphatase that had been pre-incubated with 20mM EDTA, in lambda buffer + 2.5mM $MnCl_2$. After the 60 min incubations, the four pellets were washed three times in phosphatase buffer containing 150mM NaCl, then resuspended in SDS sample buffer and analysed by immunoblotting.

Immunoblot analysis of SV2A treated with λ-phosphatase induced the dephosphorylation of SV2A as shown by the blot using the SV2A pS42,45,47 phosphospecific antibody (Figure 4.17B). The phosphatase treatment resulted in a nearly complete loss of the interactions with SPTBN2 and Syt1. These observations confirm the findings from the peptide pull-downs and definitively show that these interactions can be modulated by phosphorylation. Thus, a model whereby phosphorylation of SV2A by TTBK2 confers binding to SPTBN2 via cluster-1 and Synaptotagmin 1 via cluster-2 can be envisioned.

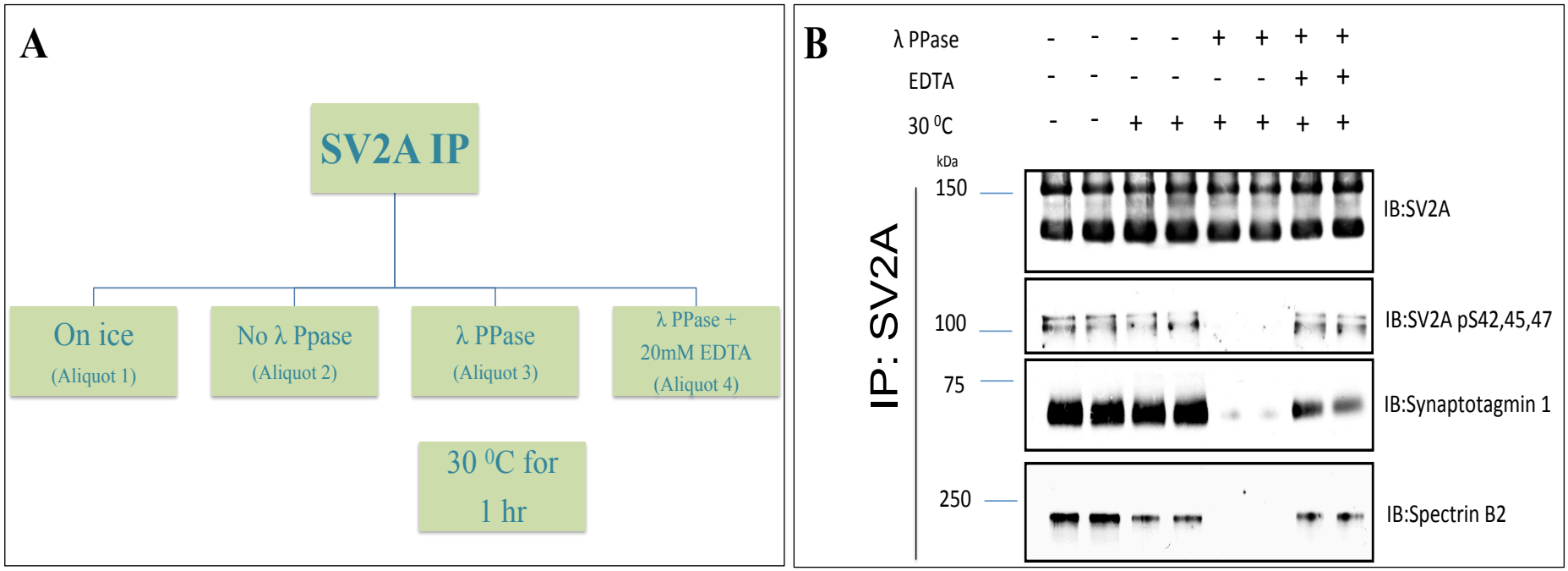

Figure 4.17. Experimental strategy and composite of immunoblots verifying the phosphorylation-dependence of SPTBN2 and Synaptotagmin 1 binding to SV2A. (A) Endogenous SV2A was immunprecipitated from 40 mg of mouse brain homogenate. The immunoprecipitate was then split into four aliquots, which were the subjected to the indicated reaction conditions. (B) After washes, each reaction was subjected to SDS-PAGE and immunoblotting in duplicate using the indicated antibodies.

4.19 Synaptotagmin 1

Synaptotagmins (Syts) make up a family of vesicle membrane proteins that includes more than 17 isoforms with diverse functions and tissue-specific expression patterns (Ullrich et al., 1994, Schiavo et al., 1998). Synaptotagmin 1 (Syt1), the best-characterised isoform, is expressed abundantly in neurons and is essential for fast Ca^{2+}-triggered neurotransmitter release (Chapman, 2008).

Syt1 is thought to function in several distinct steps during the synaptic vesicle cycle (Chapman, 2002). Among these functions, Syt1 might operate as a Ca^{2+}- sensor that triggers rapid exocytosis (Augustine, 2001). The molecular mechanism by which Syt1 transduces Ca^{2+} signals to the opening and/or dilation of fusion pores has therefore emerged as a crucial question in the study of synaptic transmission.

Syt1 is anchored to the membrane of synaptic vesicles via a single transmembrane domain near its N-terminus (Figure 4.18a). The most interesting feature of Syt1 is the presence of tandem C2 domains that make up its cytoplasmic domain; these are designated C2A and C2B (Perin et al., 1990) (Figure 4.18a). C2 domains are conserved motifs of ~135 amino acid residues that often serve as Ca^{2+} and/or effector binding domains. The name is derived from conserved or constant sequence 2 among isoforms of protein kinase C that are regulated by Ca^{2+} and phosphatidyl serine (PtdSer) (Nalefski and Falke, 1996). Early studies revealed that Syt1 binds Ca^{2+} and PtdSer-containing membranes in a mutually dependent way (Brose et al., 1992). Subsequent studies showed that isolated C2A directly binds Ca^{2+} and PtdSer (Chapman, 2002) and C2B was also later shown to be a Ca^{2+}-sensing module (Desai et al., 2000). Similar to C2A (Sutton et al., 1999), C2B is a compact β-sandwich formed by two four-stranded β-sheets with loops emerging from the top and bottom (Fernandez et al., 2001, Sutton et al., 1999) (Figure 4.18b). Nuclear magnetic resonance (NMR) studies indicate that C2B binds two Ca^{2+} ions (Fernandez et al., 2001), whereas C2A binds three Ca^{2+} ions (Ubach et al., 1998). In each C2 domain, five conserved acidic residues (Asp) in two flexible loops play crucial roles in coordinating Ca^{2+} (Sutton et al., 1995, Fernandez et al., 2001, Sutton et al., 1999) (Figure 4.18b).

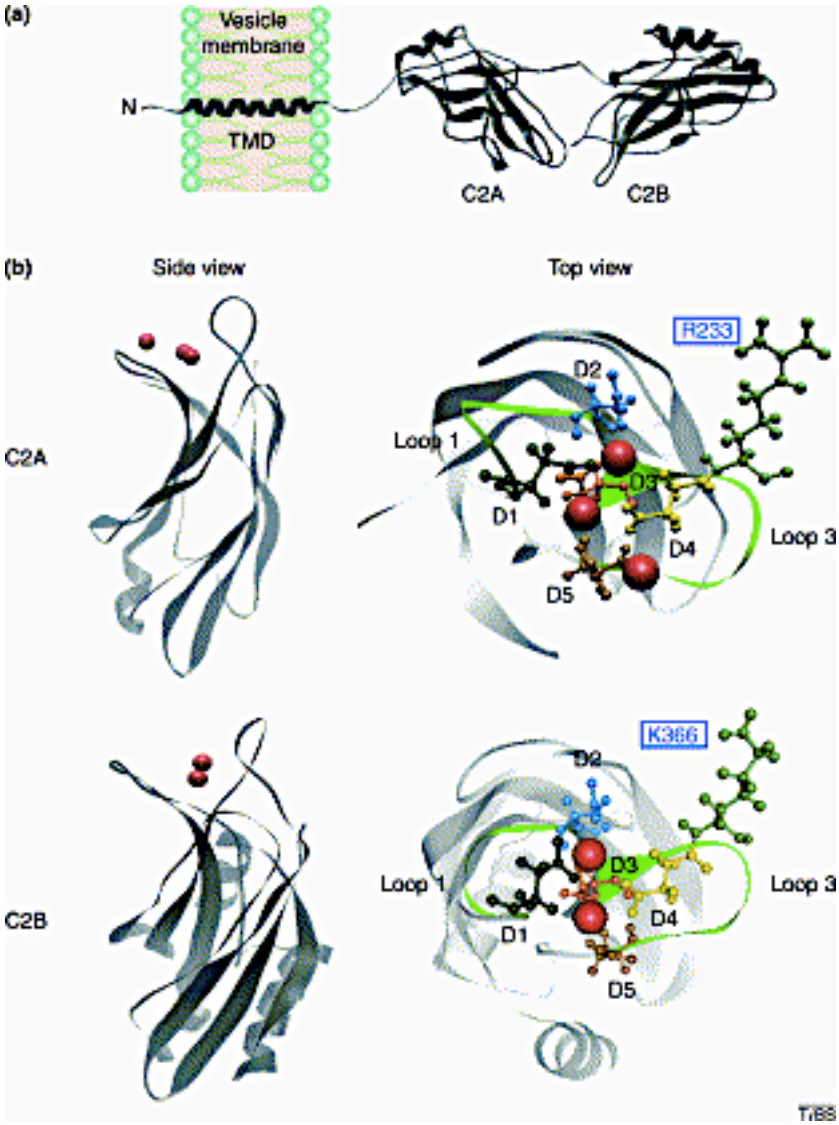

Figure 4.18. Structure of synaptotagmin 1 (Syt1). (a) Syt1 is anchored to the vesicle membrane via a single transmembrane domain (TMD) near its N terminus. The cytoplasmic domain of syt1 is composed of two conserved motifs called C2 domains (C2A and C2B). To generate this image, the crystal structure of the cytoplasmic domain of SytIII was used as a template (Sutton et al., 1995). (b) 3D structures of C2A (Shao et al., 1998) and C2B (Fernandez et al., 2001). Red spheres represent multiple Ca^{2+} ions bound to loops 1 and 3. Ca^{2+}-binding loops 1 and 3 are shown as green ribbons. Five acidic residues (D1-D5) in each domain (C2A: D172, D178, D230, D232, D238; and C2B: D303, D309, D363, D365, D371) that coordinate Ca^{2+} ions are shown as ball-and-sticks. Positively charged residues in each C2 domain that have been shown to play roles in mediating the binding of Ca^{2+} and effectors (C2A, R233; and C2B, K366) (Fernandez-Chacon et al., 2001) are also shown as ball-and-sticks. [adapted from (Bai and Chapman, 2004)].

Syt1 operates as the Ca^{2+}-sensor during neuronal exocytosis. Ca^{2+} thus has a crucial regulatory role and alters the interaction of Syt1 with effector molecules on a microsecond time-scale to drive neurotransmitter release (Bai and Chapman, 2004).

4.20 Activities of the C2 domains of Syt1

The C2A domain of Syt1 is considered to be a calcium sensor, because the binding between phospholipids and the C2A domain is Ca^{2+}-dependent (Geppert et al., 1994). The C2A domain also binds to syntaxin, a plasma membrane presynaptic protein, in the presence of Ca^{2+} (Shao et al., 1997, Chapman et al., 1995); an interaction that is necessary for SV exocytosis.

The C2B domain engages a wider array of effector molecules than the C2A domain. Several proteins, such as clathrin adaptor protein-2 (AP2) (Zhang et al., 1994), soluble NSF attachment protein (β-SNAP) (Schiavo et al., 1995), SNAP-25, and N-type calcium channels (Schiavo et al., 1997), bind to different sites in the C2B domain. AP2 is the multimeric protein complex that participates in cargo protein internalisation during the clathrin-mediated endocytosis of synaptic vesicles on the plasma membrane. The interaction between the C2B domain and AP2 was reported to play an important role in synaptic vesicle endocytosis. An in vivo study in *Caenorhabditis elegans* suggests that the C2B domain may function as a high-affinity docking site for AP2 and serve as a bridge between endo- and exocytosis in the synaptic vesicle cycle (Mizutani et al., 1997). It was also reported that the C2B domain binds inositol polyphosphates [IHPS, including inositol 1,3,4,5-tetrakisphosphate (IP4), inositol 1,3,4,5,6-pentakisphosphate (IP5), and inositol hexakisphosphate (IP6)] and phosphoinositide polyphosphates (PtdInsPn) (Fukuda et al., 1994). This binding is Ca^{2+} concentration-dependent. The binding module was determined using a liposome model system (Schiavo et al., 1996).

IP6 is generally considered to be an antinutrient because of its ability to chelate divalent minerals and reduce the extent of their absorption (Xu et al., 2008). IP6 was shown to inhibit free radical formation and weaken the lipid peroxidation catalysed by iron and ascorbic acid in human erythrocytes (Xu et al., 2008). A neuroprotective effect for IP6 was suggested because of its antioxidant effects and its ability to alter the cell signalling pathways that detoxify reactive oxygen species (ROS). A cell line assay using squid giant synapses indicated that the serial microinjection of IP6 into the presynaptic terminal inhibited synaptic transmission; this inhibition could be released by the co-injection of antibodies that recognise the C2B domain (Llinas et al., 1994). In addition, IP6 also plays an essential role in regulating the inhibition of

neurotransmitter release, and this effect might partially be due to the inhibition of the interaction between Syt1 and AP2, which blocks endocytosis (Mizutani et al., 1997).

4.21 Domain architecture and NMR structure of Synaptotagmin 1 C2B-IP6 complex

To understand the interactions between the C2B domain of Syt1 and IP6 at the molecular level, Joung et al. (2012) have used a variety of biophysical methods including isothermal titration calorimetry (ITC), circular dichroism (CD) spectrometry, and multidimensional NMR, to characterise the molecular interaction between C2B and IP6.

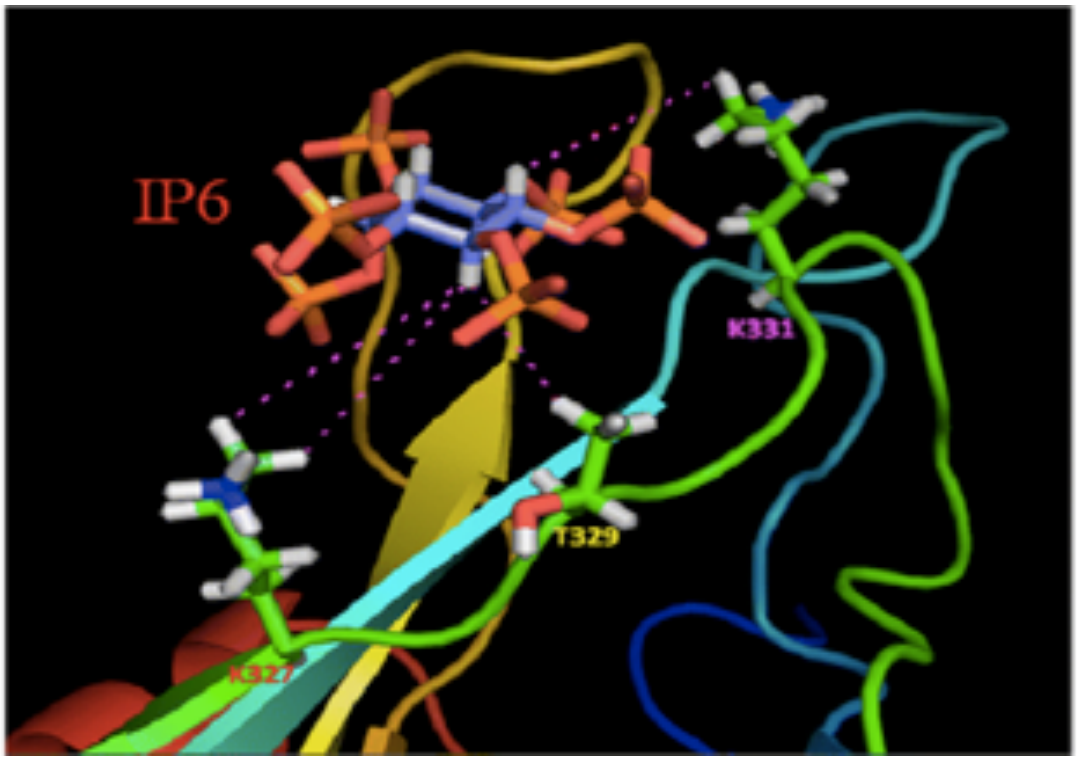

Figure 4.19. NMR structure of the C2B domain of synaptotagmin 1 complexed with IP6. A magnified view of the C2B-IP6 complex showing the binding region and the corresponding residues involved in intermolecular interaction with three phosphate groups indicated by pink dotted lines [reproduced from (Joung et al., 2012)].

IP6 binds strongly to the C2B domain and it inhibits the fusion step of Ca^{2+}-regulated exocytosis (Mochida et al., 1997, Fukuda and Mikoshiba, 1997). Therefore, IP6 was assumed to be a potential regulator of neurotransmitter release and the elucidation of the structural interactions between the IP6 and C2B domain at the molecular level provided the mechanistic information needed to understand how IP6 acts as an inhibitor of neurotransmitter release. It has been reported that point mutants in the

polybasic Lys residues (K324–K327) (see sequence alignment in Figure 4.20) within the C2B domain decreased the binding affinity of the C2B domain for IP6 (Fukuda et al., 1995).

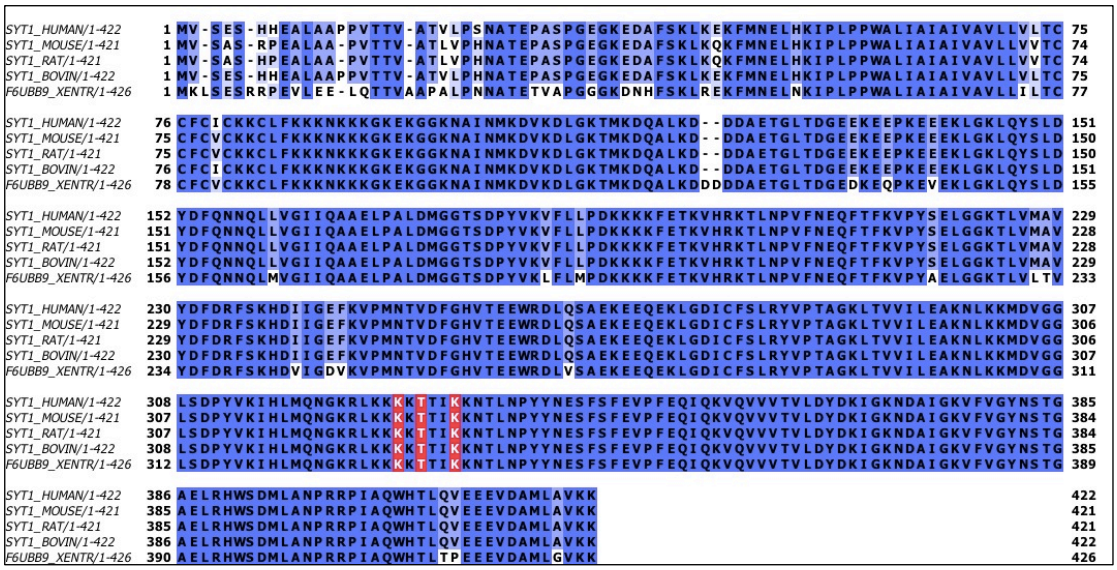

Figure 4.20. Multiple sequence alignment of human Syt1 and Syt1 from selected species. Sequence alignment showing the high degree of conservation of the Syt1 protein sequence especially in the C2A domain (residues 157-245) and the C2B domain (residues 287-422). The three charged and polar amino acids that are critical for binding three phosphate groups of IP6 are highlighted in red.

In addition, the isothermal titration calorimetry (ITC) data suggested a one-binding site mode for the C2B–IP6 complex (Joung et al., 2012). The exact binding region of IP6 on C2B was determined by the solution structure of the C2B–IP6 complex using intermolecular nuclear Overhauser enhancement (NOE) data and chemical shift perturbation data. The four intermolecular NOEs between the C2B domain and IP6 are illustrated in Figure 4.19. Residues K327, T329, and K331 in the C2B domain exhibited intermolecular NOEs with IP6. The authors thus identified a conserved cluster of charged and polar amino acids, that provide generic interactions with three phosphate groups (Figure 4.19). Those residues are therefore candidates for phosphorylation-dependent interactions with other proteins or molecular effectors.

4.22 How does the phosphorylated SV2A cluster-2 bind Syt1?

I postulated that those three residues could possibly be the critical binding sites of the three phosphate groups of SV2A cluster-2. To verify that those key phosphate-

interacting residues are required for mediating the phospho-dependent SV2A/Syt1 interaction, I mutated two of the residues predicted to be the binding sites of phosphate groups to alanine and assessed their ability to bind the triply-phosphorylated cluster-2 peptide.

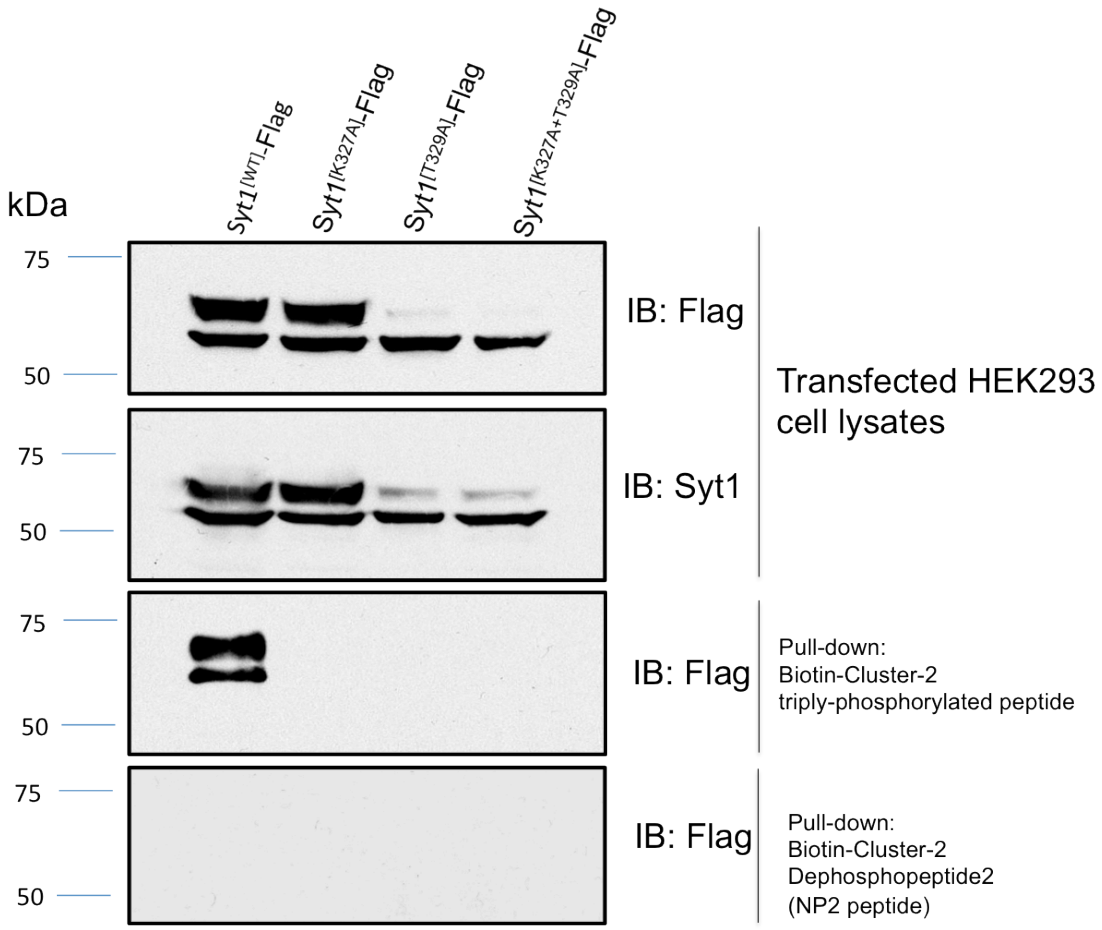

Figure 4.21. Wild-type Syt1 is retrieved by the triply-phosphorylated cluster-2 peptide but not the K327A mutant or the T329A mutant. Wild-type Syt1 with a C-terminal flag tag, single amino-acid substitution mutants (K327A and T329A) and a double amino-acid substitution mutant (K327A+T329A) were transiently expressed in HEK293 cells. Transfected cell lysates were incubated with the cluster-2 triply-phosphorylated peptide or the NP2 peptide immobilised on streptavidin beads. Proteins bound to beads were eluted and separated by SDS-PAGE. Immmunoblots were performed on whole cell lysates with anti-flag and anti-Syt1 antibodies (top two panels). Syt1 proteins bound to peptides were detected with an anti-Flag antibody.

cDNA constructs to express Syt1-Flag fusion proteins carrying a lysine-to-alanine or a threonine-to-alanine mutation in one or both of these critical IP6-binding residues were generated. The two key residues were Lys327 and Thr329 of the C2B domain of human Syt1. The resulting proteins, Syt1$^{[K327A]}$-Flag, Syt1$^{[T329A]}$-Flag and Syt1$^{[K327A+T329A]}$-Flag Wild-type and mutant (K327A and T329A) were transiently

expressed in HEK293 cells along with Syt1$^{[WT]}$-Flag. Wild-type and mutant fusion proteins were all produced by HEK293 cells (Figure 4.21).

The biotinylated cluster-2 triply-phosphorylated phosphopeptide affinity-retrieved Syt1$^{[WT]}$-Flag from HEK293 cell lysate. Remarkably, alanine mutations of either K327 or T329 within the C2B domain of Syt1 ablated the capture of Syt1 by the phosphopeptide (Figure 4.21).

As shown in Figure 4.21, mutation of either Lys327 or Thr329 in Syt1 completely abrogates the interaction with the triply-phosphorylated cluster-2 peptide, suggesting that these two residues are critical determinants for the SV2A/Syt1 interaction. This observation argues that K327 and T329 could provide generic interactions with phosphate groups of SV2A cluster-2 and is therefore critical for the phospho-dependent interaction of SV2A with synaptotagmin 1.

4.23 Discussion

As a means to understand the role of phosphorylation-dependent interactions imparted by the cytosolic N-terminus of SV2A, I employed a proteomic study to identify proteins and pathways that physically interact with the phosphorylated motifs of SV2A. In this chapter, I have described the phosphorylation-dependent interactions between SV2A and SPTBN2 via cluster-1 and the interaction between SV2A and Syt1 via cluster-2. Another noteworthy observation was that phosphorylation of the three serine residues of cluster-1, which are situated in the vicinity of SV2A's tyrosine-based endocytosis motif (amino acids 46-49), hinders the interaction between SV2A and adaptor-related protein complex 2, AP2.

4.23.1 AP2 clathrin adaptor complex

AP2 was previously reported to interact with the amino-terminus of SV2A (Yao et al., 2010). SV2A has been shown to serve as a receptor for clathrin adaptor proteins via a tyrosine-based endocytosis motif (Yao et al., 2010). SV2A contains two tyrosine-based endocytosis motifs, termed YXXΦ motifs, where Y denotes tyrosine, X denotes any amino acid, and Φ denotes a hydrophobic amino acids. The first endocytosis

motif is at amino acids 46-49 with the amino acid sequence $Y^{46}S^{47}RF$, which is in SV2A's cytoplasmic amino terminus. The serine residue, Ser47, in the endocytic motif is a major site of phosphorylation and so are two other neighbouring serine residues, Ser42 and Ser47: the three phosphosites that were previously identified and collectively grouped as cluster-1.

Importantly, Tyr46 appeared to be a major determinant of the interaction because binding was substantially lost upon mutagenesis of this residue to alanine (Yao et al., 2010). In that study, the endocytosis motif of SV2A (YSRF) was found to have the highest affinity for endocytosis-related proteins, particularly the clathrin adaptor complex AP2 (Yao et al., 2010). This high affinity binding to AP2 is consistent with SV2A acting at the point of cargo recognition in the SV cycle that ensures synaptic vesicle retrieval by endocytosis. Phosphorylation of the serine residues of cluster-1 is likely to act as additional specificity determinants for the temporal and spatial modulation of this interaction. Precedence for this supposition is provided by studies of the phospho-dependent binding of the clathrin adaptor AP2 to the $GABA_A$ receptor ($GABA_AR$) γ subunit isoforms.

Kittler et al. (2008) performed molecular analyses to delineate the amino acids responsible for binding to the μ2 subunit of AP2 (μ2–AP2) in the the $GABA_A$ receptor ($GABA_AR$) protein. This resulted in the identification of a classical tyrosine-based binding motif (YXXφ, where φ is a hydrophobic amino acid) centred on Tyr367 in the ($Y^{365}GY^{367}ECL$) in the γ2 subunit of $GABA_AR$ (Kittler et al., 2008). Significantly, both Tyr367 and the adjacent tyrosine residue Tyr365 are the principal sites of phosphorylation for Src family members in $GABA_ARs$ (Brandon et al., 2001). Using surface plasmon resonance (SPR) coupled with crystallography, it was evident that this motif bound μ2–AP2 with an affinity of 40 nM, an interaction critically dependent on Tyr367 (Kittler et al., 2008). Phosphorylation of either Tyr365 or Tyr367 ablated the interaction of μ2–AP2 to the γ2 subunit of $GABA_AR$.

The interaction of SV2A with AP2 is critically dependent Tyr46 (Yao et al., 2010), which is a potential site of phosphorylation for a tyrosine kinase. Hypothetically, there are two separate phospho-dependent mechanisms regulating the interaction of SV2A with AP2. The fact that AP2-binding motifs are regulated by different kinases

suggests that this mechanism may have evolved as a scheme to allow for tight regulation of AP2 binding, and therefore internalisation kinetics, by multiple signalling cascades that converge at the level of direct receptor phosphorylation. It will be interesting to dissect the role that phosphorylation of the three cluster-1 residues of SV2A by TTBK2 plays in regulating the binding of SV2A to μ2–AP2 by biophysical and structural approaches.

4.23.2 SPTBN2 (*β-III spectrin gene*)

The finding that the brain specific β-III spectrin (SPTBN2) interacts with SV2A in a phosphorylation-dependent manner via cluster-1 is biologically intriguing in the context of SCA pathogenesis as mutations in SPTBN2 cause spinocerebellar ataxia type 5 (SCA5) (Ikeda et al., 2006).

Spectrins, heterotetramers consisting of two α and two β subunits, are important structural components of the plasma membrane skeleton and are thought to play a significant role in restricting and stabilising membrane-spanning proteins within specific subdomains of the plasma membrane.

The core structural element of spectrins and a few other proteins, including spectrin family proteins (e.g. α-actinin, dystrophin), is a helical repeating unit referred to as a spectrin repeat (Figure 4.22B). Typically, 20 complete repeats can be found in α-spectrin, while β-spectrins contain 16 (or 29 in the case of β-heavy isoforms). Full sequence analysis of both spectrin subunits confirmed that the size of such segments varies in the range between 99 and 114 amino acid residues and the sequence homology between them does not exceed 30% (Leluk et al., 2001). Nevertheless, there is a common structural fold shared by all the spectrin repeats consisting of three helices, of which A and C are parallel and B is antiparallel. Spectrin repeats are typically found together with actin-binding calponin-homology (CH) domain, SH3 (Src homology 3) domain, PH (Pleckstrin homology) domain, EF hand type motifs; calcium-binding motifs and various signalling domains (Figure 4.22A).

β-III spectrin is primarily expressed in the nervous system with highest levels of expression in the cerebellum, where it is found in Purkinje cell soma and dendrites (Sakaguchi et al., 1998, Jackson et al., 2001). β-III spectrin interacts with EAAT4

(excitatory amino acid transporter 4), the glutamate transporter predominately expressed in Purkinje cells, and stabilises it at the plasma membrane (Jackson et al., 2001). This implicates β-III spectrin in clearance of glutamate from the synaptic cleft, and consequently both modulation of glutamatergic neurotransmission and prevention of glutamate-mediated neurotoxicity. Other investigators have shown β-III spectrin interacts with ARP1 (actin-related protein1) (Figure 4.22B) and is found in a complex with dynactin (Holleran et al., 2001). Since dynactin is the accessory protein that mediates the association of dynein with cytoplasmic vesicles, another suggested function of β-III spectrin is to facilitate protein trafficking by linking the microtubule motor to vesicle-bound cargo. An earlier study also suggested that β-III spectrin associates with Golgi and cytoplasmic vesicles (Stankewich et al., 1998).

The importance of the spectrin skeleton in the vertebrate nervous system is underscored by the discovery that mutations in human β-III spectrin cause spinocerebellar ataxia type 5 (SCA5) (Ikeda et al., 2006). SCA5 results in Purkinje cell loss, cerebellar cortical atrophy, and neuromuscular defects (Ikeda et al., 2006). The characterisation of a mouse model in which β-III spectrin expression is disrupted has been reported (Perkins et al., 2010). The functional β-III spectrin knockout mouse (β-III$^{-/-}$) develops characteristic features of cerebellar ataxia including progressive motor incoordination, a wider hind-limb gait, tremor, cerebellar atrophy and Purkinje cell loss, thus resembling the human clinical cases. The β-III$^{-/-}$ mouse was used as a new model of cerebellar ataxia and further investigations of the ataxic phenotype implicated several physiological defects: ion channel dysfunction, glutamate-mediated excitotoxicity, and vesicle-trafficking deficits, all arising from loss of β-III spectrin in disease pathogenesis.

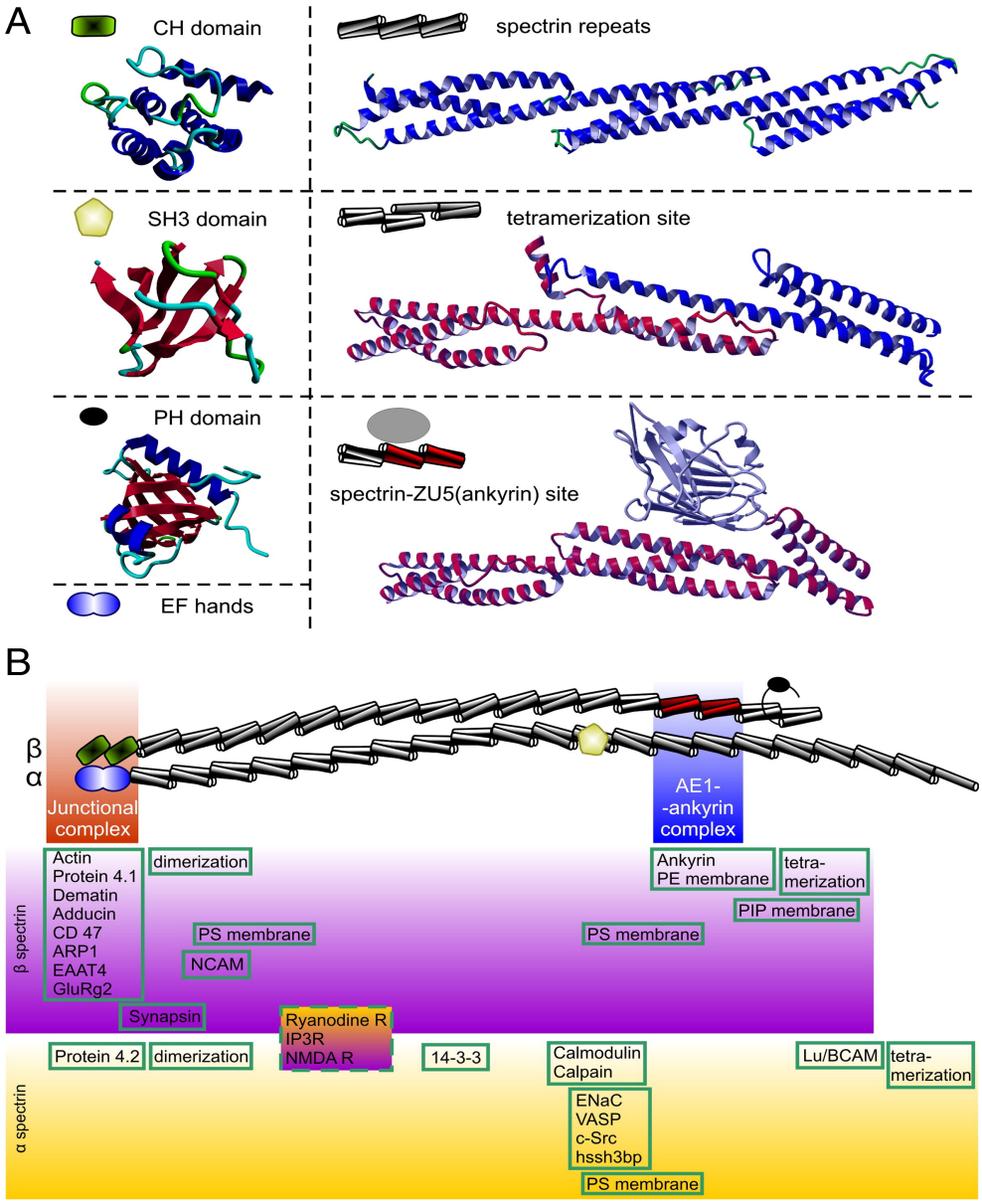

Figure 4.22. Structural and functional features of the spectrin dimer. (A) The domains of spectrin are: CH domain (PDB ID: 1BKR), SH3 domain (PDB ID: 1U06), PH domain (PDB ID: 1WJM), EF hands; major structural elements are spectrin repeats (structure of repeats 15, 16 and 17 of brain alpha spectrin PDB ID: 1U4Q; structure of erythroid spectrin tetramerisation complex PDB ID: 3LBX; structure of repeats 13, 14 and 15 of erythroid beta spectrin in complex with ZU5 domain of erythroid ankyrin; ribbon representations of helices of repeats of beta spectrin are in red and of alpha spectrin are blue). (B) Schematic representation of the domain structure of spectrin heterodimer together with examples of binding partners for each of the spectrin subunits ascribed to certain parts of the molecules (solid rectangles); double colour dashed rectangles represent binding partners of unassigned specificity to a certain part of a dimer. [adapted from (Machnicka et al., 2013)].

In *Drosophila*, spectrin function at the synapse has been extensively studied in motor neurons (Featherstone et al., 2001, Pielage et al., 2005). These studies first characterised pre- and postsynaptic spectrin localisation and function during motor neuron synaptogenesis in *Drosophila*. Loss of presynaptic spectrin reportedly eliminates several essential cell adhesion molecules from synaptic sites and leads to

defects in neurotransmission and the disassembly and elimination of synapses at the neuromuscular junction (Pielage et al., 2005, Pielage et al., 2006). In addition, the RNAi depletion of presynaptic β-spectrin has been reported to disrupt microtubule organisation at the synapse, to generate large accumulations of synaptic vesicles with motor axons, and to reduce the accumulation of synaptic vesicles within the terminal boutons. Thus, in the case of *Drosophila* and also *Caenorhabditis elegans*, which only have one form of β-spectrin, loss of β-spectrin causes an uncoordinated phenotype, which is a consequence of the destabilisation of the neuromuscular junction through loss of synaptic cell-adhesion molecules (Pielage et al., 2005) and axonal breakage (Hammarlund et al., 2007), respectively. These latter studies proposed a link between spectrin and vesicle transport either through a direct role in motor-based transport or an indirect effect on cytoskeletal organisation.

Spectrins are present in the presynaptic portion of neurons and form a dense presynaptic cytoskeletal structure known as the presynaptic particle web involved in the stabilisation of the synapse (Phillips et al., 2001). The newly identified phospho-dependent interaction between SV2A and βIII-spectrin could promote the tethering of SV2A to the pre-synaptic cytoskeleton, thereby targeting SV2A to certain membrane proteins in the neuronal plasma membrane or within specific subdomains of the plasma membrane.

Given that the spectrin cytoskeleton is required for the organisation of a diverse set of membrane proteins, including ion channels, receptors, and cell adhesion molecules, the emerging paradigm for ataxia pathogenesis follows. This paradigm is dissolution of the spectrin cytoskeleton, which causes a failure in the cellular localisation of certain membrane proteins resulting in the loss of their physiological interactions with other proteins, which leads to neuronal dysfunction that can cause ataxia.

4.23.3 Synaptotagmin 1

Several investigators have studied the physical and functional interaction between SV2A and synaptotagmin 1 previously. This interaction is direct and mediated by the amino terminus of SV2A and the C2B domain of synaptotagmin 1 (Schivell et al., 1996). It is also known to be influenced by calcium and modulated by

phosphorylation of SV2A (Pyle et al., 2000). However, the precise position of the binding site i.e. the critical SV2A phosphorylation sites that confer binding Syt1 had not been defined.

I have shown that phosphorylation of SV2A at the three cluster-2 residues (Ser80, Ser81and Thr84) confers binding to synaptotagmin 1. I have also presented evidence that the phosphorylation of cluster-2 plays a modulatory role in binding to synaptotagmin 1 as the dephosphorylation of native SV2A leads to the dissociation of synaptotagmin 1, indicating that the SV2A-synaptotagmin 1 interaction may be regulated *in vivo* through changes in SV2A phosphorylation.

The region of synaptotagmin 1 that mediates its interaction with SV2A is the second protein kinase C homology domain, the C2B domain (Schivell et al., 1996). The critical residues within the C2B domain that provide generic interactions with the phosphate groups of cluster-2 were mapped using previously published structural data. This information will be particularly useful for future biophysical, structural and functional investigations of the SV2A-synaptotagmin 1 interaction.

The SV2A-synaptotagmin 1 interaction is inhibited by calcium (Schivell et al., 1996) and this regulation is most likely mediated by calcium-induced conformational changes in synaptotagmin 1 (Davletov and Sudhof, 1994). The C2B domain is known to interact with several proteins in a calcium-independent manner. Several proteins, such as clathrin adaptor protein-2 (AP2) (Zhang et al., 1994), soluble NSF attachment protein (β-SNAP) (Schiavo et al., 1995), SNAP-25, and N-type calcium channels (Schiavo et al., 1997), bind to different sites in the C2B domain.

In addition, the C2B domain is extremely important functionally. Microinjection of peptides corresponding to a region of the C2B domain were more efficacious in disrupting neurotransmission in the squid giant synapse than peptides corresponding to the analogous region of the C2A domain (Bommert et al., 1993). Furthermore, mice in which synaptotagmin 1 has been disrupted in the C2B domain lack the fast, low calcium-affinity component of regulated secretion (Geppert et al., 1994), suggesting that the C2B domain may mediate Syt1's role as a low affinity calcium sensor.

The SV2A-synaptotagmin 1 interaction may provide calcium-regulated modulation of one or both proteins' actions. There are at least three ways in which this interaction may function. First, synaptotagmin 1 may regulate a putative transporter or channel function of SV2A. This model predicts that association with synaptotagmin 1 either inhibits or promotes transport by SV2A, with reversal of this regulation at high calcium concentrations during exocytosis. Interestingly, expression of synaptotagmin's C2B domain transforms an endogenous choline transport activity in Xenopus oocytes to one with the characteristics of neuronal choline transporters, indicating that C2B domains can regulate transporters (O'Regan et al., 1995). Moreover, the effect of C2B on transport activity in this system was eliminated by high calcium concentrations, a result which parallels the inhibitory effect of calcium on the SV2A-synaptotagmin interaction. In the synapse, synaptotagmin may activate SV2A-mediated transport of a common vesicle constituent during resting conditions. With calcium influx, the proteins dissociate, turning off SV2A activity during exocytosis and recycling.

A variation of this model incorporates another hypothesised function of SV2A; that it serves as a component of the fusion pore that mediates the initial events of transmitter release. In this model, Syt1, via its interactions with SNARE proteins, would regulate targeting of SV2A to its counterpart in the plasma membrane. This model is consistent with Syt1's proposed role as a calcium-regulated inhibitor of synaptic transmission (Nonet et al., 1993). It suggests that synaptotagmin 1 provides a "dock and hold" mechanism for the placement of SV2A. This hypothesis is also consistent with the observation that Syt1 knockout mice lack the fast component of neurotransmitter release. SV2A in these mice would not be ushered to the proper region of the plasma membrane; therefore fusion pore preassembly would be absent.

An alternative model is one in which SV2A regulates the action of synaptotagmin 1, perhaps as a function secondary to its activity as a transporter. In this model of SV2A-synaptotagmin 1 interaction, SV2A inhibits the availability of synaptotagmin 1 to form protein complexes that mediate synaptic vesicle fusion until calcium concentrations rise in response to membrane depolarisation.

I have presented evidence implicating SV2A and synaptotagmin 1 in a phosphorylation-dependent interaction. The phosphorylation of SV2A at cluster-2 may provide a temporal regulatory control of its association with the C2B domain of

synaptotagmin 1. Ca^{2+} also modulates this association as high Ca^{2+} concentrations induce conformational changes in Syt1 that mediate its dissociation from SV2A. Further insights into the SV2A-Synaptotagmin 1 interaction could be gained by co-crystallising the C2B domain of Syt1 in complex with the triply-phosphorylated SV2A cluster-2 peptide. This can reveal further insights into the binding sites and how this interaction is modulated *in vivo*.

4.24 Implications for SV2A's physiological function

Based on its structure, SV2A has been proposed to perform several actions, including transport of ions or small molecules into vesicles (Janz et al., 1999), providing the glyco-matrix to the vesicle lumen (Reigada et al., 2003), modulating the endocytosis of vesicle proteins including synaptotagmin 1 (Haucke and De Camilli, 1999), serving as a receptor for clathrin adaptor proteins and contributing to the proper trafficking of the vesicle protein synaptotagmin 1 (Yao et al., 2010).

Mutation of Tyr46, which is part of a canonical YXXΦ adaptor-binding site (Owen and Evans, 1998) in the amino terminus of SV2A, produced a protein that trafficked to synapses but did not support normal neurotransmission. In comparison to wild-type SV2A, $SV2A^{Y46A}$ demonstrated significantly reduced binding to AP2 (Yao et al., 2010). Consistent with reduced binding to the AP2 mediators of endocytosis, the Tyr46Ala mutation resulted in lowered internalisation of SV2A. Because SV2A contains an YXXΦ motif in its cytoplasmic N-terminus, those results suggested that the amino terminal endocytosis motif in SV2A plays a dominant role in its endocytosis.

Disruption of the endocytosis motif in SV2A's amino terminus by mutating Tyr46 to Ala resulted in a higher proportion of synaptotagmin 1 on the plasma membrane. This finding is consistent with SV2A playing an important role in the endocytosis of synaptotagmin 1. When viewed in light of the finding that synaptic vesicles from SV2A/B knockout mice contained significantly lower amounts of synaptotagmin 1, the most compatible conclusion is that SV2A regulates the endocytosis of synaptotagmin 1. Synaptotagmin 1 has been proposed to be required for normal vesicle endocytosis (Nicholson-Tomishima and Ryan, 2004) and to be a clathrin

adaptor receptor (Yao et al., 2010, Diril et al., 2006). Therefore, SV2A contributes to any role synaptotagmin plays in endocytosis.

SV2A influences the endocytosis of synaptotagmin 1 because peptides corresponding to the endocytosis domain of SV2A increase binding of synaptotagmin to AP2 clathrin adaptors (Haucke and De Camilli, 1999). Moreover, synaptic vesicles isolated from SV2A KO mice contain lower levels of synaptotagmin 1 than wild-type mice (Yao et al., 2010). Thus, SV2A appears to play a specific role in trafficking of synaptotagmin 1 and it also appears to exert a selective effect on the expression of synaptotagmin 1. Collectively, these observations support the view that SV2A plays a major role in regulating the amount of the synaptotagmin 1 protein in synaptic vesicles.

SV2A is essential for normal neurotransmission. In its absence, synaptic release probability decreases, a result that leads to a severe seizure phenotype and premature death (Crowder et al., 1999, Janz et al., 1999). The functional lesion in synapses lacking SV2A occurs after vesicle docking (Custer et al., 2006) and before the formation of tightly-associated SNARE complexes (Xu and Bajjalieh, 2001), indicating that SV2A contributes to the process that renders vesicles competent for calcium-stimulated fusion. Altered endocytosis could produce this phenotype by changing the protein composition of vesicles.

In the absence of SV2A, synaptotagmin 1 trafficking to synaptic vesicles becomes more random (Yao et al., 2010), leading to fewer vesicles with enough of the calcium sensor to trigger calcium-stimulated fusion. Thus this action of SV2A can explain the neurotransmission deficit observed in SV2A knockout mice. Changes in vesicle protein expression have been noted in several nervous system pathologies, including schizophrenia (Mirnics et al., 2000), epilepsy (Matveeva et al., 2007, Matveeva et al., 2008, Matveeva et al., 2003) and Alzheimer's disease, where changes in vesicle protein expression precede loss of synapses and changes in cognitive functioning (Yao, 2004, Yao et al., 2003). Protein sorting during synaptic vesicle endocytosis represents a potential point of regulation in neurotransmission because it dictates the protein composition of synaptic vesicles, the organelle that mediates neurotransmitter release.

The number and variability of each protein in synaptic vesicles has implications for

hypotheses of protein action at the synapse. Four SV proteins: SV2A, H^+/ATPase, V-glut1 and synaptotagmin 1, show little variation in number of copies per vesicles (Mutch et al., 2011), indicating that they are sorted to vesicles with high precision. This was seen despite the fact that the vesicles analysed represented all neurotransmitter classes. This finding supports a model in which protein complexes with a fixed stoichiometry interact with clathrin adaptor proteins in a stereotypical manner. In this way, vesicle protein content could be encoded into protein interactions that result in the self-assembly of vesicles with uniform protein content. This model is consistent with the report that SV2A, the most monodispersed of the vesicle proteins, regulates the amount of synaptotagmin 1 in synaptic vesicles (Yao et al., 2010).

Based on the findings presented here, a theoretical model emerges in which SV2A, via its phospho-dependent interactions with AP2 clathrin adaptors, βIII-spectrin and synaptotagmin 1 regulates the trafficking of synaptotagmin 1 and hence the vesicle content of synaptotagmin 1. SV2A impacts on the endocytosis of synaptotagmin 1 because peptides corresponding to the endocytosis domain of SV2A increase binding of synaptotagmin to AP2 clathrin adaptors (Haucke and De Camilli, 1999). However, the endocytosis of synaptotagmin 1 is also modulated by another protein called stonin 2 (Diril et al., 2006), a homolog of the μ2 subunit of AP2. SV2A's ability to influence synaptotagmin 1's endocytosis may therefore be through regulating synaptotagmin 1's ability to bind stonin 2. Alternatively, by simultaneously engaging AP2 clathrin adaptors through its YXXΦ motif and interacting with synaptotagmin 1 bound to stonin 2 via cluster-2, SV2A may help concentrate clathrin adaptors in a way that insures the inclusion of synaptotagmin 1 in vesicles.

This likely scenario may involve the coordination of the phosphorylation of SV2A at cluster-1 and cluster-2. It will be interesting to investigate the spatio-temporal regulation of SV2A phosphorylation by TTBK2 *in vivo*. Phosphorylation of SV2A at cluster-1 and cluster-2 must be tightly-coordinated to ensure the correct sequential orchestration of SV2A's interactions with AP2, β2-spectrin and synaptotagmin1 to ensure the fidelity and precise stoichiometry of protein sorting during endocytosis.

Clues to SV2A's molecular action have come largely from its structure. SV2A's most striking feature is its structural similarity to major facilitator transporters (Pao et al., 1998), which has led to the widely held hypothesis that it transports something across the vesicle membrane. Despite exhaustive efforts, the transporter function of SV2A

has never been validated (Chang and Sudhof, 2009). The fact that it affects the expression and endocytosis of synaptotagmin 1 supports the conclusion that modulation of endocytosis is an essential action of SV2A.

4.25 Enigmatic role of SV2A in clinical epilepsy and the treatment of epilepsy with Levetiracetam

The involvement of SV2A in clinical epilepsy remains unclarified. Mice with knock out of one allele of SV2A have an elevated incidence of epileptic seizures, and mice with both copies knocked out have very severe epileptic seizures after the first postnatal week and die by the third week (Crowder et al., 1999), primarily because of fulminant epilepsy.

According to the world health organisation (WHO), about 50 million people worldwide have epilepsy, and nearly 80% of epilepsy occurs in developing countries (WHO, 2012). Epilepsy becomes more common as people age (Brodie et al., 2009). Epileptic seizures may occur in recovering patients as a consequence of brain surgery. Epilepsy is usually managed with medication, but not cured.

There is no silver bullet for the medical treatment of epilepsy. Specifically, there is no single defect that can be targeted to correct the hyperexcitability and hypersynchrony that are the hallmarks of epileptic brain circuits. Vast numbers of proteins regulating neuronal excitability interact in an extraordinarily complex manner to govern cellular and network behaviour. Among the current antiepileptic therapies, only a very few proteins (e.g., voltage-gated sodium channels, GABAA receptors) have been targeted, while many potential molecular candidates for antiepileptic drug development remain unexplored. For example, a large number of proteins govern the synaptic vesicle cycle and, consequently, the strength of synaptic transmission. Once an action potential reaches the axon terminal, rather than an all-or-nothing phenomenon, these proteins regulate the probability that a vesicle will fuse and release its contents. Vesicles are filled with neurotransmitter, dock, are primed, and finally, fuse at the release site when Ca^{2+} enters the terminal. The rate at which vesicles cycle through these various stages helps to determine how synaptic responses change during repetitive activity. Thus, an ideal antiepileptic drug would not target a protein integral to the release

process, which would disrupt normal neurotransmission, but rather would be directed at a modulatory protein that regulates the vesicle cycle during high activity (e.g., a seizure).

In 1992, the potent effect of the pyrrolidone drug Levetiracetam (LEV) was discovered. By random screening, scientists at UCB (Union Chimique Belge), a Belgian biopharmaceutical company, found that this (S)-configurated ethyl derivative ((2S)-α-ethyl-2-oxo-1-pyrrolidine acetamide) of piracetam possesses pronounced anticonvulsive effects, which became evident by tests involving acoustically induced seizures in sound-sensitive mice (Gower et al., 1992). LEV underwent clinical trials and eventually was approved by the Food and Drug Administration (FDA) under the trade name Keppra® in November 1999. At that time, not much was known regarding the molecular mechanism of action and the target of LEV, which was supposed to be a highly abundant protein located in synaptic vesicle membranes of the central nervous system (Noyer et al., 1995). Five years after its approval, in 2004, this site was identified as the synaptic vesicle protein, SV2A (Lynch et al., 2004). Today, Keppra® is one of the most successful anti-epileptic drugs, being widely prescribed for partial as well as generalised seizures, as a monotherapy and as an add-on medication (De Smedt et al., 2007).

LEV represents a new class of drug for the treatment of neurological and psychiatric disorders. LEV is currently widely-used for the treatment of epilepsy, though it also shows promise in the treatment of anxiety disorders (Kinrys et al., 2007, Kinrys et al., 2006, Zhang et al., 2005), pain (Enggaard et al., 2006, Dunteman, 2005, Price, 2004), dyskinesias (Bushara et al., 2005, McGavin et al., 2003, Woods et al., 2008, Zivkovic et al., 2008, Striano et al., 2009), and post-traumatic stress disorder (Kinrys et al., 2006).

SV2A is the molecular target of the anti-epileptic drug LEV (Lynch et al., 2004). SV2A is both necessary and sufficient for LEV binding (Lynch et al., 2004). In addition, mice heterozygous for the SV2A gene disruption show reduced response to drug treatment (Kaminski et al., 2009), consistent with SV2A being required for levetiracetam action. Thus, levetiracetam appears to act by modulating the action of SV2A, though its mechanism of action remains unknown. Currently, SV2A is the

only synaptic vesicle protein known to be a drug target. LEV, the first agent in this new class of antiepileptic drugs with unknown mechanism of action, illustrates the promises and challenges faced in searching for antiepileptic medications with novel molecular targets.

Crowder et al. (1999) showed that mice with knock out of one allele for SV2A have an elevated incidence of seizures, and mice with both copies knocked out have severe seizures after the first postnatal week and die by the third week (Crowder et al., 1999). Action potential-independent release of vesicles from inhibitory neurons (i.e., spontaneous release of vesicles) is normal in hippocampal slices from SV2A-deficient mice, but action potential-dependent release (i.e., Ca^{2+}-triggered release) is markedly reduced. These findings suggested that SV2A is involved in the coupling of Ca^{2+} entry and vesicle release at inhibitory synapses i.e. in the final step in which docked vesicles are readied for rapid release in response to Ca^{2+} influx. In other words, SV2A may regulate neurotransmission indirectly by controlling the vesicle's ability to detect changes in presynaptic calcium.

Several studies report a correlation between increased SV2A expression and changes in synaptic functioning. Kindling of seizures in rats results in increased expression of several synaptic vesicle proteins including SV2A (Matveeva et al., 2007, Matveeva et al., 2003), and SV2A is at the hub of seizure-dependent changes in protein co-expression (Winden et al., 2011). In addition, mRNA encoding SV2A is a primary target of a microRNA whose expression is sensitive to changes in synaptic activity (Cohen et al., 2011). Together these findings indicate that altered expression of SV2A, is a molecular signature of altered synaptic activity.

In animals subjected to seizure kindling protocols, treatment with LEV blocks both the development of a seizure phenotype and increases in SV2A expression (Ohno et al., 2009, Matveeva et al., 2008). In hippocampal slices from non-epileptic animals, treatment with levetiracetam reduces neurotransmission in response to fast stimulus trains (Yang et al., 2007), consistent with the drug blocking SV2A's effects on vesicle priming. Most interestingly, the latency of drug action is much shorter when neurons are stimulated (Meehan et al., 2011), suggesting that LEV preferentially targets hyperactive synapses.

LEV treatment of neurons overexpressing SV2A decreased the amount of Syt1 at synapses but did not alter the ratio of SV2A/Syt1 at synapses (Nowack et al., 2011). Considered together these findings are consistent with the interpretation that the amount of Syt1 at synapses tracks the amount of SV2A, and LEV results in a reduction in the amount of both proteins available to support calcium-triggered exocytosis. The fact that both increased and decreased levels of SV2A and Syt1 are associated with reduced release probability suggests that optimal levels of these proteins are required for normal neurotransmission, a conclusion consistent with the recent observation that the number of SV2s and synaptotagmins per vesicle is tightly regulated (Mutch et al., 2011).

LEV had no effect on neurons that lacked SV2A, consistent with the conclusion that the drug acts by binding SV2A. Because SV2A expression is limited to presynaptic terminals, this means that LEV affects presynaptic events that regulate synaptic vesicle release. Given that LEV restored the concentration of SV2A at the synapse to control levels without affecting total SV2A per length of neurite, it is most likely that LEV affects the ability of SV2A to concentrate in synapses (Nowack et al., 2011). This is most consistent with the drug altering SV2A's ability to bind to proteins that influence protein trafficking or localisation, for example binding to clathrin adaptor proteins or proteins of the cytoskeleton.

The effects of LEV, in combination with the observation that LEV blocks kindling-induced increases in SV2A (Matveeva et al., 2008), suggest that levetiracetam may act by reversing the effects of increased SV2A expression. In the case of SV2A overexpression, levetiracetam may inhibit inappropriate interactions that occur when SV2A is over-abundant. What is clear is that LEV's action on protein levels at synapses represents a novel drug action.

Because SV2A's function inherently involves its phosphorylation-modulated interactions with AP2 clathrin adaptors, spectrin β2 and synaptotagmin 1, one possible mechanism of drug action is that it modulates SV2A phosphorylation, which in turn impacts on SV2A protein interactions. A direct implication of my findings

would be to investigate the effect of LEV on SV2A phosphorylation by TTBK2 *in vivo*.

Future work into the mechanisms by which LEV produces the effects will provide insight into the aetiology of nervous system disorders that are based in aberrant SV protein expression/function. Elucidating the mechanism by which LEV and SV2A interact to prevent seizures will undoubtedly open doors to the investigation of potential novel target proteins involved in the synaptic vesicle cycle.

5 Characterisation of SV2A/Syt1 interaction using biophysical and functional methods

The data presented in chapter 4 indicate that the interaction between SV2A and Syt1 is regulated by the phosphorylation of the three residues (Ser80, Ser81 and Thr84) collectively designated as SV2A cluster-2. This interaction is direct and mediated by the cluster-2 of SV2A and the C2B domain of synaptotagmin 1 (Syt1). The critical residues within the C2B domain that provide generic interactions with the phosphate groups of cluster-2 were mapped using previously published structural data. Support for the notion that a cluster of highly conserved charged and polar amino acids (K327, T329, K332) in the C2B domain Syt1 were critical in binding the three phosphate groups of SV2A cluster-2 was provided by the inability of the triply-phosphorylated SV2A cluster-2 peptide to retrieve Syt1-Flag proteins harbouring an alanine mutation of either residue. This is indicative of a phosphospecific physical and functional association between the two proteins.

The structural basis for phospho-dependent association of the amino-terminus of SV2A to the C2B domain of Syt1 may be determined by solving the high-resolution X-ray crystal structure of this complex. The resolution of the C2B domain of Syt1 in complex with the SV2A triply-phosphorylated cluster-2 phosphopeptide will provide a molecular rationale for this phosphospecific association of SV2A and Syt1.

Nevertheless, before this goal is reached, methods for determining biophysical quantitative data relating to this complex are important. Biophysical methods were employed to achieve a critical objective: an *ab initio* method of predicting the binding interface. Supporting biophysical studies are often invaluable both for sample characterisation before starting structural studies as well as for investigating structure-function relationships after structural information is available. In addition, a plethora of questions can be addressed through biophysical studies in the absence of any structural information.

To investigate the SV2A/Syt1 interaction in more detail, two independent biophysical

methods were employed: Isothermal titration calorimetry (ITC) and fluorescence polarisation anisotropy (FP) were used for quantitative analyses of the SV2A/Syt1 phosphospecific interaction.

5.1 Expression and purification of GST fusion Syt1 fragments for biophysical studies

Syt1 recombinant GST fusion proteins were expressed in BL21 DE3 strain of *E. coli* as described before in the 'Materials and Methods' section. Initial pilot expression of Syt1 fragments showed that GST-Syt1 encompassing residues 246-422 expressed very well. This fragment includes the C2B domain of Syt1 with approximately 40 residues flanking it on either side.

For the purposes of ITC and FP experiments, three different versions of GST-Syt1 [246-422] were expressed: GST-Syt1[246-422]^{WT}, GST-Syt1[246-422]^{K327A}, GST-Syt1[246-422]^{T329A}. Figure 5.1 shows a Coomassie-stained gel of those expressed fragments together with BSA (Bovine Serum Albumin) standards used to gauge the concentrations of each protein.

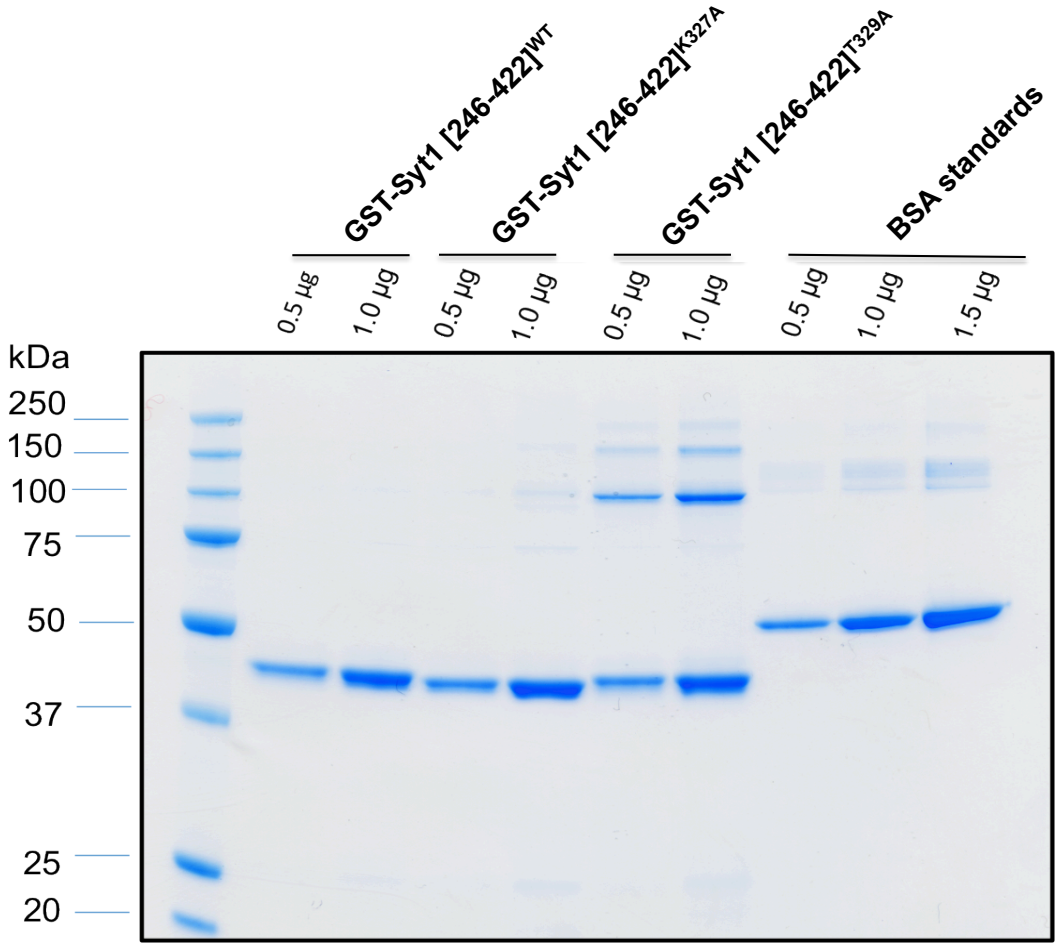

Figure 5.1. GST-Syt1[246-422] for biophysical binding studies. Coomassie Blue staining of 0.5 µg and 1.0 µg of each expressed protein fragment: GST- Syt1 [246-422]^{WT}, GST-Syt1 [246-422]^{K327A} and GST-Syt1 [246-422]^{T329A}.

5.2 Isothermal Titration Calorimetry (ITC)

Isothermal Titration Calorimetry (ITC) is considered as the most quantitative technique available for measuring the thermodynamic properties of protein–protein interactions and is a useful tool for protein–protein complex structural studies. This technique relies upon the accurate measurement of heat changes that follow the interaction of protein molecules in solution, without the need to label or immobilise the binding partners, since the absorption or production of heat is an intrinsic property of virtually all biochemical reactions. ITC provides information regarding the stoichiometry, enthalpy, entropy, and binding kinetics between two interacting proteins (Velazquez-Campoy et al., 2004).

Isothermal titration calorimetry provides a direct route to the complete thermodynamic characterisation of protein interactions. A typical ITC experiment is

carried out by the stepwise addition of one of the reactants (1-10 µl per injection) into a cell (≈ 1.4 mL) containing the other reactant. In this context, a syringe of ITC containing a ligand (peptide) is titrated into a cell containing a protein solution. As the two elements interact, heat is released or absorbed and this can be related to the extent of binding that occurs. When the protein in the cell becomes saturated with the added ligand, the heat signal diminishes until only the background heat of dilution is observed. Measurement of this heat allows for the accurate determination of binding constants (K_D), reaction stoichiometry (n), and a thermodynamic profile of the protein interaction that includes the observed molar calorimetric enthalpy (ΔH), entropy (ΔS), and change in free energy (ΔG) according to the equation:

$$\Delta G = -RT\,LnK = \Delta H - T\Delta S\,,$$

where R is the gas constant (8.3144 J K^{-1} mol^{-1} equal to 1.9872 cal K^{-1} mol^{-1}), T is the absolute temperature (Kelvin), K is the association constant, whereas ΔH, ΔS and ΔG denote, respectively, the changes in enthalpy, entropy and binding free energy upon complex association.

Unlike other methods, ITC does not require immobilisation and/or modification of proteins since the absorption or production of heat is an intrinsic property of virtually all biochemical reactions (Lakey and Raggett, 1998).

5.2.1 ITC experiments

All protein solutions for calorimetric experiments were filtered through a 0.22 µm membrane and degassed thoroughly in a vacuum chamber before use. Peptide solutions were prepared by dissolving the same buffer as protein samples. Protein and peptide samples were prepared in 20mM HEPES pH 7.5, 50mM NaCl and 0.5mM β-mercaptoethanol. The choice of buffer was based on initial trials, which revealed that this buffer offered minimal background noise and precipitation

ITC experiments were carried out on a Microcal VP-ITC (Milton Keynes, England) as described in the 'Materials and Methods' section. A typical experiment involved 30 serial 4 µl injections of the SV2A cluster-2 phosphopeptide or dephosphopeptide (10-

100 μM) into a sample cell containing 25 μM of purified GST-Syt1 [246-422]^{WT} or GST-Syt1 [246-422]^{K327A} protein. A space of 2 minutes was allowed between injections to ensure equilibration between reactants. The reaction cell was stirred at a constant speed of 300 rpm.

Heat changes within the cell were monitored during each injection of peptide and recorded as the total heat change per second over time. A binding isotherm was then fitted to data and expressed as heat change per mole of peptide against the peptide to protein ratio. For each protein and for each condition, at least 2 runs were carried out to ensure reproducibility. Between each run, the chamber was thoroughly washed with at least 10 chamber volumes of MilliQ (Millipore, England) water and the syringe rinsed thoroughly again with at least 10 volumes of MilliQ water. Each experimental condition had a blank run with protein in the chamber replaced with buffer. This data was then subtracted from the run with protein present to take into account any energy of dilution or peptide/buffer reaction.

From the isothermic data, a regression model was used to predict the number of binding sites on the protein involved in the reaction, the disssociation constants of the binding (K_D).

5.2.2 The thermodynamics of cluster-2 triply phosphorylated peptide binding to the C2B domain of synaptotagmin 1

ITC experiments were conducted on a Microcal VP-ITC instrument. The binding of the non-phosphorylated and triply-phosphorylated cluster-2 peptides to the C2B domain of Syt1 were thus examined. A series of injections of each peptide were made into an isolated chamber containing the protein: GST-Syt1[246-422]^{WT} or GST-Syt1 [246-422]^{K327A} at a constant temperature of 30 °C. Heat changes within the cell were monitored during each injection of peptide and recorded as the total heat change per second over time.

The peptides loaded into the syringe were at a concentration of 2mM. Injection parameters for the ligand were 4 μl/injection with time spacing of 200–700 seconds

depending on the progress of the titrations. The final protein concentrations used for the experiments were 26 μM concentration of Syt1[246-422].

Different concentrations were used to ensure that results were repeatable over a variety of conditions. During each experiment, 30 × 4 μL doses of peptide were injected into the chamber with protein, which was stirred constantly at 300 rpm. Each injection was followed by a 2 min period to ensure equilibration of the solution.

All the experiments presented were conducted at 30°C. The buffer used was 20mM HEPES, pH 7.5, 0.05M NaCl, 0.5mM β-mercaptoethanol. The peptides were reconstituted in the same buffer. Multiple titrations were carried out at various concentrations to optimise the conditions. The peptides taken in the syringe were at a concentration of 1 to 2.0 mM. Injection parameters for the ligand (peptide) were 4 μl/injection with time spacing of 200–700 seconds depending on the progress of the titrations.

The final protein concentrations used for the experiments were 26 μM of Syt1[246-422] and 1 μM peptide. Four sets of peptide titrations were performed; 1) cluster-2 phosphopeptide titration on GST-Syt1 $[246\text{-}422]^{WT}$, 2) cluster 2 dephosphopeptide titration on GST-Syt1 $[246\text{-}422]^{WT}$, 3) cluster 2 phosphopeptide titration on GST-Syt1 $[246\text{-}422]^{K327A}$, and 4) cluster 2 dephosphopeptide titration on GST-Syt1 $[246\text{-}422]^{K327A}$.

The results of the titration curves were corrected using a buffer–protein control. Initially, the buffer alone was titrated, using the cluster-2 phosphopeptide as the ligand. The same procedure was repeated with the protein dissolved in the buffer. The heat change of the first experiment (buffer titrated with phosphopeptide) was subtracted from that of the second (protein dissolved in buffer titrated with phosphopeptide). Finally, the Origin software supplied by Microcal was used to analyse these data.

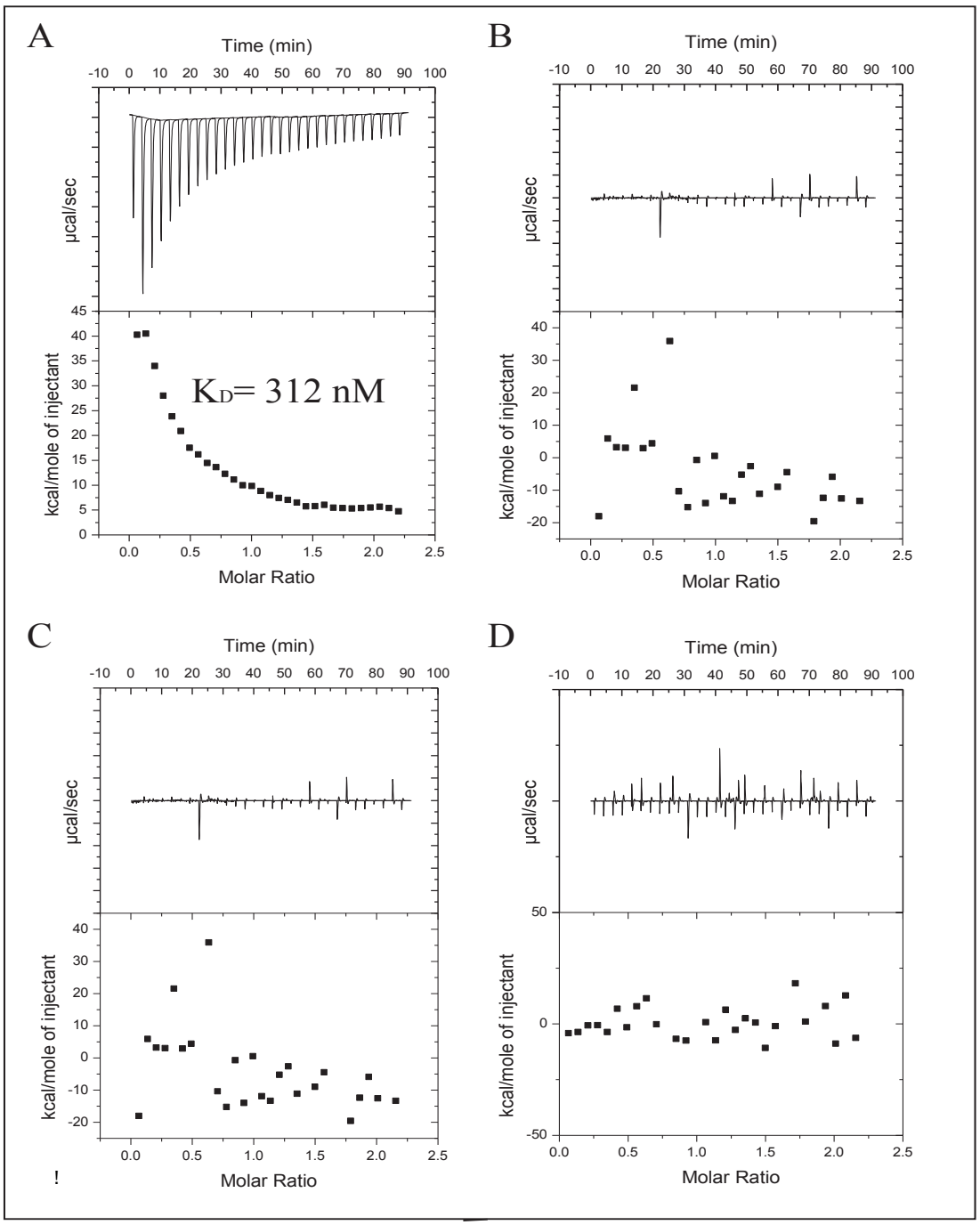

Figure 5.2. ITC Titration of SV2A peptide titrations on Syt1. Raw data are shown in the upper panels and integrated heat changes shown in the lower panels as solid squares.
(A) The triply-phosphorylated SV2A cluster-2 peptide solution was titrated into a solution containing GST-Syt1 $[246\text{-}422]^{WT}$. Each downward deflection corresponds to one injection. The area represents the heat exchanged. The total heat exchanged during each injection is fit to a single-site binding isotherm with K_D and $\Delta H°$ as independent parameters, where K_D = 312 nM.

(B) The triply-phosphorylated SV2A cluster-2 peptide solution is titrated into a solution containing GST-Syt1 $[246\text{-}422]^{K327A}$, showing no detectable binding to Syt1.

(C,D) The dephosphorylated SV2A cluster-2 peptide solution is titrated into a solution containing GST-Syt1 $[246\text{-}422]^{WT}$ (C) and GST-Syt1 $[246\text{-}422]^{K327A}$ (D) showing no detectable binding of the dephosphopeptide to Syt1.

The raw data (upper panels in Figure 5.2) consists of peaks of heat output generated by successive injections of peptide and, when integrated, these provide the total heat output per injection. Once the protein is saturated, the residual heat effects originate from dilution of the peptide and also from mechanical effects associated with the injection. Lower panels represent the data after non-specific buffer interactions have been subtracted.

In Figure 5.2A (lower panel), a clear traceable pattern of binding was observed. The heat transfer associated with each injection is plotted as a function of the peptide-to-protein concentration ratio. The Origin 7 software's non-linear regression fitting was used and fit to an equation that incorporates the enthalpy and affinity of a single phosphopeptide binding event. A single set of sites based on a MicroCal model was found to produce the lowest χ^2 values and error dependency. The binding isotherm indicates that the cluster-2 triply phosphorylated peptide bound extremely tightly to the C2B domain of Syt1 with a K_D of 312 nM. The fit corresponds to stoichiometry of binding n=1, and the data shows a two-stage binding event with one dependent site. The binding reaction is endothermic, which means that the interaction between SV2A and Syt1 is not enthalpically favoured.

Strikingly, no binding at all was observed for between triply-phosphorylated peptide and Syt1[246-422]^{K327A}, signifying that mutation of Lys327 to alanine abrogates phosphopeptide binding. In addition, none of the proteins bound to the nonphosphorylated peptide (panels C and D).

Collectively, those results show that the C2B domain of Syt1 binds with affinity the specific phosphopeptide encoding SV2A cluster-2 but not its unphosphorylated derivative, reiterating the absolute dependence of the tight association between the two proteins on the three SV2A cluster-2 residues being phosphorylated.

The ITC data also confirms the importance of residue K327 of the C2B domain of Syt1 in mediating this interaction and argue that K327 is a critical determinant of the binding specificity.

5.3 Fluorescence polarisation

Fluorescence polarisation (FP) or anisotropy can be used to measure the affinity of protein–protein or protein–ligand interactions. Typically, one binding partner is labelled with a fluorescence probe and the sample is excited with a specific frequency of light. The increase in the polarisation of the emission spectra upon binding of the labeled protein to its binding partner can be used to calculate the binding affinity (Owicki, 2000).

In broad terms, fluorescence polarisation is relevant where a small (tumbling), fluorescent molecule binds a larger target molecule. Thus the observation of small fluorescent ligands binding protein molecules are often experiments suitable for this type of detection. Fluorescence anisotropy is a method for measuring the binding interaction between two molecules, and can be used to measure the binding constant (or the inverse, the disassociation constant) for the interaction. The basic idea is that a fluorophore excited by polarised light (light whose "waves" only go one direction) will also emit polarised light. However, if a molecule is moving, it will tend to "scramble" the polarisation of the light by radiating at a different direction from the incident light (Figure 5.3). The "scrambling" effect is greatest with fluorophores freely tumbling in solution and decreases with decreased rates of tumbling. Protein interactions can be detected when one of the interacting partners is fused to a fluorophore: upon binding of the partner molecule a larger, more stable complex is formed, which will tumble more slowly (thus, increasing the polarisation of the emitted light and reducing the "scrambling" effect). This technique works best if a small molecule is fused to a fluorophore and binds to a larger partner (this maximises the difference in signal between bound and unbound states). Molecular interactions can thus be analysed using this approach where the smaller molecule is fluorescently labeled and the concentration of the larger binding partner is varied. The concept of fluorescence anisotropy is depicted in Figure 5.3 below.

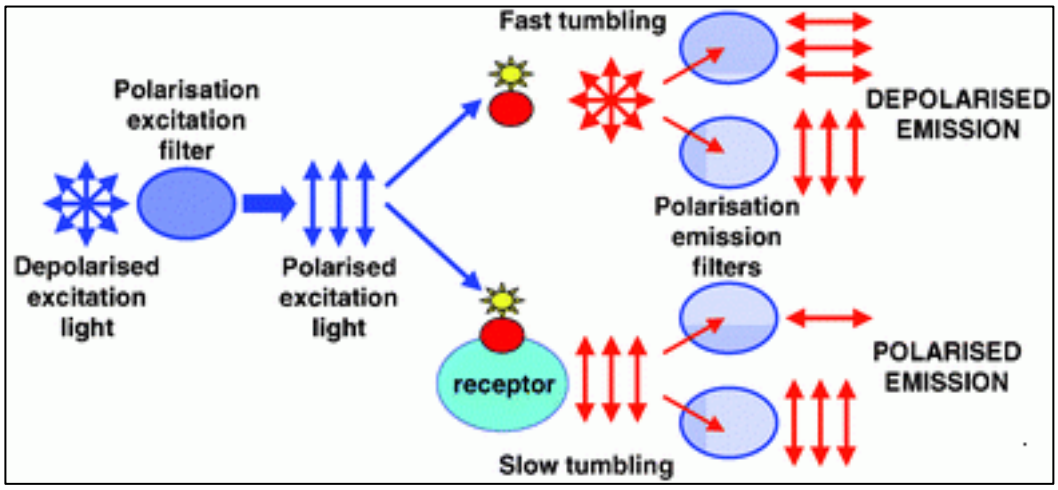

Figure 5.3. The concept of fluorescence anisotropy. As molecules tumble in solution, the emitted light is depolarised. The depolarisation of the fluorescent molecule is dependent on the size and shape of the rotating molecule and also the viscosity of the solution. The smaller the molecule, the more rapidly it rotates and the more the light is depolarised and hence the lower the anisotropy. If a larger molecule interacts with the fluorescent molecule the rotation of the complex will be slower than of the unbound molecules and result in an increase in the fluorescence anisotropy.

5.3.1 Labelling peptides with FlAsH

The FlAsH-EDT_2 labelling reagent emits a green (FlAsH) fluorescent signal when excited at the appropriate wavelength. The fluorescent excitation and emission spectra for the FlAsH reagent are shown in Figure 5.4 below. It has a maximum excitation of 508 nm and an emission maximum of 528 nm.

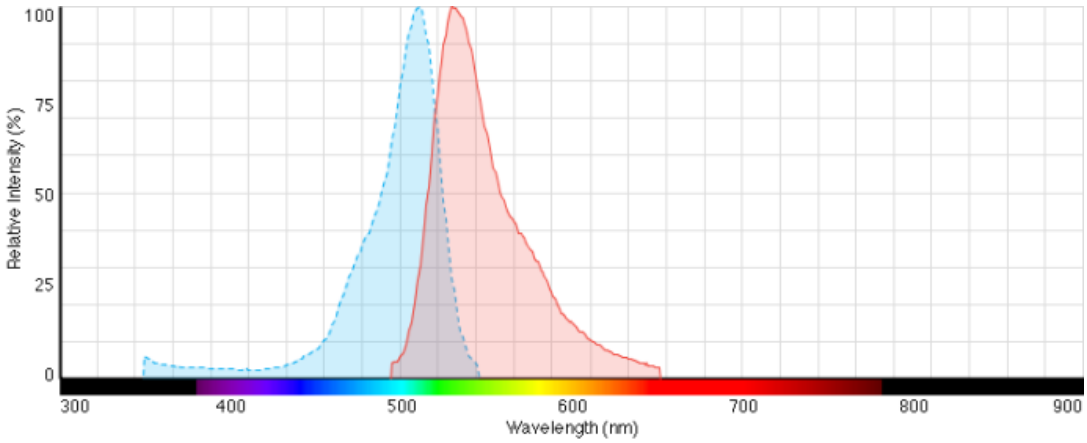

Figure 5.4. Fluorescence Excitation/Emission spectra of FlAsH-EDT_2 (Lumio green).

[adapted from http://www.lifetechnologies.com/order/catalog/product/T34563]

Peptides encoding the SV2A cluster-2 motif, with different phosphorylation status,

were custom-synthesised (Table 5.11) with a N-terminal CCPGCCGG tetra-cysteine tag (Adams et al., 2002), where two glycine residues were added to the C-terminus as a linker. This tag affords their labelling with FlAsH-EDT_2, an arsenic derivative of fluorescein. Labelling of N-terminally FlAsH-tagged (CCPGCC) peptides (Adams et al., 2002) was performed in 20mM HEPES (pH 7.5), 50mM NaCl and 5mM β-mercaptoethanol. 10nmol of each FlAsH-tagged peptide was incubated with 5µl FlAsH-EDT_2 (Lumio Green) at room temperature for 2.0 h in the dark. Excess dye was removed by overnight dialysis into the above buffer.

	Peptides for Fluorescence Polarisation
Phosphorylation status	**Peptide Sequence**
fNP2	CCPGCCGGGGRGEGAQDEEEGGASSDATEGHDEDDEIYEGEYRRRR
fSV2ApS80	CCPGCCGGGGRGEGAQDEEEGGAS*SDATEGHDEDDEIYEGEYRRRR
fSV2ApS81	CCPGCCGGGGRGEGAQDEEEGGASS*DATEGHDEDDEIYEGEYRRRR
fSV2ApT84	CCPGCCGGGGRGEGAQDEEEGGASSDAT*EGHDEDDEIYEGEYRRRR
fSV2ApS80+81	CCPGCCGGGGRGEGAQDEEEGGAS*S*DATEGHDEDDEIYEGEYRRRR
fSV2ApS80+pT84	CCPGCCGGGGRGEGAQDEEEGGAS*SDAT*EGHDEDDEIYEGEYRRRR
fSV2ApS81+pT84	CCPGCCGGGGRGEGAQDEEEGGASS*DAT*EGHDEDDEIYEGEYRRRR
fSV2ApS80+81+pT84	CCPGCCGGGGRGEGAQDEEEGGAS*S*DAT*EGHDEDDEIYEGEYRRRR

Table 5.11. Peptides for fluorescence polarisation. SV2A Cluster-2 peptides correspond to residues 67 to 98 of human SV2A where 4 Arginine residues have been added to the C-terminus to promote solubility and the tetracysteine tag (CCPGCCGGGG) has been added to the N-terminus to enable Lumio green labelling. Each of the 8 peptides has a different phosphorylation status, indicated in the first column of the table. Phosphorylated residues are highlighted with an asterisk in red.

5.3.2 Equilibrium fluorescence anisotropy measurements

All binding assays were performed by adding 100 nM of labelled peptide to increasing concentrations of recombinant GST-Syt1 $[246\text{-}422]^{WT}$ or GST-Syt1 $[246\text{-}422]^{K327A}$. End point polarisation and anisotropy measurements were made using PheraStar plate reader (BMG Labtech) using a 485/520 nm fluorescence polarisation module. Data was analysed using GraphPad Prism 5 and mean fluorescence anisotropy values (2 measurements) were plotted against protein concentration and

the curves fitted to a single-site binding model to determine K_D values.

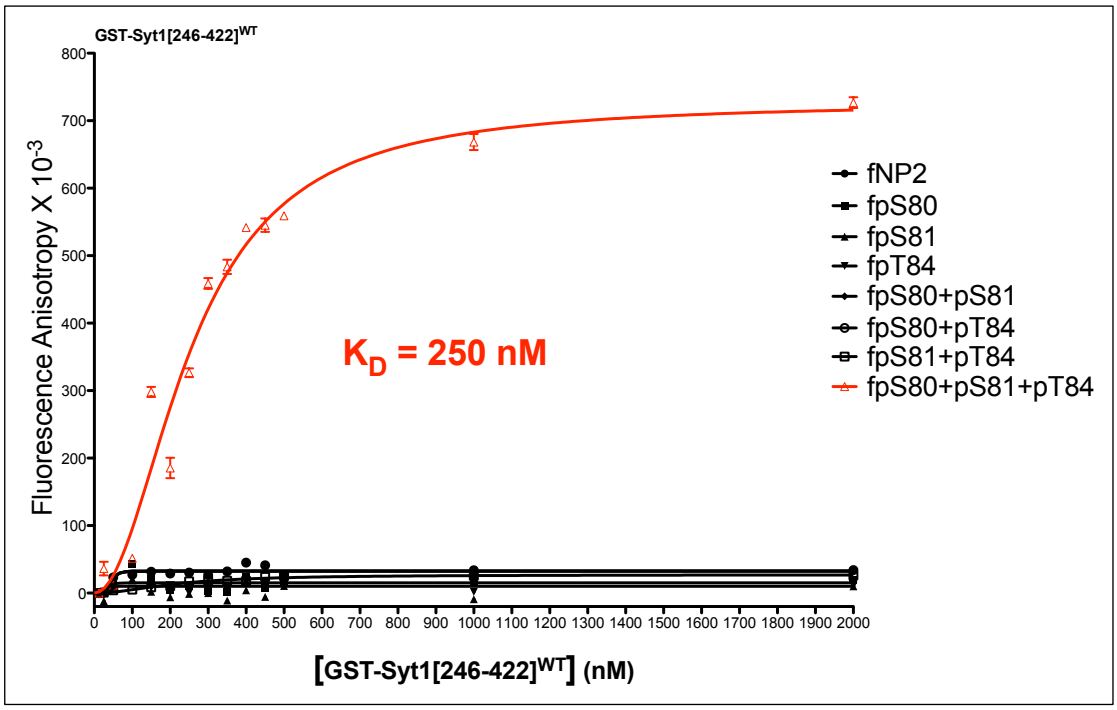

Figure 5.5. Specificity of SV2A cluster-2-encoding peptides binding to GST-Syt1[246-422]^{WT}. Binding affinities of GST-Syt1[246-422]^{WT} for FlAsH-labelled SV2Acluster-2-derived peptides were determined by fluorescence polarisation. Only the triply-phosphorylated peptide incorporating all three cluster-2 phosphorylation sites, shows significant binding affinity (250 nM). No detectable binding was observed for the dephosphopeptide, singly-phosphorylated peptides and doubly-phosphorylated peptides. The calculated K_D (shown on the graph) indicates a phosphospecific interaction. For calculation of K_D see 'Materials and Methods' section.

The binding of the eight labelled peptides shown in Table 5.11 to GST-Syt1 [246-422]^{WT} was first quantitated by FP. The triply-phosphorylated SV2A cluster-2 peptide showed very tight binding to the Syt1 protein with a K_D of 250 nM (Figure 5.5), comparable to the K_D obtained by ITC (312 nM). Notably, none of the dephosphorylated, singly-phosphorylated and doubly-phosphorylated peptides showed any demonstrable binding to Syt1, reemphasising the unconditional dependence of the tight association of SV2A to Syt1 on the concerted phosphorylation of the three SV2A cluster-2 residues.

Subsequently, the binding affinities of GST-Syt1 [246-422]^{WT} and GST-Syt1 [246-422]^{K327A} for the triply-phosphorylated peptide and dephosphopeptide were determined. In excellent agreement with the previous ITC data, the K327A mutant

protein displayed extremely weak binding to the triply-phosphorylated peptide, with a K_D several-fold higher than that observed with the wild-type protein (Figure 5.6).

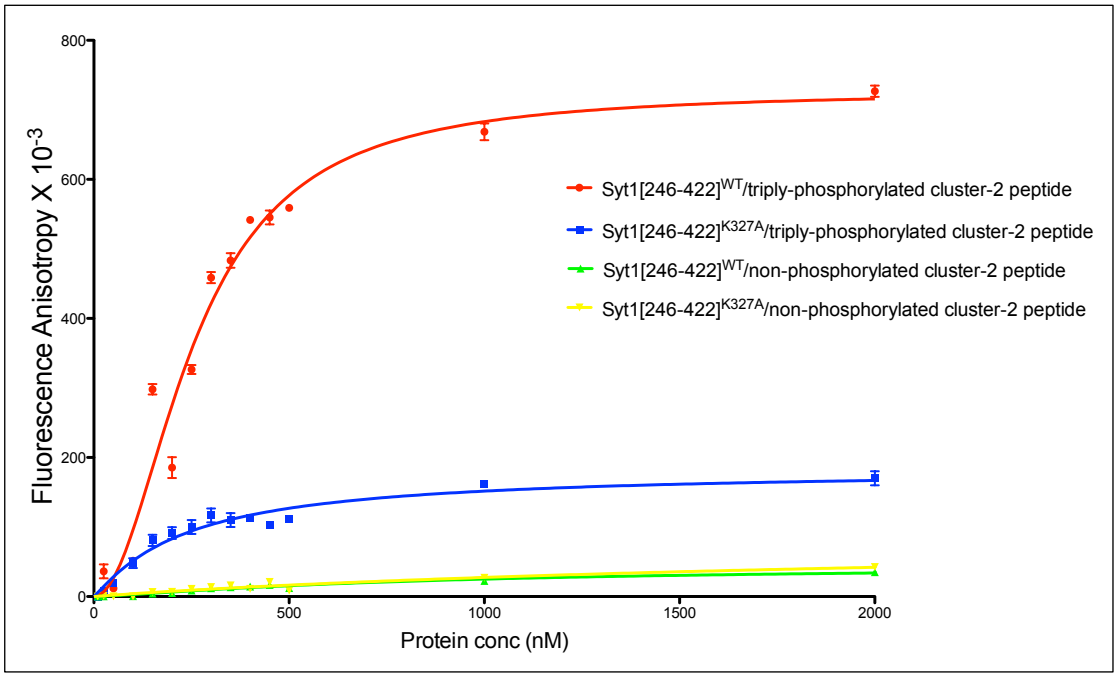

	Syt1[246-422]^{WT}/ fpS80+pS81+pT84	Syt1[246-422]^{K327A}/ fpS80+pS81+pT84	Syt1[246-422]^{WT}/ fNP2	Syt1[246-422]^{K327A}/ fNP2
K_D (nM)	252	ND	ND	ND
B_{max} (AU)	700	196	45	44

Figure 5.6. Binding of SV2A cluster-2-derived peptides to GST-Syt1 [246-422]^{WT} and GST-Syt1 [246-422]^{K327A}. The affinity of the phosphospecific interaction of GST-Syt1[246-422]^{K327A} is substantially reduced as compared to GST-Syt1[246-422]^{WT} , indicating that the Lys327 residue of the C2B domain of Syt1 is a critical determinant of this interaction. The SV2A cluster-2 dephosphopeptide showed no significant ability to bind to either GST-Syt1[246-422]^{WT} or GST-Syt1[246-422]^{K327A}. A dissociation constant could not be calculated for binding assays marked ND. ND: not determined; AU: arbitrary units.

Taken together, these data substantiate the importance of three phosphorylation sites (Ser80, Ser81 and Thr84) of SV2A, SV2A cluster-2, in the phosphospecific interaction with the C2B domain of Syt1.

Moreover, mutation of Lys327 of Syt1 to alanine abrogates phosphopeptide binding in perfect agreement with the previous ITC data and corroborates the observation that Lys327 is a critical in mediating this interaction.

5.4 Discussion

I have shown that the phosphorylated SV2A cluster-2 motif binds the C2B domain of synaptotagmin 1 with high affinity and specificity. The dissociation constant for the interaction between purified GST-Syt1[246-422]^{WT} and the triply-phosphorylated SV2A cluster-2 peptide was determined by ITC and FP. A K_D of 312 nM was obtained by ITC and 250 nM by FP. The submicromolar affinity of this interaction is comparable to other interactions of established biological importance.

The tight association of the two proteins is phospho-dependent as the dephosphorylated cluster-2 peptide showed no detectable binding to GST-Syt1[246-422]^{WT} by ITC. To confirm this unique phospho-dependent binding selectivity, eight peptides encoding SV2A cluster-2 with different phosphorylation statuses (Table 5.11) were generated and their interaction with GST-Syt1[246-422]^{WT} was examined by FP. None of those peptides displayed appreciable binding to GST-Syt1[246-422]^{WT}, except the triply-phosphorylated SV2A cluster-2 peptide. Collectively, these results showed that the C2B domain of Syt1 binds with high affinity to the phosphorylated SV2A cluster-2 motif but not to its unphosphorylated, singly-phosphorylated and doubly-phosphorylated motifs. This provides strong support to the notion that Syt1 binds SV2A by direct recognition of the SV2A cluster-2 phosphoepitope *in vivo*.

Based on the previously-published NMR structure of the C2B-IP6 complex, three critical residues (K327, T329 and K332) were predicted to provide the generic interactions with the three phosphate groups of SV2A cluster-2. GST-Syt1[246-422] fusion proteins harbouring K327A or T329A mutations were also tested for their ability to bind SV2A cluster-2 peptides. Consistent with the peptide pull-down assays described in chapter 4, ITC showed that GST-Syt1[246-422]^{K327A} did not bind the triply-phosphorylated cluster-2 peptide. Similar results were obtained by FP, which showed that neither GST-Syt1[246-422]^{K327A} nor GST-Syt1[246-422]^{T329A} bound the triply-phosphorylated cluster-2 peptide. This corroborates that this cluster of charged and polar amino acids in the C2B domain of Syt1 mediates the physical interaction with phosphorylated SV2A cluster-2.

This knowledge of the binding interface between the two proteins will be invaluable

for further structural and functional studies of the SV2A/Syt1 interaction. It will be extremely informative if the structure of the C2B domain of Syt1 complexed with the SV2A cluster-2 triply-phosphorylated peptide can be determined. This should provide a rationale of the molecular basis of this selectivity.

5.5 The use of pHluorins for optical measurements of presynaptic acitivity

Chemical synaptic transmission between neurons is a major means of communication mediating information flow in the brain. Monitoring of synaptic events during behavioural or cognitive tasks would ultimately provide important understanding of the link between collective neuronal network function and the demands placed upon cellular machinery. Clear interpretations of electrically recorded synaptic events in intact or semi-intact neuronal networks are, however, hampered by several problems. First, the complexity of the neural circuit is such that responses from single synaptic sites are often hard to extract, and second, electrical filtering properties of the dendrites strongly shape synaptic responses recorded in the postsynaptic neuron. In addition, postsynaptic electrical recordings usually obscure many of the underlying cell biological and molecular events that support presynaptic function. The advent of new optical recording techniques (Denk and Svoboda, 1997) in combination with advances in fluorescent molecular probes (Tsien, 1998) together are poised to provide new levels of information about the functioning of multicellular neuronal networks and the underlying cellular and molecular machinery that govern their behaviour. Recently, a novel approach that uses pH-sensitive green fluorescent protein (GFP) has been applied to visualise secretion at synaptic terminals (Miesenbock et al., 1998). Because this is a genetically encoded reporter, it holds significant promise for future studies in a number of genetic systems, including drosophila, nematode, zebrafish, and mouse.

The functional basis of pH-based sensors of synaptic activity is diagrammed in Figure 5.7. Synaptic vesicles are specialised endosomes that maintain an acidic lumen resulting from the activity of a vacuolar H^+-ATPase (Nelson, 1992). This activity is required to establish an electromotive force that, in turn, drives neurotransmitter uptake from the cytosol into the vesicle (Liu et al., 1999). Measurements of synaptic vesicle lumen pH indicate that it has a resting value of ~ 5.6 (Miesenbock et al., 1998). Following fusion with the plasma membrane during action potential firing, the lumenal surface of the synaptic vesicle abruptly switches to the more alkaline pH of the extracellular environment (pH ~ 7.4). Miesenbock and coworkers used a histidine-based combinatorial mutagenesis strategy combined with a pH-dependent selection

screen to obtain new variants of GFP that enable measurements of synaptic vesicle exocytosis. These new GFPs were termed pH-sensitive green fluorescent protein-based sensors (pHluorins). pHluorins targeted to the synaptic vesicle lumen (synapto-pHluorin) enabled measurements of dynamic changes in pH of vesicle lumen resulting from exocytosis and endocytosis of synaptic vesicles during presynaptic activity. The net fluorescence change observed during action potentials therefore reflect a net balance of externalised pHluorin, which is brightly fluorescent, and the endocytosed and reacidified vesicles, which are dark.

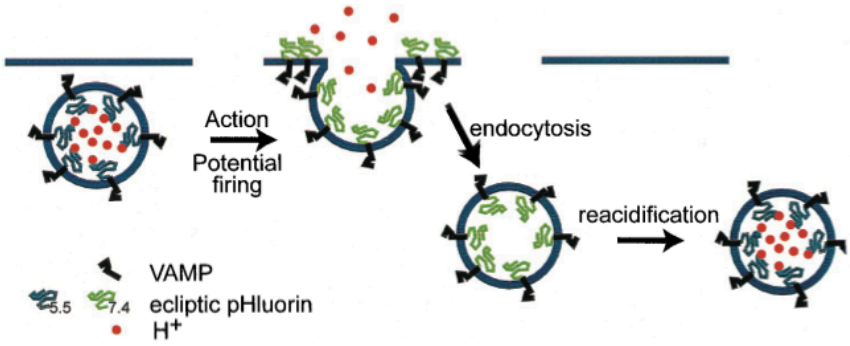

Figure 5.7. Exocytosis relieves the proton-dependent quenching of ecliptic-pHluorin fluorescence. The pHluorin molecule is attached to the lumenal aspect of VAMP. At the resting pH of 5.6 within vesicles, the fluorescence signal from pHluorin is completely quenched. During firing of action potentials, the vesicles undergo fusion with the plasma membrane leading to the externalisation of pHluorin to pH of 7.4. This relieves the proton-dependent quenching and causes an increase in fluorescence. The fluorescence signal then recovers following endocytosis by reacidification of vesicles.

5.5.1 Hippocampal neurons preparation, transfections and pHluorin imaging of neurons

To investigate the role of SV2A phosphorylation and the impact of the phospho-dependent association of SV2A and Syt1 on SV trafficking, optical imaging of pHluorin-tagged SV2A and Syt1 proteins was carried out in collaboration with Dr. Sarah Gordon from Professor Michael Cousin's laboratory (University of Edinburgh).

A chimeric reporter cDNA construct consisting of a signal-sequence-tagged pHluorin fused to the lumenal domain of mouse SV2A (SV2A-pH) was generated by inserting superecliptic pHluorin into the first intra-vesicular loop of mouse SV2A (between amino acid 197 and 198) (Figure 5.8B). Three further SV2A-pH constructs were generated; one with mutations to the cluster-1 phosphorylation sites to alanine

(Ser42Ala, Ser45Ala and Ser47Ala), another with mutations to the cluster-2 phosphorylation sites to alanine (Ser80Ala, Ser81Ala and Thr84Ala), and one with all six phosphorylation sites mutated to alanine (Ser42Ala, Ser45Ala and Ser47Ala, Ser80Ala, Ser81Ala and Thr84Ala).

Another chimeric reporter cDNA construct consisting of a signal-sequence-tagged pHluorin fused to the lumenal domain of rat synaptotagmin 1 (Syt1-pH) was kindly provided by Prof. Michael Cousin. SV2A-binding defective mutants of Syt1 were generated by mutating the three key amino acids (K327, T329 and K332) in the C2B domain of Syt1 to alanines. Those three key residues K327, T329 and K332 in the human Syt1 sequence correspond to residues K326, T328 and K331 in the rat protein sequence (see alignment in Figure 4.20). Those three residues were individually mutated to alanines to generate three independent cDNA constructs and a fourth construct with all three residues mutated to alanine was also generated.

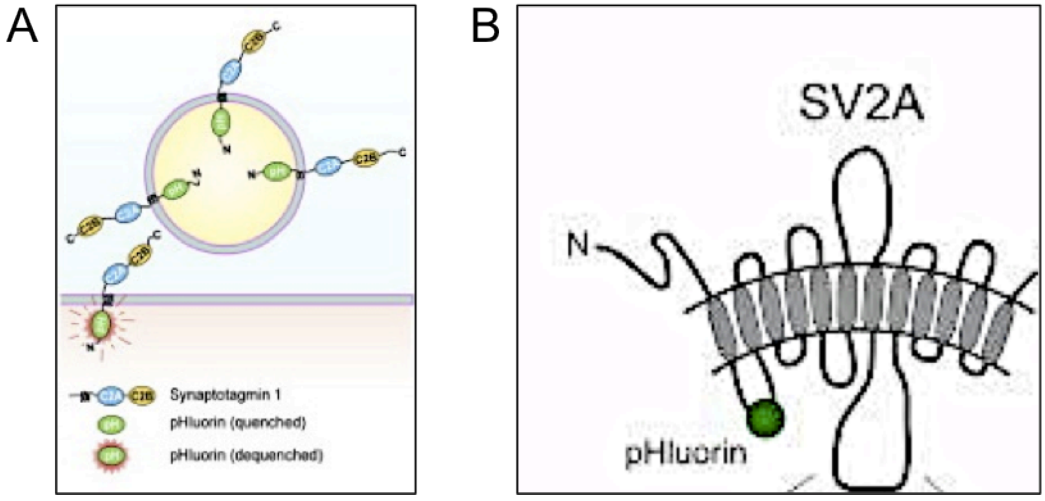

Figure 5.8. The use of Syt1-pH and SV2A-pH to monitor SV traffic. A) Because SVs are an acidic compartment, the Syt1-pHluorin reporter does not fluoresce before exocytosis but does once exposed on the cell surface. After endocytosis, this fluorescence is rapidly quenched by reacidification of the vesicle. Thus each exocytic event increases the fluorescence and each endocytic event reduces it. B) SV2A-pH was generated by inserting superecliptic pHluorin (green circle) into the first intra-vesicular loop of mouse SV2A (between amino acid 197 and 198).

Firstly, to establish the consequence of ablating the phosphorylation of SV2A and secondly the effect of disrupting the phospho-dependent association of SV2A with Syt1 in SV endocytosis, the traffic of the SV2A-pHluorin and Syt1-pHluorin wild-type and mutant proteins was monitored in primary hippocampal cultures derived from wild-type mice.

Syt1-pHluorin reports the traffic of Syt1 to and from the cell surface during SV exocytosis and endocytosis, by virtue of the pHluorin tagged to the luminal domain of Syt1 (Figure 5.8A). Its dynamic presence at the cell surface is reported by either increases (exocytosis) or decreases (endocytosis) in its signal, due to its fluorescence being quenched by the acidic environment within SVs. Similarly, SV2A-pHluorin reports the traffic of SV2A to and from the cell surface during SV exocytosis and endocytosis, by virtue of the pHluorin tagged to the luminal domain of SV2A (Figure 5.8B).

5.6 Results

5.6.1 Effect of ablating the phosphorylation of SV2A on its trafficking

In cultured primary hippocampal neurons, SV proteins, including SV2A and Syt1, undergo constitutive cycling between SVs and the presynaptic plasma membrane. A quantitative assessment of the consequence of abolishing the phosphorylation of SV2A at cluster-1 and cluster-2 sites in SV endocytosis was performed by mutating those residues to alanine.

Neurons in culture were transfected with SV2A-pHluorin reporters and were visualised at 500 nm (all >525 nm emission). Four different constructs were used for transfections: $SV2A^{WT}$-pHluorin, $SV2A^{S42A,S45A,S47A}$-pHluorin, $SV2A^{S80A,S81A,T84A}$-pHluorin, and $SV2A^{S42A,S45A,S47A,S80A,S81A,T84a}$-pHluorin ($SV2A^{6XA}$-pHluorin).

All the four SV2A-pHluorin chimeras were properly targeted to presynaptic vesicles, as electrical stimulation with 300 action potentials (APs) at 10 Hz gave rise to a stimulation-dependent SV2A-pHluorin fluorescence increase at synaptic boutons with similar characteristics as described before for pHluorin-tagged synaptobrevin (Miesenbock et al., 1998, Sankaranarayanan and Ryan, 2001). The pH dependence of the fluorescence was utilised to monitor the effect of mutating cluster-1 and cluster-2 phosphorylation sites within the presynaptic compartment of living neurons by using a simple acid quenching-dequenching protocol. Acid quenching resulted in a near complete loss of fluorescence, whereas alkalinisation of the vesicular lumen with NH_4Cl produced a maximum intensity signal at synaptic boutons, indicating that the transient fluorescence increase after stimulation was due to exocytotic externalisation

of SV2A-pHluorin.

The kinetics of SV2A-pHluorin exo-endocytosis indicated that SV2A-pHluorin can serve as a faithful reporter of SV2A recycling at presynaptic nerve terminals. This system was then used to assess the effect mutating the phosphorylation sites in living neurons both at steady state and under stimulating conditions.

A robust stimulation-dependent increase in SV2A-pHluorin fluorescence occurred in the hippocampal cultures, indicating that the reporters were efficiently delivered to the cell surface by SV exocytosis. $SV2A^{WT}$-pHluorin fluorescence decayed back to baseline with first order kinetics (Figure 5.9).

Remarkably, the three SV2A-pHluorin constructs harbouring phosphosite mutations produced similar responses; the endocytic rates remained largely unchanged (Figure 5.9A-D) with small differences in retrieval rate (i.e. relative speed of reinternalisation of SV2A-pHluorin molecules). This indicates that SV2A phosphorylation is dispensable for its normal trafficking.

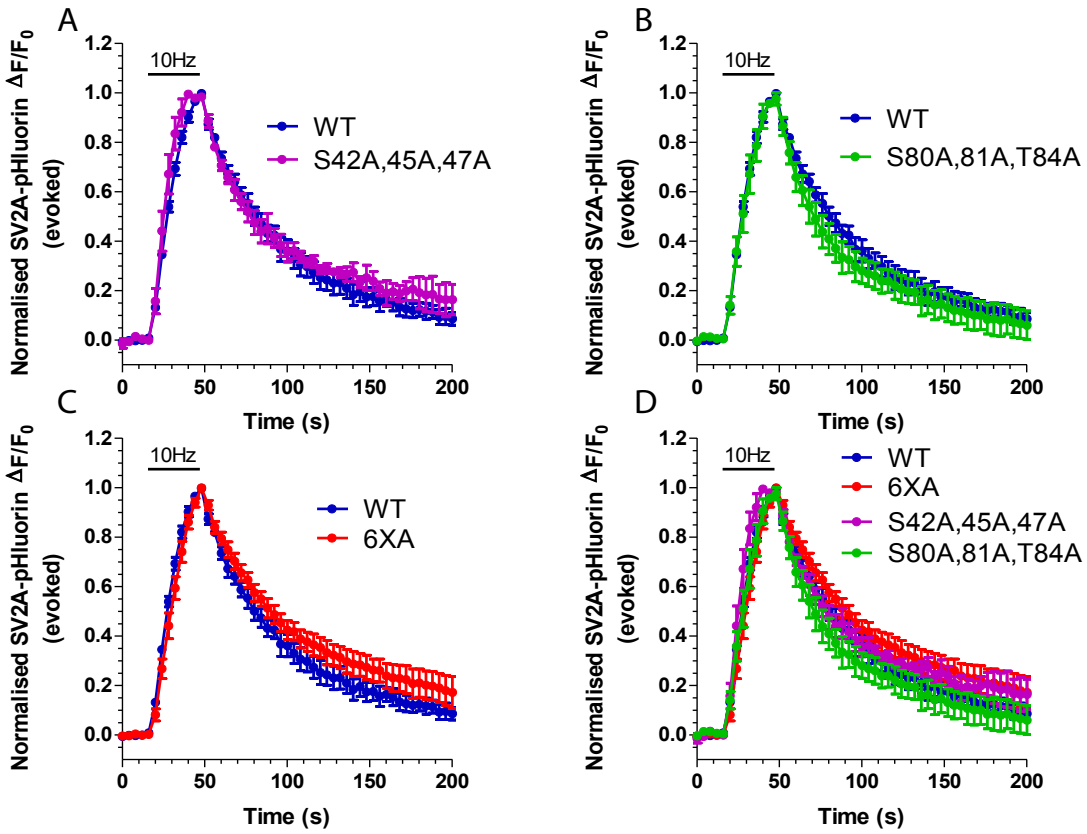

Figure 5.9. Mutation of SV2A phosphorylation sites are fully dispensable for proper SV2A trafficking. SV retrieval kinetics in WT neurons by recording SV2A-pHluorin fluorescence during and after field stimulation applied at 10 Hz for 30 s. (A) $SV2A^{S42A,S45A,S47A}$-pHluorin retrieval in WT neurons (purple line, purple bar) shows similar retrieval efficiency as compared to $SV2A^{WT}$-pHluorin retrieval in WT neurons (blue line, blue bar). (B-D) $SV2A^{S80A,S81A,T84A}$-pHluorin (green line, green bar) and $SV2A^{6XA}$-pHluorin (red line, red bar) both display very little difference in retrieval efficiency as compared to $SV2A^{WT}$-pHluorin retrieval in WT neurons (blue line, blue bar). All the four curves are plotted on the same graph in D. Data shown is mean ± SEM of five independent experiments.

5.6.2 Effect of disrupting the binding of SV2A to Syt1 on the recycling of Syt1

A quantitative assessment of the consequence of ablating the phospho-dependent association of SV2A with Syt1 in SV endocytosis was performed by mutating the three key residues, which are critical for the binding of SV2A cluster-2, in the C2B domain of Syt1.

Neurons in culture were transfected with pHluorin reporters and were visualised at 500 nm (all >525 nm emission). Five different constructs were used for transfections: $Syt1^{WT}$-pHluorin, $Syt1^{K326A}$-pHluorin, $Syt1^{T328A}$-pHluorin, $Syt1^{K331A}$-pHluorin and $Syt1^{K326A+T328A+K331A}$-pHluorin.

All the five Syt1-pHluorin chimeras were properly targeted to presynaptic vesicles, as electrical stimulation with 200 action potentials (APs) at 10 Hz gave rise to a stimulation-dependent Syt1-pHluorin fluorescence increase at synaptic boutons. The pH dependence of the fluorescence was utilised to monitor the effect of mutating those three residues on syt1-pHluorin distribution within the presynaptic compartment of living neurons by using a simple acid quenching-dequenching protocol. As observed with SV2A-pH, acid quenching resulted in a near complete loss of fluorescence, whereas alkalinisation of the vesicular lumen with NH_4Cl produced a maximum intensity signal at synaptic boutons, indicating that the transient fluorescence increase after stimulation was due to exocytotic externalisation of Syt1-pHluorin.

The kinetics of Syt1-pHluorin exo-endocytosis indicated that Syt1-pHluorin can serve as a faithful reporter of Syt1 recycling at presynaptic nerve terminals. This system then used to assess the effect mutating the three key residues, which abrogate Syt1's interaction with SV2A in the C2B domain on Syt1 recycling in living neurons both at steady state and under stimulating conditions.

A robust stimulation-dependent increase in Syt1-pHluorin fluorescence occurred in the hippocampal cultures, indicating that the reporters were efficiently delivered to the cell surface by SV exocytosis. $Syt1^{WT}$-pHluorin fluorescence decayed back to baseline with first order kinetics (Figure 5.10). The three Syt1-pHluorin constructs harbouring single mutations yielded similar responses; the endocytic events remained largely unchanged with small differences in retrieval rate (i.e., relative speed of reinternalisation of Syt1-pHluorin molecules). However, retrieval of the Syt1-pHluorin harbouring mutations in all three residues was significantly accelerated (Figure 5.10A), indicated by the increased speed of SV protein retrieval.

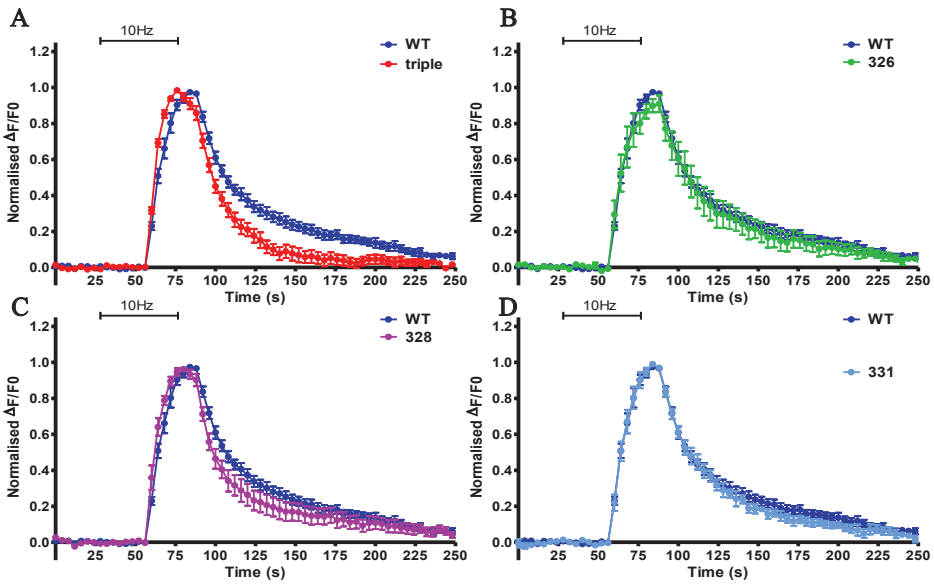

Figure 5.10. Mutation of SV2A binding site in the C2B domain of Syt1 accelerates SV retrieval. SV retrieval kinetics in WT neurons by recording Syt1-pHluorin fluorescence during and after field stimulation applied at 10 Hz for 20 s. (A) Syt1 $^{K326A+T328A+K332A}$ -pHluorin retrieval in WT neurons (red line, red bar) is faster than Syt1^{WT}-pHluorin retrieval in WT neurons (blue line, blue bar) as post-stimulation rate of fluorescence decay is higher. (B-D) Syt1^{K326A}-pHluorin (green line, green bar), Syt1^{T328A}-pHluorin (purple line, purple bar) and Syt1^{K331A}-pHluorin (light blue line, light blue bar) all display very little difference in retrieval efficiency as compared to Syt1-pHluorin^{WT} retrieval in WT neurons (blue line, blue bar). Data shown is mean ± SEM of nine independent experiments.

5.6.3 Discussion

The role of SV2A phosphorylation was studied via mutagenesis and optical imaging of pHluorin-tagged proteins in cultured neurons from wild-type mice. Surprisingly, these experiments revealed that phosphorylation is completely dispensable for the proper trafficking and retrieval of SV2A. However, the simultaneous mutation of the three residues in the C2B domain of Syt1 responsible for binding SV2A phosphocluster-2 increases the rate of SV endocytosis. This is the first direct functional evidence of a molecular role for phospho-dependent SV2A/Syt1 interaction in SV trafficking.

A potential confounding factor in this interpretation is that the same three residues are responsible for binding inositol hexaphosphate (IP6) (Joung et al., 2012), an inhibitor of SV exocytosis. Furthermore, several proteins, such as clathrin adaptor protein-2 (AP2) (Zhang et al., 1994), soluble NSF attachment protein (β-SNAP) (Schiavo et al., 1995), SNAP-25, and N-type calcium channels (Schiavo et al., 1997), bind to

different sites in the C2B domain. The mutation of those three residues could arguably affect the ability of the C2B domain to bind any of those molecular effectors, which could lead to the accelerated endocytic rate observed.

5.6.4 Synaptotagmin 1 promotes both vesicle fusion and recycling

In an active nerve terminal, exocytosis and endocytosis proceed at a frenzied pace. Each action potential releases ≈0.5% of the total supply of synaptic vesicles in the terminal (Ryan and Smith, 1995), and, with some neurons firing at a rate of 50 Hz or greater, synapses would lose the ability to secrete neurotransmitter within seconds if they could not reform and refill synaptic vesicles. Endocytosis is the principal means, and perhaps the only means, by which the used vesicles are recovered and recycled into the releasable vesicle pool (Jarousse and Kelly, 2001). Moreover, the rate of endocytosis is tightly coupled to the rate of exocytosis. In a resting terminal, endocytosis rates are low, but activity can increase this rate enormously to preserve the balance of exocytosis and endocytosis and thereby preserve the sizes of the nerve terminal and vesicle pool. A temporally linked balance of exo- and endocytosis maintains the supply of synaptic vesicles in the nerve terminal. How the rate of endocytosis is regulated, however, remains obscure.

Synaptotagmin 1 has been established as a significant contributor to exocytosis of synaptic vesicles (Sudhof and Rizo, 1996). However, Syt1 has an important role to play in promoting the efficient endocytosis of synaptic vesicles. This protein is thus of consequence to both sides of the vesicle cycle at nerve endings.

Nicholson-Tomishima and Ryan (2004) have compared exocytotic and endocytic rates in cortical cultures from wild-type and Syt1 knockout mice using synaptobrevin-pHluorin (a fusion protein of synaptobrevin tagged with pHluorin at its lumenally exposed C-terminus). For comparable levels of exocytosis, the synapses lacking synaptotagmin were substantially slower to recover their vesicles.

This evidence that Syt1 is necessary for rapid endocytosis of synaptic vesicles fits nicely with another study, in which a different approach was taken to test the involvement of Syt1 in endocytosis at the fly neuromuscular junction (Poskanzer et al., 2003). In this study, synaptobrevin-pHluorin was also used as a reporter of

exocytosis and endocytosis. The authors found that the rate of endocytosis was slower when Syt1 was inactivated. The conclusions of both studies were quite parallel and support an evolutionarily conserved and direct role of Syt1 in accelerating endocytosis.

These studies mesh well with earlier work. In particular, Syt1 has been shown to bind the clathrin–adaptor complex AP2 (Zhang et al., 1994). The binding of this complex is a mechanism by which domains of plasma membrane recruit clathrin and cargo proteins and thereby begin membrane invagination (Traub, 2003). The site of the interaction has been mapped to the C2B domain of Syt1, and this interaction can enhance the recruitment of both the AP2 complex and clathrin to liposomes (Haucke et al., 2000). The AP2 complex, however, also binds to inositol phospholipids on the membrane, and thus Syt1 was not expected to be a requisite step for AP2 recruitment to the membrane. Rather, Syt1 may assist in concentrating the clathrin apparatus at sites of recycling vesicles or may help AP2 to gather other synaptic vesicle proteins including SV2A. This model is consistent with the fact that endocytosis persisted in mice lacking Syt1 but was kinetically slower (Nicholson-Tomishima and Ryan, 2004).

Endocytosis of Syt1 is also regulated by the AP2μ related protein, stonin 2 (Diril et al., 2006), which selectively associates with Syt1 and no other SV proteins. Stonin 2 is required for the complex formation between AP2 and Syt1. Kononenko et al. (2013) compared the SV retrieval kinetics in wild-type and stonin 2 knock-out neurons by recording Syt1-pHluorin fluorescence during and after field stimulation. SV retrieval was significantly faster in stonin 2 KO neurons (Kononenko et al., 2013), an observation that echoes the accelerated rate of endocytosis with the SV2A-binding defective Syt1. Since SV2A also influences the endocytosis of Syt1, stonin 2 and SV2A could be components of a unique common mechanism for Syt1 endocytosis or they could operate via different pathways; and that remains to be determined.

The tight functional coupling between SV2A and Syt1 is a critical step in the SV cycle. SV2A impacts on the endocytosis of Syt1 because peptides corresponding to the endocytosis domain of SV2A increase the binding of Syt1 to AP2 clathrin adaptors (Haucke and De Camilli, 1999). Moreover, synaptic vesicles isolated from SV2A KO mice contain lower levels of Syt1 than wild-type mice (Yao et al., 2010). SV2A thus plays a major role in regulating the amount of the Syt1 protein in synaptic

vesicles. SV2A may help concentrate clathrin adaptors in a way that insures the inclusion of Syt1 in vesicles.

The SV2A-Syt1 interaction may influence the modulation of one or both proteins' actions. The SV2A/Syt1 complex may assist in concentrating the clathrin apparatus at sites of recycling vesicles or may help AP2 to gather other synaptic vesicle proteins. Disruption of this interaction could cause the repartitioning of SV2A and Syt1 to the active zones of neuronal membranes, which may in turn induce compensatory AP-1-mediated SV reformation from bulk endosomes to maintain the supply of synaptic vesicles. Increased bulk endocytosis and endosomal SV reformation may underlie the observed accelerated kinetics of SV protein retrieval, although other mechanisms, such as bypassing an otherwise rate-limiting step of the SV2A/Syt1 interaction, cannot be ruled out (Kononenko et al., 2013).

SV2A is essential for normal neurotransmission. In its absence, synaptic release probability decreases, a result that leads to a severe seizure phenotype and premature death (Crowder et al., 1999, Janz et al., 1999). The functional lesion in synapses lacking SV2A occurs after vesicle docking (Custer et al., 2006) and before the formation of tightly-associated SNARE complexes (Xu and Bajjalieh, 2001), indicating that SV2A contributes to the process that renders vesicles competent for calcium-stimulated fusion. In the absence of SV2A, Syt1 trafficking to synaptic vesicles becomes more random (Yao et al., 2010), leading to fewer vesicles with enough of the calcium sensor to trigger calcium-stimulated fusion. This could trigger compensatory endocytosis, which could produce the accelerated endocytic phenotype observed with the SV2A-binding defective Syt1. The role of SV2A and Syt1 in endocytosis can potentially explain the hyperexcitability and hypersynchrony that are the hallmarks of epileptic brain circuits observed in SV2A knockout mice.

5.6.5 Conclusions

By optical imaging of pHluorin-tagged SV2A in cultured neurons from wild-type mice, the phosphorylation of SV2A at cluster-1 and cluster-2 was found to play no measureable role in the normal trafficking and recycling of SV2A. Remarkably,

ablating the SV2A binding site in the C2B domain of Syt1 significantly enhances the rate of Syt1 endocytic retrieval.

The C2B domain of Syt1 engages several different proteins including clathrin adaptor protein-2 (AP2) and mutations of those critical residues could arguably affect the ability of the C2B domain to bind any of these molecular effectors. This is a potential confounding factor in the interpretation of the data. Another caveat is that the trafficking of pHluorin-tagged SV2A and Syt1 were monitored in hippocampal neurons from wild-type mice and the wild-type proteins may be masking the effect of the exogenous proteins in those neurons.

To control for off target effects of endogenous SV2A, small hairpin RNA (shRNA) that efficiently knocks down SV2A has been generated. shRNA-resistant SV2A constructs bearing alanine mutations at cluster-1 and cluster-2 have also been made. Repeat experiments involving the coexpression of the rescue constructs with SV2A-shRNA are currently underway. Further insights in the role of SV2A phosphorylation and in the functional significance SV2A/Syt1 phosphospecific interaction can be garnered by monitoring the traffic of Syt1 in neurons expressing SV2A phosphomutants in SV2A-deficient neurons.

6 Conclusions and perspectives

6.1 *In vivo* validation of SV2A as a physiological TTBK2 substrate

In conclusion, the work I have presented in this thesis postulate the first lines of evidence that TTBK2 operates at a distinct step in the synaptic vesicle trafficking cycle. I have demonstrated by immunoprecipitation of the endogenous TTBK2 protein from brain homogenates that it networks with a number of synaptic vesicle proteins including SV2A, which it potently phosphorylates *in vitro*. Subsequent phosphopeptide mapping revealed that SV2A is phosphorylated at two clusters of three highly-conserved residues by TTBK2.

The complete characterisation of this novel kinase-substrate relationship requires one crucial piece of scientific evidence. The one remaining challenge is to establish conclusively that SV2A is a physiological TTBK2 substrate *in vivo*. To validate the phosphorylation of SV2A by TTBK2 *in vivo* at the relevant sites, a set of criteria has to be satisfied. This can be achieved by a number of experimental strategies including the demonstration that the phosphorylation of the endogenous substrate is reduced at the relevant site(s) in cells by treatment with specific pharmacological inhibitors of the kinase. Another potential way to validate the substrate *in vivo* is by showing that phosphorylation does not occur in cells and tissues of mice that do not express the kinase, or in cells from knock-in mice that express a catalytically inactive mutant of the kinase. All these strategies require the monitoring of the levels of phosphorylation at the relevant sites and thus phosphospecific antibodies are very valuable tools for the *in vivo* validation of the kinase-substrate relationship.

The *in vivo* validation of SV2A phosphorylation by TTBK2 has thus far been logistically hindered by the lack of key reagents and tools. The generation of appropriate phospho-specific antibodies that are able to specifically recognize the two SV2A clusters of phosphorylation has proved to be difficult due to the close proximity of the phosphorylation sites. Moreover, as TTBK2 is not a well-studied kinase, specific inhibitors have not been developed yet. Finally, we have found that mice homozygous for the SCA11 mutation are embryonically lethal and so are complete TTBK2 gene knockouts.

Nevertheless, the validation may alternatively be accomplished by the depletion of the TTBK2 protein in neurons by RNAi (RNA interference) or shRNA (short-hairpin RNA). Due to the lack of sensitive phosphospecific antibodies, changes in phosphorylation levels may be monitored by mass spectrometry. It is also noteworthy that as synaptic vesicle traffic is a process only occurs in neurons, it will be imperative that the validation is performed in primary neuronal cultures.

6.2 Investigation of brain developmental defects in SCA11 homozygous mouse embryos

As data was gathered on TTBK2 over the course of the project, a number of key questions were raised. One such important question to be tackled is the mechanism causing developmental defects and embryonic lethality in the homozygous SCA11 knockin mice. Homozygous E10-TTBK2$^{fmly1/fmly1}$ embryos were developmentally delayed, lacking prominent subdivisions of the developing brain, and were smaller than wild-type littermates. Early embryonic lethality caused by genetic mutations have led to great insights into the genetic control of fundamental biological processes, including cell division, cell death, cell fate, differentiation, and morphogenesis. Thus, the discovery of an early embryonic lethal phenotype is an exciting opportunity for novel insights into the genetic control of biological processes with important implications for our understanding of fundamental mechanisms of neurogenesis in embryonic development.

An analysis of the mutant phenotype requires specialised embryological and analytical tools. The normal patterns of the wild-type and mutant TTBK2 gene in wild-type, heterozygous and homozygous mouse embryos will provide clues in the analysis of the lethal phenotype by pinpointing the tissue in which the mutation is likely to have its primary effect. TTBK2 expression patterns can be established by *in situ* hybridisation for mRNA or immunohistochemistry for the protein. Abnormal embryos can be assessed in comparison with their control littermates, which allow the comparison of differences in the developmental timing within and between litters.

Morphological assessment of embryos during the post-implantation period can be insightful and can be accomplished by dissection or by fixation and sectioning of embryos within the uterus. Following dissection, embryonic and placental samples can be fixed for further analysis either as whole mounts or sections for cell death and proliferation assays, gene or protein expression, or evaluation of detailed morphological and histological features. In parallel, signs of cerebellar atrophy and Purkinje cell loss can be studied in the heterozygous mice by staining and quantification of cerebellar sections using high-resolution microscopy.

6.3 Selective vulnerability of Purkinje cells in Spinocerebellar Ataxia

The most intriguing aspect of the pathogenesis of SCA11 is that although TTBK2 is widely expressed in the central nervous system and various other tissues, the pathology is confined mainly to the cerebellar Purkinje cells. It would certainly be worthwhile to examine the molecular basis of this selective vulnerability of the Purkinje cells of the cerebellum.

The issue of selective neuronal vulnerability is likely to be complex and influenced by a multitude of factors. I propose that among such contributing factors are the relative expression levels of TTBK2 in different neuronal cell populations. It is known that the levels of TTBK2 expression is higher in the cerebellar Purkinje cells than other neuronal cell populations. Therefore, if Purkinje cells express higher levels of TTBK2 as other neurons, this could put them at increased risk for degeneration when the protein is mutated. Along the same lines, the levels of TTBK2's interacting partners are likely contributors to the cell-specific vulnerabilities. For example, if SV2A or synaptotagmin 1 levels are slightly higher in vulnerable neurons, the toxic gain-of-function effects of the TTBK2 mutant protein would be more pronounced in such neurons.

There is also exploratory evidence that the SCA11 mutations markedly inhibit endogenous kinase activity. The aberrant phosphorylation of SV2A could potentially be a probable contributor to the progressive demise of Purkinje neurons. Because SV2A's interactions with synaptotagmin1 and clathrin adaptor proteins are modulated

by phosphorylation, one possible mechanism of neurotoxicity is that anomalous phosphorylation SV2A may lead to alterations in those interactions that, in turn, impact on protein trafficking and/or endocytic reinternalisation, which may lead to the accumulation of inactive (unfolded) protein intermediates that may render synaptic terminals vulnerable to activity-dependent degeneration. Research must therefore be focused on investigating these hypothetical scenarios, as they are likely to provide insights into the fundamental neurodegenerative process in SCA11.

6.4 New insights provided by the crystal structure of the C2B domain of Syt1 and the cluster-2 phosphopeptide

Since I completed my thesis work, the crystal structure of the C2B domain of synaptotagmin 1 complexed with the triply-phosphorylated cluster-2 peptide has been solved by Dr. Maximilian Fritsch (postdoc in the lab). The crystal structure has refined the binding interface between the two proteins and has exposed that Thr84 residue of SV2A is the critical determinant of the interaction and the two residues mediating this interaction in the C2B domain are Lys326 and Lys328 (not Lys327 as originally predicted from the C2B-IP6 structure). Therefore, the key residues to target in the functional dissection of the SV2A/Syt1 interaction are Lys326 and Lys328. Planned pHluorin imaging experiments and SV2A shRNA rescue experiments (in collaboration with Prof. Mike Cousin's lab) have been adjusted in the light of this relevant information.

6.5 The mechanism of action of Levetiracetam

Finally, Levetiracetam's mechanism of action remains unknown. It is conceivable that one possible mechanism of Levetiracetam (LEV) action is that it modulates SV2A's function by altering its phosphorylation by TTBK2, which in turn impacts on SV2A protein interactions. A direct implication of my findings would be to investigate the effect of LEV on SV2A phosphorylation by TTBK2 *in vivo.* From the findings presented in this thesis, a model now exists that can be used to design experiments to test these hypotheses. Elucidating the mechanism by which LEV, SV2A and TTBK2 cooperate to prevent seizures will undoubtedly open doors to the investigation of potential novel target proteins involved in the synaptic vesicle cycle.

References:

ADACHI, N., KOBAYASHI, T., TAKAHASHI, H., KAWASAKI, T., SHIRAI, Y., UEYAMA, T., MATSUDA, T., SEKI, T., SAKAI, N. & SAITO, N. 2008. Enzymological analysis of mutant protein kinase Cgamma causing spinocerebellar ataxia type 14 and dysfunction in Ca2+ homeostasis. *J Biol Chem,* 283**,** 19854-63.

ADAMS, S. R., CAMPBELL, R. E., GROSS, L. A., MARTIN, B. R., WALKUP, G. K., YAO, Y., LLOPIS, J. & TSIEN, R. Y. 2002. New biarsenical ligands and tetracysteine motifs for protein labeling in vitro and in vivo: synthesis and biological applications. *J Am Chem Soc,* 124**,** 6063-76.

AMORESANO, A., DI COSTANZO, A., LEO, G., DI CUNTO, F., LA MANTIA, G., GUERRINI, L. & CALABRO, V. 2010. Identification of DeltaNp63alpha protein interactions by mass spectrometry. *J Proteome Res,* 9**,** 2042-8.

AUGUSTINE, G. J. 2001. How does calcium trigger neurotransmitter release? *Curr Opin Neurobiol,* 11**,** 320-6.

BAI, J. & CHAPMAN, E. R. 2004. The C2 domains of synaptotagmin--partners in exocytosis. *Trends Biochem Sci,* 29**,** 143-51.

BAJJALIEH, S. M., FRANTZ, G. D., WEIMANN, J. M., MCCONNELL, S. K. & SCHELLER, R. H. 1994. Differential expression of synaptic vesicle protein 2 (SV2) isoforms. *J Neurosci,* 14**,** 5223-35.

BAJJALIEH, S. M., PETERSON, K., LINIAL, M. & SCHELLER, R. H. 1993. Brain contains two forms of synaptic vesicle protein 2. *Proc Natl Acad Sci U S A,* 90**,** 2150-4.

BAJJALIEH, S. M., PETERSON, K., SHINGHAL, R. & SCHELLER, R. H. 1992. SV2, a brain synaptic vesicle protein homologous to bacterial transporters. *Science,* 257**,** 1271-3.

BARFORD, D. 1991. Molecular mechanisms for the control of enzymic activity by protein phosphorylation. *Biochim Biophys Acta,* 1133**,** 55-62.

BARSYTE-LOVEJOY, D., GALANIS, A. & SHARROCKS, A. D. 2002. Specificity determinants in MAPK signaling to transcription factors. *J Biol Chem,* 277**,** 9896-903.

BENFENATI, F., GREENGARD, P., BRUNNER, J. & BAHLER, M. 1989. Electrostatic and hydrophobic interactions of synapsin I and synapsin I fragments with phospholipid bilayers. *J Cell Biol,* 108**,** 1851-62.

BIONDI, R. M., CHEUNG, P. C., CASAMAYOR, A., DEAK, M., CURRIE, R. A. & ALESSI, D. R. 2000. Identification of a pocket in the PDK1 kinase domain that interacts with PIF and the C-terminal residues of PKA. *EMBO J,* 19**,** 979-88.

BIONDI, R. M., KOMANDER, D., THOMAS, C. C., LIZCANO, J. M., DEAK, M., ALESSI, D. R. & VAN AALTEN, D. M. 2002. High resolution crystal structure of the human PDK1 catalytic domain defines the regulatory phosphopeptide docking site. *EMBO J,* 21**,** 4219-28.

BIONDI, R. M. & NEBREDA, A. R. 2003. Signalling specificity of Ser/Thr protein kinases through docking-site-mediated interactions. *Biochem J,* 372**,** 1-13.

BLANCO-ARIAS, P., EINHOLM, A. P., MAMSA, H., CONCHEIRO, C., GUTIERREZ-DE-TERAN, H., ROMERO, J., TOUSTRUP-JENSEN, M. S., CARRACEDO, A., JEN, J. C., VILSEN, B. & SOBRIDO, M. J. 2009. A C-terminal mutation of ATP1A3 underscores the crucial role of sodium affinity in the pathophysiology of rapid-onset dystonia-parkinsonism. *Hum Mol Genet,* 18**,** 2370-7.

BLONDEAU, F., RITTER, B., ALLAIRE, P. D., WASIAK, S., GIRARD, M., HUSSAIN, N. K., ANGERS, A., LEGENDRE-GUILLEMIN, V., ROY, L., BOISMENU, D., KEARNEY, R. E., BELL, A. W., BERGERON, J. J. & MCPHERSON, P. S. 2004. Tandem MS analysis of brain clathrin-coated vesicles reveals their critical involvement in synaptic vesicle recycling. *Proc Natl Acad Sci U S A,* 101**,** 3833-8.

BOMMERT, K., CHARLTON, M. P., DEBELLO, W. M., CHIN, G. J., BETZ, H. & AUGUSTINE, G. J. 1993. Inhibition of neurotransmitter release by C2-domain peptides implicates synaptotagmin in exocytosis. *Nature,* 363**,** 163-5.

BOUSKILA, M., ESOOF, N., GAY, L., FANG, E. H., DEAK, M., BEGLEY, M. J., CANTLEY, L. C., PRESCOTT, A., STOREY, K. G. & ALESSI, D. R. 2011. TTBK2 kinase substrate specificity and the impact of spinocerebellar-ataxia-causing mutations on expression, activity, localization and development. *Biochem J,* 437**,** 157-67.

BRADFORD, M. M. 1976. A rapid and sensitive method for the quantitation of microgram quantities of protein utilizing the principle of protein-dye binding. *Anal Biochem,* 72**,** 248-54.

BRANDON, N. J., DELMAS, P., HILL, J., SMART, T. G. & MOSS, S. J. 2001. Constitutive tyrosine phosphorylation of the GABA(A) receptor gamma 2 subunit in rat brain. *Neuropharmacology,* 41**,** 745-52.

BRODIE, M. J., ELDER, A. T. & KWAN, P. 2009. Epilepsy in later life. *Lancet Neurol,* 8**,** 1019-30.

BROSE, N., PETRENKO, A. G., SUDHOF, T. C. & JAHN, R. 1992. Synaptotagmin: a calcium sensor on the synaptic vesicle surface. *Science,* 256**,** 1021-5.

BUCKLEY, K. & KELLY, R. B. 1985. Identification of a transmembrane glycoprotein specific for secretory vesicles of neural and endocrine cells. *J Cell Biol,* 100**,** 1284-94.

BUSHARA, K. O., MALIK, T. & EXCONDE, R. E. 2005. The effect of levetiracetam on essential tremor. *Neurology,* 64**,** 1078-80.

BYRNE, J. 2013. *Neuroscience Electronic Textbook* [Online]. Houston. Available: http://neuroscience.uth.tmc.edu/ [Accessed 17 May 2013].

CANTLEY, L. C., AUGER, K. R., CARPENTER, C., DUCKWORTH, B., GRAZIANI, A., KAPELLER, R. & SOLTOFF, S. 1991. Oncogenes and signal transduction. *Cell,* 64**,** 281-302.

CASTELLUCCI, V. F., KANDEL, E. R., SCHWARTZ, J. H., WILSON, F. D., NAIRN, A. C. & GREENGARD, P. 1980. Intracellular injection of t he catalytic subunit of cyclic AMP-dependent protein kinase simulates facilitation of transmitter release underlying behavioral sensitization in Aplysia. *Proc Natl Acad Sci U S A,* 77**,** 7492-6.

CASTELLUCCI, V. F., NAIRN, A., GREENGARD, P., SCHWARTZ, J. H. & KANDEL, E. R. 1982. Inhibitor of adenosine 3':5'-monophosphate-dependent protein kinase blocks presynaptic facilitation in Aplysia. *J Neurosci,* 2**,** 1673-81.

CHANG, C. I., XU, B. E., AKELLA, R., COBB, M. H. & GOLDSMITH, E. J. 2002. Crystal structures of MAP kinase p38 complexed to the docking sites on its nuclear substrate MEF2A and activator MKK3b. *Mol Cell,* 9**,** 1241-9.

CHANG, W. P. & SUDHOF, T. C. 2009. SV2 renders primed synaptic vesicles competent for Ca2+ -induced exocytosis. *J Neurosci,* 29**,** 883-97.

CHAPMAN, E. R. 2002. Synaptotagmin: a Ca(2+) sensor that triggers exocytosis? *Nat Rev Mol Cell Biol,* 3**,** 498-508.

CHAPMAN, E. R. 2008. How does synaptotagmin trigger neurotransmitter release? *Annu Rev Biochem,* 77**,** 615-41.

CHAPMAN, E. R., HANSON, P. I., AN, S. & JAHN, R. 1995. Ca2+ regulates the interaction between synaptotagmin and syntaxin 1. *J Biol Chem,* 270**,** 23667-71.

CHEN, D. H., BRKANAC, Z., VERLINDE, C. L., TAN, X. J., BYLENOK, L., NOCHLIN, D., MATSUSHITA, M., LIPE, H., WOLFF, J., FERNANDEZ, M., CIMINO, P. J., BIRD, T. D. & RASKIND, W. H. 2003. Missense mutations in the regulatory domain of PKC gamma: a new mechanism for dominant nonepisodic cerebellar ataxia. *Am J Hum Genet,* 72**,** 839-49.

CLARK, H. B., BURRIGHT, E. N., YUNIS, W. S., LARSON, S., WILCOX, C., HARTMAN, B., MATILLA, A., ZOGHBI, H. Y. & ORR, H. T. 1997. Purkinje cell expression of a mutant allele of SCA1 in transgenic mice leads to disparate effects on motor behaviors, followed by a progressive cerebellar dysfunction and histological alterations. *J Neurosci,* 17**,** 7385-95.

COHEN, J. E., LEE, P. R., CHEN, S., LI, W. & FIELDS, R. D. 2011. MicroRNA regulation of homeostatic synaptic plasticity. *Proc Natl Acad Sci U S A,* 108**,** 11650-5.

COHEN, P. 1999. The development and therapeutic potential of protein kinase inhibitors. *Curr Opin Chem Biol,* 3**,** 459-65.

COHEN, P. 2000. The regulation of protein function by multisite phosphorylation--a 25 year update. *Trends Biochem Sci,* 25**,** 596-601.

COLLINS, B. M., MCCOY, A. J., KENT, H. M., EVANS, P. R. & OWEN, D. J. 2002. Molecular architecture and functional model of the endocytic AP2 complex. *Cell,* 109**,** 523-35.

CORRAL, J., GENIS, D., BANCHS, I., SAN NICOLAS, H., ARMSTRONG, J. & VOLPINI, V. 2005. Giant SCA8 alleles in nine children whose mother has two moderately large ones. *Ann Neurol,* 57**,** 549-53.

CROWDER, K. M., GUNTHER, J. M., JONES, T. A., HALE, B. D., ZHANG, H. Z., PETERSON, M. R., SCHELLER, R. H., CHAVKIN, C. & BAJJALIEH, S. M. 1999. Abnormal neurotransmission in mice lacking synaptic vesicle protein 2A (SV2A). *Proc Natl Acad Sci U S A,* 96**,** 15268-73.

CUMMINGS, C. J., MANCINI, M. A., ANTALFFY, B., DEFRANCO, D. B., ORR, H. T. & ZOGHBI, H. Y. 1998. Chaperone suppression of aggregation and altered subcellular proteasome localization imply protein misfolding in SCA1. *Nat Genet,* 19**,** 148-54.

CUSTER, K. L., AUSTIN, N. S., SULLIVAN, J. M. & BAJJALIEH, S. M. 2006. Synaptic vesicle protein 2 enhances release probability at quiescent synapses. *J Neurosci,* 26**,** 1303-13.

D'ANGELO, E. 2013. Handbook of the Cerebellum and Cerebellar Disorders. *In:* MANTO, M. S., J.;ROSSI, F.;GRUOL, D. AND KOIBUCHI, N (ed.) *Handbook of the Cerebellum and Cerebellar Disorders*

. Netherlands: Springer.

DAGDA, R. K., MERRILL, R. A., CRIBBS, J. T., CHEN, Y., HELL, J. W., USACHEV, Y. M. & STRACK, S. 2008. The spinocerebellar ataxia 12 gene product and protein phosphatase 2A regulatory subunit Bbeta2 antagonizes neuronal survival by promoting mitochondrial fission. *J Biol Chem,* 283**,** 36241-8.

DAJANI, R., FRASER, E., ROE, S. M., YOUNG, N., GOOD, V., DALE, T. C. & PEARL, L. H. 2001. Crystal structure of glycogen synthase kinase 3 beta: structural

basis for phosphate-primed substrate specificity and autoinhibition. *Cell,* 105**,** 721-32.
DALSKI, A., MITULLA, B., BURK, K., SCHATTENFROH, C., SCHWINGER, E. & ZUHLKE, C. 2006. Mutation of the highly conserved cysteine residue 131 of the SCA14 associated PRKCG gene in a family with slow progressive cerebellar ataxia. *J Neurol,* 253**,** 1111-2.
DAUGHTERS, R. S., TUTTLE, D. L., GAO, W., IKEDA, Y., MOSELEY, M. L., EBNER, T. J., SWANSON, M. S. & RANUM, L. P. 2009. RNA gain-of-function in spinocerebellar ataxia type 8. *PLoS Genet,* 5**,** e1000600.
DAVLETOV, B. A. & SUDHOF, T. C. 1994. Ca(2+)-dependent conformational change in synaptotagmin I. *J Biol Chem,* 269**,** 28547-50.
DE CARVALHO AGUIAR, P., SWEADNER, K. J., PENNISTON, J. T., ZAREMBA, J., LIU, L., CATON, M., LINAZASORO, G., BORG, M., TIJSSEN, M. A., BRESSMAN, S. B., DOBYNS, W. B., BRASHEAR, A. & OZELIUS, L. J. 2004. Mutations in the Na+/K+ -ATPase alpha3 gene ATP1A3 are associated with rapid-onset dystonia parkinsonism. *Neuron,* 43**,** 169-75.
DE SMEDT, T., RAEDT, R., VONCK, K. & BOON, P. 2007. Levetiracetam: part II, the clinical profile of a novel anticonvulsant drug. *CNS Drug Rev,* 13**,** 57-78.
DENK, W. & SVOBODA, K. 1997. Photon upmanship: why multiphoton imaging is more than a gimmick. *Neuron,* 18**,** 351-7.
DESAI, R. C., VYAS, B., EARLES, C. A., LITTLETON, J. T., KOWALCHYCK, J. A., MARTIN, T. F. & CHAPMAN, E. R. 2000. The C2B domain of synaptotagmin is a Ca(2+)-sensing module essential for exocytosis. *J Cell Biol,* 150**,** 1125-36.
DIRIL, M. K., WIENISCH, M., JUNG, N., KLINGAUF, J. & HAUCKE, V. 2006. Stonin 2 is an AP-2-dependent endocytic sorting adaptor for synaptotagmin internalization and recycling. *Dev Cell,* 10**,** 233-44.
DUENAS, A. M., GOOLD, R. & GIUNTI, P. 2006. Molecular pathogenesis of spinocerebellar ataxias. *Brain,* 129**,** 1357-70.
DUNTEMAN, E. D. 2005. Levetiracetam as an adjunctive analgesic in neoplastic plexopathies: case series and commentary. *J Pain Palliat Care Pharmacother,* 19**,** 35-43.
DUROCHER, Y., PERRET, S. & KAMEN, A. 2002. High-level and high-throughput recombinant protein production by transient transfection of suspension-growing human 293-EBNA1 cells. *Nucleic Acids Res,* 30**,** E9.
EDENER, U., KURTH, I., MEINER, A., HOFFMANN, F., HUBNER, C. A., BERNARD, V., GILLESSEN-KAESBACH, G. & ZUHLKE, C. 2009. Missense exchanges in the TTBK2 gene mutated in SCA11. *J Neurol,* 256**,** 1856-9.
ENGGAARD, T. P., KLITGAARD, N. A. & SINDRUP, S. H. 2006. Specific effect of levetiracetam in experimental human pain models. *Eur J Pain,* 10**,** 193-8.
FATT, P. & KATZ, B. 1952. Spontaneous subthreshold activity at motor nerve endings. *J Physiol,* 117**,** 109-28.
FEANY, M. B., LEE, S., EDWARDS, R. H. & BUCKLEY, K. M. 1992. The synaptic vesicle protein SV2 is a novel type of transmembrane transporter. *Cell,* 70**,** 861-7.
FEATHERSTONE, D. E., DAVIS, W. S., DUBREUIL, R. R. & BROADIE, K. 2001. Drosophila alpha- and beta-spectrin mutations disrupt presynaptic neurotransmitter release. *J Neurosci,* 21**,** 4215-24.
FERNANDEZ, I., ARAC, D., UBACH, J., GERBER, S. H., SHIN, O., GAO, Y., ANDERSON, R. G., SUDHOF, T. C. & RIZO, J. 2001. Three-dimensional structure of the

synaptotagmin 1 C2B-domain: synaptotagmin 1 as a phospholipid binding machine. *Neuron,* 32**,** 1057-69.

FERNANDEZ-CHACON, R., KONIGSTORFER, A., GERBER, S. H., GARCIA, J., MATOS, M. F., STEVENS, C. F., BROSE, N., RIZO, J., ROSENMUND, C. & SUDHOF, T. C. 2001. Synaptotagmin I functions as a calcium regulator of release probability. *Nature,* 410**,** 41-9.

FERNANDEZ-CHACON, R. & SUDHOF, T. C. 1999. Genetics of synaptic vesicle function: toward the complete functional anatomy of an organelle. *Annu Rev Physiol,* 61**,** 753-76.

FIOL, C. J., HASEMAN, J. H., WANG, Y. H., ROACH, P. J., ROESKE, R. W., KOWALCZUK, M. & DEPAOLI-ROACH, A. A. 1988. Phosphoserine as a recognition determinant for glycogen synthase kinase-3: phosphorylation of a synthetic peptide based on the G-component of protein phosphatase-1. *Arch Biochem Biophys,* 267**,** 797-802.

FLOOR, E. & FEIST, B. E. 1989. Most synaptic vesicles isolated from rat brain carry three membrane proteins, SV2, synaptophysin, and p65. *J Neurochem,* 52**,** 1433-7.

FLOTOW, H., GRAVES, P. R., WANG, A. Q., FIOL, C. J., ROESKE, R. W. & ROACH, P. J. 1990. Phosphate groups as substrate determinants for casein kinase I action. *J Biol Chem,* 265**,** 14264-9.

FLOTOW, H. & ROACH, P. J. 1991. Role of acidic residues as substrate determinants for casein kinase I. *J Biol Chem,* 266**,** 3724-7.

FREE, R. B., HAZELWOOD, L. A. & SIBLEY, D. R. 2009. Identifying novel protein-protein interactions using co-immunoprecipitation and mass spectroscopy. *Curr Protoc Neurosci,* Chapter 5**,** Unit 5 28.

FRIEDMAN, M. J., SHAH, A. G., FANG, Z. H., WARD, E. G., WARREN, S. T., LI, S. & LI, X. J. 2007. Polyglutamine domain modulates the TBP-TFIIB interaction: implications for its normal function and neurodegeneration. *Nat Neurosci,* 10**,** 1519-28.

FRISCHMEYER, P. A. & DIETZ, H. C. 1999. Nonsense-mediated mRNA decay in health and disease. *Hum Mol Genet,* 8**,** 1893-900.

FUKUDA, M., ARUGA, J., NIINOBE, M., AIMOTO, S. & MIKOSHIBA, K. 1994. Inositol-1,3,4,5-tetrakisphosphate binding to C2B domain of IP4BP/synaptotagmin II. *J Biol Chem,* 269**,** 29206-11.

FUKUDA, M., KOJIMA, T., ARUGA, J., NIINOBE, M. & MIKOSHIBA, K. 1995. Functional diversity of C2 domains of synaptotagmin family. Mutational analysis of inositol high polyphosphate binding domain. *J Biol Chem,* 270**,** 26523-7.

FUKUDA, M. & MIKOSHIBA, K. 1997. The function of inositol high polyphosphate binding proteins. *Bioessays,* 19**,** 593-603.

GEPPERT, M., GODA, Y., HAMMER, R. E., LI, C., ROSAHL, T. W., STEVENS, C. F. & SUDHOF, T. C. 1994. Synaptotagmin I: a major Ca2+ sensor for transmitter release at a central synapse. *Cell,* 79**,** 717-27.

GOETZ, S. C., LIEM, K. F., JR. & ANDERSON, K. V. 2012. The spinocerebellar ataxia-associated gene Tau tubulin kinase 2 controls the initiation of ciliogenesis. *Cell,* 151**,** 847-58.

GOODMAN, R. H. & SMOLIK, S. 2000. CBP/p300 in cell growth, transformation, and development. *Genes Dev,* 14**,** 1553-77.

GORDON, J. A. 1991. Use of vanadate as protein-phosphotyrosine phosphatase inhibitor. *Methods Enzymol,* 201**,** 477-82.

GOWER, A. J., NOYER, M., VERLOES, R., GOBERT, J. & WULFERT, E. 1992. ucb L059, a novel anti-convulsant drug: pharmacological profile in animals. *Eur J Pharmacol,* 222**,** 193-203.

GREENGARD, P., ALLEN, P. B. & NAIRN, A. C. 1999. Beyond the dopamine receptor: the DARPP-32/protein phosphatase-1 cascade. *Neuron,* 23**,** 435-47.

GREENGARD, P., VALTORTA, F., CZERNIK, A. J. & BENFENATI, F. 1993. Synaptic vesicle phosphoproteins and regulation of synaptic function. *Science,* 259**,** 780-5.

GREWAL, S., MOLINA, D. M. & BARDWELL, L. 2006. Mitogen-activated protein kinase (MAPK)-docking sites in MAPK kinases function as tethers that are crucial for MAPK regulation in vivo. *Cell Signal,* 18**,** 123-34.

GRONBORG, M., PAVLOS, N. J., BRUNK, I., CHUA, J. J., MUNSTER-WANDOWSKI, A., RIEDEL, D., AHNERT-HILGER, G., URLAUB, H. & JAHN, R. 2010. Quantitative comparison of glutamatergic and GABAergic synaptic vesicles unveils selectivity for few proteins including MAL2, a novel synaptic vesicle protein. *J Neurosci,* 30**,** 2-12.

HAMMARLUND, M., JORGENSEN, E. M. & BASTIANI, M. J. 2007. Axons break in animals lacking beta-spectrin. *J Cell Biol,* 176**,** 269-75.

HANKS, S. K. & HUNTER, T. 1995. Protein kinases 6. The eukaryotic protein kinase superfamily: kinase (catalytic) domain structure and classification. *FASEB J,* 9**,** 576-96.

HARLOW, E. A. L., D. 1988. *Antibodies: a laboratory manual,* New York, Cold Spring Harbor Laboratory.

HAUCKE, V. & DE CAMILLI, P. 1999. AP-2 recruitment to synaptotagmin stimulated by tyrosine-based endocytic motifs. *Science,* 285**,** 1268-71.

HAUCKE, V., WENK, M. R., CHAPMAN, E. R., FARSAD, K. & DE CAMILLI, P. 2000. Dual interaction of synaptotagmin with mu2- and alpha-adaptin facilitates clathrin-coated pit nucleation. *EMBO J,* 19**,** 6011-9.

HELMLINGER, D., HARDY, S., SASORITH, S., KLEIN, F., ROBERT, F., WEBER, C., MIGUET, L., POTIER, N., VAN-DORSSELAER, A., WURTZ, J. M., MANDEL, J. L., TORA, L. & DEVYS, D. 2004. Ataxin-7 is a subunit of GCN5 histone acetyltransferase-containing complexes. *Hum Mol Genet,* 13**,** 1257-65.

HELMLINGER, D., TORA, L. & DEVYS, D. 2006. Transcriptional alterations and chromatin remodeling in polyglutamine diseases. *Trends Genet,* 22**,** 562-70.

HENDERSON, P. J. & MAIDEN, M. C. 1990. Homologous sugar transport proteins in Escherichia coli and their relatives in both prokaryotes and eukaryotes. *Philos Trans R Soc Lond B Biol Sci,* 326**,** 391-410.

HEO, Y. S., KIM, S. K., SEO, C. I., KIM, Y. K., SUNG, B. J., LEE, H. S., LEE, J. I., PARK, S. Y., KIM, J. H., HWANG, K. Y., HYUN, Y. L., JEON, Y. H., RO, S., CHO, J. M., LEE, T. G. & YANG, C. H. 2004. Structural basis for the selective inhibition of JNK1 by the scaffolding protein JIP1 and SP600125. *EMBO J,* 23**,** 2185-95.

HERCULANO-HOUZEL, S. 2009. The human brain in numbers: a linearly scaled-up primate brain. *Front Hum Neurosci,* 3**,** 31.

HEUSER, J. E. & REESE, T. S. 1973. Evidence for recycling of synaptic vesicle membrane during transmitter release at the frog neuromuscular junction. *J Cell Biol,* 57**,** 315-44.

HOLLAND, P. M. & COOPER, J. A. 1999. Protein modification: docking sites for kinases. *Curr Biol,* 9**,** R329-31.

HOLLERAN, E. A., LIGON, L. A., TOKITO, M., STANKEWICH, M. C., MORROW, J. S. & HOLZBAUR, E. L. 2001. beta III spectrin binds to the Arp1 subunit of dynactin. *J Biol Chem,* 276**,** 36598-605.

HOLMES, S. E., O'HEARN, E. E., MCINNIS, M. G., GORELICK-FELDMAN, D. A., KLEIDERLEIN, J. J., CALLAHAN, C., KWAK, N. G., INGERSOLL-ASHWORTH, R. G., SHERR, M., SUMNER, A. J., SHARP, A. H., ANANTH, U., SELTZER, W. K., BOSS, M. A., VIERIA-SAECKER, A. M., EPPLEN, J. T., RIESS, O., ROSS, C. A. & MARGOLIS, R. L. 1999. Expansion of a novel CAG trinucleotide repeat in the 5' region of PPP2R2B is associated with SCA12. *Nat Genet,* 23**,** 391-2.

HOULDEN, H. 1993. Spinocerebellar Ataxia Type 11. *In:* PAGON, R. A., BIRD, T. D., DOLAN, C. R., STEPHENS, K. & ADAM, M. P. (eds.) *GeneReviews.* Seattle (WA).

HOULDEN, H., JOHNSON, J., GARDNER-THORPE, C., LASHLEY, T., HERNANDEZ, D., WORTH, P., SINGLETON, A. B., HILTON, D. A., HOLTON, J., REVESZ, T., DAVIS, M. B., GIUNTI, P. & WOOD, N. W. 2007. Mutations in TTBK2, encoding a kinase implicated in tau phosphorylation, segregate with spinocerebellar ataxia type 11. *Nat Genet,* 39**,** 1434-6.

HUNTER, T. 1987. A thousand and one protein kinases. *Cell,* 50**,** 823-9.

HUNTER, T. 1995. Protein kinases and phosphatases: the yin and yang of protein phosphorylation and signaling. *Cell,* 80**,** 225-36.

HUTTI, J. E., JARRELL, E. T., CHANG, J. D., ABBOTT, D. W., STORZ, P., TOKER, A., CANTLEY, L. C. & TURK, B. E. 2004. A rapid method for determining protein kinase phosphorylation specificity. *Nat Methods,* 1**,** 27-9.

ICHISE, T., KANO, M., HASHIMOTO, K., YANAGIHARA, D., NAKAO, K., SHIGEMOTO, R., KATSUKI, M. & AIBA, A. 2000. mGluR1 in cerebellar Purkinje cells essential for long-term depression, synapse elimination, and motor coordination. *Science,* 288**,** 1832-5.

IKEDA, Y., DAUGHTERS, R. S. & RANUM, L. P. 2008. Bidirectional expression of the SCA8 expansion mutation: one mutation, two genes. *Cerebellum,* 7**,** 150-8.

IKEDA, Y., DICK, K. A., WEATHERSPOON, M. R., GINCEL, D., ARMBRUST, K. R., DALTON, J. C., STEVANIN, G., DURR, A., ZUHLKE, C., BURK, K., CLARK, H. B., BRICE, A., ROTHSTEIN, J. D., SCHUT, L. J., DAY, J. W. & RANUM, L. P. 2006. Spectrin mutations cause spinocerebellar ataxia type 5. *Nat Genet,* 38**,** 184-90.

INOUE, H., NOJIMA, H. & OKAYAMA, H. 1990. High efficiency transformation of Escherichia coli with plasmids. *Gene,* 96**,** 23-8.

ISHIGAKI, Y., LI, X., SERIN, G. & MAQUAT, L. E. 2001. Evidence for a pioneer round of mRNA translation: mRNAs subject to nonsense-mediated decay in mammalian cells are bound by CBP80 and CBP20. *Cell,* 106**,** 607-17.

ISKEN, O. & MAQUAT, L. E. 2007. Quality control of eukaryotic mRNA: safeguarding cells from abnormal mRNA function. *Genes Dev,* 21**,** 1833-56.

IZQUIERDO, I., MEDINA, J. H., BIANCHIN, M., WALZ, R., ZANATTA, M. S., DA SILVA, R. C., BUENO E SILVA, M., RUSCHEL, A. C. & PACZKO, N. 1993. Memory processing by the limbic system: role of specific neurotransmitter systems. *Behav Brain Res,* 58**,** 91-8.

JACKSON, M., SONG, W., LIU, M. Y., JIN, L., DYKES-HOBERG, M., LIN, C. I., BOWERS, W. J., FEDEROFF, H. J., STERNWEIS, P. C. & ROTHSTEIN, J. D. 2001. Modulation of the neuronal glutamate transporter EAAT4 by two interacting proteins. *Nature,* 410**,** 89-93.

JACOBS, D., GLOSSIP, D., XING, H., MUSLIN, A. J. & KORNFELD, K. 1999. Multiple docking sites on substrate proteins form a modular system that mediates recognition by ERK MAP kinase. *Genes Dev,* 13**,** 163-75.
JAHN, R. & SUDHOF, T. C. 1993. Synaptic vesicle traffic: rush hour in the nerve terminal. *J Neurochem,* 61**,** 12-21.
JANZ, R., GODA, Y., GEPPERT, M., MISSLER, M. & SUDHOF, T. C. 1999. SV2A and SV2B function as redundant Ca2+ regulators in neurotransmitter release. *Neuron,* 24**,** 1003-16.
JANZ, R., HOFMANN, K. & SUDHOF, T. C. 1998. SVOP, an evolutionarily conserved synaptic vesicle protein, suggests novel transport functions of synaptic vesicles. *J Neurosci,* 18**,** 9269-81.
JANZ, R. & SUDHOF, T. C. 1999. SV2C is a synaptic vesicle protein with an unusually restricted localization: anatomy of a synaptic vesicle protein family. *Neuroscience,* 94**,** 1279-90.
JAROUSSE, N. & KELLY, R. B. 2001. Endocytotic mechanisms in synapses. *Curr Opin Cell Biol,* 13**,** 461-9.
JOHNSON, G. 2005. *The synapse revealed* [Online]. San francisco. Available: http://www.grahamj.com/ [Accessed 01.11.13 2013].
JOHNSON, L. N. & BARFORD, D. 1990. Glycogen phosphorylase. The structural basis of the allosteric response and comparison with other allosteric proteins. *J Biol Chem,* 265**,** 2409-12.
JOHNSON, L. N. & O'REILLY, M. 1996. Control by phosphorylation. *Curr Opin Struct Biol,* 6**,** 762-9.
JOHNSTON, P. A., CAMERON, P. L., STUKENBROK, H., JAHN, R., DE CAMILLI, P. & SUDHOF, T. C. 1989. Synaptophysin is targeted to similar microvesicles in CHO and PC12 cells. *EMBO J,* 8**,** 2863-72.
JOUNG, M. J., MOHAN, S. K. & YU, C. 2012. Molecular level interaction of inositol hexaphosphate with the C2B domain of human synaptotagmin I. *Biochemistry,* 51**,** 3675-83.
KAMINSKI, R. M., GILLARD, M., LECLERCQ, K., HANON, E., LORENT, G., DASSESSE, D., MATAGNE, A. & KLITGAARD, H. 2009. Proepileptic phenotype of SV2A-deficient mice is associated with reduced anticonvulsant efficacy of levetiracetam. *Epilepsia,* 50**,** 1729-40.
KATZ, B. 1969. *The release of neural transmitter substances,* Liverpool, Liverpool University Press.
KEBABIAN, J. W. & GREENGARD, P. 1971. Dopamine-sensitive adenyl cyclase: possible role in synaptic transmission. *Science,* 174**,** 1346-9.
KEMP, B. E., BYLUND, D. B., HUANG, T. S. & KREBS, E. G. 1975. Substrate specificity of the cyclic AMP-dependent protein kinase. *Proc Natl Acad Sci U S A,* 72**,** 3448-52.
KINRYS, G., WORTHINGTON, J. J., WYGANT, L., NERY, F., REESE, H. & POLLACK, M. H. 2007. Levetiracetam as adjunctive therapy for refractory anxiety disorders. *J Clin Psychiatry,* 68**,** 1010-3.
KINRYS, G., WYGANT, L. E., PARDO, T. B. & MELO, M. 2006. Levetiracetam for treatment-refractory posttraumatic stress disorder. *J Clin Psychiatry,* 67**,** 211-4.
KIRCHHAUSEN, T. 1999. Adaptors for clathrin-mediated traffic. *Annu Rev Cell Dev Biol,* 15**,** 705-32.
KITTLER, J. T., CHEN, G., KUKHTINA, V., VAHEDI-FARIDI, A., GU, Z., TRETTER, V., SMITH, K. R., MCAINSH, K., ARANCIBIA-CARCAMO, I. L., SAENGER, W.,

HAUCKE, V., YAN, Z. & MOSS, S. J. 2008. Regulation of synaptic inhibition by phospho-dependent binding of the AP2 complex to a YECL motif in the GABAA receptor gamma2 subunit. *Proc Natl Acad Sci U S A,* 105**,** 3616-21.

KNIGHT, M. A., HERNANDEZ, D., DIEDE, S. J., DAUWERSE, H. G., RAFFERTY, I., VAN DE LEEMPUT, J., FORREST, S. M., GARDNER, R. J., STOREY, E., VAN OMMEN, G. J., TAPSCOTT, S. J., FISCHBECK, K. H. & SINGLETON, A. B. 2008. A duplication at chromosome 11q12.2-11q12.3 is associated with spinocerebellar ataxia type 20. *Hum Mol Genet,* 17**,** 3847-53.

KONONENKO, N. L., DIRIL, M. K., PUCHKOV, D., KINTSCHER, M., KOO, S. J., PFUHL, G., WINTER, Y., WIENISCH, M., KLINGAUF, J., BREUSTEDT, J., SCHMITZ, D., MARITZEN, T. & HAUCKE, V. 2013. Compromised fidelity of endocytic synaptic vesicle protein sorting in the absence of stonin 2. *Proc Natl Acad Sci U S A,* 110**,** E526-35.

KREBS, E. G. 1985. The phosphorylation of proteins: a major mechanism for biological regulation. Fourteenth Sir Frederick Gowland Hopkins memorial lecture. *Biochem Soc Trans,* 13**,** 813-20.

KREBS, E. G. & FISCHER, E. H. 1955. Phosphorylase activity of skeletal muscle extracts. *J Biol Chem,* 216**,** 113-20.

KUO, J. F. & GREENGARD, P. 1970. Cyclic nucleotide-dependent protein kinases. VI. Isolation and partial purification of a protein kinase activated by guanosine 3',5'-monophosphate. *J Biol Chem,* 245**,** 2493-8.

KURET, J., WOODGETT, J. R. & COHEN, P. 1985. Multisite phosphorylation of glycogen synthase from rabbit skeletal muscle. Identification of the sites phosphorylated by casein kinase-I. *Eur J Biochem,* 151**,** 39-48.

KUTAY, U., AHNERT-HILGER, G., HARTMANN, E., WIEDENMANN, B. & RAPOPORT, T. A. 1995. Transport route for synaptobrevin via a novel pathway of insertion into the endoplasmic reticulum membrane. *EMBO J,* 14**,** 217-23.

LAKEY, J. H. & RAGGETT, E. M. 1998. Measuring protein-protein interactions. *Curr Opin Struct Biol,* 8**,** 119-23.

LEE, T., HOOFNAGLE, A. N., KABUYAMA, Y., STROUD, J., MIN, X., GOLDSMITH, E. J., CHEN, L., RESING, K. A. & AHN, N. G. 2004. Docking motif interactions in MAP kinases revealed by hydrogen exchange mass spectrometry. *Mol Cell,* 14**,** 43-55.

LELUK, J., HANUS-LORENZ, B. & SIKORSKI, A. F. 2001. Application of genetic semihomology algorithm to theoretical studies on various protein families. *Acta Biochim Pol,* 48**,** 21-33.

LI, C., ULLRICH, B., ZHANG, J. Z., ANDERSON, R. G., BROSE, N. & SUDHOF, T. C. 1995. Ca(2+)-dependent and -independent activities of neural and non-neural synaptotagmins. *Nature,* 375**,** 594-9.

LI, F., MACFARLAN, T., PITTMAN, R. N. & CHAKRAVARTI, D. 2002. Ataxin-3 is a histone-binding protein with two independent transcriptional corepressor activities. *J Biol Chem,* 277**,** 45004-12.

LIM, J., HAO, T., SHAW, C., PATEL, A. J., SZABO, G., RUAL, J. F., FISK, C. J., LI, N., SMOLYAR, A., HILL, D. E., BARABASI, A. L., VIDAL, M. & ZOGHBI, H. Y. 2006. A protein-protein interaction network for human inherited ataxias and disorders of Purkinje cell degeneration. *Cell,* 125**,** 801-14.

LIPINSKI, M. M. & YUAN, J. 2004. Mechanisms of cell death in polyglutamine expansion diseases. *Curr Opin Pharmacol,* 4**,** 85-90.

LIU, J., TANG, T. S., TU, H., NELSON, O., HERNDON, E., HUYNH, D. P., PULST, S. M. & BEZPROZVANNY, I. 2009. Deranged calcium signaling and neurodegeneration in spinocerebellar ataxia type 2. *J Neurosci,* 29**,** 9148-62.

LIU, Y., KRANTZ, D. E., WAITES, C. & EDWARDS, R. H. 1999. Membrane trafficking of neurotransmitter transporters in the regulation of synaptic transmission. *Trends Cell Biol,* 9**,** 356-63.

LLINAS, R., GRUNER, J. A., SUGIMORI, M., MCGUINNESS, T. L. & GREENGARD, P. 1991. Regulation by synapsin I and Ca(2+)-calmodulin-dependent protein kinase II of the transmitter release in squid giant synapse. *J Physiol,* 436**,** 257-82.

LLINAS, R., MCGUINNESS, T. L., LEONARD, C. S., SUGIMORI, M. & GREENGARD, P. 1985. Intraterminal injection of synapsin I or calcium/calmodulin-dependent protein kinase II alters neurotransmitter release at the squid giant synapse. *Proc Natl Acad Sci U S A,* 82**,** 3035-9.

LLINAS, R., SUGIMORI, M., LANG, E. J., MORITA, M., FUKUDA, M., NIINOBE, M. & MIKOSHIBA, K. 1994. The inositol high-polyphosphate series blocks synaptic transmission by preventing vesicular fusion: a squid giant synapse study. *Proc Natl Acad Sci U S A,* 91**,** 12990-3.

LONGENECKER, K. L., ROACH, P. J. & HURLEY, T. D. 1996. Three-dimensional structure of mammalian casein kinase I: molecular basis for phosphate recognition. *J Mol Biol,* 257**,** 618-31.

LOWE, A. W., MADEDDU, L. & KELLY, R. B. 1988. Endocrine secretory granules and neuronal synaptic vesicles have three integral membrane proteins in common. *J Cell Biol,* 106**,** 51-9.

LYNCH, B. A., LAMBENG, N., NOCKA, K., KENSEL-HAMMES, P., BAJJALIEH, S. M., MATAGNE, A. & FUKS, B. 2004. The synaptic vesicle protein SV2A is the binding site for the antiepileptic drug levetiracetam. *Proc Natl Acad Sci U S A,* 101**,** 9861-6.

MACHNICKA, B., CZOGALLA, A., HRYNIEWICZ-JANKOWSKA, A., BOGUSLAWSKA, D. M., GROCHOWALSKA, R., HEGER, E. & SIKORSKI, A. F. 2013. Spectrins: A structural platform for stabilization and activation of membrane channels, receptors and transporters. *Biochim Biophys Acta*.

MAIDEN, M. C., DAVIS, E. O., BALDWIN, S. A., MOORE, D. C. & HENDERSON, P. J. 1987. Mammalian and bacterial sugar transport proteins are homologous. *Nature,* 325**,** 641-3.

MALTECCA, F., MAGNONI, R., CERRI, F., COX, G. A., QUATTRINI, A. & CASARI, G. 2009. Haploinsufficiency of AFG3L2, the gene responsible for spinocerebellar ataxia type 28, causes mitochondria-mediated Purkinje cell dark degeneration. *J Neurosci,* 29**,** 9244-54.

MANNING, G., WHYTE, D. B., MARTINEZ, R., HUNTER, T. & SUDARSANAM, S. 2002. The protein kinase complement of the human genome. *Science,* 298**,** 1912-34.

MARIN, O., MEGGIO, F. & PINNA, L. A. 1994. Design and synthesis of two new peptide substrates for the specific and sensitive monitoring of casein kinases-1 and -2. *Biochem Biophys Res Commun,* 198**,** 898-905.

MATILLA, A., KOSHY, B. T., CUMMINGS, C. J., ISOBE, T., ORR, H. T. & ZOGHBI, H. Y. 1997. The cerebellar leucine-rich acidic nuclear protein interacts with ataxin-1. *Nature,* 389**,** 974-8.

MATILLA-DUENAS, A. 2008. The highly heterogeneous spinocerebellar ataxias: from genes to targets for therapeutic intervention. *Cerebellum,* 7**,** 97-100.
MATILLA-DUENAS, A., GOOLD, R. & GIUNTI, P. 2008. Clinical, genetic, molecular, and pathophysiological insights into spinocerebellar ataxia type 1. *Cerebellum,* 7**,** 106-14.
MATILLA-DUENAS, A., SANCHEZ, I., CORRAL-JUAN, M., DAVALOS, A., ALVAREZ, R. & LATORRE, P. 2010. Cellular and molecular pathways triggering neurodegeneration in the spinocerebellar ataxias. *Cerebellum,* 9**,** 148-66.
MATVEEVA, E. A., VANAMAN, T. C., WHITEHEART, S. W. & SLEVIN, J. T. 2007. Asymmetric accumulation of hippocampal 7S SNARE complexes occurs regardless of kindling paradigm. *Epilepsy Res,* 73**,** 266-74.
MATVEEVA, E. A., VANAMAN, T. C., WHITEHEART, S. W. & SLEVIN, J. T. 2008. Levetiracetam prevents kindling-induced asymmetric accumulation of hippocampal 7S SNARE complexes. *Epilepsia,* 49**,** 1749-58.
MATVEEVA, E. A., WHITEHEART, S. W. & SLEVIN, J. T. 2003. Accumulation of 7S SNARE complexes in hippocampal synaptosomes from chronically kindled rats. *J Neurochem,* 84**,** 621-4.
MAYCOX, P. R., LINK, E., REETZ, A., MORRIS, S. A. & JAHN, R. 1992. Clathrin-coated vesicles in nervous tissue are involved primarily in synaptic vesicle recycling. *J Cell Biol,* 118**,** 1379-88.
MCCAMPBELL, A., TAYLOR, J. P., TAYE, A. A., ROBITSCHEK, J., LI, M., WALCOTT, J., MERRY, D., CHAI, Y., PAULSON, H., SOBUE, G. & FISCHBECK, K. H. 2000. CREB-binding protein sequestration by expanded polyglutamine. *Hum Mol Genet,* 9**,** 2197-202.
MCGAVIN, C. L., JOHN, V. & MUSSER, W. S. 2003. Levetiracetam as a treatment for tardive dyskinesia: a case report. *Neurology,* 61**,** 419.
MEEHAN, A. L., YANG, X., MCADAMS, B. D., YUAN, L. & ROTHMAN, S. M. 2011. A new mechanism for antiepileptic drug action: vesicular entry may mediate the effects of levetiracetam. *J Neurophysiol,* 106**,** 1227-39.
MIESENBOCK, G., DE ANGELIS, D. A. & ROTHMAN, J. E. 1998. Visualizing secretion and synaptic transmission with pH-sensitive green fluorescent proteins. *Nature,* 394**,** 192-5.
MILLER, W. T. 2003. Determinants of substrate recognition in nonreceptor tyrosine kinases. *Acc Chem Res,* 36**,** 393-400.
MIRNICS, K., MIDDLETON, F. A., MARQUEZ, A., LEWIS, D. A. & LEVITT, P. 2000. Molecular characterization of schizophrenia viewed by microarray analysis of gene expression in prefrontal cortex. *Neuron,* 28**,** 53-67.
MIYAMOTO, E., KUO, J. F. & GREENGARD, P. 1969. Adenosine 3',5'-monophosphate-dependent protein kinase from brain. *Science,* 165**,** 63-5.
MIZUTANI, A., FUKUDA, M., NIINOBE, M. & MIKOSHIBA, K. 1997. Regulation of AP-2-synaptotagmin interaction by inositol high polyphosphates. *Biochem Biophys Res Commun,* 240**,** 128-31.
MOCHIDA, S., FUKUDA, M., NIINOBE, M., KOBAYASHI, H. & MIKOSHIBA, K. 1997. Roles of synaptotagmin C2 domains in neurotransmitter secretion and inositol high-polyphosphate binding at mammalian cholinergic synapses. *Neuroscience,* 77**,** 937-43.
MOK, J., KIM, P. M., LAM, H. Y., PICCIRILLO, S., ZHOU, X., JESCHKE, G. R., SHERIDAN, D. L., PARKER, S. A., DESAI, V., JWA, M., CAMERONI, E., NIU, H., GOOD, M., REMENYI, A., MA, J. L., SHEU, Y. J., SASSI, H. E., SOPKO, R., CHAN, C. S., DE VIRGILIO, C., HOLLINGSWORTH, N. M., LIM, W. A., STERN, D. F.,

STILLMAN, B., ANDREWS, B. J., GERSTEIN, M. B., SNYDER, M. & TURK, B. E. 2010. Deciphering protein kinase specificity through large-scale analysis of yeast phosphorylation site motifs. *Sci Signal,* 3**,** ra12.

MUTCH, S. A., KENSEL-HAMMES, P., GADD, J. C., FUJIMOTO, B. S., ALLEN, R. W., SCHIRO, P. G., LORENZ, R. M., KUYPER, C. L., KUO, J. S., BAJJALIEH, S. M. & CHIU, D. T. 2011. Protein quantification at the single vesicle level reveals that a subset of synaptic vesicle proteins are trafficked with high precision. *J Neurosci,* 31**,** 1461-70.

NAGY, E. & MAQUAT, L. E. 1998. A rule for termination-codon position within intron-containing genes: when nonsense affects RNA abundance. *Trends Biochem Sci,* 23**,** 198-9.

NAKIELNY, S., CAMPBELL, D. G. & COHEN, P. 1991. The molecular mechanism by which adrenalin inhibits glycogen synthesis. *Eur J Biochem,* 199**,** 713-22.

NALEFSKI, E. A. & FALKE, J. J. 1996. The C2 domain calcium-binding motif: structural and functional diversity. *Protein Sci,* 5**,** 2375-90.

NELSON, N. 1992. Structure and function of V-ATPases in endocytic and secretory organelles. *J Exp Biol,* 172**,** 149-53.

NICHOLSON-TOMISHIMA, K. & RYAN, T. A. 2004. Kinetic efficiency of endocytosis at mammalian CNS synapses requires synaptotagmin I. *Proc Natl Acad Sci U S A,* 101**,** 16648-52.

NOBLE, W., PLANEL, E., ZEHR, C., OLM, V., MEYERSON, J., SULEMAN, F., GAYNOR, K., WANG, L., LAFRANCOIS, J., FEINSTEIN, B., BURNS, M., KRISHNAMURTHY, P., WEN, Y., BHAT, R., LEWIS, J., DICKSON, D. & DUFF, K. 2005. Inhibition of glycogen synthase kinase-3 by lithium correlates with reduced tauopathy and degeneration in vivo. *Proc Natl Acad Sci U S A,* 102**,** 6990-5.

NONET, M. L., GRUNDAHL, K., MEYER, B. J. & RAND, J. B. 1993. Synaptic function is impaired but not eliminated in C. elegans mutants lacking synaptotagmin. *Cell,* 73**,** 1291-305.

NOWACK, A., MALARKEY, E. B., YAO, J., BLECKERT, A., HILL, J. & BAJJALIEH, S. M. 2011. Levetiracetam reverses synaptic deficits produced by overexpression of SV2A. *PLoS One,* 6**,** e29560.

NOYER, M., GILLARD, M., MATAGNE, A., HENICHART, J. P. & WULFERT, E. 1995. The novel antiepileptic drug levetiracetam (ucb L059) appears to act via a specific binding site in CNS membranes. *Eur J Pharmacol,* 286**,** 137-46.

O'REGAN, S., BIRMAN, S. & MEUNIER, F. M. 1995. Regulation of hemicholinium-3 sensitive choline uptake in Xenopus laevis oocytes by the second C2 domain of synaptotagmin. *Brain Res Mol Brain Res,* 32**,** 135-42.

OHNO, Y., ISHIHARA, S., TERADA, R., KIKUTA, M., SOFUE, N., KAWAI, Y., SERIKAWA, T. & SASA, M. 2009. Preferential increase in the hippocampal synaptic vesicle protein 2A (SV2A) by pentylenetetrazole kindling. *Biochem Biophys Res Commun,* 390**,** 415-20.

ORR, H. T. 2012. Cell biology of spinocerebellar ataxia. *J Cell Biol,* 197**,** 167-77.

OWEN, D. J. & EVANS, P. R. 1998. A structural explanation for the recognition of tyrosine-based endocytotic signals. *Science,* 282**,** 1327-32.

OWICKI, J. C. 2000. Fluorescence polarization and anisotropy in high throughput screening: perspectives and primer. *J Biomol Screen,* 5**,** 297-306.

PAO, S. S., PAULSEN, I. T. & SAIER, M. H., JR. 1998. Major facilitator superfamily. *Microbiol Mol Biol Rev,* 62**,** 1-34.

PASSOT, J. B., SHEYNIKHOVICH, D., DUVELLE, E. & ARLEO, A. 2012. Contribution of cerebellar sensorimotor adaptation to hippocampal spatial memory. *PLoS One,* 7**,** e32560.

PATON, W. D. 1958. Central and synaptic transmission in the nervous system; pharmacological aspects. *Annu Rev Physiol,* 20**,** 431-70.

PAWSON, T. 1995. Protein modules and signalling networks. *Nature,* 373**,** 573-80.

PAWSON, T. & GISH, G. D. 1992. SH2 and SH3 domains: from structure to function. *Cell,* 71**,** 359-62.

PAWSON, T. & NASH, P. 2000. Protein-protein interactions define specificity in signal transduction. *Genes Dev,* 14**,** 1027-47.

PAWSON, T. & SCOTT, J. D. 1997. Signaling through scaffold, anchoring, and adaptor proteins. *Science,* 278**,** 2075-80.

PEARSE, B. M., SMITH, C. J. & OWEN, D. J. 2000. Clathrin coat construction in endocytosis. *Curr Opin Struct Biol,* 10**,** 220-8.

PERIN, M. S., FRIED, V. A., MIGNERY, G. A., JAHN, R. & SUDHOF, T. C. 1990. Phospholipid binding by a synaptic vesicle protein homologous to the regulatory region of protein kinase C. *Nature,* 345**,** 260-3.

PERKINS, E. M., CLARKSON, Y. L., SABATIER, N., LONGHURST, D. M., MILLWARD, C. P., JACK, J., TORAIWA, J., WATANABE, M., ROTHSTEIN, J. D., LYNDON, A. R., WYLLIE, D. J., DUTIA, M. B. & JACKSON, M. 2010. Loss of beta-III spectrin leads to Purkinje cell dysfunction recapitulating the behavior and neuropathology of spinocerebellar ataxia type 5 in humans. *J Neurosci,* 30**,** 4857-67.

PHILLIPS, G. R., HUANG, J. K., WANG, Y., TANAKA, H., SHAPIRO, L., ZHANG, W., SHAN, W. S., ARNDT, K., FRANK, M., GORDON, R. E., GAWINOWICZ, M. A., ZHAO, Y. & COLMAN, D. R. 2001. The presynaptic particle web: ultrastructure, composition, dissolution, and reconstitution. *Neuron,* 32**,** 63-77.

PIELAGE, J., FETTER, R. D. & DAVIS, G. W. 2005. Presynaptic spectrin is essential for synapse stabilization. *Curr Biol,* 15**,** 918-28.

PIELAGE, J., FETTER, R. D. & DAVIS, G. W. 2006. A postsynaptic spectrin scaffold defines active zone size, spacing, and efficacy at the Drosophila neuromuscular junction. *J Cell Biol,* 175**,** 491-503.

PIETROBON, D. 2013. Calcium channels and migraine. *Biochim Biophys Acta,* 1828**,** 1655-65.

POSKANZER, K. E., MAREK, K. W., SWEENEY, S. T. & DAVIS, G. W. 2003. Synaptotagmin I is necessary for compensatory synaptic vesicle endocytosis in vivo. *Nature,* 426**,** 559-63.

PRICE, M. J. 2004. Levetiracetam in the treatment of neuropathic pain: three case studies. *Clin J Pain,* 20**,** 33-6.

PURVES, D. A., G.; FITZPATRICK, D.; KATZ, L.; LAMANTIA, A.S.; MCNAMARA, J.; WILLIAMS, SM. 2001. *Neuroscience*, Sinauer Associates.

PYLE, R. A., SCHIVELL, A. E., HIDAKA, H. & BAJJALIEH, S. M. 2000. Phosphorylation of synaptic vesicle protein 2 modulates binding to synaptotagmin. *J Biol Chem,* 275**,** 17195-200.

REIGADA, D., DIEZ-PEREZ, I., GOROSTIZA, P., VERDAGUER, A., GOMEZ DE ARANDA, I., PINEDA, O., VILARRASA, J., MARSAL, J., BLASI, J., ALEU, J. & SOLSONA, C. 2003. Control of neurotransmitter release by an internal gel matrix in synaptic vesicles. *Proc Natl Acad Sci U S A,* 100**,** 3485-90.

REMENYI, A., GOOD, M. C., BHATTACHARYYA, R. P. & LIM, W. A. 2005. The role of docking interactions in mediating signaling input, output, and discrimination in the yeast MAPK network. *Mol Cell,* 20**,** 951-62.

ROSS, C. A. & POIRIER, M. A. 2004. Protein aggregation and neurodegenerative disease. *Nat Med,* 10 Suppl**,** S10-7.

RYAN, T. A. & SMITH, S. J. 1995. Vesicle pool mobilization during action potential firing at hippocampal synapses. *Neuron,* 14**,** 983-9.

SABATINI, B. L. & REGEHR, W. G. 1999. Timing of synaptic transmission. *Annu Rev Physiol,* 61**,** 521-42.

SAKAGUCHI, G., ORITA, S., NAITO, A., MAEDA, M., IGARASHI, H., SASAKI, T. & TAKAI, Y. 1998. A novel brain-specific isoform of beta spectrin: isolation and its interaction with Munc13. *Biochem Biophys Res Commun,* 248**,** 846-51.

SAKMANN, B. 1992. Nobel Lecture. Elementary steps in synaptic transmission revealed by currents through single ion channels. *Neuron,* 8**,** 613-29.

SANCHEZ, I., HUGHES, R. T., MAYER, B. J., YEE, K., WOODGETT, J. R., AVRUCH, J., KYRIAKIS, J. M. & ZON, L. I. 1994. Role of SAPK/ERK kinase-1 in the stress-activated pathway regulating transcription factor c-Jun. *Nature,* 372**,** 794-8.

SANCHEZ, I., XU, C. J., JUO, P., KAKIZAKA, A., BLENIS, J. & YUAN, J. 1999. Caspase-8 is required for cell death induced by expanded polyglutamine repeats. *Neuron,* 22**,** 623-33.

SANKARANARAYANAN, S. & RYAN, T. A. 2001. Calcium accelerates endocytosis of vSNAREs at hippocampal synapses. *Nat Neurosci,* 4**,** 129-36.

SASTRY, B. R., MORISHITA, W., YIP, S. & SHEW, T. 1997. GABA-ergic transmission in deep cerebellar nuclei. *Prog Neurobiol,* 53**,** 259-71.

SATO, S., CERNY, R. L., BUESCHER, J. L. & IKEZU, T. 2006. Tau-tubulin kinase 1 (TTBK1), a neuron-specific tau kinase candidate, is involved in tau phosphorylation and aggregation. *J Neurochem,* 98**,** 1573-84.

SATO, S., XU, J., OKUYAMA, S., MARTINEZ, L. B., WALSH, S. M., JACOBSEN, M. T., SWAN, R. J., SCHLAUTMAN, J. D., CIBOROWSKI, P. & IKEZU, T. 2008. Spatial learning impairment, enhanced CDK5/p35 activity, and downregulation of NMDA receptor expression in transgenic mice expressing tau-tubulin kinase 1. *J Neurosci,* 28**,** 14511-21.

SCHIAVO, G., GMACHL, M. J., STENBECK, G., SOLLNER, T. H. & ROTHMAN, J. E. 1995. A possible docking and fusion particle for synaptic transmission. *Nature,* 378**,** 733-6.

SCHIAVO, G., GU, Q. M., PRESTWICH, G. D., SOLLNER, T. H. & ROTHMAN, J. E. 1996. Calcium-dependent switching of the specificity of phosphoinositide binding to synaptotagmin. *Proc Natl Acad Sci U S A,* 93**,** 13327-32.

SCHIAVO, G., OSBORNE, S. L. & SGOUROS, J. G. 1998. Synaptotagmins: more isoforms than functions? *Biochem Biophys Res Commun,* 248**,** 1-8.

SCHIAVO, G., ROSSETTO, O., BENFENATI, F., POULAIN, B. & MONTECUCCO, C. 1994. Tetanus and botulinum neurotoxins are zinc proteases specific for components of the neuroexocytosis apparatus. *Ann N Y Acad Sci,* 710**,** 65-75.

SCHIAVO, G., STENBECK, G., ROTHMAN, J. E. & SOLLNER, T. H. 1997. Binding of the synaptic vesicle v-SNARE, synaptotagmin, to the plasma membrane t-SNARE, SNAP-25, can explain docked vesicles at neurotoxin-treated synapses. *Proc Natl Acad Sci U S A,* 94**,** 997-1001.

SCHIVELL, A. E., BATCHELOR, R. H. & BAJJALIEH, S. M. 1996. Isoform-specific, calcium-regulated interaction of the synaptic vesicle proteins SV2 and synaptotagmin. *J Biol Chem,* 271**,** 27770-5.

SCHMIDT, T., LINDENBERG, K. S., KREBS, A., SCHOLS, L., LACCONE, F., HERMS, J., RECHSTEINER, M., RIESS, O. & LANDWEHRMEYER, G. B. 2002. Protein surveillance machinery in brains with spinocerebellar ataxia type 3: redistribution and differential recruitment of 26S proteasome subunits and chaperones to neuronal intranuclear inclusions. *Ann Neurol,* 51**,** 302-10.

SCHULMAN, H. & GREENGARD, P. 1978. Stimulation of brain membrane protein phosphorylation by calcium and an endogenous heat-stable protein. *Nature,* 271**,** 478-9.

SERRA, H. G., BYAM, C. E., LANDE, J. D., TOUSEY, S. K., ZOGHBI, H. Y. & ORR, H. T. 2004. Gene profiling links SCA1 pathophysiology to glutamate signaling in Purkinje cells of transgenic mice. *Hum Mol Genet,* 13**,** 2535-43.

SHAO, X., FERNANDEZ, I., SUDHOF, T. C. & RIZO, J. 1998. Solution structures of the Ca2+-free and Ca2+-bound C2A domain of synaptotagmin I: does Ca2+ induce a conformational change? *Biochemistry,* 37**,** 16106-15.

SHAO, X., LI, C., FERNANDEZ, I., ZHANG, X., SUDHOF, T. C. & RIZO, J. 1997. Synaptotagmin-syntaxin interaction: the C2 domain as a Ca2+-dependent electrostatic switch. *Neuron,* 18**,** 133-42.

SHARROCKS, A. D., YANG, S. H. & GALANIS, A. 2000. Docking domains and substrate-specificity determination for MAP kinases. *Trends Biochem Sci,* 25**,** 448-53.

SHIMOHATA, T., NAKAJIMA, T., YAMADA, M., UCHIDA, C., ONODERA, O., NARUSE, S., KIMURA, T., KOIDE, R., NOZAKI, K., SANO, Y., ISHIGURO, H., SAKOE, K., OOSHIMA, T., SATO, A., IKEUCHI, T., OYAKE, M., SATO, T., AOYAGI, Y., HOZUMI, I., NAGATSU, T., TAKIYAMA, Y., NISHIZAWA, M., GOTO, J., KANAZAWA, I., DAVIDSON, I., TANESE, N., TAKAHASHI, H. & TSUJI, S. 2000. Expanded polyglutamine stretches interact with TAFII130, interfering with CREB-dependent transcription. *Nat Genet,* 26**,** 29-36.

SNYDER, S. H. & INNIS, R. B. 1979. Peptide neurotransmitters. *Annu Rev Biochem,* 48**,** 755-82.

SON, Y. J., SCRANTON, T. W., SUNDERLAND, W. J., BAEK, S. J., MINER, J. H., SANES, J. R. & CARLSON, S. S. 2000. The synaptic vesicle protein SV2 is complexed with an alpha5-containing laminin on the nerve terminal surface. *J Biol Chem,* 275**,** 451-60.

STANKEWICH, M. C., TSE, W. T., PETERS, L. L., CH'NG, Y., JOHN, K. M., STABACH, P. R., DEVARAJAN, P., MORROW, J. S. & LUX, S. E. 1998. A widely expressed betaIII spectrin associated with Golgi and cytoplasmic vesicles. *Proc Natl Acad Sci U S A,* 95**,** 14158-63.

STRIANO, P., ELEFANTE, A., COPPOLA, A., TORTORA, F., ZARA, F. & MINETTI, C. 2009. Dramatic response to levetiracetam in post-ischaemic Holmes' tremor. *BMJ Case Rep,* 2009.

SUDHOF, T. C. 1995. The synaptic vesicle cycle: a cascade of protein-protein interactions. *Nature,* 375**,** 645-53.

SUDHOF, T. C. 2004. The synaptic vesicle cycle. *Annu Rev Neurosci,* 27**,** 509-47.

SUDHOF, T. C., DE CAMILLI, P., NIEMANN, H. & JAHN, R. 1993. Membrane fusion machinery: insights from synaptic proteins. *Cell,* 75**,** 1-4.

SUDHOF, T. C. & RIZO, J. 1996. Synaptotagmins: C2-domain proteins that regulate membrane traffic. *Neuron,* 17**,** 379-88.
SUTHERLAND, E. W. 1972. Studies on the mechanism of hormone action. *Science,* 177**,** 401-8.
SUTTON, R. B., DAVLETOV, B. A., BERGHUIS, A. M., SUDHOF, T. C. & SPRANG, S. R. 1995. Structure of the first C2 domain of synaptotagmin I: a novel Ca2+/phospholipid-binding fold. *Cell,* 80**,** 929-38.
SUTTON, R. B., ERNST, J. A. & BRUNGER, A. T. 1999. Crystal structure of the cytosolic C2A-C2B domains of synaptotagmin III. Implications for Ca(+2)-independent snare complex interaction. *J Cell Biol,* 147**,** 589-98.
TAKAHASHI, M., TOMIZAWA, K., SATO, K., OHTAKE, A. & OMORI, A. 1995. A novel tau-tubulin kinase from bovine brain. *FEBS Lett,* 372**,** 59-64.
TAKAMORI, S., HOLT, M., STENIUS, K., LEMKE, E. A., GRONBORG, M., RIEDEL, D., URLAUB, H., SCHENCK, S., BRUGGER, B., RINGLER, P., MULLER, S. A., RAMMNER, B., GRATER, F., HUB, J. S., DE GROOT, B. L., MIESKES, G., MORIYAMA, Y., KLINGAUF, J., GRUBMULLER, H., HEUSER, J., WIELAND, F. & JAHN, R. 2006. Molecular anatomy of a trafficking organelle. *Cell,* 127**,** 831-46.
TANOUE, T., ADACHI, M., MORIGUCHI, T. & NISHIDA, E. 2000. A conserved docking motif in MAP kinases common to substrates, activators and regulators. *Nat Cell Biol,* 2**,** 110-6.
TARONI, F. & DIDONATO, S. 2004. Pathways to motor incoordination: the inherited ataxias. *Nat Rev Neurosci,* 5**,** 641-55.
TOMIZAWA, K., OMORI, A., OHTAKE, A., SATO, K. & TAKAHASHI, M. 2001. Tau-tubulin kinase phosphorylates tau at Ser-208 and Ser-210, sites found in paired helical filament-tau. *FEBS Lett,* 492**,** 221-7.
TRAUB, L. M. 2003. Sorting it out: AP-2 and alternate clathrin adaptors in endocytic cargo selection. *J Cell Biol,* 163**,** 203-8.
TSIEN, R. Y. 1998. The green fluorescent protein. *Annu Rev Biochem,* 67**,** 509-44.
TSUJI, S., ONODERA, O., GOTO, J., NISHIZAWA, M. & STUDY GROUP ON ATAXIC, D. 2008. Sporadic ataxias in Japan--a population-based epidemiological study. *Cerebellum,* 7**,** 189-97.
TURK, B. E., HUTTI, J. E. & CANTLEY, L. C. 2006. Determining protein kinase substrate specificity by parallel solution-phase assay of large numbers of peptide substrates. *Nat Protoc,* 1**,** 375-9.
UBACH, J., ZHANG, X., SHAO, X., SUDHOF, T. C. & RIZO, J. 1998. Ca2+ binding to synaptotagmin: how many Ca2+ ions bind to the tip of a C2-domain? *EMBO J,* 17**,** 3921-30.
ULLRICH, B., LI, C., ZHANG, J. Z., MCMAHON, H., ANDERSON, R. G., GEPPERT, M. & SUDHOF, T. C. 1994. Functional properties of multiple synaptotagmins in brain. *Neuron,* 13**,** 1281-91.
VALENSTEIN, E. S. 2006. *The War of the Soups and the Sparks: The Discovery of Neurotransmitters and the Dispute Over How Nerves Communicate,* New York, Columbia University Press.
VAN DE LEEMPUT, J., CHANDRAN, J., KNIGHT, M. A., HOLTZCLAW, L. A., SCHOLZ, S., COOKSON, M. R., HOULDEN, H., GWINN-HARDY, K., FUNG, H. C., LIN, X., HERNANDEZ, D., SIMON-SANCHEZ, J., WOOD, N. W., GIUNTI, P., RAFFERTY, I., HARDY, J., STOREY, E., GARDNER, R. J., FORREST, S. M., FISHER, E. M., RUSSELL, J. T., CAI, H. & SINGLETON, A. B. 2007. Deletion at

ITPR1 underlies ataxia in mice and spinocerebellar ataxia 15 in humans. *PLoS Genet,* 3**,** e108.

VAN SWIETEN, J. C., BRUSSE, E., DE GRAAF, B. M., KRIEGER, E., VAN DE GRAAF, R., DE KONING, I., MAAT-KIEVIT, A., LEEGWATER, P., DOOIJES, D., OOSTRA, B. A. & HEUTINK, P. 2003. A mutation in the fibroblast growth factor 14 gene is associated with autosomal dominant cerebellar ataxia [corrected]. *Am J Hum Genet,* 72**,** 191-9.

VAZQUEZ-HIGUERA, J. L., MATEO, I., SANCHEZ-JUAN, P., RODRIGUEZ-RODRIGUEZ, E., POZUETA, A., CALERO, M., DOBATO, J. L., FRANK-GARCIA, A., VALDIVIESO, F., BERCIANO, J., BULLIDO, M. J. & COMBARROS, O. 2011. Genetic variation in the tau kinases pathway may modify the risk and age at onset of Alzheimer's disease. *J Alzheimers Dis,* 27**,** 291-7.

VELAZQUEZ-CAMPOY, A., LEAVITT, S. A. & FREIRE, E. 2004. Characterization of protein-protein interactions by isothermal titration calorimetry. *Methods Mol Biol,* 261**,** 35-54.

VERBEEK, D. S., GOEDHART, J., BRUINSMA, L., SINKE, R. J. & REITS, E. A. 2008. PKC gamma mutations in spinocerebellar ataxia type 14 affect C1 domain accessibility and kinase activity leading to aberrant MAPK signaling. *J Cell Sci,* 121**,** 2339-49.

WAKAMIYA, M., MATSUURA, T., LIU, Y., SCHUSTER, G. C., GAO, R., XU, W., SARKAR, P. S., LIN, X. & ASHIZAWA, T. 2006. The role of ataxin 10 in the pathogenesis of spinocerebellar ataxia type 10. *Neurology,* 67**,** 607-13.

WALTHER, T. C. & MANN, M. 2010. Mass spectrometry-based proteomics in cell biology. *J Cell Biol,* 190**,** 491-500.

WATERS, M. F., MINASSIAN, N. A., STEVANIN, G., FIGUEROA, K. P., BANNISTER, J. P., NOLTE, D., MOCK, A. F., EVIDENTE, V. G., FEE, D. B., MULLER, U., DURR, A., BRICE, A., PAPAZIAN, D. M. & PULST, S. M. 2006. Mutations in voltage-gated potassium channel KCNC3 cause degenerative and developmental central nervous system phenotypes. *Nat Genet,* 38**,** 447-51.

WHITTAKER, V. P. 1968. The storage of transmitters in the central nervous system. *Biochem J,* 109**,** 20P-21P.

WHO. 2012. *Epilepsy. Fact sheet N°999. October 2012* [Online]. Available: http://www.who.int/mediacentre/factsheets/fs999/en/ [Accessed 03.11.13 2013].

WINDEN, K. D., KARSTEN, S. L., BRAGIN, A., KUDO, L. C., GEHMAN, L., RUIDERA, J., GESCHWIND, D. H. & ENGEL, J., JR. 2011. A systems level, functional genomics analysis of chronic epilepsy. *PLoS One,* 6**,** e20763.

WOODS, S. W., SAKSA, J. R., BAKER, C. B., COHEN, S. J. & TEK, C. 2008. Effects of levetiracetam on tardive dyskinesia: a randomized, double-blind, placebo-controlled study. *J Clin Psychiatry,* 69**,** 546-54.

WORTH, P. F., HOULDEN, H., GIUNTI, P., DAVIS, M. B. & WOOD, N. W. 2000. Large, expanded repeats in SCA8 are not confined to patients with cerebellar ataxia. *Nat Genet,* 24**,** 214-5.

XU, J., SATO, S., OKUYAMA, S., SWAN, R. J., JACOBSEN, M. T., STRUNK, E. & IKEZU, T. 2010. Tau-tubulin kinase 1 enhances prefibrillar tau aggregation and motor neuron degeneration in P301L FTDP-17 tau-mutant mice. *FASEB J,* 24**,** 2904-15.

XU, Q., KANTHASAMY, A. G. & REDDY, M. B. 2008. Neuroprotective effect of the natural iron chelator, phytic acid in a cell culture model of Parkinson's disease. *Toxicology,* 245**,** 101-8.

XU, R. M., CARMEL, G., SWEET, R. M., KURET, J. & CHENG, X. 1995. Crystal structure of casein kinase-1, a phosphate-directed protein kinase. *EMBO J,* 14**,** 1015-23.

XU, T. & BAJJALIEH, S. M. 2001. SV2 modulates the size of the readily releasable pool of secretory vesicles. *Nat Cell Biol,* 3**,** 691-8.

YABE, I., SASAKI, H., CHEN, D. H., RASKIND, W. H., BIRD, T. D., YAMASHITA, I., TSUJI, S., KIKUCHI, S. & TASHIRO, K. 2003. Spinocerebellar ataxia type 14 caused by a mutation in protein kinase C gamma. *Arch Neurol,* 60**,** 1749-51.

YANG, X. F., WEISENFELD, A. & ROTHMAN, S. M. 2007. Prolonged exposure to levetiracetam reveals a presynaptic effect on neurotransmission. *Epilepsia,* 48**,** 1861-9.

YAO, J., NOWACK, A., KENSEL-HAMMES, P., GARDNER, R. G. & BAJJALIEH, S. M. 2010. Cotrafficking of SV2 and synaptotagmin at the synapse. *J Neurosci,* 30**,** 5569-78.

YAO, P. J. 2004. Synaptic frailty and clathrin-mediated synaptic vesicle trafficking in Alzheimer's disease. *Trends Neurosci,* 27**,** 24-9.

YAO, P. J., ZHU, M., PYUN, E. I., BROOKS, A. I., THERIANOS, S., MEYERS, V. E. & COLEMAN, P. D. 2003. Defects in expression of genes related to synaptic vesicle trafficking in frontal cortex of Alzheimer's disease. *Neurobiol Dis,* 12**,** 97-109.

YU, N. N., YU, J. T., XIAO, J. T., ZHANG, H. W., LU, R. C., JIANG, H., XING, Z. H. & TAN, L. 2011. Tau-tubulin kinase-1 gene variants are associated with Alzheimer's disease in Han Chinese. *Neurosci Lett,* 491**,** 83-6.

ZARSKY, V. 2012. Jan Evangelista Purkyne/Purkinje (1787-1869) and the establishment of cellular physiology--Wroclaw/Breslau as a central European cradle for a new science. *Protoplasma,* 249**,** 1173-9.

ZHANG, J. Z., DAVLETOV, B. A., SUDHOF, T. C. & ANDERSON, R. G. 1994. Synaptotagmin I is a high affinity receptor for clathrin AP-2: implications for membrane recycling. *Cell,* 78**,** 751-60.

ZHANG, S., XU, L., LEE, J. & XU, T. 2002. Drosophila atrophin homolog functions as a transcriptional corepressor in multiple developmental processes. *Cell,* 108**,** 45-56.

ZHANG, W., CONNOR, K. M. & DAVIDSON, J. R. 2005. Levetiracetam in social phobia: a placebo controlled pilot study. *J Psychopharmacol,* 19**,** 551-3.

ZHUCHENKO, O., BAILEY, J., BONNEN, P., ASHIZAWA, T., STOCKTON, D. W., AMOS, C., DOBYNS, W. B., SUBRAMONY, S. H., ZOGHBI, H. Y. & LEE, C. C. 1997. Autosomal dominant cerebellar ataxia (SCA6) associated with small polyglutamine expansions in the alpha 1A-voltage-dependent calcium channel. *Nat Genet,* 15**,** 62-9.

ZIVKOVIC, S. A., COSTA, G., BOND, G. & ABU-ELMAGD, K. M. 2008. Treatment of tardive dyskinesia with levetiracetam in a transplant patient. *Acta Neurol Scand,* 117**,** 351-3.

ZOGHBI, H. Y. & ORR, H. T. 2000. Glutamine repeats and neurodegeneration. *Annu Rev Neurosci,* 23**,** 217-47.